

Dissecting the Role of Oxidative Stress in Spinal Muscular Atrophy (SMA)

Paloma Pacheco Torres, BSc

Submitted to the University of Hertfordshire in partial fulfilment of the requirements of the
degree of Doctor of Philosophy

School of Life and Medical Sciences, University of Hertfordshire, Hatfield, Hertfordshire, AL10
9AB

May 2025

Abstract

Spinal muscular atrophy (SMA) is a fatal inherited neurodegenerative disorder of childhood characterised by progressive motor neuron degeneration, extreme muscle weakness and atrophy. SMA results from biallelic mutations or deletions in the *survival motor neuron 1 (SMN1)* gene, which lead to diminished levels of the survival motor neuron (SMN) protein. SMN is a ubiquitously expressed protein localised in the nucleus and cytoplasm of cells and plays an essential role in several cellular processes. Its canonical function lies in the biogenesis of small nuclear ribonucleoproteins (snRNPs) required for pre-mRNA splicing. In addition, SMN regulates neuron-specific processes such as mRNA trafficking, local translation at synaptic terminals, and synaptic vesicle dynamics. These specialised functions contribute to the heightened vulnerability of spinal cord motor neurons to SMN deficiency. The approval of three therapeutic interventions for SMA patients in recent years has markedly improved patient outcome by significantly extending their lifespan. However, variability in treatment response among patients and the limited evidence of long-term effects has indicated that current therapies, despite being beneficial, do not represent a definitive cure for SMA.

In recent years, mitochondrial dysfunction and oxidative stress have emerged as potential contributors to SMA pathology. Various *in vitro* and *in vivo* models of SMA have highlighted that SMN deficiency leads to a range of mitochondrial abnormalities, such as increased mitochondrial fragmentation and altered mitochondrial membrane potential, impairing energy production and elevating reactive oxygen species (ROS) levels. Consequently, markers of oxidative damage to proteins, lipids and DNA have been detected in both SMA patients and preclinical SMA models. Additionally, oxidative stress can destabilise SMN and interfere with its primary function in pre-mRNA splicing, suggesting a bidirectional relationship between SMN depletion and oxidative stress that may accelerate SMA progression. Despite this evidence, the involvement of oxidative stress in SMA pathology remains poorly understood. This thesis investigates the role of oxidative stress in SMA by utilising a combination of targeted pharmacological interventions, genetic

manipulation and behavioural assays in the *Caenorhabditis elegans* (*C. elegans*) *smn-1(ok355)* SMA model, which is known to be characterised by neuromuscular defects and reduced lifespan. Reminiscent to mammalian studies, mutant *smn-1(ok355)* animals displayed transcriptional downregulation of mitochondrial energy metabolism pathways and elevated levels of cytoplasmic ROS. Interestingly, these mutants displayed increased sensitivity to oxidative stress, despite maintaining resistance to other types of stressors, suggesting a selective impairment of oxidative stress response mechanisms in SMA. To evaluate whether ROS reduction could improve neuromuscular function in SMA, five known antioxidant compounds were administered to *smn-1(ok355)* mutant animals. N-acetylcysteine was found to reduce ROS levels and improved motor phenotypes, as previously documented in the mammalian system. Interestingly, other chemical compounds unexpectedly increased ROS yet enhanced neuromuscular function (i.e. epigallocatechin gallate and melatonin). Additionally, SMN-1 protein levels were increased under both ROS-reducing and ROS-elevating conditions, indicating that redox state does not strictly govern SMN-1 abundance *in vivo*. Finally, the role of specific oxidative stress-response genes in SMA pathology was examined. A set of antioxidant genes from the *superoxide dismutase* (*SOD*) family were identified to be dysregulated in *smn-1(ok355)* animals. Pharmacological and behavioural analysis revealed that deletion of *sod-1* and *sod-2* increased *smn-1* oxidative stress sensitivity, although only *sod-1* deletion exacerbated neuromuscular defects. In contrast, loss of *sod-4* or *sod-5* improved both *smn-1* oxidative stress resilience and motor function. These findings demonstrated that modulating specific ROS-detoxifying pathways can influence SMA phenotypes.

Overall, our study highlights the intricate regulation of ROS in SMA, emphasising the necessity for precise modulation of oxidative stress responses. Our findings may inform the development of more effective, targeted antioxidant therapies for SMA in the future.

Acknowledgements

I would like to express my deepest gratitude to my supervisor, Dr Maria Dimitriadi, for her unwavering support throughout this journey. When all I had was the dream to become a scientist, she trusted my potential and gave me the opportunity to pursue this PhD, providing me with the tools and encouragement to help me make my own path in academia. I would also like to extend my gratitude to my second and third supervisors for their support and insightful feedback. Dr Maria Braoudaki, always kind, approachable and with encouraging words; and Dr George Poulogiannis, his guidance and insights during key moments of my PhD have made a significant difference in my progress.

My sincere thanks to all the members of the Dimitriadi Lab, for generously sharing their knowledge and offering words of encouragement: Toni, Amy, Fathama, Saman, Patricia, Ana, Coral, Lucia, Sandra, Ariadna, Marina, Lucia, Christine, and Emili. A special mention goes to Patricia Barnes and Sandra Hernández Sánchez, whom I have closely worked with and mentored; our work together have been particularly rewarding, and I genuinely admire their scientific rigour, and I have no doubt they will achieve great success in their careers. I would also like to thank the researchers and peers who provided constructive feedback during lab meetings, helping to shape this project through thoughtful discussions, especially Dr Caroline Formstone, Dr Lisa Lione, and Dr Helen Foster.

I am also thankful to the Society of Spanish Researchers in the UK, whose admirable efforts help to promote scientific collaborations between both British and Spanish institutions. I would like to extend my appreciation to the University of Hertfordshire, for providing funding support which has enabled me to attend and present my work at several conferences; and to the technical staff at the Science Building, whose dedicated work behind the scenes ensures that research runs smoothly. Finally, to my colleagues from the office and visiting lecturer team — thank you for your companionship and support throughout this journey.

I would like to express my heartfelt gratitude to my family and friends, who have stood by me with patience, love, and endless encouragement throughout this process. At times, I have felt

defeated when things have not worked out as I expected in the lab, but then I found Javi and Laura around the building, and they instantly brightened my day. Laura —free-spirited, talkative, kind, and loving —makes me feel at home whenever we are together. Javi —the coolest guy in Hatfield, the life of every social gathering —always knows how to reassure me; his optimism, laughter, and empathy have been invaluable during these years. Maria and Virginia —although your stay here was brief, I have missed you both since. Maria radiates peace and warmth simply through her presence. Virginia’s passion and dedication are an infinite source of motivation, and a constant reminder of how much this career means to me.

Thank you to those who became my family in Hatfield, Àlex and Ana. My initial plan was to stay in the UK for only one year, but then I met you. Our time here has been filled with challenges, celebrations, and so many crazy adventures that we could write a book about them. We have grown together through these experiences, and I will forever treasure them as some of the most special years of my life. Àlex, you are more than my best friend; you’re my brother. Words cannot express how much it has meant to me to count on your support during these years. Thank you for always being there for me —I’ll always be here for you too.

To my boyfriend, Szilveszter. Your mere presence in my life makes the top at the list of “things that I am grateful for”, every day. Thank you for believing in my dreams as if they were your own, for loving and taking care of me every day, and for being proud of me no matter what. I have my entire life to thank you for your unconditional support.

And finally, to my family. To my grandparents, Antonio and Faustina, thank you for dedicating your life to take care of our family. To my brother, Ismael, for being a role model for as long as I can remember. And to my parents, Paloma and Manuel, thank you for all the hard work and sacrifices you have made to help me achieve this long-held dream. To develop “the pill of immortality” has proven to be more challenging than what I imagined when I was kid, but I promise I will keep trying! ☺

Dedicated to the memory of my grandfather, Antonio Torres.

List of Publications, Presentations and Awards

1.1. Publications

Published

Hoolachan, J. M., McCallion, E., Sutton, E. R., Çetin, Ö., Pacheco-Torres, P., Dimitriadi, M., Sari, S., Miller, G. J., Okoh, M., Walter, L. M., Claus, P., Wood, M. J. A., Tonge, D. P., & Bowerman, M. (2023). A transcriptomics-based drug repositioning approach to identify drugs with similar activities for the treatment of muscle pathologies in spinal muscular atrophy (SMA) models. *Human Molecular Genetics*, 33(5), 400. <https://doi.org/10.1093/HMG/DDAD192>. (**Appendices 1B**).

Under peer review

Sutton, E. R., McCallion, E., Hoolachan, J. M., Cetin, Ö., Pacheco-Torres, P., Bouhmidi, S., Churchill, L., Scaife, T., Chaytow, H., Huang, Y.-T., Duguez, S., Schneider, B. L., Gillingwater, T. H., Dimitriadi, M., & Bowerman, M. (2025). Mifepristone alone and in combination with scAAV9-SMN1 gene therapy improves disease phenotypes in *Smn2B^{-/-}* spinal muscular atrophy mice. *BioRxiv*, 2025.02.17.638672. <https://doi.org/10.1101/2025.02.17.638672>. (**Appendices 1A**).

1.2. Presentations

Internal

- ❖ Life and Medical School Annual Research Conference 2021 – 22 June 2021 – University of Hertfordshire (online), Hatfield, United Kingdom – Poster presentation – (**Anexo II A1**).

- ❖ Life and Medical School Annual Research Conference 2022 – 21 June 2022 – University of Hertfordshire, Hatfield, United Kingdom – Poster presentation (**Anexo II A2**).
- ❖ Postgraduate Research Seminars 2022 – 10 Oct 2022 – University of Hertfordshire, Hatfield, United Kingdom – Presentation – (**Anexo II A3**).
- ❖ 3 Minute Thesis Competition – 5 May 2022 – University of Hertfordshire, Hatfield, United Kingdom – Presentation – (**Anexo II A4**).
- ❖ Life and Medical School Annual Research Conference 2024 – 11 Jun 2024 – University of Hertfordshire, Hatfield, United Kingdom – Presentation – (**Anexo II A5**).
- ❖ Postgraduate Research Seminars 2024 – 11 Nov 2024 – University of Hertfordshire, Hatfield, United Kingdom – Presentation – (**Anexo II A6**).

National

- ❖ Worm Club Seminars 2021 – 3 Nov 2021 – The London Worm Club (online), United Kingdom – Presentation – (**Anexo II B1**).
- ❖ 15th UK Neuromuscular Translational Research Conference (online) – 26-27 Apr 2022 – Muscular Dystrophy UK (online) – Poster presentation – (**Anexo II B2**).
- ❖ IX International Symposium SRUK – 1-3 July 2022 – Spanish Researchers in the UK, Oxford, United Kingdom – Poster presentation – (**Anexo II B3**).
- ❖ SRUK Ageing and Diseases Conference – 9 Jun 2023 – Spanish Researchers in the United Kingdom, Cambridge, United Kingdom – Presentation – (**Anexo II B4**).
- ❖ UK Worm Meeting 2023 – 13 Jan 2023 – University of East Anglia, Norwich, United Kingdom – Poster presentation – (**Anexo II B5**).
- ❖ 16th UK Neuromuscular Translational Research Conference – 29-30 Mar 2023 – Muscular Dystrophy UK, University College London, London, United Kingdom – Poster presentation – (**Anexo II B6**).

International

- ❖ 3rd International Scientific Congress on Spinal Muscular Atrophy – 21-23 October 2022 – SMA Europe, Barcelona, Spain – Poster presentation – (**Anexo II C1**).
- ❖ 24th International C. elegans Conference – 24-28 June 2023 – Genetics Society of America, Glasgow, Scotland – Poster presentation – (**Anexo II C2**).
- ❖ 4th International Scientific Congress on Spinal Muscular Atrophy – 14-16 March 2024 – SMA Europe, Ghent, Belgium – Poster presentation – (**Anexo II C3**).

1.3. Awards

- ❖ IX International Symposium SRUK – 1-3 July 2022 – Spanish Researchers in the UK, Oxford, United Kingdom – Poster presentation – (**Anexo II B3**).
- ❖ SRUK Ageing and Diseases Conference – 9 Jun 2023 – Spanish Researchers in the United Kingdom, Cambridge, United Kingdom – Presentation – (**Anexo II B4**).

Table of Contents

| | |
|--|-------|
| Abstract | ii |
| Acknowledgements | iv |
| List of Publications, Presentations and Awards..... | viii |
| 1.1. Publications | viii |
| 1.2. Presentations..... | viii |
| 1.3. Awards..... | x |
| List of Figures | xvi |
| List of Tables..... | xviii |
| List of Acronyms..... | xix |
| Chapter I. Introduction | 1 |
| 1.1. Spinal muscular atrophy..... | 2 |
| 1.1.1. Clinical and physiological pathology..... | 2 |
| 1.1.2. Molecular genetics..... | 7 |
| 1.1.3. The survival motor neuron protein | 11 |
| 1.1.3.1. Ribonucleoprotein assembly | 12 |
| 1.1.3.2. RNA trafficking and cytoskeleton dynamics..... | 14 |
| 1.1.3.4. Regulation of local translation | 15 |
| 1.1.3.5. Regulation of the ubiquitin pathway | 15 |
| 1.1.3.6. Regulation of endocytosis | 16 |
| 1.1.3.7. Modulation of autophagy | 16 |
| 1.1.3.8. Mitochondrial function..... | 17 |
| 1.1.4. Genetic modifiers..... | 17 |
| 1.1.5. Approved therapies | 20 |
| 1.2. Spinal muscular atrophy models | 24 |
| 1.2.1. Cell-culture | 24 |
| 1.2.2. Mice | 25 |
| 1.2.3. Zebrafish..... | 26 |
| 1.2.4. <i>Drosophila melanogaster</i> | 27 |
| 1.2.5. <i>Caenorhabditis elegans</i> | 28 |
| 1.3. Oxidative stress | 36 |
| 1.3.1. Evolution of the scientific knowledge of free radicals and oxidative agents..... | 36 |
| 1.3.2. Definitions | 37 |
| 1.3.3. ROS in physiology: oxidative eustress | 41 |
| 1.3.3.1. Cellular sources of ROS and its role | 41 |
| 1.3.3.2. Antioxidant defence | 43 |

| | | |
|----------|---|----|
| 1.3.4. | ROS in pathology: oxidative stress..... | 49 |
| 1.3.4.1. | Non-specific oxidation of biomolecules | 49 |
| 1.3.4.2. | Oxidative stress in neurodegeneration | 51 |
| 1.4. | Oxidative stress in spinal muscular atrophy..... | 56 |
| 1.4.1. | Increased ROS and elevated oxidative damage in spinal muscular atrophy..... | 56 |
| 1.4.2. | Mechanisms triggering oxidative stress in spinal muscular atrophy | 60 |
| 1.4.3. | Oxidative stress in spinal muscular atrophy: cause or consequence? | 64 |
| 1.5. | Aims and objectives | 69 |
| | Chapter II. Materials and Methods..... | 70 |
| 2.1. | General solutions and media | 71 |
| 2.2. | Strains and maintenance..... | 73 |
| 2.3. | Freezing and thawing stocks | 78 |
| 2.4. | Decontamination of stocks | 78 |
| 2.5. | Synchronisation of <i>Caenorhabditis elegans</i> populations | 79 |
| 2.6. | Genotyping..... | 80 |
| 2.6.1. | DNA extraction..... | 80 |
| 2.6.2. | Polymerase chain reaction (PCR) | 81 |
| 2.6.3. | Agarose gel DNA electrophoresis..... | 83 |
| 2.7. | Dihydroethidium assay..... | 83 |
| 2.8. | MitoSOX assay | 84 |
| 2.9. | Fluorescence imaging..... | 85 |
| 2.10. | Fluorescence quantification | 86 |
| 2.11. | Survival assays | 86 |
| 2.12. | Juglone sensitivity assay | 87 |
| 2.13. | Paraquat sensitivity assay..... | 88 |
| 2.14. | Heat stress sensitivity assay | 88 |
| 2.15. | Osmotic stress sensitivity assay | 89 |
| 2.16. | Pharyngeal pumping..... | 89 |
| 2.17. | WormLab® locomotion assay | 90 |
| 2.17.1. | Locomotion assay | 90 |
| 2.17.2. | WormLab® detection and tracking system | 90 |
| 2.17.3. | Evaluation of automatic tracking quality..... | 91 |
| 2.17.4. | WormLab® data processing | 91 |
| 2.18. | Antioxidant treatment..... | 94 |
| 2.19. | RNA isolation..... | 95 |
| 2.20. | RNA sequencing..... | 95 |
| 2.21. | Bioinformatic analysis | 96 |

| | | |
|---|---|-----|
| 2.21.1. | Principal component analysis | 97 |
| 2.21.2. | Differentially expressed genes analysis..... | 97 |
| 2.21.3. | Functional analysis | 97 |
| 2.21.4. | Gene Set Expression analysis..... | 98 |
| 2.21.5. | Identification of oxidative stress hub genes in SMA..... | 99 |
| 2.22. | Statistical analysis | 99 |
| Chapter III. Investigating oxidative stress involvement in the <i>Caenorhabditis elegans</i> spinal muscular atrophy model..... | | 101 |
| 3.1. | Introduction..... | 102 |
| 3.1.1. | ROS induction in <i>Caenorhabditis elegans</i> | 102 |
| 3.1.2. | ROS detection in <i>Caenorhabditis elegans</i> | 105 |
| 3.1.3. | Research Objectives..... | 107 |
| 3.2. | Results | 107 |
| 3.2.1. | SMN-1 depletion induces changes in gene expression in <i>Caenorhabditis elegans</i> . | 107 |
| 3.2.2. | SMN-1 depletion increases oxidative stress sensitivity in <i>Caenorhabditis elegans</i> | 123 |
| 3.2.3. | SMN-1 depletion increases cytoplasmic ROS in <i>Caenorhabditis elegans</i> | 132 |
| 3.3. | Discussion | 140 |
| 3.3.1. | Gene expression changes in the <i>Caenorhabditis elegans</i> spinal muscular atrophy model | 140 |
| 3.3.2. | Dissecting stress vulnerabilities in spinal muscular atrophy | 141 |
| 3.3.3. | ROS imbalance in the <i>Caenorhabditis elegans</i> spinal muscular atrophy model | 144 |
| Chapter IV. Therapeutic potential of antioxidant treatment in spinal muscular atrophy | | 146 |
| 4.1. | Introduction..... | 147 |
| 4.1.1. | Antioxidant treatment in neurodegenerative diseases: mechanisms of action and therapeutic potential | 148 |
| | N-acetylcysteine..... | 148 |
| | Curcumin..... | 149 |
| | Vitamin C | 151 |
| | Epigallocatechin gallate | 152 |
| | Melatonin | 154 |
| 4.1.2. | Research objectives..... | 155 |
| 4.2. | Results | 156 |
| 4.2.1. | Characterisation of the <i>Caenorhabditis elegans</i> locomotion..... | 156 |
| 4.2.2. | Evaluation of antioxidant treatment efficacy in modulating neuromuscular activity in SMA | 159 |
| 4.2.2.1. | N- acetyl cysteine | 159 |
| 4.2.2.2. | Curcumin..... | 164 |
| 4.2.2.3. | Vitamin C | 169 |

| | | |
|--|---|-----|
| 4.2.2.4. | Epigallocatechin gallate | 173 |
| 4.2.2.5. | Melatonin | 178 |
| 4.2.3. | Impact of ROS on SMN-1 protein levels..... | 183 |
| 4.3. | Discussion | 189 |
| 4.3.1. | Neuromuscular function and ROS levels..... | 189 |
| 4.3.2. | SMN-1 protein and ROS levels | 191 |
| 4.3.3. | Neuromuscular function and SMN-1 protein levels | 192 |
| 4.3.4. | Relationship between ROS, neuromuscular function and SMN-1 protein levels.... | 193 |
| Chapter V. Investigating the oxidative stress response in the <i>Caenorhabditis elegans</i> spinal muscular atrophy model..... | | 196 |
| 5.1. | Introduction..... | 197 |
| 5.1.1. | Transcription factors that regulate the oxidative stress response | 197 |
| 5.1.1.1. | DAF-16 | 197 |
| 5.1.1.2. | SKN-1 | 199 |
| 5.1.2. | Endogenous antioxidant enzymes..... | 204 |
| 5.1.2.1. | Superoxide dismutase..... | 204 |
| 5.1.2.2. | Catalase | 205 |
| 5.1.2.3. | Glutathione peroxidase..... | 206 |
| 5.1.2.4. | Peroxiredoxin | 206 |
| 5.1.3. | Research objectives..... | 207 |
| 5.2. | Results..... | 208 |
| 5.2.1. | Dysregulated genes controlling the oxidative stress response in spinal muscular atrophy..... | 208 |
| 5.2.2. | Evaluation of the impact of <i>sod</i> knockouts on neuromuscular function..... | 217 |
| 5.2.2.1. | <i>Superoxide dismutase 1</i> | 217 |
| 5.2.2.2. | <i>Superoxide dismutase 2</i> | 220 |
| 5.2.2.3. | <i>Superoxide dismutase 3</i> | 223 |
| 5.2.2.4. | <i>Superoxide dismutase 4</i> | 226 |
| 5.2.2.5. | <i>Superoxide dismutase 5</i> | 229 |
| 5.3. | Discussion | 233 |
| 5.3.1. | Identification of central oxidative stress related genes differentially expressed..... | 233 |
| 5.3.2. | SOD isoforms can modulate oxidative stress sensitivity in the <i>Caenorhabditis elegans</i> spinal muscular atrophy model | 235 |
| 5.3.3. | SOD isoforms can modulate neuromuscular function in the <i>Caenorhabditis elegans</i> spinal muscular atrophy model | 237 |
| 5.3.3.1. | Cytoplasmic <i>sods</i> | 238 |
| 5.3.3.2. | Mitochondrial <i>sods</i> | 239 |
| 5.3.3.3. | Extracellular <i>sod</i> | 240 |

| | |
|---|-----|
| Chapter VI. Discussion | 245 |
| 6.1 Project outcomes | 246 |
| 6.2 Future directions..... | 248 |
| 6.2.1. Methodological considerations | 249 |
| 6.2.2. Refine molecular targets modulated by ROS in spinal muscular atrophy | 251 |
| 6.3 Therapeutic opportunities..... | 254 |
| 6.4 Conclusion | 254 |
| References..... | 256 |
| Anexo I..... | 301 |
| Anexo II | 313 |

List of Figures

| | |
|---|-----|
| Figure 1.1. Pathophysiology of spinal muscular atrophy | 4 |
| Figure 1.2. SMN expression in healthy individuals and SMA patients..... | 9 |
| Figure 1.3. Developmental lifecycle of <i>Caenorhabditis elegans</i> and phenotypic consequences of SMN-1 depletion..... | 30 |
| Figure 1.4. Free radicals and non-radicals derived from oxygen..... | 39 |
| Figure 1.5. Cellular sources and fates of reactive oxygen species | 48 |
| Figure 1.6. Hypothetical models illustrating the interplay between SMN depletion and oxidative stress in the pathophysiology of spinal muscular atrophy..... | 68 |
| | |
| Figure 2.1. The <i>Caenorhabditis elegans smn-1</i> endogenous gene and the <i>C. elegans</i> SMA severe models and maintenance | 76 |
| Figure 2.2. Experimental workflow utilised to quantify nematode locomotion using the WormLab® software..... | 92 |
| | |
| Figure 3.1. SMN-1 depletion induces widespread changes in gene expression of the <i>smn-1(ok355)</i> <i>C. elegans</i> SMA model | 109 |
| Figure 3.2. Gene Ontology (GO) molecular function enrichment analysis of the <i>smn-1(ok355)</i> <i>C. elegans</i> SMA model..... | 112 |
| Figure 3.3. Gene Ontology (GO) biological processes enrichment analysis of the <i>smn-1(ok355)</i> <i>C. elegans</i> SMA model | 115 |
| Figure 3.4. Gene Ontology (GO) cellular components enrichment analysis of the <i>smn-1(ok355)</i> <i>C. elegans</i> SMA model | 118 |
| Figure 3.5. Kyoto Encyclopedia of Genes and Genomes (KEGG) pathways enrichment analysis of <i>smn-1(ok355)</i> <i>C. elegans</i> SMA model..... | 121 |
| Figure 3.6. Depletion of the SMN-1 protein increases sensitivity to oxidative stress in <i>C. elegans</i> | 126 |
| Figure 3.7. SMN-1 depletion modifies the stress response in the <i>smn-1(ok355)</i> <i>C. elegans</i> SMA model following exposure to heat and osmotic stress..... | 130 |
| Figure 3.8. Depletion of the SMN-1 protein does not alter whole-body MitoSOX fluorescence in the <i>smn-1(ok355)</i> <i>C. elegans</i> SMA model..... | 133 |
| Figure 3.9. Depletion of the SMN-1 protein does not alter head-specific mitochondrial MitoSOX fluorescence in the <i>smn-1(ok355)</i> <i>C. elegans</i> SMA model. | 136 |
| Figure 3.10. The SMN-1 protein prevents the cytoplasmic accumulation of ROS in <i>C. elegans</i> | 139 |
| | |
| Figure 4.1. WormLab parameters selected to measure differences in locomotion among <i>smn-1(ok355)</i> and control animals..... | 158 |
| Figure 4.2. N-acetylcysteine partially ameliorates neuromuscular defects in the <i>smn-1(ok355)</i> <i>C. elegans</i> SMA model..... | 160 |
| Figure 4.3. N-acetyl cysteine prevents the accumulation of cytoplasmic ROS in the <i>smn-1(ok355)</i> <i>C. elegans</i> SMA model | 162 |
| Figure 4.4. Curcumin does not ameliorate neuromuscular defects in the <i>smn-1(ok355)</i> <i>C. elegans</i> SMA model | 165 |
| Figure 4.5. Curcumin prevents the accumulation of cytoplasmic ROS in the <i>smn-1(ok355)</i> <i>C. elegans</i> SMA model..... | 167 |
| Figure 4.6. Vitamin C does not ameliorate neuromuscular defects in the <i>smn-1(ok355)</i> <i>C. elegans</i> SMA model | 170 |

| | |
|--|-----|
| Figure 4.7. Vitamin C does not prevent the accumulation of cytoplasmic ROS in the <i>smn-1(ok355)</i> <i>C. elegans</i> SMA model | 172 |
| Figure 4.8. Epigallocatechin gallate partially ameliorates neuromuscular defects in the <i>smn-1(ok355)</i> <i>C. elegans</i> SMA model | 174 |
| Figure 4.9. Epigallocatechin gallate might induce accumulation of cytoplasmic ROS in the <i>smn-1(ok355)</i> <i>C. elegans</i> SMA model at low concentrations | 176 |
| Figure 4.10. Melatonin partially ameliorates neuromuscular defects in the <i>smn-1(ok355)</i> <i>C. elegans</i> SMA model | 179 |
| Figure 4.11. Melatonin induces the accumulation of cytoplasmic ROS in the <i>smn-1(ok355)</i> <i>C. elegans</i> SMA model | 181 |
| Figure 4.12. Visualization of the SMN-1 protein in the <i>smn-1(ok355)</i> <i>C. elegans</i> SMA model | 185 |
| Figure 4.13. N-acetyl cysteine increases SMN-1 protein levels in the <i>smn-1(ok355)</i> <i>C. elegans</i> SMA model | 187 |
| Figure 4.14. Melatonin increases SMN-1 protein levels in the <i>smn-1(ok355)</i> <i>C. elegans</i> SMA model | 188 |
| | |
| Figure 5.1. Regulatory pathways controlling the activation of the transcription factors DAF-16 and SKN-1 in <i>Caenorhabditis elegans</i> | 202 |
| Figure 5.2. Oxidative stress-response genes differentially expressed (OxSR-DE) in the <i>smn-1(ok355)</i> <i>C. elegans</i> SMA model | 210 |
| Figure 5.3. Identification of oxidative stress hub genes in the <i>smn-1(ok355)</i> <i>C. elegans</i> SMA model using protein-protein interaction (PPI) network analysis | 213 |
| Figure 5.4. Transcription-factor (TF) network of oxidative stress hub genes identified in <i>smn-1(ok355)</i> animals | 216 |
| Figure 5.5. Deletion of <i>sod-1</i> increases sensitivity to oxidative stress and exacerbates neuromuscular defects in the <i>smn-1(ok355)</i> <i>C. elegans</i> SMA model | 219 |
| Figure 5.6. Deletion of <i>sod-2</i> increases sensitivity to oxidative stress without exacerbating neuromuscular defects in the <i>smn-1(ok355)</i> <i>C. elegans</i> SMA model | 222 |
| Figure 5.7. Deletion of <i>sod-3</i> did not increase sensitivity to oxidative stress or affect neuromuscular function in the <i>smn-1(ok355)</i> <i>C. elegans</i> SMA model | 225 |
| Figure 5.8. Deletion of <i>sod-4</i> decreases sensitivity to oxidative stress and ameliorates neuromuscular defects in the <i>smn-1(ok355)</i> <i>C. elegans</i> SMA model | 228 |
| Figure 5.9. Deletion of <i>sod-5</i> decreases sensitivity to oxidative stress and ameliorates neuromuscular defects in the <i>smn-1(ok355)</i> <i>C. elegans</i> SMA model | 231 |
| Figure 5.10. Hypothetical model illustrating how loss of <i>sod-4</i> modulates IIS signalling and enhances stress responses in the <i>C. elegans</i> SMA model | 243 |
| | |
| Supplementary Figure 1. Venn diagram illustrating the overlap of molecular components involved in the oxidative, heat and osmotic stress responses in <i>C. elegans</i> | 302 |
| Supplementary Figure 2. WormLab shape-based parameters | 303 |
| Supplementary Figure 3. WormLab movement-behaviour parameters | 304 |
| Supplementary Figure 4. WormLab distance-travelled parameters | 305 |
| Supplementary Figure 5. WormLab time-based parameters | 307 |
| Supplementary Figure 6. WormLab speed measurements | 309 |
| Supplementary Figure 7. Deletion of individual <i>sod</i> genes modifies the sensitivity to oxidative stress in <i>smn-1(ok355)</i> <i>C. elegans</i> SMA | 310 |
| Supplementary Figure 8. Deletion of <i>sod-4</i> gene can modify <i>smn-1(ok355)</i> <i>C. elegans</i> neuromuscular defects | 311 |

List of Tables

| | |
|---|-----|
| Table 1.1. Reactive oxygen species: origin, reactivity and biological impact..... | 40 |
| Table 1.2. Cofactors, subcellular locations, and overall reaction of antioxidants enzymes | 46 |
| Table 1.3. Effect of antioxidant treatment in Alzheimer’s Disease and Parkinson’s Disease pre-clinical models | 54 |
| Table 1.4. Evidence of elevated reactive oxygen species in spinal muscular atrophy | 57 |
| Table 1.5. Evidence of oxidative damage in spinal muscular atrophy | 59 |
| Table 1.6. Evidence of mitochondrial defects on spinal muscular atrophy | 62 |
| Table 1.7. Effect of reactive oxygen species modulation in spinal muscular atrophy..... | 66 |
| | |
| Table 2.1. List of <i>C. elegans</i> strains used in this project | 73 |
| Table 2.2. Standard egg-laying procedure to synchronise <i>C. elegans</i> populations at day-3 post-hatching, as described by Dimitriadi et al., 2010 | 79 |
| Table 2.3. Egg-laying experimental procedure for obtaining synchronous <i>C. elegans</i> L4-stage populations | 80 |
| Table 2.4. Thermal cycler programs for <i>C. elegans</i> lysis and PCR..... | 81 |
| Table 2.5. Primers used for PCR genotyping | 81 |
| Table 2.6. PCR master mix for genes utilised in this thesis | 82 |
| Table 2.7. Antioxidant compounds used for <i>C. elegans</i> drug treatment..... | 94 |
| Table 2.8. List of software packages and parameters utilised for transcriptomic analysis..... | 96 |
| | |
| Table 4.1. Differential effects of antioxidant treatment on <i>smn-1(ok355)</i> neuromuscular function and intracellular ROS levels..... | 183 |
| Table 4.2. Modulation of molecular pathways by antioxidants utilised in this study | 194 |
| | |
| Table 5.1. Conversion of candidate <i>C. elegans</i> OxSR-DE genes to their closest human ortholog | 214 |
| Table 5.2. Transcription factor analysis of hub oxidative stress hub genes identified in <i>smn-1(ok355)</i> animals | 215 |
| Table 5.3. Summary of phenotypic outcomes observed in <i>C. elegans</i> single <i>sod</i> mutants and <i>smn-1(ok355);sod</i> double mutants across oxidative stress and neuromuscular function assays..... | 232 |

List of Acronyms

•HO₂ = Hydroperoxyl

•OH = Hydroxyl

3NT = 3-nitrotyrosine

4HNE = Protein Carbonylation

8OHdG = Nucleic Acid Oxidation

AAV9 = Adeno-associated Vector 9

AB = Amyloid-B

ACOX = Acyl-CoA Oxidases

AD = Alzheimer's Disease

AGE-1 = Advanced Glycation End-products-1

AKT = Akt strain Transforming

ALS = Amyotrophic Lateral Sclerosis

AMPK = AMP-activated Protein Kinase

ANOVA = Analysis of Variance

AOX1 = Aldehyde Oxidase-1

ASI = Acidogenic

ASO = Antisense Oligonucleotide

AT1 = angiotensin II receptor 1

ATP = Adenosine Triphosphate

ATPase = Adenosine Triphosphatase

AVI = Audio Video Interleave

BDM = 2,3-Butanedione Monoxime

C. elegans = Caenorhabditis elegans

CAT = Catalase

CGC = Caenorhabditis Genetics Center

COP1 = Coat Protein 1

COX2 = Cyclooxygenase-2

CP-SOH = Cysteine Sulfenic Acid

CR = Resolving Cysteine

CTL = Catalases

Cu = Copper

CUR = Curcumin

CYP = Cytochrome P450

Cys = Cystine

DAB = Diaminobenzidine

DAF-16 = Decay-acceleration Factor-16

DEG = Differentially Expressed Genes

dH₂O = Distilled water

DHCR24 = 24-Dehydrocholesterol Reductase

DHE = Dihydroethidium

DIC = Differential Interference Contrast

DIM = Dimitriadi Lab

DJR = Glutathione-independent Glyoxalase System

DMD = Duchenne Muscular Dystrophy

DMSO = Dimethyl Sulfoxide

DNA = Deoxyribonucleic acid

dNTPs = Deoxynucleoside Triphosphates

EGCG = Epigallocatechin Gallate

ER = Endoplasmic Reticulum

ErbB = Erythroblastic leukemia viral oncogene homologue

ERK = Extracellular Regulated Kinase

ERK1/2 = Extracellular signal-regulated protein kinase 1/2

ERO1 = Endoplasmic Reticulum Oxidoreductin-1

ESE = Exon Splicing Enhancer

ESE2 = Exonic Splicing Enhancer 2

ETC = Electron Transport Chain

FDR = False Discovery Rate

FOXC1 = Forkhead box C1

FOXO = Forkhead box O

FUdR = 5-fluoro-2'-deoxyuridine

GABA = Gamma-Aminobutyric Acid

GATA2 = GATA-binding transcription factor-2

GFP = Green Fluorescent Protein

GO = Gene Ontology

GPx = Glutathione Peroxidases

GSEA = Gene Set Enrichment Analysis

GSH = Glutathione

GSSG = Oxidised Glutathione

GST = Glutathione S-transferase

H₂O₂ = Hydrogen Peroxide

HA = Hart Lab

HD = Huntington's Disease

HDAC = Histone Deacetylase

HDD = Hard Disk Drive

hESC = Human Embryonic Stem Cell

HMOX1 = Heme Oxygenase-1

HNE = 4-Hydroxynonenal

HOXA5 = Homeobox A5

HPLC = High-performance liquid chromatography

hT2 = Serotonin receptor

IGF-1 = Insulin-like Growth Factor-1

IIS = Insulin/IGF-1 signalling

ILP = Insulin-like Peptides

iPSC = induced Pluripotent Stem Cells

ISTL1 = Internal Stem-Loop 1

JNK = c-Jun N-terminal kinase

KEGG = Kyoto Encyclopedia of Genes and Genomes

LC-MS = Liquid Chromatography-Mass Spectrometry

LMNs = Lower Motor Neurons

M9 = M9 minimal medium

MAPK = Mitogen-activated protein kinase

MCODE = Molecular Complex Detection Technology

MDA = Malondialdehyde

MEL = Melatonin

MF = Molecular Function

MitoSOX = Mitochondrial Superoxide Indicator

MMP = Matrix Metalloproteinases

Mn = Manganese

MNs = Motor Neurons

MO = Morpholino Oligonucleotides

MPP = 1-methyl-4-phenylpyridinium

MPTP = 1-methyl-4-phenyl-1,2,3,6-tetrahydropyridine

MS = Multiple Sclerosis

MSRA = Methionine Sulfoxide Reductase

mTOR = Mechanistic/Mammalian Target of Rapamycin

n = Sample size

NAC = N-acetyl cysteine

NaCl = Sodium Chloride

NADPH = Nicotinamide Adenine Dinucleotide Phosphate

NCALD = Neuroclaritin Delta

NES = Negative enrichment scores

NFE2L2 = Nuclear Factor Erythroid 2-like2

NFT = Neurofibrillary Tangles

NF- κ B = Nuclear factor kappa-light-chain-enhancer of activated B cells

NGM = Nematode Growth Medium

NMJ = Neuromuscular Junction

NO = Nitric Oxide

NOX = NADPH Oxidases

NPC = Neuronal Progenitor Stage

NRF2 = Nuclear factor erythroid 2-related factor 2

NRTK = Non-receptor tyrosine kinases

OL2 = OrthoList 2

OP50 E.coli = Escherichia coli

OxSR = Oxidative Stress Response

OxSR-DE = Oxidative stress related genes Differentially Expressed

p38 MAPK = p38 mitogen-activated protein kinase

P47-Phox = Neutrophil cytosolic factor-1

PC1 = First principal component

PC2 = Second principal component

PCA = Principal Component Analysis

PCR = Polymerase Chain Reaction

PD = Parkinson`s disease

PDI = Protein Disulphide Isomerases

PKC-1 = Phosphoinositide-dependent protein kinase-1

PGK1 = Phosphoglycerate Kinase-1

pH = potential of Hydrogen

PHA-4 = Pharynx-4

PI3K = Phosphoinositide 3-kinase

PIP = Phosphatidylinositol Phosphate

PLS3 = Platin 3

PPI = Protein-Protein Interaction

PQ = Plastoquinone

PRDXs = Perxiredoxins

PRx = Peroxiredoxins

Prxs = Peroxiredoxin

PTEN = Phosphatase and TENsin homolog deleted on chromosome 10

PTPases = Protein-Tyrosine Phosphatases

qRT-PCR = Quantitative Reverse Transcription Polymerase Chain Reaction

RAC1 = Ras-related C3 botulinum toxin substrate-1

Ras-ERK = Extracellular signal-regulated kinase

RBP = RNA-Binding Proteins

RELA = RELA protooncogene NF-kB subunit

RNA = Ribonucleic acid

RNA-seq = RNA sequencing

ROCK = Rho Kinase
ROS = Reactive Oxygen Species
rRNA = Ribosomal RNA
RTK = receptor tyrosine kinases
SBS = Sequencing by Synthesis
SEK-1 = Stress-Activated Protein Kinase-1
SEM = Standard Error of the Mean
-SeOH = Selenenic Acid
SEPP1 = Selenoprotein P
SIP1 = SMN-Interacting Protein
SKN-1 = Skinhead-1
SMA = Spinal Muscular Atrophy
SMA-OSRGs = SMA-Oxidative Stress-Related-Genes
SMN = Survival Motor Neuron
SMN1 = Survival Motor Neuron One
snoRNPs = Small nucleolar RNAs
SnRNPs = Small Nuclear Ribonucleoproteins
SOD = Superoxide Dismutase
TBARs = Thiobarbituric Acid Reactive Substances
TF = Transcription Factor
TPP = Triphenylphosphonium
tRNA = Transfer Ribonucleic acid
TRX = Thioredoxin
TSL2 = Terminal Stem-Loop 2
TSL3 = Terminal Stem-Loop 3
TTN = Transient Tachypnea of the Newborn
TVA = Transversus Abdominis
UPR = Unfolded Protein Response
UPS = Ubiquitin-proteasome system
UR = Urate Oxidase
UV = UltraViolet

VITC = Vitamin C

VST = Variance-Stabilizing Transformation

Wnt/ β -catenin = Wingless-related integration site

XOR = Xanthine Oxidoreductase

Chapter I. Introduction

1.1. Spinal muscular atrophy

Spinal Muscular Atrophy (SMA) is an inherited neuromuscular disease, caused by biallelic mutations or deletions in the *survival motor neuron one (SMN1)* gene (Burr and Reddivari, 2023). The main pathological marker of SMA is the progressive and irreversible loss of lower motor neurons in the spinal cord and the brain stem nuclei, which causes severe muscle weakness and atrophy (Burr and Reddivari, 2023). As consequence, patients suffering from SMA have difficulties in walking, sitting independently and controlling head movements, among others (Kolb and Kissel, 2015). As the disease progresses, the motor ability of these patients is subsequently affected, ultimately leading to mortality (mainly in infancy) as a consequence of multi systemic complications, such as cardiac arrest or respiratory failure (Burr and Reddivari, 2023). Population studies have estimated that approximately 1 in 50 individuals are carriers of SMA, with an incidence of one affected newborn per 10,000 live births for this debilitating disorder (Macdonald, Hamilton and Kuhle, 2014).

1.1.1. Clinical and physiological pathology

Before the advent of molecular diagnosis, clinicians classified SMA into different clinical subtypes. Based on age of onset, severity and highest motor function achieved, SMA can be classified into five subtypes, from SMA type 0 to SMA type IV (Kolb and Kissel, 2015). SMA type 0 represents the most severe form of the condition, manifesting prenatally with significant muscular weakness, respiratory failure and mortality within the first month of life. SMA type I, which presents before six months of age, is characterised by hypotonia, an inability to sit, and early mortality due to respiratory complications, generally occurring before the age of two. SMA type II emerges between 6 and 18 months and is characterised by progressive muscular weakness and musculoskeletal complications. Patients can sit independently and, although they lose the ability to walk, many survive until adulthood. SMA type III, with onset after 18 months, initially permits ambulation but often progresses to wheelchair dependence. Clinical features include proximal leg weakness, tremor, and diminished reflexes. SMA type IV is the mildest form, with

adult onset and mild proximal weakness, is characterised by extreme fatigue without significant motor disability (Kolb and Kissel, 2015). Although supportive care can enhance quality of life, it does not arrest disease progression, rendering these phenotypes critical baselines for assessing the efficacy of new treatments.

The primary pathological hallmark of SMA, evident in all human patients, is the loss of lower motor neurons (MNs) and muscle atrophy (Burr and Reddivari, 2023) (**Figure 1.1**). However, in the most severe forms of the disease, the overall clinical manifestations can reflect the contribution from various cell types and tissues, including not only motor neurons but also other neuronal types, muscles, brain, cardiac tissue and liver, among others (Hamilton and Gillingwater, 2013).

To initiate movement, a signal begins in the primary motor cortex, where the upper motor neurons originate. Their axons descend through the brain to the anterior horn of the spinal cord, where they synapse with lower motor neurons (LMNs), which then transmit the signal to the muscle for movement (Zayia and Tadi, 2023). LMNs are classified into somatic motor neurons, branchial motor neurons, and visceral motor neurons. Somatic motor neurons, including alpha, beta, and gamma types, are located in the brainstem and spinal cord and innervate skeletal muscle fibres, coordinating precise and synchronous muscle contraction. Alpha motor neurons innervate extrafusal muscle fibres and are responsible for generating skeletal muscle contraction, while gamma motor neurons innervate intrafusal fibres within muscle spindles to regulate their sensitivity and fine-tune muscle tone. Beta motor neurons, which are less well characterised, innervate both extrafusal and intrafusal fibres and may contribute to integrating motor and sensory functions (Zayia and Tadi, 2023). Branchial motor neurons control head and neck muscles. Visceral motor neurons innervate ganglia, which in turn regulate organs such as the heart, lungs, kidneys, and digestive tract (Stifani, 2014).

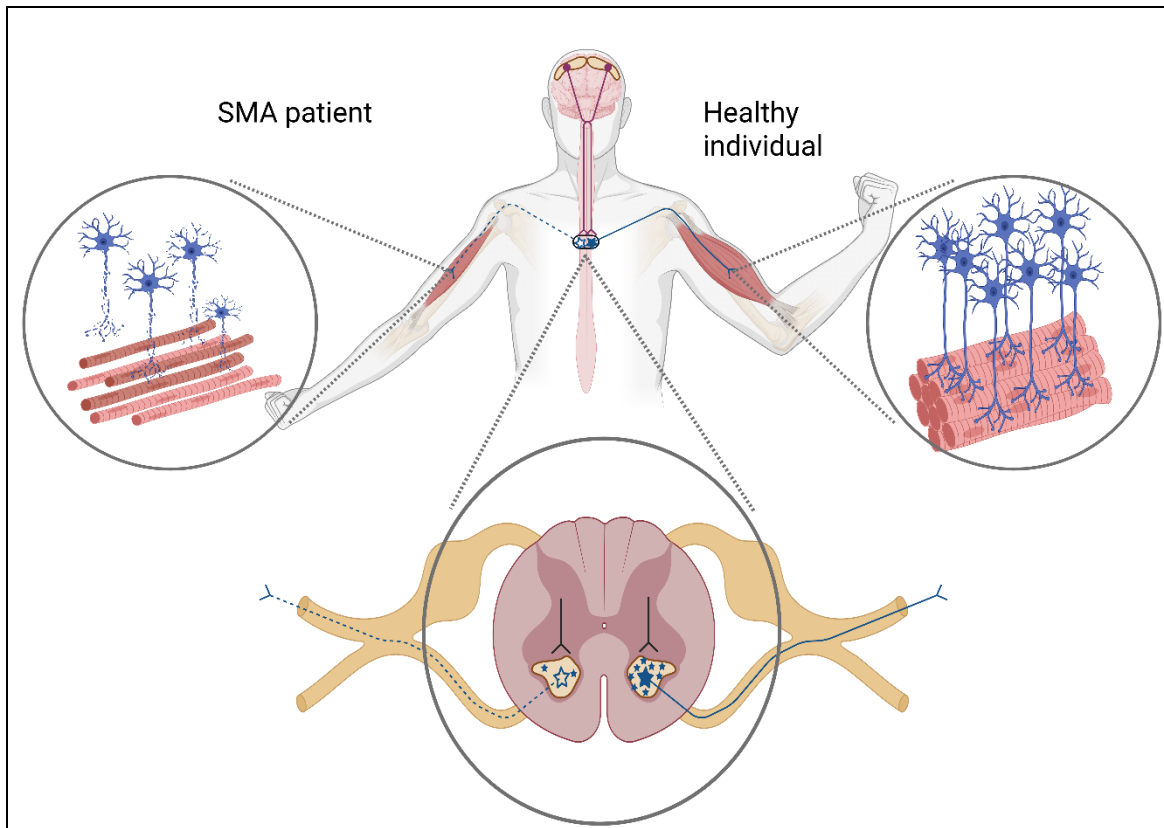


Figure 1.1. Pathophysiology of spinal muscular atrophy

Schematic illustration of spinal muscular atrophy (SMA) pathophysiology, highlighting neuromuscular differences between healthy individuals (right) and SMA patients (left).

The axons of the upper motor neurons (depicted in red) descend from the primary motor cortex in the brain to the anterior horn of the spinal cord, where they form synapses with lower motor neurons (depicted in blue). The central panel at the bottom illustrates a transversal section of the spinal cord, emphasising the abundance of motor neuron somas in healthy individuals (right), in contrast to the loss of motor neurons observed in this region in patients with SMA (left). The axons of these neurons extend through the spinal ganglion to the muscles they innervate, facilitating the maintenance of muscular tone in healthy individuals (upper panel, right). Conversely, in SMA patients, the loss and degeneration of motor neurons results in myofiber loss, degeneration and muscle atrophy/weakness (upper panel, left).

In postmortem examinations of infants who perished to SMA, quantitative analyses of neurons from the anterior horn of the spinal cord (i.e. LMNs) revealed a 73% reduction in neuronal count compared to healthy controls (Simic et al., 2000). Additionally, many of the surviving neurons displayed morphological changes, including swelling, peripheral displacement of the nucleus, and indicators of advanced degeneration, such as cytoplasmic vacuolisation. These morphological changes, in combination with specific methodologies for detecting apoptotic death, confirm that these neurons undergo apoptosis (Simic et al., 2000).

Notably, not all LMNs are equally affected in SMA, instead, specific pools of motor neurons show distinct vulnerability to degeneration. For instance, a study performed in $Smn^{-/-};SMN2$ and $Smn^{-/-};SMN2;\Delta 7$ severe SMA mouse models demonstrated that MNs innervating the transversus abdominis (TVA) muscles were more severely affected than MNs innervating lumbrical muscles (Murray et al., 2008), suggesting that MN vulnerability might be related with the innervation of anatomically distinct muscle targets. Additionally, another study revealed that alpha motor neurons within the spinal cord of a $Smn^{-/-};SMN2$ severe SMA mouse model were uniquely vulnerable to degeneration, while gamma motor neurons and other cholinergic populations were largely spared (Powis and Gillingwater, 2016). However, a later study in a $Smn^{-/-};SMN2$ severe SMA mouse model demonstrated that this vulnerability does not depend on gross morphological features, such as function subtype, nerve length, motor unit size or branching pattern (Thomson et al., 2012). Instead, researchers suggested that specific vulnerability may arise from subtle molecular distinction, such as different dependence on SMN related functions by different neuronal populations (See **1.3.The survival motor neuron protein**) (Tu et al., 2017) or increased bioenergetic demands (Boyd et al., 2017).

Other neuronal cell types have also demonstrated to be implicated in SMA pathology. For instance, a study that used human SMA spinal cord cells found an abnormal increase in the number of astrocytes, as well as signs of astrocyte activation and consequently elevated levels of proinflammatory cytokines (Rindt et al., 2015). Astrocytes are a crucial type of glial cells in the central nervous system (CNS) responsible for various critical functions, including maintaining

blood-brain barrier integrity, regulating neuron differentiation, supporting, nourishing, protecting, insulating, and repairing neurons (Cheng et al., 2019). Importantly, astrocyte activation has been found in nearly all neurodegenerative diseases (Rama Rao and Kielian, 2015), suggesting that astrocyte pathology might play a role in accelerating neurodegeneration in SMA.

The degeneration of MNs contributes to the observed defects at the levels of the neuromuscular junction (NMJ) in SMA. NMJs are specialised synapses that connect motor neurons and skeletal muscle fibres, thereby facilitating the transfer of electrical signals that initiates muscle contraction (Khalil, Marwaha and Bollu, 2025). Defects at the NMJ represent some of the earliest pathological changes in SMA. In prenatal and postnatal human samples, as well as SMA mouse models, changes in acetylcholine receptor clustering and abnormal presynaptic accumulation of vesicles without proper contact with muscle cells were identified (Kariya et al., 2008; Martínez-Hernández et al., 2013). Additionally, studies have shown that axons of SMA motor neurons exhibit massive accumulation of neurofilaments in the synaptic terminals, which is associated with lack of axonal sprouting and dramatic axonal degeneration (Rafii et al., 2002). All these defects contribute to NMJ immaturity and to the disruption of the establishment and maintenance of muscle innervation.

Motor neuron survival and skeletal muscle development are tightly interdependent, requiring continuous cell-cell contact. Histological and morphometric analysis from type I SMA fetuses demonstrated that SMA myotubes (i.e. cells that compose the muscle fibres), are smaller than those of healthy controls and present impaired myogenesis (i.e. fusion of myotubes that precedes muscle fibre formation) (Martínez-Hernández et al., 2009; Mutsaers et al., 2011). Additionally, abnormal cluster of nicotinic acetylcholine receptors that was associated with impaired NMJ maturation were also observed (Mutsaers et al., 2011). A later study using the *Smn*^{-/-};SMN2 severe SMA mice found evidence of myofiber degeneration and atrophy and that these alone were sufficient to trigger NMJ abnormalities, motor function impairment and premature death (Kim et al., 2020). These findings demonstrated that muscle atrophy in SMA is not only a consequence of motor neuron degeneration, but also an active contributor to SMA pathology.

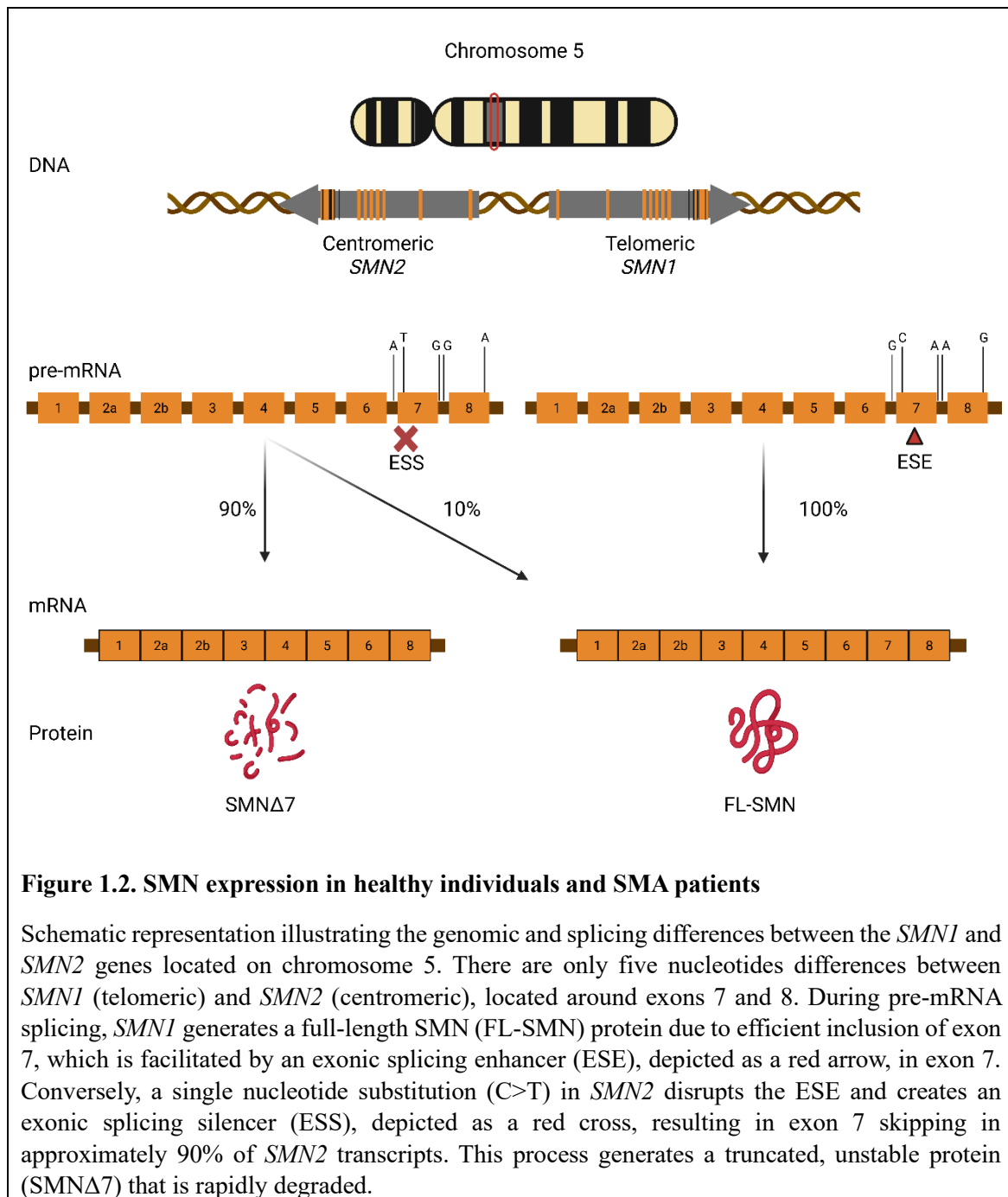
Notably, SMA is increasingly recognised as a multi-system disorder, affecting not only the neuromuscular system but also other organs such as the brain, heart, vasculature, bone, pancreas, liver, lung and intestine, particularly in severe cases (Hamilton and Gillingwater, 2013). The involvement of multiple organ systems in SMA may gain relevance in treated SMA patients, particularly those receiving intrathecal therapies that do not address peripheral tissues, underscoring the complexity of the disease and the need for a comprehensive approach to patient care, treatment strategies, and long-term prognosis.

1.1.2. Molecular genetics

In 1995, Lefebvre et al. identified the *survival motor neuron one (SMN1)* gene, located on chromosome 5q13, as the gene responsible for SMA (Lefebvre et al., 1995). The *SMN1* gene encompasses 27 kb (i.e. 27,000 base pairs) and contains 9 exons that encode a 294-amino acid protein, known as the survival motor neuron (SMN) protein (Chen et al., 1998; Lefebvre et al., 1995). Lefebvre et al., found that 93% of SMA patients lacked both copies of *SMN1*, while 5.6% of patients presented a mutated version of *SMN1* that lacked exon 7 in both gene copies. The remaining 1.3% of patients exhibited other intragenic mutations in one or both *SMN1* copies. Other studies demonstrated that SMA patients can carry several types of mutations within the *SMN1* gene, the majority of which affected exons 7 and 8, although other mutations have been reported in exons 1, 2a, 2b, 3, 4, 5 and 6, as well as introns 6 and 7 (Lefebvre et al., 1995). These mutations include large-scale deletions, nonsense mutations (nucleotide changes that introduce a premature stop codon), frameshift mutations (addition or loss of nucleotides that changes the gene's reading frame), missense mutations (nucleotide changes that alter the translation of one amino acid) and splice site mutations (nucleotide changes that disrupt normal splicing) (Wirth, 2000). Approximately 95% of all SMA cases are caused by deletions or mutations in the *SMN1* gene. The remaining 5% of patients present SMA-like clinical features but have no identifiable deletions or mutations in *SMN1* and are therefore classified as non-*SMN1*-related SMA patients (Burr and Reddivari, 2023). Currently, there are more than 20 genes that have been associated

with non-*SMN1*-related SMA, including *UBE1* (associated with X-linked infantile SMA type 2), *SCO2* (associated with SMA due to mitochondrial dysfunction), or *IGHMBP2* (associated with SMA with respiratory distress) (Farrar and Kiernan, 2014). This thesis focuses exclusively on *SMN1*-related SMA.

The 5q region, where the *SMN1* gene is located, is particularly unstable and contains multiple duplications and repetitive sequences. The arrangement of these repetitive gene motifs is polymorphic between individuals, which means that different individuals have different patterns or numbers of these repeated gene sequences, which some researchers associate with the high incidence and worldwide distribution of SMA (Theodosiou et al., 1994; Crawford, 1996). Notably, the *SMN1* gene is part of a 500 kb inverted duplication region within the 5q13 chromosome, which means that humans possess two nearly identical copies of the *survival motor neuron* gene: a telomeric copy, designated as *SMN1*, and a centromeric copy, designated as *SMN2* (Lefebvre et al., 1995). There are only 5 single nucleotide differences between *SMN1* and *SMN2* genes, localised in intron 6 (G-to-A substitution), exon 7 (C-to-T substitution), intron 7 (A-to-G substitution), intron 7 (another A-to-G substitution 114 bp upstream of the previous one) and exon 8 (G-to-A substitution) (Lorson et al., 1999) (**Figure 1.2**).



The functional divergence between *SMN1* and *SMN2* stems from the C-to-T substitution located at the position +6 of exon 7. Despite being a translationally silent mutation that does not alter the amino acid sequence of the protein, this mutation alters the pre-mRNA splicing pattern of *SMN1* by disrupting the proper functioning of a nearby exon splicing enhancer (ESE) situated at the centre of exon 7 (Lorson et al., 1999; Monani et al., 1999). ESEs are sequences within pre-mRNA molecules that are required for the efficient recognition of exons by the splicing machinery, facilitating the incorporation of the exon in the mature mRNA, which is later translated into a protein (Blencowe, 2000). In *SMN1*, the cytosine (C+6) creates an efficient ESE that facilitates the binding of splicing activators. Conversely, in *SMN2* the thymine (T+6) disrupts this ESE and instead, creates an exonic splicing silencer (ESS), which enhances the binding of inhibitory splicing factors that promote the exclusion of exon 7 from the mature mRNA (Kashima and Manley, 2003). These mature mRNA transcripts lacking exon 7 are translated into a truncated SMN isoform, known as SMN Δ 7, that is highly unstable and is marked for degradation by the ubiquitin proteasome system (UPS) (Gray et al., 2018). Consequently, the levels of functional SMN protein produced by *SMN2* are significantly lower than those produced by *SMN1* (Lorson et al., 1999; Monani et al., 1999). This finding was pivotal in understanding why *SMN1*, but not *SMN2*, is the primary gene responsible for determining SMA.

Although *SMN1* is the gene responsible for determining SMA, there is a strong correlation between the number of *SMN2* copies and the severity of the disease. This correlation arises because, as calculated using the blood data of patients with SMA, *SMN2* produces about 10% to 20% full-length *SMN* mRNA (Crawford et al., 2012; Wadman et al., 2016). Consequently, a higher *SMN2* copy number is associated with increased levels of SMN protein in patients, thereby reducing disease severity. A cohort analysis conducted in 2018, which included 2834 SMA patients worldwide, indicated that the majority of type I SMA patients possess between 2 and 3 *SMN2* copies (69% and 23%, respectively), the majority of type II patients have between 2 and 3 copies (75% and 17%, respectively), while the majority of type III SMA patients have between 3 and 4 copies (47% and 46%, respectively) (Calucho et al., 2018). Moreover, several studies have

compared the levels of full-length SMN protein in patients with varying severity and found that while type I SMA patients exhibit a 60% reduction in total SMN protein levels compared to controls, type II SMA patients show a 44.4% reduction in functional SMN protein levels, and type III SMA patients demonstrate a 41.7% reduction (Crawford et al., 2012). Altogether, these findings led to a shift in focus from gene presence to protein expression, highlighting that the disease severity is largely determined by how much full-length SMN protein a patient can produce.

1.1.3. The survival motor neuron protein

The full-length human SMN protein (hereafter referred as SMN) is a 294-polypeptide translated from full-length SMN mRNA. The translation stop codon occurs within exon 7, leaving exon 8 untranslated. SMN adopts a three-dimensional structure comprising distinct functional domains essential for its diverse cellular roles. At its N-terminus, a lysine-rich domain mediates interactions with RNA molecules. The central Tudor domain facilitates protein-protein interactions crucial for assembling the cellular splicing machinery. Adjacent to this, a proline-rich domain engages proteins involved in actin dynamics, influencing cytoskeletal organisation. Finally, the YG box at the C-terminal end is vital for SMN oligomerisation, a property essential for the protein's stability and activity, and notably impaired in the truncated SMN Δ 7 variant (Singh et al., 2017).

In humans, the SMN protein is ubiquitously expressed throughout the body and is localised in both the cytoplasm and nucleus of cells. Despite its widespread expression, the levels of SMN protein vary significantly across different tissues. Post-mortem analyses comparing tissues from healthy individuals and patients with type I SMA revealed that SMN is highly expressed in the brain, spinal cord, and liver of healthy individuals, whereas skeletal and cardiac muscles exhibited a more moderate expression (Coovert et al., 1997). Additionally, the same study examined those tissues from type I SMA patients and found that the SMN protein was moderately reduced in muscle tissue but profoundly decreased (~100-fold) in the spinal cord, aligning with the selective

vulnerability of MNs observed in SMA pathology (Coover et al., 1997). More recently, Ramos et al., 2019 demonstrated that SMN expression also varies greatly with developmental stage, showing a pronounced physiological decline during the perinatal period and low, stable levels after early infancy in both healthy and SMA tissues. These findings highlight the importance of tissue specificity and developmental timing in determining therapeutic efficacy.

The SMN protein is involved in several cellular processes critical for maintaining protein homeostasis, including the assembly of small nuclear ribonucleoproteins (snRNPs) essential for pre-mRNA splicing (Gubitz, Feng and Dreyfuss, 2004), RNA trafficking (Rossoll et al., 2003; Fallini et al., 2011), translation (Bernabò et al., 2017a; Fallini et al., 2016) and protein degradation pathways (Wishart et al., 2014). Moreover, SMN indirectly affects other critical cellular processes, such as endocytosis (Dimitriadi et al., 2016), autophagy (Rashid & Dimitriadi, 2024a), and mitochondrial function (James et al., 2021). These indirect roles have been identified through observations that demonstrate that SMN reduction disrupts these processes, although precise mechanisms by which SMN deficiency causes such disruptions are not yet fully elucidated (Chaytow et al., 2018; Singh et al., 2017; Wirth, 2021).

The ubiquitous expression of SMN and its involvement in numerous essential cellular processes underscore its critical biological significance. Nonetheless, some researchers have suggested that SMN has MN-specific functions, such as axonal mRNA transport and local translation, which are crucial for proper MN development and function (Monani, 2005; Chaytow et al., 2018; Wirth, 2021). The disruption of these functions disproportionately affects motor neurons, contributing to their increased vulnerability to degeneration, highlighting why specific SMN-dependent processes become particularly relevant in the context of SMA.

1.1.3.1. Ribonucleoprotein assembly

The SMN protein plays an essential role in the biogenesis of small nuclear ribonucleoproteins (snRNPs), which are critical components of the cellular splicing machinery that catalyse the excision of introns and the ligation of exons to form mature mRNA (Zhang et al., 2013). The

critical role of SMN in snRNP biogenesis is underscored by findings that link decreased snRNP availability directly with increased disease severity in SMA (Gabanella et al., 2007).

Each snRNPs consist of a uridylic acid-rich small nuclear RNA (U1, U2, U4, U5 and U6 snRNAs) and Sm proteins that are post-transcriptionally modified by methylation and then imported to the nucleus, where they assist with mRNA splicing (Patel and Bellini, 2008). The critical role of SMN in snRNP biogenesis involves the facilitation of snRNPs assembly and transport to the nucleus. Briefly, SMN assembles into a multiprotein complex in the cytoplasm, known as the SMN complex, constituted by SMN and eight other proteins, known as Gemin 2-8 and Unrip (Gubitz, Feng and Dreyfuss, 2004). The SMN complex facilitates the binding of Sm proteins onto small nuclear RNAs (snRNAs) (Gubitz, Feng and Dreyfuss, 2004). Following this, snRNAs are modified through methylation, enabling their transport into the nucleus via interaction with nuclear transport proteins (Friesen et al., 2001; Narayanan et al., 2004; Henriksson and Farnebo, 2015). Within the nucleus, snRNPs are targeted to specialised structures termed Cajal bodies or Gems, where they dissociate from the SMN complex and undergo final maturation steps (Henriksson and Farnebo, 2015).

SMN has been directly involved in the biogenesis of U1 and U7 snRNPs (Pillai et al., 2003; So et al., 2016). SMN depletion causes widespread splicing perturbations that affect the transcription of hundreds of genes in different tissues, including brain, spinal cord, and skeletal muscle among others (Zhang et al., 2008). Importantly, some of these genes play critical roles in MN function. For example, stasimon and neuroxin2a were found strongly downregulated and displayed changes in alternative splicing patterns in fruit fly, zebrafish and mouse models of SMA, where they play an essential role in synaptic transmission (Lotti et al., 2012; See et al., 2014). These findings could elucidate the relationship between the role of SMN in snRNPs biogenesis and increased motor neuron vulnerability in SMA pathology.

1.1.3.2. RNA trafficking and cytoskeleton dynamics

SMN plays a crucial role in RNA trafficking, a process of particular significance in MNs, which, due to their long and complex axonal projections, require efficient intracellular transport mechanisms for metabolic and functional maintenance (Wirth, 2021). Research indicates that the depletion of SMN leads to significant reduction in the localisation of mRNA transcripts along MN axons (Rossoll et al., 2003; Fallini et al., 2011). Specifically, a study conducted in SMN-deficient MNs found that the location of β -actin mRNA within axons was particularly decreased, despite no alterations in overall protein expression levels (Rossoll et al., 2003). Notably, β -actin plays a role in axon elongation and maturation and contributes to the dynamic nature of the axonal cytoskeleton (Moradi et al., 2017). Additionally, SMN deficiency has been demonstrated to impair mitochondrial transport, thereby reducing mitochondrial presence in MN axons, which rely on mitochondrial ATP for proper functioning (Xu et al., 2016). These findings highlight the critical role of SMN in maintaining synaptic transmission at the NMJs (Fallini et al., 2011, 2013, 2016).

SMN facilitates RNA transport by interacting with various RNA-binding proteins (RBPs) through its Tudor domain (Fallini et al., 2011). Subsequently RBPs interact with specific mRNA transcripts and cytoskeletal structures, facilitating their transport through the axon (Chaytow et al., 2018). Among the various RBPs that interact with SMN, IMP1 and HuD are particularly noteworthy, as they have been identified to bind mRNAs essential for axonal growth, such as β -actin and GAP-43 (Fallini et al., 2013). Furthermore, SMN has been shown to interact with the coat protein I (COPI), a family of vesicle proteins involved in the intracellular transport of proteins between the endoplasmic reticulum (ER) and Golgi apparatus within cells (Beck et al., 2009). In spinal cord MNs, SMN facilitates the interaction between COPI and β -actin mRNA, thereby aiding its transport across the axon (Peter et al., 2011).

SMN has also demonstrated to play a role in regulating cytoskeleton dynamics. In neurons, the maintenance of cytoskeleton dynamics is crucial for axon formation and axonal transport (Kevenaar and Hoogenraad, 2015). The extensive evidence of axonal growth defects in neuronal cultures with depleted SMN expression (Rafii et al., 2002), as well as evidence of direct

interaction between SMN and components of the cytoskeleton, such as actin proteins (Peter et al., 2011; Fallini et al., 2013) and profilin (Nölle et al., 2011), suggests that SMN may contribute to the maintenance of cytoskeleton dynamics within neurons. However, it remains unclear whether this is an SMN-independent role or if it is associated with its involvement in mRNA trafficking (Chaytow et al., 2018).

1.1.3.4. Regulation of local translation

SMN has been implicated in the spatial regulation of protein synthesis, a critical function in neurons where local translation at distal axonal sites is necessary for axonal integrity and synaptic function (Chaytow et al., 2018). Comparative analyses of transcriptomes and translomes in SMA models revealed extensive translation defects, notably impacting ribosome biogenesis (Bernabò et al., 2017a). Notably, studies in SMN-deficient neurons demonstrated that somatic translation remains largely unaffected, whereas axonal translation is significantly impaired, underscoring a specialised role for SMN in the spatial control of translation (Fallini et al., 2016).

SMN's role in local translation is believed to be mediated through its interactions with RBPs such as HuD and IMP1, which regulate the localisation of mRNAs involved in axon growth (Fallini et al., 2016). Furthermore, biochemical assays have demonstrated that SMN associates with polyribosomes, directly influencing translation efficiency in a dose-dependent manner (Sanchez et al., 2013).

1.1.3.5. Regulation of the ubiquitin pathway

SMN also contributes to cellular protein homeostasis through its interactions with components of the ubiquitin-proteasome system (UPS). SMN itself undergoes ubiquitination and subsequent proteasomal degradation via direct interaction with UBA1, an E1 ubiquitin-activating enzyme, and Itch, a type of E3 ubiquitin ligase (Han et al., 2012). Conversely, interactions with deubiquitinating enzymes, such as UCHL1, has shown to increase SMN stability (Hsu et al.,

2010). Interestingly, SMN reduction led to the reduction of UBA1, which subsequently affected the ubiquitination of other cellular proteins (Wishart et al., 2014), reflecting the broader impact of SMN depletion on cellular protein homeostasis beyond its own degradation.

1.1.3.6. Regulation of endocytosis

SMN plays a crucial role in regulating endocytosis, a cellular process vital for synaptic vesicle recycling and neurotransmission, particularly at the NMJ (Chaytow et al., 2018; Wirth, 2021). Research has demonstrated that depletion of SMN results in the disruption of endocytic function in various SMA models. For example, in a severe *C. elegans* SMA model, reduction of SMN-1 led to the altered localisation of presynaptic endocytic proteins in motor neurons and a reduction of presynaptic vesicles near the presynaptic region, indicating impaired endosomal trafficking in SMA (Dimitriadi et al., 2016). These findings were corroborated in a severe SMA mouse model, where SMN depletion was associated with reduced endocytosis (Hosseinibarkooie et al., 2016). Notably, these endocytic defects were linked to the disruption of the NMJ and impaired synaptic transmission (Dimitriadi et al., 2016; Hosseinibarkooie et al., 2016). The role of SMN in endocytosis could be mediated through interactions with cytoskeletal regulators such as Plastin 3 (PLS3) and Neurocalcin Delta (NCALD), which will be further elaborated in following sections (See 1.4. Genetic modifiers).

1.1.3.7. Modulation of autophagy

SMN regulates autophagy, a conserved process within cells that breaks down and recycles damaged components through lysosomal degradation. SMN deficiency has been associated with increased autophagosome formation across different SMA models, suggesting a blockage in lysosomal degradation (Rashid & Dimitriadi, 2024a). However, it is not yet elucidated whether increased autophagosome formation is protective or deleterious in SMA and further research is required to fully elucidate the direct relationship between SMN and the autophagy pathway. (Rashid & Dimitriadi, 2024a).

1.1.3.8. Mitochondrial function

Emerging evidence indicates that SMN plays a significant role in mitochondrial trafficking, function and homeostasis, as demonstrated by the significant mitochondrial dysfunction, increased oxidative stress, impaired mitochondrial transport, among others, observed after SMN depletion (See 4.2.Mechanisms triggering oxidative stress in). Although SMN does not localise to mitochondria directly (Acsadi et al., 2009), its effects on mitochondrial function are thought to be indirect, possibly through affecting the splicing, translation, or mRNA transport of genes fundamental to mitochondrial homeostasis (James et al., 2021).

1.1.4. Genetic modifiers

Although it is well-established that homozygous deletions or mutations within the *SMN1* gene lead to SMA, there are rare, documented cases of discordant families where siblings of SMA patients are unaffected despite identical homozygous absence of *SMN1* (Cobben et al., 1995; Hahnen et al., 1995; Wang et al., 1996). This observation indicates that SMA is influenced by additional factors that modify *SMN1* activity or expression, known as protective modifiers. Since then, several SMA protective modifiers in humans have been reported (Lamar and McNally, 2014). From those, *SMN2* constitutes the clearest example of a genetic modifier in SMA. As discussed in previous sections, the number of *SMN2* copies inversely correlates with SMA severity, due to its limited production of functional SMN protein. This relationship has been corroborated in a severe SMA mouse model with homozygous deletion of the endogenous *Smn* gene, where the expression of 8 *SMN2* copies completely rescued the SMA mice-associated phenotypes (Monani et al., 2000).

While numerous genetic modifiers have been identified (Lamar and McNally, 2014), each exhibiting distinct mechanisms of action, this section will focus on two genetic modifiers found in SMA discordant families that illustrate either positive protective effect (i.e. increased gene

expression or presence of specific gene variants confers protection against SMA), or negative protective effect (i.e. reduced gene expression or complete absence of the gene confers protection against SMA).

In 2008, a study identified six SMA discordant families, where female siblings of SMA patients were unaffected by the disease despite carrying the same *SMN1* and *SMN2* alleles than their affected siblings (Oprea et al., 2008). Researchers selected one of these discordant families and conducted a transcriptome-wide differential expression analysis, which included two males with SMA and two females that were fully asymptomatic. The analysis revealed 18 transcripts that were differentially expressed between affected and unaffected individuals (Oprea et al., 2008). Subsequent examination of the expression of those genes in the other five discordant families indicated that only one gene was consistently differentially expressed between affected and unaffected individuals. This gene, identified as *Plastin 3 (PLS3)*, was significantly overexpressed in all unaffected females with homozygous *SMN1* deletion, whereas all related males with SMA exhibited strong downregulation (Oprea et al., 2008). Additionally, the study included unrelated type I, II, and III patients and found that some individuals also expressed elevated *PLS3* levels, which was associated with decreased severity only in female patients (Oprea et al., 2008; Yanyan et al., 2013), demonstrating that *PLS3* functions as a gender-specific protective modifier in SMA.

PLS3 is located on the X chromosome and encodes a calcium-sensitive actin-binding protein, that is predominantly expressed in the spinal cord (Oprea et al., 2008). *PLS3* plays a critical role in organising and stabilising the actin cytoskeleton by facilitating the cross-linking of actin filaments into bundles, ensuring proper actin dynamics (Delanote, Vandekerckhove and Gettemans, 2005). In neurons, this process is critical for axon growth and branching, as well as for vesicle trafficking and endocytosis (Dent & Gertler, 2003; Engqvist-Goldstein & Drubin, 2003). In severe SMA mouse models, overexpression of *PLS3* restored several defects depending on actin dynamics, such as reduced axon length and outgrowth, thereby enhancing neuronal connectivity at the NMJ (Oprea et al., 2008; Ackermann et al., 2013). Furthermore, in a severe *C. elegans* SMA model,

PLS3 overexpression improved endocytic function and mitigated the neuromuscular defects associated with SMN-1 depletion (Walsh et al., 2020).

Another SMA modifier was identified in a USA discordant family, where from seven individuals carrying homozygous deletions in *SMN1*, two were affected by SMA type I, whereas five were completely asymptomatic (Riessland et al., 2017). While the two SMA type I patients expressed 2 *SMN2* copies, unaffected individuals carried 4 *SMN2* copies (Riessland et al., 2017), which is usually associated with type III SMA (Calucho et al., 2018). Researchers performed a genome-wide linkage analysis that included 14 family members, with the aim to identify chromosomal regions that may contain genetic variations that explain the SMA differential phenotypes. This analysis yielded 8 regions of interest (Riessland et al., 2017). Additionally, in a transcriptome-wide differential expression analysis, researchers found 17 transcripts that were significantly differentially expressed in asymptomatic individuals. From the 17 transcripts that were differentially expressed, only one of them localised to one of the eight regions of interest, making it a highly likely SMA genetic modifier (Riessland et al., 2017). This gene was significantly downregulated in asymptomatic patients and was identified as the neuronal calcium sensor *Neurocalcin delta* (*NCALD*) (Riessland et al., 2017).

NCALD encodes a calcium (Ca^{2+})-dependent molecular sensor highly abundant in axonal growth cones of motor neurons (Iino, Kobayashi and Hidaka, 1998; Braunewell and Gundelfinger, 1999). Upon binding to Ca^{2+} , *NCALD* undergoes conformational changes that facilitate its attachment to the plasma membrane when intracellular Ca^{2+} concentrations are elevated, and its release into the cytoplasm when Ca^{2+} levels are decreased (Hoareau et al., 2019). In the cytoplasm, *NCALD* directly interacts with clathrin molecules, thereby interfering with their proper trafficking and localisation to endocytic sites at the neuronal membrane (Riessland et al., 2017). Importantly, clathrin is a crucial protein involved in the coating of endocytic vesicles, which allow synaptic vesicle recycling and neurotransmission (Slepnev and De Camilli, 2000). In the pathological context of SMA, synaptic Ca^{2+} influx is significantly reduced (Jablonka et al., 2007), resulting in an increased proportion of cytoplasmic *NCALD* that binds to clathrin, thereby impairing clathrin-

mediated formation of endocytic vesicles. Consequently, neurotransmitter recycling at the synapse is disrupted, leading to impaired synaptic transmission (Riessland et al., 2017). However, the downregulation of NCALD in SMA diminishes its inhibitory interaction with clathrin, facilitating clathrin redistribution to the plasma membrane and restoring endocytic vesicle formation. This mechanism elucidates why the reduction of NCALD levels effectively rescued endocytic and synaptic deficits observed in SMA models (Riessland et al., 2017). These findings were further validated in four well-characterised SMA models, including *C. elegans*, zebrafish and intermediate and severe SMA mice. In all cases, *NCALD* downregulation ameliorated the neuromuscular dysfunction exhibited in these SMA models (Riessland et al., 2017). Additionally, NCALD downregulation restored synaptic maturation at the NMJ and the muscle response in severe and intermediate SMA mouse models (Riessland et al., 2017), positioning NCALD a strong SMA modifier candidate.

The discovery of protective modifiers not only enhanced our understanding of SMA pathogenesis, but also opened new avenues for developing targeted interventions that could potentially ameliorate the devastating effects of this neurodegenerative disorder.

1.1.5. Approved therapies

Spinal muscular atrophy represents one of the most common genetic causes of death in infants (Wojcik et al., 2019), however, advancements in SMA therapeutics are significantly shifting the disease's natural progression. Currently, three treatments have been approved for SMA: Nusinersen (Spinraza), Risdiplam (Evrysdi), and Onasemnogene abeparvovec (Zolgensma).

Nusinersen, commercially known as Spinraza, is an antisense oligonucleotide (ASO) drug that rectifies the splicing defects of *SMN2* pre-mRNA transcripts (Finkel et al., 2017). Due to the inability of ASOs to cross the intact blood-barrier, this drug is injected directly into the spinal fluid, achieving elevated concentrations in the spinal cord over a period of four months (Biliouris et al., 2018), at which point the next dose is administered. Notably, its distribution to peripheral

tissues has been demonstrated to be limited (Biliouris et al., 2018). Once within cells, Nusinersen rectify the splicing defects in *SMN2* pre-mRNA by binding to an intronic splicing silencer (ISS) located in the intron 7 (position 10-27) of *SMN2*. Some researchers believe that this interaction directly inhibits the binding of the splicing repressor hnRNP-A1, which promotes exon 7 exclusion (Singh et al., 2011). Additionally, others researchers suggest that Nusinersen's binding to *SMN2* pre-mRNA modifies the structure of the pre-mRNA molecule, disrupting inhibitory structures such as the Terminal Stem-Loop 3 (TSL3) and the Internal Stem-Loop 1 (ISTL1), which normally interfere with exon 7 inclusion, thereby increasing the accessibility of the 5' splice site of exon 7 and facilitating the recruitment of U1 snRNP to exon 7, which promotes exon 7 inclusion (Singh et al., 2015). In either case, increased SMN protein levels have been observed in mice and non-human primates following Nusinersen treatment (Rigo et al., 2014).

Nusinersen effects can vary significantly depending on the severity of the disease and the stage at which the treatment is administered. Notably, a study including 122 SMA infants showed that patients who received the treatment were more likely to be alive and show improvements in motor function than in the control group (Finkel et al., 2017). Additionally, another clinical study including patients with type II and III SMA reported that those who received Nusinersen had also significant and clinically meaningful improvement in their motor function (Mercuri et al., 2018). Notably, when Nusinersen was administered to pre-symptomatic infants with type I or II SMA, all participants remained alive without requiring constant ventilation, and many achieved significant motor milestones including independent walking (De Vivo et al., 2019).

Risdiplam, commercially known as Evrysdi, is a small-molecule compound developed to treat SMA by correcting the splicing of *SMN2* pre-mRNA, thereby increasing the production of full-length SMN protein (Sivaramakrishnan et al., 2017). Risdiplam is administered orally in a daily basis and has a broad distribution throughout the body, including both central and peripheral tissues (Sturm et al., 2019). Risdiplam facilitates the inclusion of exon 7 in mRNA transcripts from *SMN2* by two different mechanisms. First, it facilitates the recognition of exon 7 by the splicing machinery through the binding to the terminal stem-loop 2 (TSL2) structure at the 5'

splice site of exon 7, facilitating its interaction with snRNPs (Sivaramakrishnan et al., 2017). Additionally, Risdiplam alters the stem-loop structure (TSL1) around the exonic splicing enhancer 2 (ESE2) region of exon 7, preventing the binding of hnRNPG, a splicing repressor that typically inhibits exon 7 inclusion (Sivaramakrishnan et al., 2017). In either case, Risdiplam promotes the inclusion of exon 7 in *SMN2* mRNA, increasing the levels of full-length SMN transcripts.

Risdiplam has shown significant clinical benefits for SMA patients across various age groups and disease severity. Clinical studies have demonstrated that type I, II and III SMA patients achieved notable motor milestones after 12 months of treatment (Baranello et al., 2021; Servais et al., 2023). Significantly, 29% of type I SMA patients were able to sit independently at the end of the study, a milestone that is rarely achieved without treatment (Baranello et al., 2021). Notably, clinical studies in pre-symptomatic patients show that early treatment is associated with better outcomes, and that improvements in motor function are sustained or increase over time with continued use (Finkel et al., 2022).

Onasemnogene abeparvovec (commercially known as Zolgensma), is a revolutionary gene replacement medicine approved for the treatment of SMA. The European Medicine Agency states that Zolgensma is indicated for the treatment of patients with bi-allelic mutation in *SMN1* and a clinical diagnosis of SMA type 1, or bi-allelic mutations in *SMN1* and up to 3 copies of *SMN2*. Zolgensma utilises a non-replicating, self-complementary adeno-associated vector 9 (AAV9) where the viral DNA is replaced by a functional copy of the human *SMN1* gene (Dominguez et al., 2011). The self-complementary feature of the vector combined with a hybrid cytomegalovirus enhancer–chicken beta-actin promoter enables rapid and sustained expression of SMN. AAV9 can cross the blood-brain barrier, allowing the delivery of the *SMN1* gene through the body, reaching motor neurons as well as other peripheral tissues, enabling the production of full-length, functional SMN protein (Dominguez et al., 2011).

The first clinical trial with Zolgensma found that all 15 SMA type I patients included in the study survived at 20 months without requiring permanent mechanical ventilation (Mendell et al., 2017),

in contrast with only 8% survival at the same age in previously reported studies with SMA patient that did not received treatment (Finkel et al., 2014). Other clinical trials have shown that patients treated with Zolgensma demonstrated improved swallowing and speaking abilities, with reduced need for pulmonary and nutritional support. Additionally, patients also achieved significant milestones such as sitting unassisted rolling over, and in some cases, even walking independently (Al-Zaidy et al., 2019; Day et al., 2021). The most significant side effect of Zolgensma is the potential for liver toxicity. A clinical study including 325 patients demonstrated that 90% of patients presented elevated liver function enzymes, and more than 40% needed medications to treat hepatotoxicity (Chand et al., 2021); its early administration (less than 8 months of age) significantly reduced the risk of hepatic complications (Waldrop et al., 2020).

While SMN-targeted therapies have demonstrated significant clinical benefits, data regarding their long-term efficacy and safety remain limited (Varone, Esposito and Bitetti, 2025). Additionally, clinical studies indicate that the effectiveness of these treatments is highly contingent upon the timing of intervention, with earlier administration producing more favourable outcomes (De Vivo et al., 2019; Waldrop et al., 2020; Finkel et al., 2022). Importantly, once motor neuron degeneration has advanced, SMN restoration alone is inadequate to reverse certain pathological changes, suggesting that some disease mechanisms become irreversible over time (Hensel, Kubinski and Claus, 2020). This underscores the necessity for comprehensive newborn genetic screenings to identify genetic mutations that cause SMA before the onset of symptoms, thereby enhancing the response to treatments (Hensel, Kubinski and Claus, 2020). Additionally, this situation leaves a significant number of patients with suboptimal responses to these therapies, who may require additional therapies (combinatorial therapy approach) targeting the remaining symptoms, which include respiratory issues, feeding difficulties, loss of mobility, communication impairments, and distress, among others (Cruz et al., 2018). To address these pathologies, researchers are developing SMN-independent therapies aimed at modifying altered pathways downstream of SMN deficiency, such as the Rho kinase (ROCK), and the extracellular regulated kinase (ERK) (Hensel et al., 2014, 2017). However, the application of combinatorial therapies in

SMA is still under investigation and must be approached with caution due to the potential risks and complexities associated with combining treatments (Proud et al., 2023).

1.2. Spinal muscular atrophy models

Several experimental strategies, ranging from *in vitro* cell cultures to *in vivo* animal systems, have been developed to investigate how depletion of the SMN protein gives rise to SMA. This section provides a brief description of different strategies employed to study SMA, with special emphasis on the suitability of *C. elegans* as an animal model for investigating the disease.

1.2.1. Cell-culture

Human *in vitro* systems are attractive because they eliminate the interspecies differences in SMN processing. Earlier SMA cell culture studies relied on immortal HeLa cells (Wan et al., 2008), skin-derived fibroblasts from patients (Köstel, Bora-Tatar and Erdem-Yurter, 2012), and murine NSC-34 motor neuron cultures (Acsadi et al., 2009), where SMN was depleted by DNA- or RNA-mediated knockdown. However, these systems lack either authentic lower-motor neuron physiology or the patient's native genetic context, limiting their translational relevance. These limitations have been overcome with the emergence of pluripotent stem cell technologies, most notably induced pluripotent stem cells (iPSC) (Ng and Rubin, 2017). More specifically, iPSCs are immortal, can be generated from routine skin or blood samples, and retain the donor's precise *SMN1/SMN2* genotype, capturing the full clinical spectrum of SMA, making iPSCs a powerful tool for modelling SMA and studying relevant disease-mechanisms *in vitro* (Corti et al., 2012; Ebert et al., 2008; Liu et al., 2015). Additionally, they differentiate efficiently into spinal motor neurons, astrocytes, skeletal muscle fibres, and other lineages and therefore, iPSC-based models permit researchers to differentiate the effect of SMN disease mechanism in different cell types (Ng and Rubin, 2017).

1.2.2. Mice

Mouse models constitute an invaluable tool for understanding SMA pathogenesis and developing potential treatments. Unlike humans, mice possess a single survival motor neuron gene, termed *Smn*. The mouse *Smn* gene encodes an SMN protein with approximately 83% amino acid identity to human SMN. Homozygous deletion of *Smn* in mice (*Smn*^{-/-}) results in embryonic lethality (Schrack et al., 1997), confirming the conserved essential role of SMN in cell survival across species. Similar to humans, SMA severity in mice directly correlates with SMN protein levels. Heterozygous *Smn*^{+/-} mice exhibit a 46% reduction in the SMN protein within the spinal cord. Yet, at one year old, *Smn*^{+/-} animals do not show signs of muscle weakness, and display either mild lumbar spinal motor neuron loss (Jablonka et al., 2000; Simon et al., 2010) or no detectable degeneration (Bowerman et al., 2014).

Researchers have employed different genetic strategies to modulate the levels of full-length SMN protein, generating various SMA mouse models that display different severity. For example, the severe Taiwanese SMA mouse model (*Smn*^{-/-}*SMN2*^{+/+}) was generated by inserting a genomic fragment containing the human *SMN2* gene into an *Smn*-null background (Hsieh-Li et al., 2000). Another severe SMA model, the SMNΔ7, was developed by introducing a transgene encoding the truncated SMNΔ7 protein into the Taiwanese model, producing *Smn*^{-/-};*SMN2*^{+/+};*SMNΔ7*^{+/+} animals (Le et al., 2005). The main difference between the Taiwanese and the SMNΔ7 mouse models is that while *SMN2* gives rise to both full-length SMN and predominantly exon 7-skipped SMNΔ7 protein, the SMNΔ7 transgene produces only the truncated isoform. To model SMA of intermediate severity, the endogenous *Smn* gene was modified with point mutations in exon 7, generating the *Smn2B* allele, which was then introduced into the *Smn*-null background. The *Smn2B* allele promotes exon 7 skipping, resulting in only 15% expression of full-length SMN protein and increased levels of SMNΔ7 isoform.

As with any model system, findings in SMA models should be interpreted within the context of differences in genetic background, and specific individual responses. Nonetheless, the availability of SMA mouse models with varying degrees of severity continues to provide valuable insights

into disease mechanisms and therapeutic efficacy, complementing data obtained from other model organisms and human studies.

1.2.3. Zebrafish

Zebrafish constitute a useful animal model for investigating neurodegenerative diseases, such as SMA, due to their well-defined motor neuron circuits and optical transparency during larval stages (Bandmann and Burton, 2010). Zebrafish have an ortholog of the human *SMN1* gene termed *Smn*, which render it as a useful model to study the impact of SMN reduction on motor neuron development *in vivo* (McWhorter et al., 2003). Different strategies have been utilised to mimic SMA in zebrafish.

Early SMA studies were performed by knocking down the levels of the endogenous SMN protein by injecting antisense morpholino oligonucleotides (MO) in embryos. MO are designed to bind complementary sequences of the target mRNA, inhibiting its translation (Nasevicius and Ekker, 2000). In zebrafish, higher doses of SMN mRNA-targeted MO correlated with lower SMN protein expression, which was associated with increased embryonic lethality, and defects in motor axon development, demonstrating the essential role that *Smn* plays on early development (McWhorter et al., 2003).

Additionally, transgenic SMA zebrafish models have been developed by introducing various genetic mutations on their endogenous *Smn* gene, allowing the evaluation of phenotypes associated with later stages of SMA. For example, the transgenic alleles *smnY262stop* and *smnL265stop* introduced an anticipated stop codon at exon 6 or exon 7, respectively, resulting in a truncated SMN protein that gets rapidly degraded. The presence of maternal *Smn* contribution allow those mutants to survive an average of 12 days, which allowed researchers to associate SMN depletion with a decrease in the synaptic vesicle protein SV2 at the NMJ (Boon et al., 2009).

Additionally, a more recent study generated an intermediate zebrafish SMA model called *smnA6T^{ind27}*, which introduced an amino acid substitution in exon 7 of zebrafish *Smn* mimicking

human *SMN2*. The *smnA6T^{ind27}* mutants presented with normal SMN protein levels in early developmental stages but showed a gradual decline in SMN as animals developed into juvenile stages. Notably, as SMN protein levels decrease, by day 21 motor neurons and NMJ formed initially progressively degenerate, until mutants eventually die at 39 days post fertilization (Tay et al., 2021).

The zebrafish models offer different levels of SMN deficiency and disease severity, providing complementary platforms for dissecting SMA pathogenesis and testing genetic or pharmacological modifiers in a transparent vertebrate.

1.2.4. *Drosophila melanogaster*

Drosophila melanogaster is known for its high conservation of genes associated with human diseases, which are expressed in analogous tissues (Chintapalli et al., 2007; Yamamoto et al., 2014). This characteristic facilitates the investigation of conserved cellular pathways within a complex nervous system, thereby providing an effective model for human diseases, including neurodegenerative disorders such as SMA (Liguori, Pandey and Digilio, 2023).

Drosophila encodes a single ortholog of the *SMN* gene, called *Smn* (Miguel-Aliaga et al., 2000). Initial studies replicated the most severe aspect of SMA by introducing point mutations into the endogenous *Drosophila* *Smn* gene, analogous to those observed in SMA patients (Chan et al., 2003). These mutations, known as *Smn^A* and *Smn^B* alleles, led to the disruption of the SMN protein, which was believed to undergo rapid degradation, resulting in reduced postsynaptic transmission, NMJ degeneration, and motor dysfunction. Although these mutants can survive beyond embryogenesis due to maternal SMN contribution, they ultimately perish as early third instar larvae (Chan et al., 2003). A later study generated a zygotic protein null *Smn* allele, *Smn^{x7}*, by removing the entire *Smn* coding region (Chang et al., 2008). Homozygous *Smn^{x7}* mutants displayed a 94% depletion of SMN expression at third instar larval stage, reduced muscle size, defective NMJ neurotransmission, defective locomotion and lethality at the third instar larvae

(Chang et al., 2008), similar to the previous loss-of-function alleles *Smn^A* and *Smn^B* (Chan et al., 2003).

To replicate more intermediate SMA phenotypes, several research groups have developed hypomorphic alleles of *Smn* with varying degrees of SMN knockdown in specific tissues. For instance, animals carrying the homozygous *Smn^E* mutation, which leads to a depletion of SMN expression exclusively in the thoracic segment, were completely viable and fertile but exhibited signs of neuromuscular degeneration and motor dysfunction in adulthood (Rajendra et al., 2007). Another study employed RNAi for SMN knockdown and discovered that while both muscle and neuronal knockdown affected NMJ morphology, muscle-specific knockdown resulted in more severe lethality compared to neuronal knockdown (Chang et al., 2008).

These *Drosophila* models span a spectrum of SMN reduction, from complete absence to tissue-limited depletion, thereby reproducing severe through mild SMA phenotypes and enabling dissection of cell-autonomous versus non-autonomous disease mechanisms within a genetically tractable, highly conserved system.

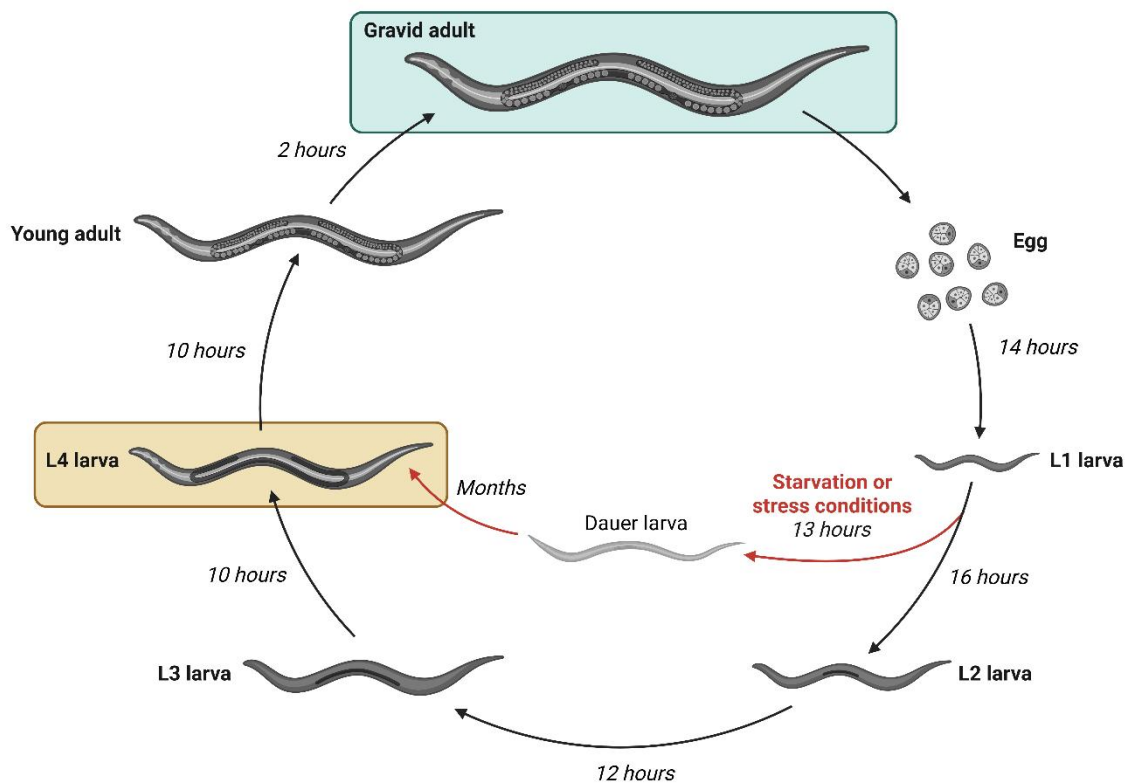
1.2.5. *Caenorhabditis elegans*

Caenorhabditis elegans (*C. elegans*) is a free-living, non-parasitic nematode found worldwide in temperate, nutrient-rich environments, such as rotting vegetal substrates (Félix and Duveau, 2012). In laboratory settings, this nematode is easily maintained using agar plates or liquid medium supplemented with *Escherichia coli*, at 15 °C to 25 °C (Brenner, 1974a).

The nematode *C. elegans* exist predominantly as a self-fertilising hermaphrodite, with a wildtype animal producing approximately 300 embryos encased in impermeable eggshells (Corsi, Wightman and Chalfie, 2015). Typically, embryos are retained within the hermaphrodite until reaching the 24-cell stage, after which they are laid. The development of *C. elegans* from embryo to self-fertilising adult encompasses four larval stages, designated L1 to L4, with each stage lasting approximately 13 h (**Figure 1.3**). Upon reaching adulthood, these nematodes commence the production of self-progeny and can survive for several additional weeks (Raizen et al., 2008).

The capacity for self-fertilisation and a rapid life cycle are among the most distinguished features of *C. elegans*, as it facilitates the maintenance of stocks and enable faster experimental cycles. Notably, *C. elegans* body is transparent throughout all developmental stages, which provides several significant advantages for researchers, including the observation of internal structures and use of fluorescent markers *in vivo* (Corsi, Wightman and Chalfie, 2015).

The use of *C. elegans* in research has led to important discoveries, including the incorporation of the green fluorescent protein (GFP) into the genomes of different organisms through genetic engineering to track biological processes within cells, (Chalfie et al., 1994), the discovery of RNA interference (RNAi) (Fire et al., 1998), and the discovery of microRNAs (Lee et al., 1993). Notably, *C. elegans* was the first animal model in which the entire neuronal connectome was characterised at the level of individual neurons and synapses. This connectome comprises 302 neurons, 5000 chemical synapses, 2000 neuromuscular junctions and 600 gap junctions in the adult hermaphrodite (White et al., 1986). In addition, *C. elegans* is equipped with a total of 75 motor neurons, each innervating a specific group of muscle cells. For instance, while muscles in the head receive innervation for motor neurons in the nerve ring, the rest of the body-wall muscles are innervated by motor neurons of the ventral cord (White et al., 1986; Smith et al., 2024). The precise identification and connectivity patterns of each neuron facilitate the indirect assessment of their functional state through behavioural assays. For instance, the pharyngeal pumping behaviour is indicative of the activity of a well-defined neuronal circuit comprising 20 neurons that coordinate the excitation and inhibition of the pharyngeal muscles, including key motor neurons such as MC, M2 and M4 (Trojanowski et al., 2014). Since this pioneering work, *C. elegans* has become an essential model for investigating neurobiological questions through the application of a diverse array of assays that assess neuronal function, such as locomotion, feeding, and chemosensation among others (Hart, 2006).





| SMN-1 protein | Diminished SMN-1 protein |
|---|--|
|  |  |
| Reaches fertile adulthood | Slow growth, fails to reach adulthood |
| Retains typical intestinal pigmentation | Loss of intestinal pigmentation |
| Regular swimming, feeding, and coordinated locomotion. | Reduced swimming and feeding behaviours due to synaptic defects |

Figure 1.3. Developmental lifecycle of *Caenorhabditis elegans* and phenotypic consequences of SMN-1 depletion

Schematic representation illustrating the developmental lifecycle of *C. elegans* at 20°C, progressing from embryonic state (egg) to a gravid adult through four larval stages (L1–L4). In response to starvation or stress, nematodes enter the dauer diapause stage, characterised as a stress-resistant condition, where the animal is capable of surviving for several months. The bottom panels provide a comparative analysis of the animals' phenotypes under normal (left) or depleted (right) SMN-1 protein levels. Wildtype animals progress through all developmental stages, exhibiting characteristic intestinal pigmentation and coordinated motor behaviours. Conversely, SMN-1-depleted animals demonstrate delayed development, larval arrest, loss of pigmentation, and reduced swimming and feeding capabilities, indicative of neuromuscular dysfunction.

Another important feature of *C. elegans* is its significant genetic conservation with humans. It is estimated that approximately 70% of human genes have orthologs within the *C. elegans* genome (Kaletta and Hengartner, 2006), and around 40% of genes implicated in human diseases possess clear orthologs in *C. elegans*. Importantly, the role that many of those genes fulfil in the nematode are similar or nearly identical to those in humans (Carrol, Grenier and Weatherbee, 2002), thereby enabling researchers to explore complex biological processes in a more simplified organism.

Due to its well-characterised nervous system and genetic conservation, *C. elegans* has emerged as a powerful tool for investigating neurodegenerative diseases, including SMA. *C. elegans* possesses a single ortholog of the human *SMN1* gene, known as *smn-1*, with an overall sequence similarity of 36% between the human and nematode sequences (Miguel-Aliaga et al., 1999). This conservation is particularly pronounced in three critical regions: the N-terminus, involved in RNA binding and interaction with SMN-interacting protein (SIP1); the central Tudor domain, involved in RNA binding and metabolism; and the C-terminal end, involved in binding to Sm proteins and oligomerisation (Miguel-Aliaga et al., 1999). The conservation of these regions indicates that the *C. elegans* SMN protein possess a significant homology to its human counterpart, retaining similar functional properties, thereby making *C. elegans* a powerful model for studying SMA. Since then, different SMA models have been engineered utilising *C. elegans*.

The first approach employed to mimic SMA in *C. elegans* involved the injection of RNAi to decrease endogenous SMN transcript levels (Miguel-Aliaga et al., 1999). While this approach did not produce noticeable effects in the injected animals, significant impacts were observed in their progeny. Most of the offspring exhibited lethality during late embryonic stages, and the few survivors displayed various deficiencies affecting neuronal, muscular, and reproductive tissues (Miguel-Aliaga et al., 1999), highlighting the critical role of SMN as an essential protein during embryonic development.

The first *smn-1* loss-of-function allele described, designated as *smn-1(ok355)*, involves a 975 bp deletion that abrogates most of the *C. elegans* endogenous *smn-1* gene (Briese et al., 2008). This deletion includes the 246 bp upstream of the *smn-1* coding sequence, including the start codon,

leaving only 87 bp at the 3' end of the gene, including the stop codon. The strain is maintained as a heterozygous line that presents no phenotypic differences with wildtype *C. elegans*. Conversely, homozygous *smn-1(ok355)* animals, which appear overtly normal in early developmental stages, exhibit a progressive decline in health, characterised by slow growth, arrest at the late larval developmental stage, loss of intestinal pigmentation, and sterility (Briese et al., 2008) (**Figure 1.3**). These animals also displayed significant neuromuscular defects by day 2 post-L1, especially for behaviours that require rhythmic and constantly contraction of muscles, such as decreased swimming and feeding behaviours (Briese et al., 2008; Dimitriadi et al., 2016). Interestingly, these functional deficits occur without overt motor-neuron loss (Briese et al., 2008), despite the observed defects in synaptic transmission and altered localisation of presynaptic proteins (Dimitriadi et al., 2016). The absence of phenotypic manifestations in early stages, followed by a progressive health decline, is attributed to the maternal loading of *smn-1* mRNA transcripts from heterozygous parental nematodes to their progeny (Miguel-Aliaga et al., 1999). Consequently, as maternal SMN levels diminish, defects begin to manifest in *smn-1(ok355)* nematodes, replicating core features observed in severe SMA patients. The severe *C. elegans* SMA model is particularly well-suited for studying postembryonic roles of SMN-1, identifying genetic modifiers and developing potential therapeutic strategies through genetic or drug screens.

Researchers have also developed an additional severe *C. elegans* SMA model, known as *smn-1(rt248)* (Dimitriadi et al., 2016). The *smn-1(rt248)* allele was generated by utilising CRISPR-Cas9 technology and involves an 8 bp deletion in exon 2 of the endogenous *C. elegans smn-1* gene. This mutation introduces a premature stop codon at the 19th amino acid position within the RNA binding region, thereby skipping the translation of the Tudor and oligomerisation domains (Dimitriadi et al., 2016). The truncated protein encoded is hypothesised to undergo rapid degradation by the proteasome, thereby losing its function. Consequently, homozygous *smn-1(rt248)* animals, similar to *smn-1(ok355)* nematodes, appear phenotypically normal during early larval stages. However, exhibit a progressive decline in health as maternal SMN-1 is diminished, characterised by arrest at the late larval stage, loss of intestinal pigmentation and sterility

(Dimitriadi et al., 2016). Additionally, *smn-1(rt248)* animals showed significant neuromuscular impairment by day 2 post-L1, defects in synaptic transmission and altered localization of presynaptic proteins (Dimitriadi et al., 2016). The *smn-1(rt248)* *C. elegans* SMA model is particularly useful for studying the effects of SMN-1 depletion in *C. elegans*, complementing the existing *smn-1(ok355)* model and allowing researchers to confirm that observed defects are indeed caused by *smn-1* loss.

Milder phenotypes of SMA have also been developed in *C. elegans*. For instance, the *smn-1(cb131)* allele harbours a single-nucleotide substitution in exon 2 of the endogenous gene, converting codon 27 from aspartic acid to asparagine (D27N) (Sleigh et al., 2011a). This allele was designed to mimic a mutation found in a type III SMA patient, which destabilises the SMN complex and impairs its function in snRNP assembly (Ogawa et al., 2007). Unlike the most severe *C. elegans* SMA models, homozygous *smn-1(cb131)* nematodes reach adulthood and remain fertile, although their progeny exhibited increased embryonic lethality (Sleigh et al., 2011a). Notably, adult nematodes displayed selective neuromuscular deficits that progress with age. For example, while swimming behaviour is impaired from day 1 post-L1, feeding behaviour remains indistinguishable from wildtype until day 9 post-L1. Interestingly, despite the neuromuscular behavioural impairments, these nematodes do not exhibit overt structural abnormalities in body-wall muscle or motor neurons, although they present impaired synaptic transmission (Sleigh et al., 2011a). The milder phenotype of *smn-1(cb131)* nematodes make this *C. elegans* SMA model particularly well-suited for performing large-scale chemical compound screening to identify potential therapeutic agents for SMA. Notably, *N*-acetylneuraminic acid was identified in a chemical screen as a potential therapeutic agent for SMA, improving several features of the *smn-1(cb131)* phenotype, including egg-laying defects, and enhancing the pharyngeal pumping rate in the more severe *smn-1(ok355)* *C. elegans* SMA model. Mechanistically, *N*-acetylneuraminic acid has been shown to act as a scavenger of hydrogen peroxide, suggesting that its beneficial effects may derive from reducing oxidative damage (Sleigh et al., 2011).

Another intermediate *C. elegans* SMA model, known as *smn-1(gk118916)*, was generated by inducing a C-to-T nucleotide change in the *C. elegans* endogenous *smn-1* gene, resulting in the conversion of glutamate 167 to lysine (E167K). This mutation affects the central helical domain of SMN-1, yielding a protein with only partial loss of function (Doyle et al., 2021). Homozygous *smn-1(gk118916)* nematodes complete larval development, reach adulthood and remain fertile. However, the nematodes exhibited signs of muscle degeneration by day 3 of adulthood, followed by a decline in motor function by day 5 of adulthood and degeneration of GABAergic motor neurons, but not cholinergic motor neurons, by day 9 of adulthood (Doyle et al., 2021). While GABAergic motor neurons use gamma-aminobutyric acid (GABA) as their neurotransmitter and are typically involved in the transmission of inhibitory signals, cholinergic motor neurons use acetylcholine as their neurotransmitter and are involved in stimulating muscle contraction (Smith et al., 2024). These findings suggest that muscle dysfunction, which in this study precedes neurodegeneration, could be a critical factor for the observed motor function decline, while the degeneration of GABAergic motor neurons, which play a crucial role in coordinating movement, could be a contributing factor. The late onset of SMA-like phenotypes in *smn-1(gk118916)* animals make this *C. elegans* SMA model particularly useful for studying the onset and progression of SMA phenotypes.

Finally, SMN knockdown in specific tissues in *C. elegans* have been utilised to understand cell-autonomous roles of SMN-1. For example, pan-neuronal expression, but not muscle-specific expression, of SMN in a null *smn-1* background rescues both motility and pharyngeal defects (Briese et al., 2008). Additionally, specific knockdown of SMN in *C. elegans* in D-type motor neuron, a subclass of GABAergic neurons in the ventral nerve cord of *C. elegans* that play a specific role in regulating the nematode's backward movement (Cooper et al., 1993), was enough to mimic some of the key features of SMA, such as impaired locomotion and neuron degeneration (Gallotta et al., 2016). These tissue-specific studies in *C. elegans* highlight the importance of SMN function in neurons for proper neuromuscular activity and development, while also revealing roles in other tissues such as muscle and the germline.

1.3. Oxidative stress

Oxygen is an abundant and highly reactive element essential for life. Yet, akin to a double-edged sword, it is capable of inducing great cellular damage. This duality was described by Kelvin Davies, who termed it as “the paradox of aerobic life” (Davies, 1995). Since its discovery in 1775 by Joseph Priestley (Priestley, 1775; De Sequeira and Hancock, 2022), our understanding of oxygen and its role on physiological and pathological processes has been shaped by the integration of key discoveries in the fields of chemistry and biology, which will be summarised in the following section.

1.3.1. Evolution of the scientific knowledge of free radicals and oxidative agents

In the late 19th century, Henry John Horstman Fenton demonstrated that hydrogen peroxide, in the presence of ferrous salts, promotes the oxidation of organic compounds, a reaction now termed the Fenton reaction (Fenton, 1894). Initially, chemists attributed these oxidative transformations to highly reactive, unstable atom groups within molecules, referred to as "radicals," which were thought to exist only transiently during chemical reactions (Villamena, 2013). This perception shifted dramatically in 1900 when Moses Gomberg isolated, for the first time, the stable organic radical triphenylmethyl, providing unequivocal evidence that radicals could exist as independent chemical entities (Gomberg, 1900). Gomberg's landmark discovery led directly to the introduction of the term "free radical". Applying the emerging knowledge in free radicals, Fritz Haber and Joseph Weiss revisited the mechanism of the original Fenton reaction. They proposed that the oxidation of organic substrates observed by Fenton was specifically due to the formation of hydrogen peroxide-derived free radicals, namely, hydroxyl ($\bullet\text{OH}$) and hydroperoxyl ($\bullet\text{HO}_2$) radicals (Haber et al., 1934). The resulting Haber–Weiss reaction offered a mechanistic explanation for the biological generation of highly reactive hydroxyl radicals, thereby elucidating their potential to cause substantial cellular damage.

Building upon these foundations, Denham Harman later hypothesised that intracellular iron ions could catalyse the production of oxygen-derived radicals during enzymatic reactions, particularly aerobic respiration. According to Harman's theory, these radicals initiate chain reactions that result in cellular deterioration, genetic mutations, and degenerative processes associated with biological aging, a concept known today as the "free radical theory of aging" (Harman, 1956).

Subsequent research revealed that oxidative damage arises not only from free radicals but also from certain non-radical oxidants, such as hydrogen peroxide (H_2O_2). Recognizing the broader spectrum of chemically reactive species, Weiss introduced the collective term "reactive oxygen species (ROS)" in 1977 (Weiss, King and LoBuglio, 1977). Later, in 1985, Helmut Sies coined the term "oxidative stress" to describe conditions in which an imbalance favouring pro-oxidants over antioxidants occurs, resulting in oxidative damage to proteins, lipids, and DNA (Sies, 1985).

1.3.2. Definitions

Biological free radicals are atoms or molecules present in living organisms, characterised by a chemically unstable configuration due to the presence of one or more unpaired electrons (Villamena, 2013) (**Figure 1.4**). This instability causes free radicals to rapidly react with surrounding molecules through electron-transfer reactions, either accepting electrons (oxidation) or donating electrons (reduction), to achieve a stable electron-paired state (Villamena, 2013). These oxidation-reduction (redox) reactions are essential for the proper function of a wide arrange of physiological processes, such as cellular respiration (**See 3.3.1. Cellular sources of ROS and its role**).

Among the various reactive species generated during cellular redox reactions, oxygen-derived molecules play particularly prominent roles due to their involvement in multiple physiological processes (Sies and Jones, 2020). The generic term "reactive oxygen species" (ROS) collectively describes diverse molecules derived from oxygen formed through redox reactions or electronic excitation. It is important to emphasise that "ROS" is not a defined chemical compound, but a

group of diverse atoms or molecules with vastly different properties and biological functions (Sies, Berndt and Jones, 2017).

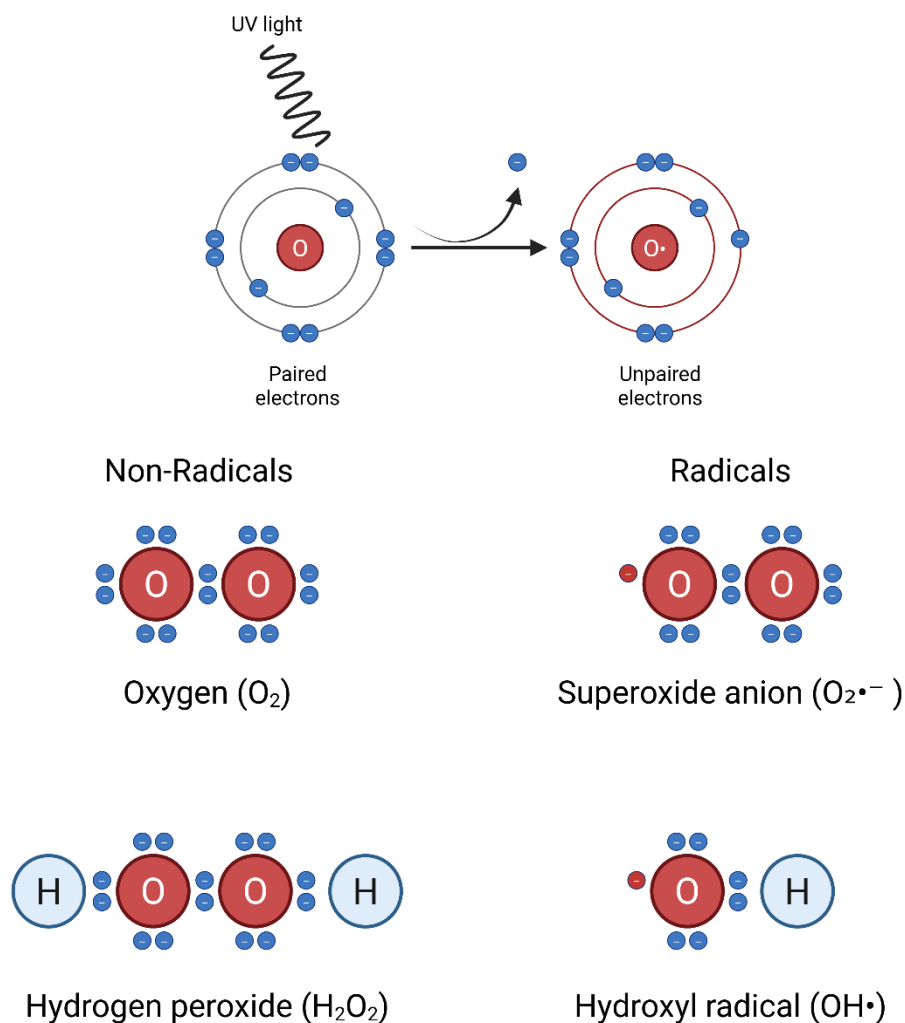


Figure 1.4. Free radicals and non-radicals derived from oxygen

Atoms or molecules with paired electron configurations exhibit chemical stability. However, this stability can be disrupted by external factors such as ultraviolet (UV) radiation or the presence of highly electronegative molecules that attract electrons. The loss of an electron results in the formation of a molecule with an unpaired electron configuration, referred to as free radical. Reactive oxygen species (ROS) encompass both non-radical and radical oxygen-derived compounds. Non-radicals, such as molecular oxygen (O_2) and hydrogen peroxide (H_2O_2), maintain paired electrons, whereas radical species, such as superoxide anion ($O_2^{\bullet-}$) and hydroxyl radical ($^{\bullet}OH$), possess one or more unpaired electrons.

ROS include radical species, such as the superoxide radical ($O_2^{\bullet-}$) and hydroxyl radical (OH^{\bullet}), as well as non-radical species, like hydrogen peroxide (H_2O_2) and singlet oxygen (1O_2), formed sequentially from molecular oxygen (O_2) (Weiss, King and LoBuglio, 1977). Each of these chemical entities exhibit a varying degree of reactivity with neighbouring molecules and different biological significance, ranging from signalling to pathological damage, which are summarised in **Table 1.1**. Among those molecules, hydrogen peroxide (H_2O_2) and the superoxide anion radical ($O_2^{\bullet-}$), stand out due to their carefully controlled production within cells and their interactions with critical metabolic and signalling pathways (Sies and Jones, 2020).

Table 1.1. Reactive oxygen species: origin, reactivity and biological impact

UV= ultraviolet light, ETC = electron transport chain, NADPH = , SOD= superoxide dismutase.

| Name | Free radical / Reactivity | Main generation pathways | Biological significance |
|---------------------------------------|---------------------------|---------------------------|---|
| Singlet oxygen (1O_2) | No / Highly reactive | Excitation of O_2 by UV | Cellular damage |
| Superoxide anion ($O_2^{\bullet-}$) | Yes / Weak oxidant | ETC NADPH oxidase | Cellular signalling |
| Hydrogen peroxide (H_2O_2) | No / Mild oxidant | SOD NADPH oxidase | Cellular signalling |
| Hydroxyl radical (HO^{\bullet}) | Yes / Extremely reactive | Fenton reaction | Cellular damage |
| Peroxyl radicals (ROO^{\bullet}) | Yes / Moderate reactivity | Lipid peroxidation | Cellular signalling and cellular damage |
| Alkoxy radicals (RO^{\bullet}) | Yes / Highly reactive | Lipid peroxidation | Cellular damage |

Early studies emphasised the implication of ROS in cellular damage and pathological processes, such as aging, oxygen toxicity and radiation-induced damage (Harman, 1956). However, under physiological conditions, the concentration of these molecules within cells is meticulously

controlled by distinct mechanisms, including regulated expression of ROS-producing enzymes, endogenous antioxidants, and molecules facilitating inter-compartment ROS transport (Sies and Jones, 2020). Such tightly regulated ROS levels result in specific and reversible oxidation of protein targets integral to a wide range of cellular processes (i.e. cell proliferation and differentiation). The maintenance of physiological levels of oxidants essential for redox signalling is defined as “oxidative eustress” (Sies, Berndt and Jones, 2017). Conversely, oxidative stress occurs when there is an imbalance between oxidative stress production and removal, favouring oxidants over antioxidants, leading to a disruption of redox signalling and causing molecular damage (Sies, Berndt and Jones, 2017).

1.3.3. ROS in physiology: oxidative eustress

1.3.3.1. Cellular sources of ROS and its role

The intracellular distribution of ROS within cells is not homogeneous. Instead, each cell maintains a distinct redox gradient, shaped by subcellular compartmentalisation, differential enzyme expression, and localized physiological processes that contribute to the generation of ROS (Snezhkina et al., 2019) (**Figure 1.5**).

Mitochondria are one of the primary sources of ROS within cells due to their high oxygen consumption utilised for cellular respiration (Mori et al., 2021). Within mitochondria, the electron transport chain (ETC) engages in a series of electron transfer reactions to generate cellular ATP via oxidative phosphorylation (Nolfi-Donagan, Braganza and Shiva, 2020). In this process, the mitochondrial complex IV catalyses the four-electron reduction of O_2 to H_2O (Faxén et al., 2005). However, leak of electrons from complexes I, II, and III into the mitochondrial matrix or intermembrane space results on the reduction of oxygen into superoxide anion ($O_2^{\bullet-}$) (Henderson et al., 2009; Zhang et al., 1998). Superoxide dismutase enzymes located in these compartments rapidly catalyse the conversion of $O_2^{\bullet-}$ into H_2O_2 (Nolfi-Donagan et al., 2020; Zhao et al., 2019). Importantly, ROS production in mitochondria is an essential element of mitochondrial physiology,

functioning as an important regulator of various cellular processes, including differentiation, autophagy, metabolic adaptation, and immune cell activation (Sena and Chandel, 2012).

The endoplasmic reticulum (ER), recognised for its involvement in protein synthesis, modification and transport, among other functions (Snezhkina et al., 2019), is also a significant source of cellular ROS. Notably, during protein folding, each disulphide bond introduced by protein disulphide isomerases (PDIs) and endoplasmic reticulum oxidoreductin-1 (ERO1) generates one molecule of H_2O_2 (Tu & Weissman, 2002; Zito, 2015). Additional sources of ROS, including NADPH oxidases (NOX) and cytochrome P450 (CYP) enzymes localised in the ER membrane, also contribute to ROS generation within the ER (Roscoe and Sevier, 2020; Sies and Jones, 2020). ROS generation in the ER plays an important role in redox signalling, protein folding and the regulation of calcium storage (Roscoe & Sevier, 2020; Zhang et al., 2019). For instance, increased ROS production due to the activation of NOX can activate ROS dependent branches of the unfolded protein response, which in turn, activate apoptotic pathways (Zeeshan et al., 2016; Bhattarai et al., 2021).

Peroxisomes are cell organelles that play a central role in lipid and protein metabolism, generating ROS as a byproduct of those metabolic processes. For instance, during fatty acid β -oxidation, acyl-CoA oxidases (ACOX) enzymes catalyse the initial step of β -oxidation, which generates H_2O_2 as secondary products (Del Río and López-Huertas, 2016; Sies and Jones, 2020). Furthermore, enzymes such as xanthine oxidoreductase (XOR) and urate oxidase (UR), are involved in the generation of uric acid within peroxisomes during purine metabolism, producing $\text{O}_2^\bullet -$ and H_2O_2 during this process (Schrader and Fahimi, 2006). ROS produced in peroxisomes can diffuse out of this organelle, functioning as signalling molecules that influence mitochondrial function of modulating transcription factors such as NF- κ B that affects various cellular processes including inflammation, immunity, and cell growth (Fransen et al., 2012).

Lastly, the plasma membrane itself contributes to the production of both extracellular and intracellular ROS. The primary sources of ROS at the plasma membrane are NOXs enzymes (Brandes, Weissmann and Schröder, 2014; Sies and Jones, 2020; Vermot et al., 2021). The NOX

family constitute a family of transmembrane proteins that transfer electrons from NADPH to oxygen, reducing it to $O_2^{\bullet-}$ or to H_2O_2 (Brandes, Weissmann and Schröder, 2014). ROS generated in the plasma membrane play a crucial role in several physiological processes such as host defence, inflammation, cell growth, redox signalling and cell death (Vermot et al., 2021).

In summary, while uncontrolled production of ROS results in oxidative damage, the regulated generation of ROS from cellular organelles plays essential roles in redox regulation. This suggests the importance of maintaining ROS at basal levels for normal physiological function.

1.3.3.2. Antioxidant defence

The term antioxidant is defined as any substance that delays, prevents or removes oxidative damage to a target molecule (Halliwell and Gutteridge, 2007). In biological systems, there are three lines of antioxidant defence that work together to protect against oxidative stress and free radical damage. A first line of antioxidant defence is constituted by endogenous antioxidant enzymes, a second line of antioxidant defence involves exogenous low-molecular-weight antioxidants derived from diet, and a third line of antioxidant defence involves the repair or removal of damaged biomolecules (Jomova et al., 2024). This section focusses on the first line of antioxidant defence, endogenous enzymatic antioxidants, as they constitute the most powerful protective barrier against oxidative stress. These enzymatic antioxidants include superoxide dismutase (SOD), catalase (CAT), glutathione peroxidase (GPx), and peroxiredoxins (PRx) (Table 1.2) (Figure 1.5).

Superoxide dismutases (SOD) constitute the first line of defence against ROS. SOD enzymes utilise either copper (Cu) or manganese (Mn) as catalytic cofactors in their active sites and perform their antioxidant function through a mechanism of action that involves the alternate reduction and reoxidation of the metal cofactor (Fukai and Ushio-Fukai, 2011). During the reduction phase, $O_2^{\bullet-}$ reduces the metal cofactor from Cu^{2+} or Mn^{2+} to Cu^+ or Mn^+ , generating an oxygen molecule. During the reoxidation phase, the reduced SOD donates the exceeding electron

and proton to $O_2^{\bullet-}$, producing H_2O_2 and reverting Cu^+ or Mn^+ to its active form (Jomova et al., 2024). Through this process, SOD facilitates the conversion of two superoxide anions into hydrogen peroxide and molecular oxygen (Hsu et al., 1996; McCord & Fridovich, 1969). The specific metal cofactor varies among different SOD isoforms, which are localised to distinct cellular compartments. While SOD1 (CuZnSOD), is found in the cytoplasm, mitochondrial intermembrane space and nucleus (Chang et al., 1988; Sturtz et al., 2001); SOD2 (MnSOD), is located in the mitochondrial matrix (Weisiger and Fridovich, 1973); and SOD3 (Cu/ZnSOD) is present on cell surface or secreted extracellularly (Marklund, 1984).

Catalase (CAT) is a tetrameric heme protein that facilitates the conversion of hydrogen peroxide into water and molecular oxygen (Karnati et al., 2013). This reaction occurs in two distinct phases. In the first phase, the heme group of CAT is oxidised by a hydrogen peroxide molecule, resulting in the formation of a hypervalent iron intermediate, known as compound I, and the release of water. Subsequently, compound I is reduced back to its original state by another hydrogen peroxide molecule, culminating in the production of two water molecules and oxygen (Kettle and Winterbourn, 2001; Alfonso-Prieto et al., 2009). CAT is predominantly found in peroxisomes, although some studies have also observed its presence in cytosol as cells age (Walton and Pizzitelli, 2012; Karnati et al., 2013).

Glutathione peroxidases (GPxs) constitute a family of enzymes that catalyse the reduction of hydrogen peroxide or organic hydroperoxides to water or corresponding alcohols, utilising glutathione (GSH) as a reductant (Maiorino et al., 1995). There are eight human isoforms of GPxs, classified into two distinct groups: selenium-containing GPxs (GPx1-4 and GPx6) and non-selenium congeners (GPx5, 7, and 8) (Brigelius-Flohé and Maiorino, 2013). The mechanisms of action for these two groups differ slightly. Selenium-containing GPxs participate in a cyclic reaction wherein the selenenic group reacts with H_2O_2 to form selenenic acid ($-SeOH$). This selenenic acid is subsequently reduced back to selenol by two GSH molecules, resulting in the formation of oxidised glutathione (GSSG) and water, thereby enabling GPx to continuously reduce hydroperoxides as long as GSH is available (Flohà et al., 1972; Takebe et al., 2002).

Conversely, in cysteine-containing GPxs, the peroxidatic cysteine in their catalytic site is oxidised to sulfenic acid by H_2O_2 , which is then reduced by a redoxin, typically thioredoxin (Trx) (Flohé et al., 2011; Maiorino et al., 2007). The cellular compartments where these enzymes perform their antioxidant functions also vary for each isoform. For instance, GPx1 and GPx4 are predominantly located in the cytoplasm and mitochondria (Asayama et al., 1994; Brigelius-Flohé et al., 1994). Additionally, GPx3 and GPx4 can be found in the extracellular space and cell membrane, respectively (Maiorino et al., 2007; Wei et al., 2024). Moreover, GPx7 and GPx8 are situated in the lumen of the endoplasmic reticulum (Nguyen et al., 2011).

Peroxiredoxins (PRx) enzymes facilitate the conversion of peroxide into water, utilising cysteine (Cys) as an acceptor of electrons (Zeida et al., 2014). This cysteine is referred to as peroxidatic cysteine (CP) and a characteristic shared by all PRx isoforms. Additionally, certain isoforms contain a second Cys, termed resolving cysteine (CR), which contributes to their catalytic activity (Wood et al., 2003). Based on the presence or absence of CR and its specific location within the protein, PRx can be classified into distinct categories. PRx1-4 are designated as 2-Cys PRx and contain both CP and CR, which are located in different subunits of the protein. PRx5 is an atypical 2-Cys PRx isoform, also containing both CP and CR, with the distinction that these residues are in close proximity within the same subunit. In contrast, PRx6 is classified as a 1-Cys PRx, containing only CP (Wood et al., 2003). PRx isoforms are distributed across various cellular compartments, including cytoplasm (PRx1, 2, 4, 5, and 6), mitochondria (PRx3), plasma membrane (PRx1 and 2), nucleus (PRx1,2 and 5), and extracellular location (PRx4 and 6), among others (Heo, Kim and Kang, 2020).

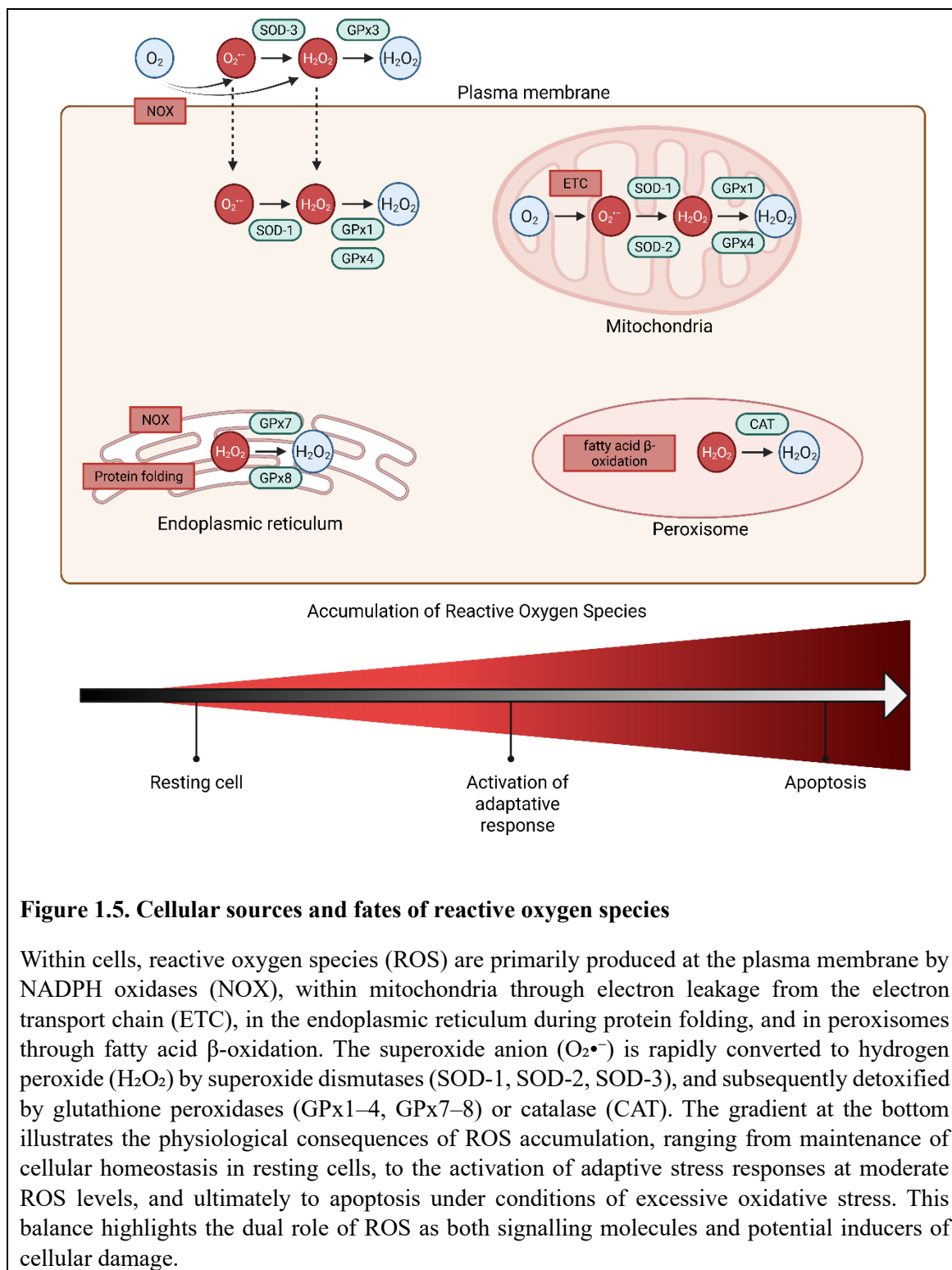
The mechanism of action of PRx enzymes is characterised by a redox cycle that includes two separate oxidations by H_2O_2 and a subsequent reduction by a reducing agent that restores PRx to its active form. The first round of oxidation occurs similarly in all isoforms. The CP residue is oxidised by H_2O_2 resulting in the formation of cysteine sulfenic acid (CP-SOH) (Zeida et al., 2014). During the second round of oxidation by another H_2O_2 molecule, typical 2-Cys PRx interacts with the resolving cysteine (CR) of the adjacent PRx subunit, forming a disulfide bond

between both subunits (Wood et al., 2002). In contrast, in atypical 2-Cys PRx, with a nearby CR residing close to the CP-SOH, the disulfide bond is intramolecular, occurring within the same PRx subunit (Choi et al., 2003). Conversely, in 1-Cys PRx, there is no disulfide bond formation, due to the absence of CR (Monteiro et al., 2007). The reduction reaction that completes the cycle also differ among the different classes of PRx. While both typical and atypical 2-Cys isoforms are reduced by TRx, 1-Cys PRx utilize GSH as an electron donor (Montemartini et al., 1999; Manevich, Feinstein and Fisher, 2004). In all instances, the oxidised CP-SOH is reverted to its active CP form, enabling the initiation of a new cycle. The main biological implication of this structural variations among isoforms is that 2-Cys PRx are more susceptible to hyperoxidation due to their higher affinity to react with H₂O₂, whereas hyperoxidation of atypical 2-Cys and 1-Cys PRx is considerably less frequent (Montemartini et al., 1999; Hyun et al., 2005). Notably, hyperoxidation can lead to enzyme inactivation, which can be reversed by sulfiredoxin in an ATP-dependent mechanism (Biteau, Labarre and Toledano, 2003).

Table 1.2. Cofactors, subcellular locations, and overall reaction of antioxidants enzymes

| Enzyme | Cofactor(s) | Location | Overall reaction |
|---------------|-------------|---|--|
| SOD1 | Cu, Zn | Cytoplasm, mitochondrial intermembrane space, nucleus | $2 \text{O}_2^{\bullet-} + 2 \text{H}^+ \rightarrow \text{H}_2\text{O}_2 + \text{O}_2$ |
| SOD2 | Mn | Mitochondrial matrix | |
| SOD3 | Cu, Zn | Extracellular space, cell surface | |
| CAT | Fe | Peroxisomes | $2 \text{H}_2\text{O}_2 \rightarrow 2 \text{H}_2\text{O} + \text{O}_2$ |
| GPx1 | Sec, GSH | Cytoplasm, mitochondria | $\text{H}_2\text{O}_2 + 2 \text{GSH} \rightarrow 2 \text{H}_2\text{O} + \text{GSSG}$ |
| GPx3 | Sec, GSH | Extracellular space | |
| GPx4 | Sec, GSH | Cytoplasm, mitochondria, cell membrane | |
| GPx7/8 | Cys, Trx | Endoplasmic reticulum lumen | |

| | | | |
|-------------|------------|-------------------------------------|--|
| PRx1 | 2-Cys, Trx | Cytoplasm, plasma membrane, nucleus | $\text{H}_2\text{O}_2 + \text{Prx-SH} \rightarrow \text{H}_2\text{O} + \text{Prx-SOH}$ |
| PRx2 | 2-Cys, Trx | Cytoplasm, plasma membrane, nucleus | |
| PRx3 | 2-Cys, Trx | Mitochondria | |
| PRx4 | 2-Cys, Trx | Cytoplasm, extracellular space | |
| PRx5 | 2-Cys, Trx | Cytoplasm, nucleus | |
| PRx6 | 1-Cys, GSH | Cytoplasm, extracellular space | |



1.3.4. ROS in pathology: oxidative stress

1.3.4.1. Non-specific oxidation of biomolecules

When the rate of ROS production exceeds the cellular antioxidant capacity, the excessive production of ROS causes cellular damage through non-specific oxidation of biological molecules such as lipids, proteins and DNA, which compromise cellular integrity (Sies, Berndt and Jones, 2017).

Lipid peroxidation

ROS, particularly hydroxyl radicals, can attack the carbon chains of fatty acids through hydrogen abstraction, initiating the so-called lipid peroxidation (Tejero et al., 2007). During lipid peroxidation, lipid radicals and peroxy radicals are generated, further propagating the damage to other biological molecules (Ayala, Muñoz and Argüelles, 2014). Accumulation of lipid peroxidation-derived radicals can alter the structure of the membranes, perturbing physiological processes that depend on it, such as channels, or electron transport activities (Yadav et al., 2019). Furthermore, fragmentation of the membrane can generate other toxic products such as malondialdehyde (MDA) and 4-hydroxynonenal (HNE) (Ayala, Muñoz and Argüelles, 2014; Juan et al., 2021). The accumulation of toxic byproducts as a consequence of lipid peroxidation has been associated with various pathological conditions, such as diabetes (Slatter, Bolton and Bailey, 2000), cardiovascular diseases (Uchida, 2000) and cancer (Cai et al., 2012), among others (Juan et al., 2021).

Protein oxidation

Oxidation of proteins can be reversible, in normal conditions as part of signalling processes; or irreversible, in pathological conditions (Spickett and Pitt, 2012). There are different types of irreversible protein modification, depending on the amino acids that are target of the oxidation or the oxidant molecules, such as oxidation of sulfur-containing or aromatic amino acids,

glycoxidation, lipoxidation, carbonylation and nitration (Kehm et al., 2021). Those molecules can be measured in lab settings as a biomarker of oxidative damage (Spickett and Pitt, 2012; Kehm et al., 2021). Irreversible oxidation of protein causes changes in its conformation that lead them to lose their function. As such, protein oxidation is sometimes related with the ethology of diseases such as autoimmune rheumatic diseases (Smallwood et al., 2018), skin diseases (Bickers and Athar, 2006), or neurological disorders (Uttara et al., 2009).

Nucleic-acid oxidation

ROS can inflict damage on DNA and RNA by directly attacking different structures of the molecule. For instance, ROS can attack guanine bases in DNA generating 8-OH-Gua (Ock et al., 2012). Furthermore, ROS can target the sugar molecules of DNA through hydrogen abstraction, potentially resulting in strand breaks (Sharma et al., 2016). Additionally, they can create DNA cross linking, impairing processes such as DNA replication or transcription (Kühbacher and Duxin, 2020). The accumulation of DNA damage over time is associated with the aging process (Van Remmen, Hamilton and Richardson, 2003), as well as several pathologies, such as autoimmune diseases (Bashir et al., 1993), and cancer (Tubbs and Nussenzweig, 2017).

One of the primary consequences of increased oxidative damage to biomolecules is the activation of programmed cell death, known as apoptosis (Redza-Dutordoir and Averill-Bates, 2016). For instance, ROS lipid peroxidation in the mitochondrial membrane leads to the release of cytochrome c, which triggers the initiation of the mitochondrial apoptosis pathway (Petrosillo et al., 2001). Additionally, oxidative modifications to proteins, leading to misfolding or loss of function, trigger the unfolded protein response (UPR) in the endoplasmic reticulum, which if prolonged, can lead to apoptosis (Tabas and Ron, 2011). Additionally, studies have shown that oxidative damage to both nuclear and mitochondrial DNA can trigger p53 activation, which activate the transcription of pro-apoptotic genes (Yoshida and Miki, 2010). These mechanisms underscore the critical role of oxidative stress in the pathogenesis of numerous diseases.

1.3.4.2. Oxidative stress in neurodegeneration

Oxidative stress has the potential to impact every tissue of the body, depending on the site of ROS production, and may either cause or contribute to the pathogenesis of both acute and chronic diseases (Kruk et al., 2019). Notably, research indicates that neuronal tissue is particularly susceptible to oxidative stress. This vulnerability is attributed to the high metabolic demands of neurons and glial cells, which primarily depend on mitochondrial oxidative phosphorylation for energy, a process intrinsically linked to ROS generation (Bélanger, Allaman and Magistretti, 2011; Friedman, 2011; Lundgaard et al., 2015). Additionally, the brain's elevated content of lipids, which make it especially prone to lipid peroxidation (Shichiri, 2014), and limited regenerative capacity of neuronal tissue (Kvistad et al., 2024), further exacerbates this vulnerability. As oxidative damage escalates with aging (Mecocci et al., 1993), and given that advanced age is the primary risk factor for neurodegenerative diseases (Hou et al., 2019), oxidative stress has been proposed as a significant contributor to both aging and neurodegenerative diseases. This concept is encapsulated in the free radical theory of aging (Harman, 1956). Consequently, the role that oxidative stress plays on neurodegeneration has been investigated in various neurodegenerative diseases, such as Alzheimer's disease, Parkinson's disease (PD), Huntington's disease (HD), and amyotrophic lateral sclerosis (ALS) (Singh et al., 2019).

Alzheimer's disease (AD) exemplifies the profound role of oxidative stress in the pathogenesis of neurodegenerative disorders. AD is neuropathologically defined by the formation of amyloid plaques, constituted by amyloid-beta ($A\beta$) peptides, and neurofibrillary tangles (NFT), formed by hyperphosphorylated tau protein aggregates, within neurons of the hippocampus (Serrano-Pozo et al., 2011). This pathological accumulation of proteins leads to progressive neurodegeneration, initially observed on the hippocampus and ultimately to widespread brain atrophy (De-Paula et al., 2012). As a consequence, AD patients manifest with progressive memory loss, disorientation, and impaired judgment (De-Paula et al., 2012). Notably, several markers demonstrated the

presence of oxidative stress in the brain of AD patients (Zhao & Zhao, 2013). There are several mechanisms that explain the presence of oxidative stress in AD. For instance, the accumulation of A β peptides within mitochondria disrupt mitochondrial function, reduce ATP production and enhance ROS generation (Wang et al., 2014). Additionally, the interaction of both A β plaques and NFTs with hydrogen peroxide led to the generation of hydroxyl radicals, via Fenton-type reaction (La Penna et al., 2013). Excessive production of ROS is thought to contribute to the pathogenesis of AD by propagating oxidative damage to lipids, proteins, and nucleic acids. This results in impaired signal transduction, compromised protein functionality, and both genetic and epigenetic alterations that disrupt normal gene expression (Zhao & Zhao, 2013). These alterations create a self-perpetuating cycle of oxidative damage and cellular dysfunction, accelerating neurodegeneration and cognitive decline.

Parkinson's disease (PD) further illustrates the detrimental consequences of oxidative stress within the brain. PD is characterised by the accumulation of α -synuclein aggregates within neurons of the substantia nigra, a specific region of the midbrain. This pathological accumulation leads to progressive loss of dopaminergic neurons in this region of the brain with a central role in motor control (Cai et al., 2011). Consequently, PD patient manifest motor impairments such as slow movements and freezing, resting tremor and muscular rigidity (La Penna et al., 2013). Notably, there is wide evidence of oxidative stress and increased oxidative damage in PD (Dias, Junn and Mouradian, 2013). The presence of oxidative stress in PD is mechanistically linked to disturbances in dopamine metabolism. For instance, dopamine is susceptible to auto-oxidation, which together with mitochondrial dysfunction leads to the overproduction of dopamine quinones and ROS, generating the observed oxidative damage to biomolecules (Muñoz et al., 2012). Importantly, oxidative stress has been observed to play a direct role in the physiopathology of PD, promoting α -synuclein misfolding and aggregation and exacerbating mitochondrial dysfunction (Dias, Junn and Mouradian, 2013). These interconnected mechanisms perpetuate a cycle of oxidative damage, cellular dysfunction, and neurodegeneration, which collectively drive disease progression.

Notably, numerous antioxidants have demonstrated neuroprotective effects in a wide range of preclinical models of AD and PD. In both conditions, antioxidant compounds have consistently enhanced endogenous antioxidant defences, mitigated oxidative stress, reduced protein aggregation, and improved neuronal outcomes (**Table 1.3**). However, despite substantial evidence supporting the involvement of oxidative stress and the consistent efficacy of antioxidants in preclinical studies, their performance in clinical trials has been inconsistent (Kim et al., 2015). These inconsistencies are attributed to factors such as insufficient dosage, inappropriate timing, or inadequate duration of treatments, highlighting the challenges in translating promising preclinical findings into effective clinical interventions. This emphasises the necessity for a more comprehensive understanding of antioxidant mechanisms, the development of reliable biomarkers of oxidative stress, and more targeted therapeutic strategies before clinical translation can be fully implemented (Kim et al., 2015). Nonetheless, acknowledging the role of oxidative stress in the pathology of neurodegenerative diseases provides a valuable framework for developing combinatorial or adjunctive therapies and continues to inform the design of more refined and effective treatment approaches.

Table 1.3. Effect of antioxidant treatment in Alzheimer's Disease and Parkinson's Disease pre-clinical models

MDA= Malondialdehyde (lipid peroxidation derivate), TBARs= Thiobarbituric acid reactive substances (lipid peroxidation derivate), GSH= Glutathione (antioxidant), SOD= Superoxide dismutase (antioxidant), NO= Nitric oxide (reactive nitrogen Specie), CAT= Catalase (Antioxidant).

| | Antioxidant | References | ↓ oxidative stress | ↓ protein aggregation | ↓ apoptosis | Improved neuronal function |
|-----------|-------------|---|--|---|--|---|
| AD | NAC | (1) Fu et al., 2006 (2) Tchantchou et al., 2005 | ↓ MDA (1), ↓ TBARs (2), ↑ GSH (1,2) | | Reduced neuronal loss (1) | Improved cognitive function and memory retention (1,2) |
| | CUR | (1) Kawamoto et al., 2012 (2) Shao et al., 2023 (3) Lim et al., 2001 (4) Liu et al., 2016 (5) Wang et al., 2014 | ↓ MDA (2), ↓ inflammatory markers (2,4), ↓ protein carbonylation (3) | ↓ Aβ deposition (2,3,5) | ↓ markers of apoptosis in brain (↑ Bax, ↓ Bcl-2) | Improved cognitive function (1,2,5), spatial memory (2,4,5), motor skills (1) |
| | VITC | (1) Murakami et al., 2011 | ↓ protein carbonylation (1) and ↑ GSH (1) | ↓ Aβ deposition (1) and ↓ tau phosphorylation (1) | | Behavioural improvements (1) |
| | EGCG | (1) Rezai-Zadeh et al., 2005 (2) Rezai-Zadeh et al., 2008 (3) Lee et al., 2009 (4) Lee et al., 2013 | ↓ inflammatory markers (3,4) | ↓ Aβ deposition (1,2,3,4) and ↓ tau phosphorylation (2) | ↓ markers of apoptosis (3,4) | Improved cognitive function (2) and memory retention (3,4) |
| | MEL | (1) Li et al., 2005 (2) Feng & Zhang, 2004 (3) Matsubara et al., 2003 (4) Feng et al., 2004 (5) Rosales-Corral et al., 2003 | ↓ MDA (1,5), ↓ inflammatory markers (5), ↑ SOD (1), ↓ NO (2,5) | ↓ Aβ deposition (3,4) and ↓ tau phosphorylation (1) | ↓ markers of apoptosis (2,4) | Improved memory and learning (1,2) |
| PD | NAC | (1) Offen et al., 1996 (2) Cocco et al., 2005 | ↓ protein carbonylation (2), ↑ GSH (2) | | Reduced markers of apoptosis (1) | |

| | | | | | | |
|--|------|--|---|-------------------------------|----------------------------------|--|
| | CUR | (1) Siddique et al., 2014 (2) Chakraborty et al., 2017 (3) He et al., 2022 | ↓ MDA (1,3), ↓ protein carbonylation (1), ↓ ROS (2,3) | | Reduced markers of apoptosis (1) | Improved motor skills (1,3) and spatial memory (3) |
| | VITC | (1) Sil et al., 2016 | | ↓ α-synuclein aggregation (1) | | |
| | EGCG | (1) Levites et al., 2001 (2) Xu et al., 2017 (3) Zhou et al., 2018 (4) Tseng et al., 2020 | ↓ protein carbonylation (2), ↓ inflammatory markers (3), ↑ SOD (1), ↑ CAT (1) | | Reduced markers of apoptosis (4) | Improved motor skills (2,3) |
| | MEL | (1) Sharma et al., 2006 (2) Dabbeni-Sala et al., 2001 (3) Mayo et al., 1998 | ↑ SOD (3), ↑ GSH (3) | | Reduced markers of apoptosis (3) | Improved motor skills (1,2) |

1.4. Oxidative stress in spinal muscular atrophy

A growing body of evidence supports a central role for oxidative stress in the pathophysiology of SMA as demonstrated by the accumulation of ROS, oxidative damage to biomolecules, and mitochondrial dysfunction across diverse *in vitro* and *in vivo* models.

1.4.1. Increased ROS and elevated oxidative damage in spinal muscular atrophy

Elevated levels of ROS in SMA have been documented by *in vitro* and *in vivo* models of SMA, as summarised in **Table 1.4**. The first research that observed increased ROS production in SMA employed siRNA-reduced *Smn* expression in NSC-34 (mouse neuron-like cultured cells) and demonstrated that the extent of SMN depletion directly correlates with an increase in ROS generation (Acsadi et al., 2009). These findings were later replicated in cell cultures from SMA patients. For instance, the presence of ROS in fibroblasts from patients with SMA type I (null *SMN1*), healthy family carriers (possessing only one copy of *SMN1*), and healthy control individuals (possessing two *SMN1* copies) were evaluated. The study identified an inverse correlation between the number of *SMN1* copies and ROS levels, with SMA type I patients exhibiting the highest ROS content, and SMA carriers displaying higher ROS levels than healthy subjects (although not statistically significant), yet lower than those in SMA type I patients (Köstel, Bora-Tatar and Erdem-Yurter, 2012).

This research was later extended to human neuronal lineages. A study compared human embryonic stem cell (hESC)-derived spinal motor neurons with either full-length SMN knockdown or SMN Δ 7 knockdown (lacking exon 7) revealed that elevated mitochondrial ROS levels were observed exclusively in the full-length SMN-deficient neurons (Wang et al., 2013). In this study, FL-SMN motor neurons showed a reduction of the FL-SMN protein to approximately 20% compared to the control group, while SMN Δ 7 motor neurons did not

demonstrate differences in FL-SMN protein levels. Consequently, FL-SMN motor neurons, and not SMN Δ 7, exhibited neurodegeneration, suggesting that only FL-SMN depletion triggers both neurodegeneration and increased ROS production. Notably, mitochondrial ROS levels were only elevated in motor neurons, but not in forebrain neuron cultures, indicating that the increased ROS production may be cell-specific rather than systemic (Wang, Zhang and Li, 2013). These differences in ROS among different cells could be behind the particular vulnerability of SMA motor neurons to degeneration. Another study in pluripotent stem cells corroborates these findings, as it was observed that increased ROS levels in both mitochondria and cytoplasm of induced pluripotent stem cell (iPSC)-derived motor neurons from skin fibroblasts of a patient with SMA type III (Ando et al., 2017).

Additionally, studies in SMA mouse model have also demonstrated elevated ROS production within motor neurons (Miller et al., 2016; Thelen, Wirth and Kye, 2020) and muscle tissue (Chemello et al., 2023), demonstrating that although increased ROS might not apply to all cell types, it is not constricted to motor neurons only.

Table 1.4. Evidence of elevated reactive oxygen species in spinal muscular atrophy

NPS= neuronal progenitor stage, E= embryonic, P= postnatal, H₂DCFDA= unspecific cellular ROS, MitoSOX= mitochondrial O₂^{•-}, DHE= cytoplasmic O₂^{•-}, mito-roGFP= mitochondrial H₂O₂, CellRox= unspecific cellular ROS, Amplex Red= cytoplasmic H₂O₂.

| Study | SMA Model | Cell type | ROS detection method | ROS levels | Stage at what measurements took place |
|---------------------|--------------------------------------|-------------------------|----------------------|--|--|
| Acsadi et al., 2009 | Mouse NSC-34 SMN knockdown | Motor neuron-like cells | H ₂ DCFDA | Increased ROS with decreasing SMN levels | 48 and 72 h after <i>Smn</i> knockdown |
| Köstel et al., 2012 | Fibroblasts from SMA type I patients | Fibroblast | H ₂ DCFDA | Increased | NA |

| | | | | | |
|-------------------------|--|--|-------------------------------|-----------------|---|
| Wang et al., 2013 | hESC with SMN-FL or SMN-Δ7 knockdown | Culture was differentiated to motor neurons | MitoSOX | Increased | Day 26 post differentiation (NPS) |
| Ando et al., 2017 | iPSC from SMA type III patients | Culture was differentiated to motor neurons | H ₂ DCFDA, MitoSOX | Increased | Day 42-56 post differentiation (complete differentiation) |
| Patitucci & Ebert, 2016 | iPSC from SMA type I patients | Culture was differentiated to astrocytes and motor neurons | DHE | Decreased | Day 28-42 post differentiation (NPS) |
| Miller et al., 2016 | Δ7 SMA mouse | Spinal cord motor neurons | mito-roGFP | Increased | Post-symptomatic (P9) |
| Thelen et al., 2020 | Taiwanese SMA mouse | Spinal cord motor neurons | CellROX | Increased | Pre-symptomatic (E 13) |
| Chemello et al., 2023 | Muscle-specific <i>Smn1</i> knockout mouse model | Skeletal muscle | Amplex Red | Increased | Post-symptomatic (3 months old) |
| El Khoury et al., 2023 | Taiwanese SMA mouse | Spinal cord motor neurons | DHE | Increased at P8 | Pre-symptomatic (P 6) and disease onset (P8) |

Altogether, those findings demonstrate that the extent of SMN depletion correlates with the observed increase in ROS levels, which could be suggestive of a role for oxidative damage as mechanism leading or exacerbating neurodegeneration. Supporting this idea, histopathological and cellular studies have documented oxidative damage in motor neurons and peripheral tissues in SMA (**Table 1.5**). For instance, in type I SMA patient autopsy samples, Hayashi et al., (2002) reported elevated protein carbonylation (4HNE) in spinal motor neurons, and elevated nucleic acid oxidation (8OHdG) in other tissues of the central nervous system such as precentral cortex,

thalamus and cerebellum, indicating that oxidative damage does not occur only in motor neurons. Another study confirmed the presence of oxidative damage in motor neurons utilising a severe SMA mouse model, which displayed increased protein carbonylation (Thelen, Wirth and Kye, 2020). Notably, the evidence for oxidative damage is not restricted to the central nervous system. For example, increased levels of 3-nitrotyrosine (3NT) and the cardiac oxidative stress marker angiotensin II receptor 1 (AT1) have been detected in the hearts of intermediate and severe SMA mouse models, respectively (Shababi et al., 2012; Maxwell et al., 2018).

Table 1.5. Evidence of oxidative damage in spinal muscular atrophy

4HNE= 4-hydroxynonenal, 8OHdG= 8-hydroxydeoxyguanosine, 3NT= 3-nitrotyrosine, AT-1= angiotensin II receptor 1, E= embryonic, P=postnatal.

| Study | SMA Model | Cell Type | Evidence of Oxidative Damage | Stage |
|-------------------------|----------------------|---------------------------|---|--|
| Hayashi et al., 2002 | Type I SMA patient | Motor neurons | Increased lipid peroxidation (4HNE) and nucleic acid oxidation (8OHdG) | Post-mortem |
| Shababi et al., 2012 | $\Delta 7$ SMA mouse | Cardiomyocytes | Increased protein carbonylation (3NT) | Post-symptomatic (P9) |
| Patitucci & Ebert, 2016 | $\Delta 7$ SMA mouse | Spinal cord motor neurons | No difference in nucleic acid oxidation (8OHdG) | Pre and post symptomatic (P4, 6, and 8) |
| Maxwell et al., 2018 | Taiwanese SMA mouse | Cardiomyocytes | Increased cardiac oxidative damage markers (AT-1 and ATP-synthase FO) from P3 | Pre-symptomatic (P1 and P3) and early onset (P5) |
| Thelen et al., 2020 | Taiwanese SMA mouse | Spinal cord motor neurons | Increased protein carbonylation | Pre-symptomatic (E3) |

1.4.2. Mechanisms triggering oxidative stress in spinal muscular atrophy

The presence of increased ROS production and oxidative damage in SMA support a model of interaction where oxidative stress may participate in the neurodegeneration observed on SMA. Studies have highlighted that oxidative damage to biomolecules, including lipids, proteins and DNA, can induce apoptosis, which could contribute to the observed cell death in SMA.

This idea is nicely described in research conducted utilising in motor neurons derived from pluripotent stem cells mimicking SMA. In a 2013 study employing human embryonic stem cell (hESC)-derived motor neurons with FL-SMN knockdown, researchers demonstrated that SMN depletion was associated with increased oxidative stress and elevated apoptosis, as indicated by heightened caspase-3/7 activity (Wang et al., 2013), key executors of apoptotic cell death (Porter & Jänicke, 1999). These changes were accompanied by impaired axonal outgrowth and motor neuron loss, hallmarks of spinal muscular atrophy (Wang et al., 2013). Notably, treatment with the antioxidant N-acetylcysteine (NAC) led to the complete restoration of the caspase-3/7 activity to control levels and a significant increase in motor neuron survival, although it did not rescue the impaired axonal outgrowth observed in SMA motor neuron cultures (Wang et al., 2013). Furthermore, another study performed in SMA-iPSCs derived spinal motor neurons (Ando et al., 2017) found evidence of increased mitochondrial ROS accompanied of increased apoptotic markers, such as caspase-3 and increased DNA fragmentation, which resulted from apoptotic signalling cascades (Majtnerová and Roušar, 2018). Importantly, treatment with the antioxidant edaravone decreased mitochondrial ROS levels and reduced the presence of apoptotic markers (Ando et al., 2017), supporting the idea that antioxidants can alleviate neurodegeneration in SMA. Additionally, this work focused on elucidating the factors that triggered apoptosis, excluding the involvement of endoplasmic reticulum stress signalling and the mitogen-activated protein kinase (MAPK) family signalling pathway. The findings suggest that the increased apoptosis observed in untreated cultures likely originates from mitochondria, and that the mitochondria targeted-antioxidant effect of edaravone is the responsible for reducing this oxidative stress-induced apoptosis (Ando et al., 2017).

Notably, mitochondrial dysfunction is a recurring feature in SMA (**Table 1.6**), which could explain the elevated levels of ROS and oxidative damage in SMA. Whole proteome and transcriptomic analyses have shown widespread mitochondrial protein dysregulation (Miller et al., 2016; Thelen, Wirth and Kye, 2020; Chemello et al., 2023), which could explain the observed mitochondrial defects, such as abnormal morphology (Schultz et al., 2017; Xu et al., 2016) and increased fragmentation (Miller et al., 2016). Additionally, decreased complex I and IV activity (Thelen, Wirth and Kye, 2020; Chemello et al., 2023), reduced oxygen consumption and respiration (Miller et al., 2016; Chemello et al., 2023), altered membrane potential (Acsadi et al., 2009; Miller et al., 2016; Xu et al., 2016) and decreased ATP production (Acsadi et al., 2009; Thelen et al., 2020) have indicated that mitochondria are dysfunctional in SMA. Importantly, it has been demonstrated that, in SMA mice, the presence of mitochondrial defects precede neurodegeneration suggesting a role for mitochondria in initiating SMA (Miller et al., 2016).

Other studies have also attempted to bridge the knowledge gap between SMN depletion and mitochondrial defects. For instance, in a *C. elegans* severe SMA model, muscle mitochondria were noticed to abnormally positioned throughout the body (Schultz et al., 2017), while in motor neurons from intermediate SMA mice and SMA type I iPSC there was evidence of reduced transport of mitochondria through the axons (Miller et al., 2016; Xu et al., 2016). This aberrant mitochondrial localisation may provide direct evidence linking SMN protein function in intracellular transport to the observed mitochondrial dysfunction and the associated increase in ROS. Furthermore, other studies have shown that treatment with the antioxidant NAC showed promising results in alleviating various mitochondrial defects, such as the impaired mitochondrial dynamics, reduced mitochondrial potential and ATP production, as well as reducing motor neuron degeneration (Thelen et al., 2020; Xu et al., 2016). Collectively, these findings support a model in which SMN deficiency leads to mitochondrial dysfunction, resulting in elevated ROS production and oxidative damage. This cascade contributes to neurodegeneration and may partially explain cell-type specific vulnerability in SMA, as the nervous system is particularly reliant on mitochondrial.

Table 1.6. Evidence of mitochondrial defects on spinal muscular atrophy

$\Delta\Psi_m$ = mitochondrial membrane potential, CcO= cytochrome C oxidase, E=embryonic.

| Study | SMA model | Cell type | Evidence of Mitochondrial Defects | Stage |
|-------------------------|-------------------------------|---|---|---------------------------------------|
| Acsadi et al., 2009 | Mouse NSC-34 SMN knockdown | Motor neuron-like cells | Reduced ATP levels, increased $\Delta\Psi_m$, increased CcO activity, | 48 and 72 h post <i>Smn</i> knockdown |
| Xu et al., 2016 | iPSC from SMA type I patients | Culture was differentiated to motor neurons | Reduced axonal transport, number of mitochondria in axons, and $\Delta\Psi_m$ | Day 24 post differentiation |
| Patitucci & Ebert, 2016 | iPSC from SMA type I | Culture was differentiated to astrocytes | No difference in mitochondrial respiration | Day 14-52 post differentiation |
| Miller et al., 2016 | $\Delta 7$ SMA mouse | Spinal cord motor neurons | Dysregulation of mitochondrial genes, reduced mitochondrial respiration, reduced $\Delta\Psi_m$, reduced axonal transport; increased fragmentation | Day 7 post differentiation |
| Thelen et al., 2020 | Taiwanese SMA mouse | Spinal cord motor neurons | Dysregulation of mitochondrial proteins, reduced number of mitochondria in axons, reduced mitochondrial respiration, decreased complex I activity | Pre-symptomatic (E13) |

| | | | | |
|-----------------------|---|-----------------|---|---------------------------------|
| Chemello et al., 2023 | Muscle-specific Smn1 knockout mouse model | Skeletal muscle | Dysregulation of mitochondrial genes, ultrastructural alterations, reduced mitochondrial respiration, reduced complex I and IV activity | Post-symptomatic (3 months old) |
|-----------------------|---|-----------------|---|---------------------------------|

A recent study has associated the increased presence of ROS with the overexpression of NOX4 in a severe SMA mouse model (El Khoury et al., 2023). NOX4 is expressed in endoplasmic reticulum, plasma membrane, and nucleus and contribute to the generation of H₂O₂ (Sies and Jones, 2020). In this study, it was demonstrated that pharmacological inhibition of NOX4 in SMA mice resulted in decreased ROS levels and provided significant neuroprotection for motor neurons, evident by reduced motor neuron degeneration, reduced NMJ atrophy, improved motor behaviour and extension of lifespan (El Khoury et al., 2023). NOX4 constitutes an alternative mechanism independent of mitochondria that could explain elevated ROS and oxidative damage in SMA.

Interestingly, El Khoury et al., (2023) not only demonstrated that NOX4 inhibition reduced ROS levels, but also increased SMN protein expression in the spinal cord and motor neurons. Moreover, it was found that antioxidant treatment in SMA fibroblasts led to the concentration dependent increase in the number of Gemini that are nuclear aggregates that contain concentrated SMN protein levels (Ando et al., 2017). We have already explored that ROS can directly attack nucleic acid (Ock et al., 2012; Sharma et al., 2016), and that there is evidence of oxidative damage to DNA in SMA (Hayashi et al., 2002). Importantly, there are studies that have explored the specific interplay between oxidative stress and SMN expression. For instance, an *in vitro* study performed in HeLa cells highlighted that, due to the presence of cysteine residues within its amino acid sequence, the SMN protein might be particularly vulnerable to oxidation (Wan et al., 2008). It was demonstrated that inducing oxidative stress can promote the formation of disulfide cross-links between SMN proteins *in vitro*, potentially reducing their functionality and facilitating its degradation by the proteosome system (Wan et al., 2008). Additionally, a later report suggested

that induction of oxidative stress can decrease exon 7 inclusion in *SMN2* transcripts, potentially diminishing the levels of full-length functional SMN protein (Seo et al., 2016). Notably, this effect can be reverted by some antioxidant compounds, such as curcumin (CUR), epigallocatechin gallate (EGCG), and resveratrol. Studies have shown that treatment with the aforementioned antioxidants promoted exon 7 inclusion in the *SMN2* gene of SMA type I patient's fibroblasts, which lacked *SMN1* but retained two intact copies of *SMN2*, increasing SMN protein levels (Dayangac-Erden et al., 2011; Sakla & Lorson, 2008a). Although SMA type I fibroblasts have been shown to exhibit elevated levels of ROS (Köstel, Bora-Tatar and Erdem-Yurter, 2012), and a reduction in ROS could plausibly account for the observed therapeutic effects — given the capacity of oxidative stress to diminish SMN protein levels (Wan et al., 2008; Seo et al., 2016) — the authors did not select the compounds based on their antioxidant properties, nor did they attribute the observed benefits to a reduction in ROS. Instead, these compounds were proposed to act as histone deacetylase (HDAC) inhibitors, which act by relaxing the chromatin structure and enabling the binding of the transcriptional machinery to targeted genes (Kelly, O'Connor and Marks, 2002). Nevertheless, these studies indicated that increased oxidative stress can reduce SMN protein levels *in vitro*, highlighting the relevance of antioxidant treatment, which could potential increase SMN protein levels. Overall, these findings underscore the importance of evaluating the off-target effects of antioxidant compounds and caution against drawing definitive conclusions regarding their mechanisms of action solely based on observed therapeutic benefits.

1.4.3. Oxidative stress in spinal muscular atrophy: cause or consequence?

All the studies reviewed until now support a model in which increased ROS levels lead or exacerbate neurodegeneration, highlighting the importance of antioxidant treatment as an effective therapeutic avenue for SMA. However, few studies have challenged that interpretation. Despite the extensive evidence of increased ROS production in SMA (**Table 1.4**), Patitucci & Ebert (2016) found that neither SMA iPSC-derived motor neurons nor astrocytes exhibited

increased ROS levels; in fact, they displayed a reduction in ROS compared to control cells. Although measurements were taken at the neuronal progenitor stage (NPC), when cells are not fully differentiated into motor neurons or astrocytes, at this stage motor neurons already exhibited neurodegeneration, and astrocytes showed altered morphology and dysfunction (Patitucci and Ebert, 2016). Notably, this observation contradicts the results obtained in other studies, which can be attributed to differing methodologies or SMA models employed.

For instance, although both Patitucci & Ebert (2016) and Ando et al., (2017) utilised SMA-iPSCs, the former study measured ROS levels at the NPC stage when the cells were not fully differentiated, whereas the later assessed ROS levels when cells were fully differentiated. This could indicate that ROS does not occur before neurodegeneration, but it is produced afterwards as a secondary consequence of SMN depletion. Another study in pluripotent stem cells, however, found that ROS was increased at the NPC stage (Wang et al., 2013). Researchers employed RNAi SMN knockdown in human hESCs, which may have resulted in a more pronounced generation of ROS than the one observed in iPSC cultures at the same stage. The discrepancies between studies highlight the necessity of employing different SMA models to confirm the results before moving to clinical trials, as small differences in the genetics of methodologies can lead to different results. Nevertheless, research conducted by Patitucci & Ebert (2016) suggested that, at least in the context of iPSC cultures, the generation of ROS does not precede neurodegeneration in SMA, suggesting a different relationship between oxidative stress and SMA than the one suggested by other studies. However, these findings do not rule out the potential role of ROS in exacerbating SMA physiopathology.

These findings raise important considerations regarding previously reported beneficial effects of antioxidants in SMA (**Table 1.7**). A significant limitation in many studies is the use of a single antioxidant, typically NAC or edaravone, making it difficult to conclusively attribute therapeutic benefits solely to ROS modulation. For instance, Thelen et al., (2020) demonstrated that NAC treatment reduced ROS, increased ATP, and improved protein synthesis in SMA cells. Interestingly, treatment with pyruvate similarly reduced ROS and increased ATP but failed to

restore protein synthesis, suggesting that NAC's beneficial effects on protein synthesis might be independent of its antioxidant capacity (Thelen, Wirth and Kye, 2020). If researchers had exclusively focused on NAC, they might have erroneously concluded that the enhancement in protein synthesis was attributable solely to the reduction in oxidative stress. Consequently, employing a diverse array of antioxidants is essential to ascertain whether the observed benefits are genuinely reliant on ROS or if they involve alternative molecular targets. The existing variability in ROS measurement methodologies, experimental models, developmental stages assessed, and limited use of multiple antioxidants complicates comparisons between studies. Therefore, distinguishing whether oxidative stress contributes causally to SMA or occurs merely as a downstream consequence remains challenging.

Table 1.7. Effect of reactive oxygen species modulation in spinal muscular atrophy

| Study | SMA model | Cell type | Pro-oxidative/Antioxidant compound used | Observed Effects |
|---------------------|---|--|--|---|
| Wan et al., 2008 | NA | HeLa cells | Pro-oxidant β -lapachone | SMN disulfide crosslinks |
| Seo et al., 2016 | Mild SMA mouse | Brain, heart, kidney, liver, lung, muscle, spinal cord | Pro-oxidant Paraquat | Skipping of exons 7 and 5 in <i>SMN2</i> |
| Köstel et al., 2012 | Fibroblasts from SMA type I patients | Fibroblasts | Antioxidants Curcumin, Vitamin E, NAC | Reduced ROS |
| Wang et al., 2013 | hESC with SMN-FL or SMN- $\Delta 7$ knockdown | Culture was differentiated to motor neurons | Antioxidant NAC | Prevented motor degeneration; did not rescue axonal outgrowth defects |
| Xu et al., 2016 | iPSC from SMA type I patients | Culture was differentiated to motor neurons | Antioxidant NAC | Reduced mitochondrial defects; rescued neurodegeneration |
| Ando et al., 2017 | iPSC from SMA type III patients | Culture was differentiated to motor neurons | Edaravone | Reduced apoptosis |

| | | | | |
|------------------------|---------------------------|------------------------------|-----------------------------------|--|
| Thelen et al., 2020 | Taiwanese SMA mouse | Spinal cord motor neurons | Antioxidants NAC, and Pyruvate | NAC reduced ROS, increased ATP, improved protein synthesis; pyruvate reduced ROS but did not affect protein synthesis |
|------------------------|---------------------------|------------------------------|-----------------------------------|--|

To address this complexity, Van Raamsdonk & Hekimi, (2010) proposed a clear experimental framework to differentiate between causality (contribution) and association (consequence) of oxidative stress in neurodegeneration (**Figure 1.6**). According to their model, if oxidative stress directly contributes to disease pathology, increasing ROS levels by utilising pharmacological or genetic approaches should accelerate the disease onset or exacerbate its severity, whereas reducing ROS should mitigate or delay symptoms. Conversely, if oxidative stress arises solely as a consequence of neurodegeneration, without a direct impact on the disease, altering ROS levels would have minimal or no impact on disease progression. To robustly test this hypothesis in SMA, experiments must evaluate multiple antioxidants simultaneously as well as identifying the main dysregulated pathways that contribute to increased ROS levels. If oxidative stress truly drives SMA pathology, diverse antioxidants should yield consistent beneficial effects, as observed in Alzheimer's and Parkinson's disease models (Table 1.3).

Conclusively determining whether oxidative stress is causative or consequential in SMA pathogenesis is fundamental to elucidate the underlying mechanisms of neurodegeneration in SMA and develop targeted therapies that improve beneficial effects for patients.

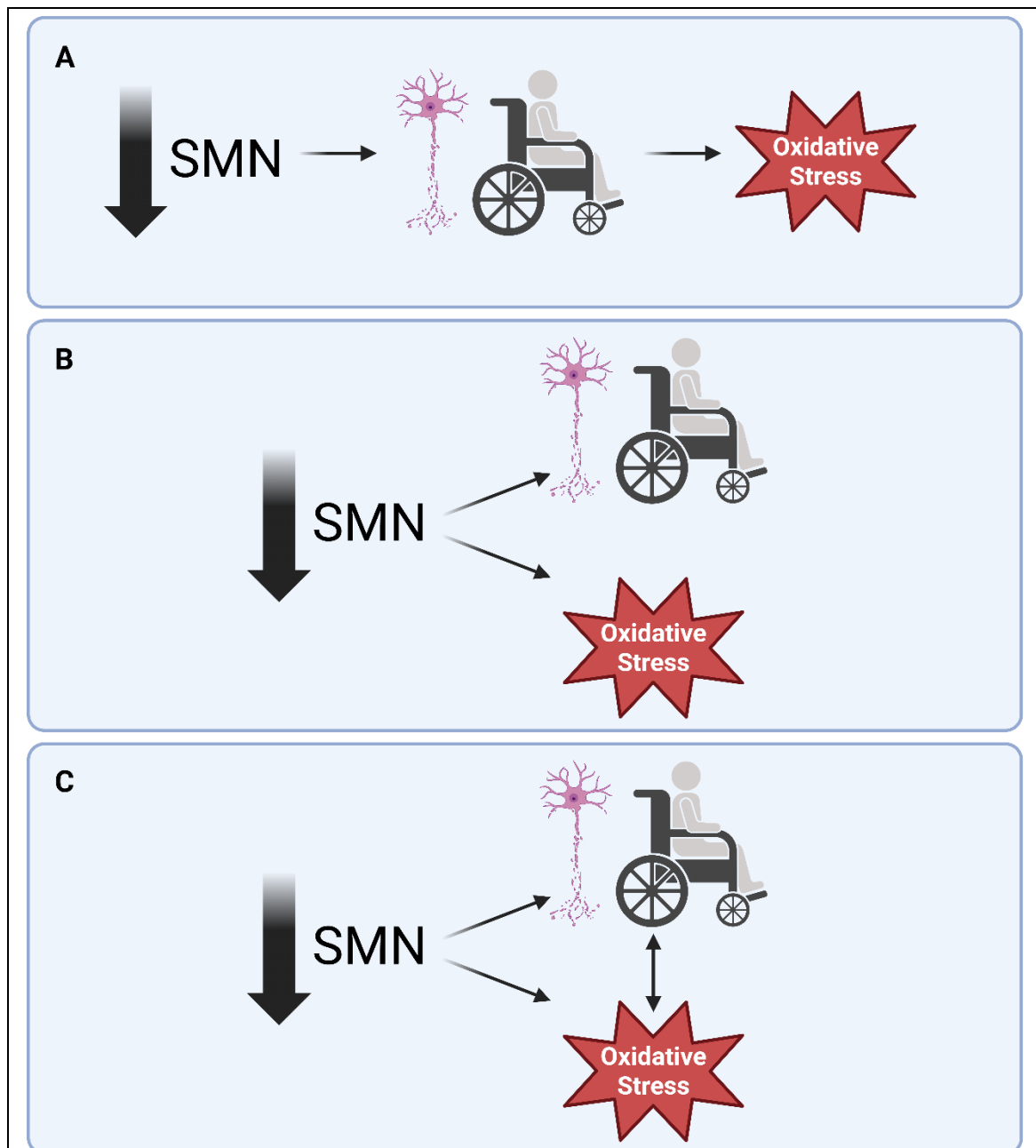


Figure 1.6. Hypothetical models illustrating the interplay between SMN depletion and oxidative stress in the pathophysiology of spinal muscular atrophy

(A) Oxidative stress emerges as a downstream effect of motor neuron degeneration caused by SMN deficiency. In this scenario, antioxidant treatment is likely to be ineffective in alleviating SMA neuromuscular phenotypes.

(B) Oxidative stress and neurodegeneration are parallel outcomes independently triggered by SMN deletion, but without direct correlation. In this scenario, antioxidant treatment is likely to be ineffective in alleviating SMA neuromuscular phenotypes.

(C) Oxidative stress is both a parallel consequence of SMN deficiency and an exacerbating factor that worsens neurodegeneration and muscular dysfunction, thereby contributing to disease progression. In this scenario, antioxidant treatment could ameliorate SMA neuromuscular phenotypes.

1.5. Aims and objectives

The overall aim of this thesis is to investigate the role of oxidative stress in SMA pathology with the ultimate goal to elucidate whether antioxidant therapies hold a genuine therapeutic promise.

The project is structured around three experimental chapters, each addressing a key aspect of the relationship between oxidative stress and SMA.

1. Evaluate whether oxidative stress can be identified in the *smn-1(ok355)* severe *C. elegans* SMA model and evaluate its potential contribution to disease pathology.
2. To determine whether antioxidant treatment can mitigate SMA neuromuscular phenotypes.
3. To identify whether precise modulation of endogenous redox pathways alters disease severity, thereby identifying potential redox-based therapeutic targets specifically relevant to SMA.

Altogether, the integrated objectives of this thesis aim to clarify whether oxidative stress is a causative factor, a contributing amplifier, or a downstream consequence in SMA pathology. By combining physiological, pharmacological, and genetic approaches in a tractable model organism, this work seeks to resolve key scientific questions regarding the role of redox imbalance in SMA and to inform the design of targeted therapeutic strategies that go beyond SMN restoration.

Chapter II. Materials and Methods

2.1. General solutions and media

Solutions used throughout this project were prepared and stored as followed.

1. 1X M9 buffer.

Chemicals (for 1 L):

| | |
|---------------------------------|---------------|
| KH ₂ PO ₄ | 3 g |
| Na ₂ PO ₄ | 6 g |
| NaCl | 5 g |
| Deionised H ₂ O | Top up to 1 L |

After adding the listed chemicals, the solution was sterilized by autoclaving. Then, the following sterilized solution was added:

| | |
|-----------------------|-----|
| 1 M MgSO ₄ | 1mL |
|-----------------------|-----|

Store at room temperature.

2. Lysis Buffer

Chemicals (for 10 mL):

| | |
|-----------------------|---------|
| 1 M KCl | 500 µL |
| 1 M Tris (pH 8.2) | 100 µL |
| MgCl ₂ | 1000 µL |
| 20% NP-40 | 225 µL |
| 20% Tween 20 | 225 µL |
| 10% Gelatine | 10 µL |
| Sterile Milli-Q water | 7940 µL |

Aliquot 250mL of the lysis buffer solution into 1.5 mL Eppendorf tubes and store at -20°C.

3. Freezing solution.

Chemicals (for 1L):

| | |
|---------------------------------|--------|
| NaCl | 5.85 g |
| KH ₂ PO ₄ | 6.8 g |
| 1M NaOH | 5.6 mL |

| | |
|----------------------------|------------------|
| Deionised H ₂ O | 800 mL |
| Glycerol | 300 g |
| Deionised H ₂ O | Top up until 1 L |

Store at room temperature.

4. Freezing solution agar.

Chemicals (for 100 mL):

| | |
|-------------------|--------|
| Freezing solution | 100 mL |
| Agar | 0.4 g |

Store at room temperature.

5. Nematode Growth Media (NGM) agar.

Chemicals (for 500 mL):

| | |
|----------------------------|----------|
| Agar bacteriological | 8.5 g |
| Peptone | 1.25 g |
| NaCl | 1.5 g |
| Deionised H ₂ O | 487.5 mL |

The media was sterilized by autoclaving, after which the following sterilized solutions were added:

| | |
|----------------------------|---------|
| 1M Potassium phosphate pH6 | 12.5 mL |
| 1M MgSO ₄ | 0.5 mL |
| 1M CaCl ₂ | 0.5 mL |
| 5 mg/mL cholesterol | 0.5 mL |

NGM agar was poured into 55 mm triple-vented Petri dishes while still hot. Agar plates were left to dry on the bench for 24 h, covered with filter paper. The following day, plates were seeded with 200 μ L of OP50 *Escherichia coli* (*E. coli*) in a sterile environment. Seeded plates were left on the bench, covered with filter paper, for three days until the bacterial lawn was completely dry. Plates were stored at room temperature in plastic boxes and used within one week, with a fresh batch of plates prepared weekly.

2.2. Strains and maintenance

Caenorhabditis elegans (*C. elegans*) strains listed in **Table 2.1** were maintained on Nematode Growth Media (NGM) plates seeded with OP50 *E. coli* and incubated at 20°C as previously described (Brenner, 1974). To prevent starvation, four early L4 animals of each strain were transferred to freshly seeded plates every few days using a dissection microscope, and a platinum wire sterilised with an ethanol burner.

Table 2.1. List of *C. elegans* strains used in this project

The ‘strain’ column lists the designated *C. elegans* strain name, the ‘identifier’ column highlights the name used in this thesis to refer to each strain and the ‘genotype’ column specifies the genetic modification(s) that characterise each strain, including allele names and chromosome location.

| Strain | Identifier | Genotype |
|--------|---------------------------------------|---|
| N2 | N2 | Wildtype |
| LM99 | <i>smn-1(ok355)</i> | <i>smn-1(ok355) I/hT2[bli-4(e937) qIs48[myo-2p::GFP; pes-10p::GFP; ges-1p::GFP]] (I;III)</i> |
| HA1981 | <i>smn-1(+)</i> | <i>(+)/hT2[bli-4(e937) qIs48[myo-2p::GFP; pes-10p::GFP; ges-1p::GFP]] (I;III)</i> |
| HA2824 | <i>smn-1(rt248)</i> | <i>smn-1(rt248) I/hT2[bli-4(e937) qIs48[myo-2p::GFP; pes-10p::GFP; ges-1p::GFP]] (I;III)</i> |
| HA2452 | <i>smn-1(ok355); rtSi9</i> | <i>smn-1(ok355) I/hT2[bli-4(e937) qIs48[myo-2p::GFP; pes-10p::GFP; ges-1p::GFP]] (I;III); rtSi9[<i>Cb-unc-119(+)</i>] IV</i> |
| HA2454 | <i>smn-1(ok355); [smn-1(+)]</i> | <i>smn-1(ok355) I/hT2[bli-4(e937) qIs48[myo-2p::GFP; pes-10p::GFP; ges-1p::GFP]] (I;III); rtSi10[<i>smn-1p::smn-1;Cb-unc-119(+)</i>] IV</i> |
| GA187 | <i>sod-1(tm776)</i> | <i>sod-1(tm776) II</i> |
| DIM17 | <i>sod-1(tm776)</i> | <i>(+)/hT2[bli-4(e937) qIs48[myo-2p::GFP; pes-10p::GFP; ges-1p::GFP]] (I;III); sod-1(tm776) II</i> |
| DIM18 | <i>smn-1(ok355); sod-1(tm776)</i> | <i>smn-1(ok355) I/hT2[bli-4(e937) qIs48[myo-2p::GFP; pes-10p::GFP; ges-1p::GFP]] (I;III); sod-1(tm776) II</i> |
| RB1072 | <i>sod-2(ok1030)</i> | <i>sod-2(ok1030) I</i> |

| | | |
|----------------|--|--|
| DIM42 | <i>sod-2(ok1030)</i> | <i>sod-2(ok1030) I/hT2[bli-4(e937) qls48[myo-2p::GFP; pes-10p::GFP; ges-1p::GFP]] (I,III)</i> |
| PHX6174 | <i>smn-1(ok355); sod-2(ok1030)</i> | <i>sod-2 (ok1030) smn-1(ok355) I/hT2[bli-4(e937) qls48[myo-2p::GFP; pes-10p::GFP; ges-1p::GFP]] (I,III)</i> |
| GA186 | <i>sod-3(tm760)</i> | <i>sod-3(tm760) X</i> |
| DIM13 | <i>sod-3(tm760)</i> | <i>(+)/hT2[bli-4(e937) qls48[myo-2p::GFP; pes-10p::GFP; ges-1p::GFP]] (I,III); sod-3(tm760) X</i> |
| DIM14 | <i>smn-1(ok355); sod-3(tm760)</i> | <i>smn-1(ok355) I/hT2[bli-4(e937) qls48[myo-2p::GFP; pes-10p::GFP; ges-1p::GFP]] (I,III); sod-3(tm760) X</i> |
| GA416 | <i>sod-4(gk101)</i> | <i>sod-4(gk101) III</i> |
| DIM15 | <i>sod-4(gk101)</i> | <i>sod-4(gk101) III/hT2[bli-4(e937) qls48[myo-2p::GFP; pes-10p::GFP; ges-1p::GFP]] (I,III)</i> |
| DIM16 | <i>smn-1(ok355); sod-4(gk101)</i> | <i>smn-1(ok355) I;sod-4(gk101) III/ hT2[bli-4(e937) qls48[myo-2p::GFP; pes-10p::GFP; ges-1p::GFP]] (I,III)</i> |
| GA503 | <i>sod-5(tm1146)</i> | <i>sod-5(tm1146) II</i> |
| DIM19 | <i>sod-5(tm1146)</i> | <i>(+)/hT2[bli-4(e937) qls48[myo-2p::GFP; pes-10p::GFP; ges-1p::GFP]] (I,III); sod-5(tm1146) II</i> |
| DIM20 | <i>smn-1(ok355); sod-5(tm1146)</i> | <i>smn-1(ok355) I/hT2[bli-4(e937) qls48[myo-2p::GFP; pes-10p::GFP; ges-1p::GFP]] (I,III); sod-5(tm1146) II</i> |
| PHX8399 | <i>smn-1(ok355) I/hT2[smn- 1(syb8399)]</i> | <i>smn-1(ok355) I/hT2 [smn-1(syb8399); bli-4(e937) qls48[myo-2p::GFP; pes-10p::GFP; ges-1p::GFP]] (I,III)</i> |

Strains used in this study were sourced by the *Caenorhabditis* Genetics Center (CGC), the Hart Lab (designated by "HA") or the Dimitriadi Lab (designated by "DIM") PHX6174 and PHX8399 strains were generated by Suny Biotech (Zhejiang University Sunny Technology Co.,Ltd). The heterozygous PHX8399 (*smn-1(ok355) I/hT2[smn-1(syb8399)*) strain carries an endogenous wild-type copy of *smn-1* tagged to *wrmScarlet* using CRISPR/Cas9-mediated genome editing to allow for the visualisation of the endogenous SMN-1 protein. All strains were confirmed by PCR-genotyping and/or sequencing prior to experimental procedures.

Maintenance of homozygous *smn-1(ok355)* animals is restricted by their lethality at the L4 stage (Briese et al., 2008). To overcome this we used the well characterised LM99 strain where *smn-1(ok355)* animals are the progeny of heterozygous hermaphrodites; the latter carry the *smn-1(ok355)* mutation in one allele of chromosome I and an *hT2[bli-4(e937) qIs48[myo-2p::GFP; pes-10p::GFP; ges-1p::GFP]] (I;III)* balancer chromosome on the other allele (Briese et al., 2008). To maintain a consistent genetic background, all strains used throughout the project were crossed into the *hT2 (I;III)* balancer chromosome. Therefore, homozygous animals used in all experimental procedures were first-generation offspring from *hT2* parents (**Figure 2.1**). All strains carrying *hT2 (I;III)* integrated transgene were maintained based on their pharyngeal GFP fluorescence (*myo-2p::GFP*) (Briese et al., 2008).

Throughout this thesis, control animals were always the non-GFP progeny of HA1981 animals (*smn-1(+)*), with the only exception in the antioxidant drug treatment experiments, where heterozygous *smn-1(ok355)/hT2* animals (LM99) were used instead of *smn-1(+)*. Previous work by (Briese et al., 2008) has demonstrated that N2 (wild type) and heterozygous *smn-1(ok355)/hT2* animals look identical and behave similarly in various neuromuscular assays used herein such as pharyngeal pumping and locomotion. The same applies for other behavioural assays tested in *C. elegans* such as swimming (thrashing) and lifespan (Briese et al., 2008). Furthermore, our own data have also indicated that the non-GFP progeny of HA1981 (*smn-1(+)*) and *smn-1(ok355)/hT2* heterozygous animals both exhibit no significant difference in their cytoplasmic ROS content. Therefore, *smn-1(ok355)/hT2* heterozygous animals were considered suitable controls for the drug treatment experiments. It should also be noted that as these experiments required the use of NGM plates containing drugs, using *smn-1(ok355)/hT2* animals as controls allowed for a more efficient use of resources, as both *smn-1(ok355)/hT2* controls and *smn-1(ok355)* mutant animals could be derived from the same strain (i.e. LM99), reducing the amount of chemical substance needed to carry out the experiments.

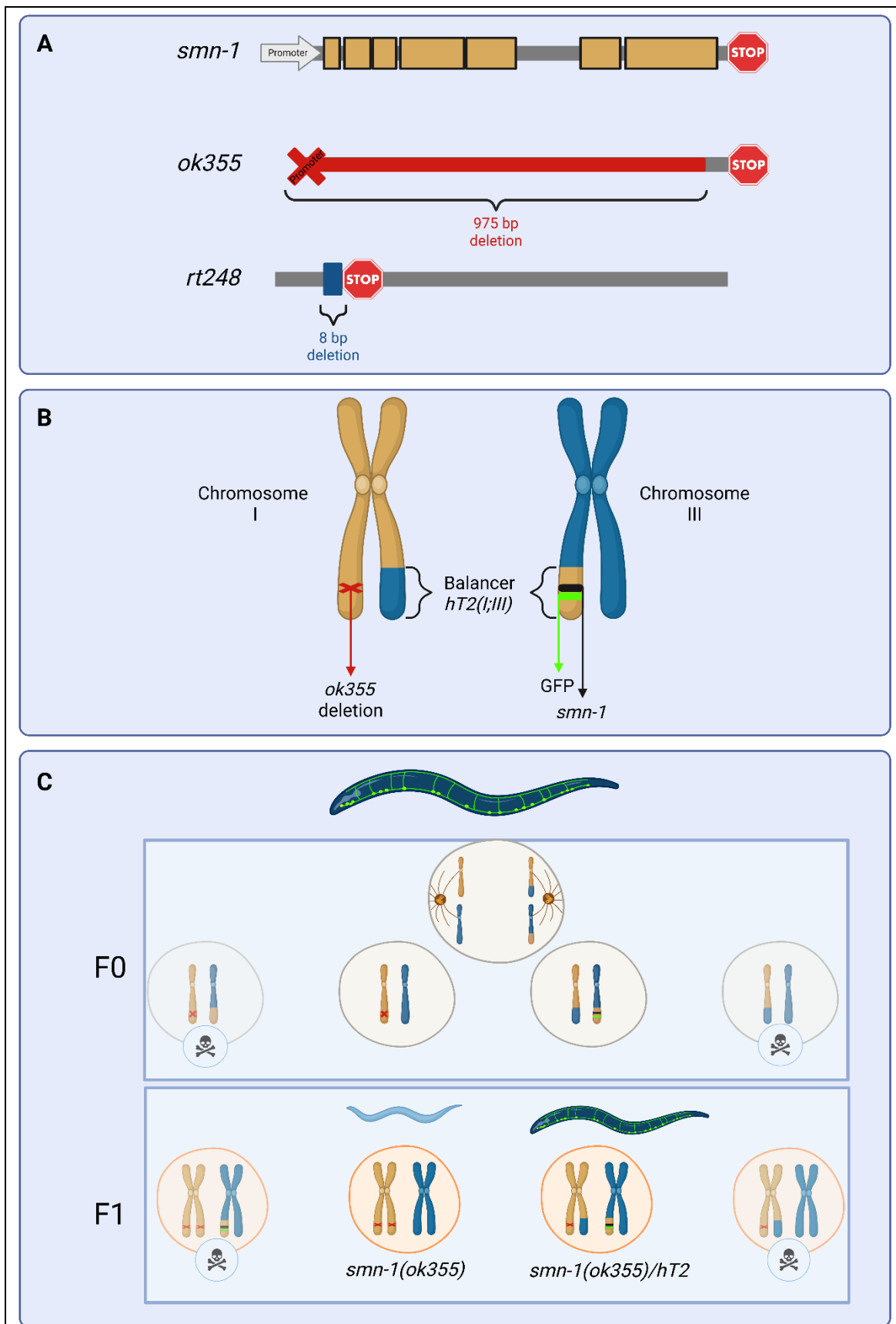


Figure 2.1. The *Caenorhabditis elegans smn-1* endogenous gene and the *C. elegans* SMA severe models and maintenance

(A) Schematic representation of the *smn-1* gene and the mutations used in this study. The *ok355* allele consists of a 975 bp deletion that abrogates the majority of the *C. elegans smn-1* gene, including the promoter and initial coding region, and leaving only 87 bp at the 3' end of the gene, including the stop codon. The *rt248* allele contains an 8bp deletion in exon 2, introducing a premature stop codon.

(B) Schematic representation of the *hT2(I;III)* genetic balancer utilised to maintain the lethal *smn-1(ok355)* allele. The *ok355* deletion is located on chromosome I. The *hT2 (I;III)* balancer compromise a reciprocal translocation of chromosomal segments between chromosomes I and III. A GFP marker located within the chromosomal segment of the hT2 balancer allows the distinction of homozygous *smn-1(ok355)* (no GFP) and heterozygous *smn-1(ok355)/hT2* animals (GFP).

(C) Genetic crosses illustrating the maintenance strategy for *smn-1(ok355)* animals. During meiosis in heterozygous *smn-1(ok355)/hT2* hermaphrodites (F0 generation), homologous chromatids segregate randomly, generating haploid gametes with only one copy of each chromosome. Following fertilization, the resulting F1 embryos are diploid. Only two genotypes are viable: *smn-1(ok355)/hT2* animals (green fluorescent) and homozygous *smn-1(ok355)* mutants (non-fluorescent), which exhibit SMA-like phenotypes.

2.3. Freezing and thawing stocks

C. elegans strains can be frozen and preserved for long-term storage with minimal impact on their fitness (Stiernagle, 2006; Stastna et al., 2020). The nematodes were cultivated on five to ten NGM plates at 20°C until the bacterial lawn was fully consumed, resulting in a population primarily consisting of L1 larvae since these animals have an increased survival rate (Brenner, 1974). Nematodes were then washed off the plates using 1x M9 buffer and collected in a Falcon tube. The suspension was centrifuged at 1000 rpm for 1 min to pellet the animals, and the supernatant was then carefully removed. A 0.4% agar-freezing solution was added to the nematode suspension in a 1:1 ratio, and gently mixed. The glycerol contained in the freezing solution acts as a cryoprotectant, minimising osmotic shock and ice crystal formation, thereby enhancing the survival rate of the frozen strains (Murray & Gibson, 2022).

The nematode-freezing solution mixture was transferred to 1mL cryovials, which were then placed in styrofoam rack to facilitate gradual cooling at -80 °C. To verify the success of the freezing process, a small aliquot from a cryovial was thawed onto a seeded NGM plate and incubated at 20 °C one week after freezing. If nematodes are observed crawling on the plate within a few days, the freezing process is deemed successful. When using a thawed strain, it is essential to decontaminate the animals upon reaching adulthood.

2.4. Decontamination of stocks

Although aseptic technique must be always maintained to prevent the contamination of *C. elegans* stocks, strains may occasionally become contaminated with bacteria, yeast or mould. Contaminated strains cannot be used for experiments, as contamination can alter various scientific parameters, such as gene expression, survival rates, and behavioural assays (O'Donnell et al., 2020; Ahamefule et al., 2021).

Most contaminants can be effectively eliminated by treating with a hypochlorite solution (Stiernagle, 2006). A 10% hypochlorite solution was prepared by adding 10 µL of commercially

available hypochlorite (1x bleach solution) to 90 µL of 1x M9 buffer. A drop of 10% hypochlorite (10 µL) was placed on the edge of a NGM plate away from food, before adding seven to ten gravid contaminated adults to the hypochlorite solution. Plates are subsequently incubated at 20°C overnight. The eggshell of *C. elegans* is impermeable (Stein and Golden, 2018), allowing eggs to remain unaffected, while contaminants and live nematodes are eliminated by the bleach treatment. Once eggs hatch and the larvae emerge into the clean OP50 food, a single L1 animal was transferred to a freshly seeded NGM plate (one L1/plate) and allowed to grow at 20°C to confirm the removal of any subsequent contamination.

2.5. Synchronisation of *Caenorhabditis elegans* populations

All experiments detailed in this thesis were performed using *smn-1(ok355)* animals at day-3 post hatching, as previously described (Dimitriadi et al., 2010, 2016) (**Table 2.2**). Briefly, gravid adults were placed onto seeded NGM plates and allowed to lay eggs for 5 h while incubating at 25°C. Adult animals were then removed, and the egg-containing plates were placed at 25°C for 48 h. Lastly, plates were shifted to 20°C for 24 h prior to selecting day 3 animals for assaying.

Table 2.2. Standard egg-laying procedure to synchronise *C. elegans* populations at day-3 post-hatching, as described by Dimitriadi et al., 2010

All genotypes used in the experiments were obtained following incubation for three days at 25 °C, 25 °C and 20°C on day one, two and three of development, respectively.

| Procedure A | Parental strain genotype | Day 0 | | | Day 1 | Day 2 | Day 3 offspring genotype | Stage |
|--|--------------------------------|-----------------------------------|---------------|------|-------|-------|--------------------------------|-------|
| Standard egg-laying (Dimitriadi et al., 2010) | <i>smn-1(ok355)/hT2</i> | Egg- lay 25°C for 5 h | Remove adults | 25°C | 25°C | 20°C | <i>smn-1(ok355)</i> | L4 |
| | | | | | | | <i>smn-1(ok355)/hT2</i> | Adult |
| | <i>smn-1(+)/hT2</i> | | | | | | <i>smn-1(+)</i> | Adult |

An additional an egg laying protocol was optimised for experimental procedures to match the developmental stage observed in *smn-1(ok355)* animals at day-3. The egg-laying protocol was optimised with a different temperature paradigm to slow down the growth of control animals, so they would match the growth rate of *smn-1(ok355)* nematodes (**Table 2.3**). All animals were incubated at 20°C 24h prior to experiments.

Table 2.3. Egg-laying experimental procedure for obtaining synchronous *C. elegans* L4-stage populations

smn-1(ok355) nematodes were obtained by standard egg-laying procedures as described above (25°C, 25°C, 20°C). Day-3 L4-stage *smn-1(ok355)/hT2* nematodes were obtained by lowering the temperature paradigm of incubation to 15°C, 20°C, 20°C on day one, two and three of development, respectively. L4-stage *smn-1(+)* animals were obtained after two days of incubation at 20°C.

| Procedure B | Parental strain genotype | Day 0 | | | Day 1 | | | Day 2 | Day 3 offspring genotype | Stage |
|--|--------------------------|----------------------|---------------|-------|--------------|---------------|------|-------|--------------------------|-------|
| Egg-laying for synchronous L4 populations, adapted from Dimitriadi et al., 2010. | smn-1(ok355)/hT2 | Egg-lay 25°C for 5 h | Remove adults | 25°C | 25°C | | | 20°C | smn-1(ok355) | L4 |
| | | | | 15 °C | 20°C | | | 20°C | smn-1(ok355)/hT2 | L4 |
| | smn-1(+)/hT2 | | | | Day 0 | | | Day 1 | Day 2 Genotype | Stage |
| | | | | | Egg-lay 25°C | Remove adults | 20°C | 20°C | smn-1(+) | L4 |

2.6. Genotyping

2.6.1. DNA extraction

For DNA extraction from single nematodes a lysis solution was prepared by gently mixing 10 µL of 10mg/ml proteinase K into 250 µL of lysis buffer. Aliquots of 5 µL of lysis solution were dispensed into each PCR tube. Single nematodes were picked and placed into the 5 µL of lysis solution in the appropriate labelled tube, ensuring minimal transfer of OP50 bacteria.

PCR-genotyping was then performed using a thermal cycler program (add the make of the PCR machine here) set to 60°C for 1 hour, followed by 95°C for 15 min, and then cooling at 4°C (**Table 2.4**). At this point, *C. elegans* lysates could be used directly for PCR or stored at -20 °C for future analysis.

Table 2.4. Thermal cycler programs for *C. elegans* lysis and PCR

| Program | No of cycles | Temperature | Time |
|--|--------------|-------------|--------|
| Nematode lysis | 1 | 60°C | 1 h |
| | 1 | 95°C | 15 sec |
| | 1 | 4°C | Hold |
| PCR for <i>smn-1</i> , <i>sod-2</i> and <i>sod-4</i> genes | 1 | 95°C | 2 sec |
| | 30 | 95°C | 30 sec |
| | | 61°C | 30 sec |
| | | 68°C | 1 min |
| | 1 | 68°C | 5 min |
| | 1 | 4°C | Hold |
| PCR for <i>sod-1</i> , <i>sod-3</i> and <i>sod-5</i> genes | 1 | 95°C | 2 min |
| | 30 | 95°C | 30 sec |
| | | 63°C | 30 sec |
| | | 68°C | 1 min |
| | 1 | 68°C | 5 min |
| | 1 | 4°C | Hold |

2.6.2. Polymerase chain reaction (PCR)

Each PCR-genotyping reaction included 1x PCR buffer, 200 µM dNTPs and 0.05 units/µL Taq polymerase to a final volume of 20 µL per PCR tube by using autoclaved distilled dH₂O. **Table 2.4** highlights the thermal cycling conditions used, whereas primer sequences for each gene investigated are outlined in **Table 2.5**.

Table 2.5. Primers used for PCR genotyping

| Gene | Primers | |
|--------------|-----------|-----------------------------|
| <i>smn-1</i> | Forward 1 | 5'- gctcaaaacttaaactccgcctc |
| | Forward 2 | 5' - tgaagaagctattgcggacg |
| | Reverse | 5'- agcctccaaatatcgtctcc |

| | | |
|--------------|-----------|-----------------------------|
| <i>sod-1</i> | Forward 1 | 5'- ccttctccgtcagaactgttg |
| | Forward 2 | 5' - ccctcgctggaaagttag |
| | Reverse | 5'- ctatcgactgtgatctgcctg |
| <i>sod-2</i> | Forward 1 | 5' - agaagagatgggctaaggac |
| | Reverse | 5' - gtagtaagegtgctcccaga |
| <i>sod-3</i> | Forward 1 | 5'- tctactgctgcactgcttc |
| | Forward 2 | 5' - ccaagcacactctcccagatc |
| | Reverse | 5'- cagagccttgaaccgaatag |
| <i>sod-4</i> | Forward 1 | 5'- ggtggaatcgaactcggagtg |
| | Forward 2 | 5'- accagcacttagacaaccatttc |
| | Reverse | 5'- agccgcttccgaaggtaaac |
| <i>sod-5</i> | Forward 1 | 5'- gttgtgtgtgtggtcgttgagc |
| | Forward 2 | 5'- ctcgttaggtattggcgacag |
| | Reverse | 5'- gagcaatgactccacaagcag |

Table 2.6. PCR master mix for genes utilised in this thesis

| Master mix | Components | μL per tube |
|-------------------------------|--------------------------------|-------------|
| <i>smn-1, sod-2 and sod-4</i> | dH ₂ O | 15.025 |
| | Buffer (1x) | 2.5 |
| | dNTPs (200 μM) | 0.25 |
| | F1 (10 μM) | 0.7 |
| | F2 (10 μM) | 0.7 |
| | R1 (10 μM) | 0.7 |
| | Taq Polymerase (0.05 units/μL) | 0.125 |
| <i>sod-1, sod-3 and sod-5</i> | dH ₂ O | 14.325 |
| | Buffer (10x) | 2.5 |
| | dNTPs (25 mM) | 0.25 |
| | F1 (10 μM) | 0.7 |
| | F2 (10 μM) | 1.4 |
| | R1 (10 μM) | 0.7 |
| | Taq Polymerase (0.05 units/μL) | 0.125 |

All reagents were stored at -20 °C. The PCR buffer, dNTPs and primers were thawed at room temperature and briefly vortexed before added to the PCR master mix (**Table 2.6**). Taq polymerase was collected from the freezer briefly prior to adding it to the master mix and returned to -20 °C. The PCR master mix was gently mixed and aliquoted at 20 μL per PCR tube used, on top of the 5 μL *C. elegans* lysate that contained the genomic DNA.

PCR-genotyping was conducted using a thermal cycler program set to 1 cycle at 95°C for 2 min for DNA denaturation, 30 cycles at a sequence of 95°C for 30 seconds, 61°C o 63°C for 30 seconds (depending on primers used) and 68°C for 1 min, followed by a final extension of 1 cycle at 68°C for 5 min with a hold at 4°C.

2.6.3. Agarose gel DNA electrophoresis

PCR products were mixed with 10 µL of 6x orange gel loading dye and loaded onto a 1% agarose gel containing 0.01% GelRed® Nucleic Acid Gel Stain (Biotium). A 100 bp DNA ladder (Quick-Load®, New England Biolabs) was loaded in the first lane for size reference. Samples were electrophoresed at 120V for 40 min and visualised under a Syngene™ UV transillumination (Ingenius3). All strains were confirmed by PCR genotyping prior to their use in experiments.

2.7. Dihydroethidium assay

C. elegans intracellular ROS levels were detected using the commercial dye dihydroethidium (DHE) (ThermoFisher #D23107). Upon receipt from the supplier, DHE was transferred into 0.5 mL Eppendorf tubes in 3 µl aliquots (5mM), ensuring minimal exposure to air and light. Tubes were sealed with parafilm and wrapped with foil to protect them from humidity and light, and stored at -20°C, according to the manufacturer's guidelines.

DHE oxidation assay was performed as previously described (Roux et al., 2016; Aspernig et al., 2019). Briefly, 25-30 L4-stage nematodes were transferred to unseeded NGM plates and allowed to crawl for 15 min to remove any bacteria adhering to their bodies. Animals were washed off the plates with 1x M9 buffer and transferred to 1 mL Eppendorf tubes. Three additional washing steps with 1x M9 were performed to eliminate any remaining bacterial debris, resulting in a final pellet of 100 µL containing the nematodes after the last washing step.

A 3 µl DHE aliquot of 5mM was retrieved from the freezer and diluted with 900 µl of 1x M9 buffer, resulting in a 30 µM DHE solution. Thereafter, 50 µL from this DHE solution was

immediately added to the Eppendorf tubes containing the animals, achieving a final working concentration of 10 μM DHE. Then, the nematodes were incubated in a thermomixer at 20°C for 2 h while shaking at 300rpm. DHE tubes were protected from light throughout the procedure.

Following incubation, DHE was carefully removed from the Eppendorf tubes with a glass Pasteur pipette. Animals were then washed three times with 1ml 1x M9 buffer and transferred to unseeded plates, where they were allowed to crawl for 15 min prior to imaging. Whole-body fluorescence of stained animals was captured at a total magnification of 50X. Final data represent a minimum of three independent trials, with each replicate including a minimum of 10 nematodes and with at least one trial blinded for each genotype or condition assessed.

2.8. MitoSOX assay

C. elegans mitochondria ROS was detected using the commercial dye MitoSOX (ThermoFisher #M36008). MitoSOX was provided in vials of 50 μg dye and was stored at -20°C protected from light and humidity, as per the manufacturer's guidelines.

MitoSOX oxidation assay was optimised following previously described protocols (Aspernig et al., 2019; Coppa et al., 2020; Hsiung et al., 2020). Briefly, 25-30 L4-stage nematodes were transferred to unseeded NGM plates and allowed to crawl for 15 min to remove any bacteria adhering to their bodies. Similarly to DHE, animals were washed off the plates with 1x M9 buffer and transferred to 1 mL Eppendorf tubes. Three additional washing steps with 1x M9 were performed to eliminate any remaining bacterial debris, resulting in a final pellet of 100 μL containing the nematodes after the last washing step.

A MitoSOX vial was retrieved from the freezer and dissolved in 3 μL DMSO, creating a 5 mM MitoSOX stock solution that was stored at -20°C for a maximum of 2 days, as per manufacturer's instructions. During the day of the assay, the 5mM MitoSOX stock solution was further diluted at 133.3 μM with 146 μL DMSO and added to three Eppendorf tubes containing the nematodes at a final working concentration of 5 μM , 10 μM or 20 μM , respectively. The nematodes were then

incubated with MitoSOX solution at 20°C in a thermomixer while shaking at 300rpm for 30 min, 1 hour or 2 h for each concentration used. MitoSOX tubes and stained animals were protected from light throughout the procedure.

Following incubation, MitoSOX was carefully removed from the Eppendorf tubes. Animals were then washed three times with 1ml 1x M9 buffer and transferred to unseeded plates, where they were allowed to crawl for 15 min prior to imaging. Whole-body fluorescence of stained animals was captured at a total magnification of 50X, while fluorescence concentrating in the head region only was captured at a total magnification of 200X. Final data represent a minimum of two independent trials, with each replicate including a minimum of 10 nematodes.

2.9. Fluorescence imaging

For fluorescence microscopy 5–10 L4-stage nematodes were transferred to a drop of 30 mg/mL 2,3-Butanedione monoxime (BDM; $\geq 98\%$, Sigma-Aldrich) on a coverslip and incubated at room temperature for approximately 3 min till nematodes were fully immobilised. Agar pads were prepared by pipetting 120 μ L of 2% melted agar on the centre of a 75 mm \times 25 mm glass slide and immediately placing a second one on top to spread the agar. After cooling for 2 min, the slides were carefully separated by sliding one over the other, leaving the agar pad on one of the slides. The agar pad was then carefully placed on top of the coverslip with the immobilised nematodes, minimising air bubbles and ensuring gentle contact to avoid harming the animals.

C. elegans fluorescence imaging acquisition was performed using a ZEISS AxioImage.M2 microscope attached to an AxioCam 503 mono camera, operated by the ZEN 3.3 software (blue edition). The microscope features eyepieces allowing for 10X magnification, and a set of objectives offering 5X, 10X or 20X magnification. Images were captured using the Texas Red filter (Ex λ 335-383 nm, Em λ 593-668 nm) at a 75% light source intensity and 1.6-second exposure under 50X or 100X total magnification (5X and 10X objectives, respectively), or at a 20% light intensity and 150-millisecond exposure under 200X total magnification (20X

objective). The following settings were used to measure the fluorescence emitted by DHE (Ex λ 370 nm, Em λ 420 nm), MitoSOX (Ex λ 396, Em λ 610 nm) and wrmScarlet (Ex λ 569 nm, Em λ 594 nm).

2.10. Fluorescence quantification

Fluorescence images were processed using the imaging processing tab included in the Zeiss ZEN 2.3 Lite (blue edition) software. This approach enables the experimenter to outline manually each animal's silhouette and subsequently, quantify the fluorescence intensity of each pixel contained within the area selected. The *C. elegans* whole-body 'mean fluorescence intensity' is yielded as a result and can be directly used in statistical analysis without any further adjustments.

It should be noted that Zeiss ZEN 2.3 Lite software possesses a built-in range indicator function that highlights pixels within the images captured that fall outside the optimal detection range. When this function is enabled, overexposed areas (i.e. pixels that exceed the maximum detectable signal) are automatically marked in red. Because these values are no longer accurately quantifiable, images with pixels exceeding the range indicator were excluded from the analysis to ensure data reliability. For each image included in the analysis, the 'mean fluorescence intensity' value for each animal was exported to Excel for statistical analysis in GraphPad.

2.11. Survival assays

To determine *C. elegans* lifespan, synchronised day-3 animals were placed on seeded NGM plates. For each genotype, experimental plates were prepared in duplicate with 30 animals per plate. Animals were incubated and maintained at 20°C throughout the assay. Survival was scored daily until all animals were assigned as dead and/or censored. More specifically, each animal was observed individually at 30x magnification without disruption for 5 seconds. If body or grinder activity was detected, animals were scored as alive. In the absence of visible movement, the

nematode was gently poked with a platinum wire on one side of the body, just below the head. Following a 5 second observation period, nematodes were scored as dead and removed from the plate if no body or grinder movement was detected. Nematodes that died due to (a) picking, (b) internal hatching of progeny, (c) vulva protrusion or (d) escaped on the walls of the plate were removed from the assay and were censored. The aforementioned animals were included the assay up to the day prior to censoring.

In survival assays, 5-fluoro-2'-deoxyuridine (FUdR) has been used to control animal population and minimise their handling, as nematodes fed on FUdR are known to lay eggs which are defective in hatching (Gandhi et al., 1980). The use of this chemical compound was avoided herein, as recent studies have shown that FUdR can affect mitochondrial function and activate *C. elegans* stress response pathways (Anderson et al., 2016; Rooney et al., 2014). To prevent strain starvation during survival assessment, animals were transferred onto new NGM plates every two days until egg laying was ceased. Final data represent three independent trials, with each replicate including a minimum of 30 nematodes and with at least one trial blinded per genotype.

2.12. Juglone sensitivity assay

A 12mM juglone (5-Hydroxy-1,4-naphthoquinone 97%; Sigma-Aldrich #H47003) stock solution was prepared in 100% ethanol. NGM plates containing juglone were prepared at a final concentration of 60 μ M. Plates were allowed to solidify before being seeded with 40 μ l of 5x concentrated OP50 to minimise animals crawling off the plates during the assay (Van Remmen et al., 2004). Importantly, plates were prepared on the day of the assay and always protected from light, as juglone is light-sensitive and losses its toxicity over time (Senchuk et al., 2017). To measure juglone sensitivity, day-3 nematodes were transferred to juglone-containing plates and their survival was assessed hourly for up to 4 h. Final data represent four independent trials, with each replicate including a minimum of 10 nematodes and with at least one trial blinded for each genotype assessed.

2.13. Paraquat sensitivity assay

A 500 mM paraquat (Methyl viologen dichloride hydrate 98%; Sigma-Aldrich #856177) stock solution was prepared in autoclaved distilled water. NGM plates containing paraquat were then prepared to a final concentration of 4 mM. The plates were allowed to solidify before being seeded with 200 μ l OP50. Plates were allowed to dry for three days before use. Although it is generally accepted that paraquat plates can be stored at 4°C for up to a month (Senchuk et al., 2017), plates were freshly prepared three days before the assay and were kept away from light to increase the consistency of the assays.

Synchronised day-3 animals were transferred to paraquat-containing plates, and their survival was scored every 24 h, until all animals were dead or censored. Final data represent four independent trials, with each replicate including a minimum of 30 nematodes and with at least one trial blinded per each genotype assessed.

2.14. Heat stress sensitivity assay

L4-stage nematodes maintained at 20°C were transferred to seeded NGM plates. Importantly, animals were selected at L4-stage to match the developmental stage of *smn-1(ok355)* mutants, as previous literature has shown that *C. elegans* thermotolerance varies markedly depending on the life cycle (Zevian and Yanowitz, 2014). Experimental plates were placed individually, not stacked, within a pre-heated mini incubator at 35°C, and animals were incubated for 4, 5, 6 or 7 h, respectively. The incubator door remained closed throughout the experiment to maintain a stable temperature, only being opened to retrieve experimental plates at the specified time-points. Following heat exposure, animals were allowed to recover at 20°C for 24 h prior to assessing their survival. Final data represent the percentage of animals alive (\pm SEM) from three independent trials, with each replicate consisting of a minimum of 10 nematodes and including at least one trial blinded for each genotype studied.

2.15. Osmotic stress sensitivity assay

Day-3 animals were transferred from standard isotonic NGM plates (50 mM NaCl) to hyperosmotic plates (450 mM NaCl) and incubated at 20°C for 24 h. Animals were then collected into Eppendorf tubes and washed three times with hyperosmotic 1x M9 solution (300 mM NaCl). Nematodes were returned to standard isotonic plates, ensuring minimal transfer of M9 solution, and allowed to recover at 20°C for 24 h prior to evaluating their survival. Final data represent the percentage of animals alive (\pm SEM) from three independent trials, with each replicate consisting of a minimum of 10 nematodes and including at least one trial blinded for each genotype used.

Hyperosmotic NGM was prepared by modifying the standard NGM protocol and by increasing the salt concentration of NaCl from 1.5 g/L to 26.3 g/L. Similarly, hyperosmotic 1x M9 was prepared by increasing NaCl from 5 g/L to 17.5 g/L. The concentration of NaCl in M9 was chosen to be intermediate between isotonic and hypertonic to avoid osmotic shock (Wheeler and Thomas, 2006).

2.16. Pharyngeal pumping

Pharyngeal pumping rates were assessed in day-3 nematodes using the Zen Pro software on a Discovery.V8 SteREO microscope attached to an AxioCam ICc5 camera, as previously described (Dimitriadi et al., 2010). Briefly, animals were filmed for 10 seconds at 17.5 frames per second to produce a slow-motion video for manual counting of pumps. A pumping event was defined as any grinder contraction along any axis. Since pumping rates are influenced by food availability (Scholz et al., 2016), only animals placed on the food were recorded.

2.17. WormLab[®] locomotion assay

2.17.1. Locomotion assay

Day 3 animals were allowed to crawl on unseeded NGM plates for 3 min to remove any bacteria adhering to their bodies. Meanwhile, experimental plates were set up by embedding a metallic ring onto the NGM agar. Eight to ten animals were transferred within the metallic ring/filming area and allowed to acclimate to the microscope light for 2 min. Animals were then filmed while crawling for 5 min at 15 frames per second using the Zen Pro software on a Discovery.V8 SteREO microscope equipped with an AxioCam ICc5 camera (**Figure 2.2A**). Each video was converted into an AVI format movie at 15 frames per second for later analysis.

2.17.2. WormLab[®] detection and tracking system

Locomotion movies were processed utilising the individually imported into WormLab software (MBF Bioscience Version 2020.1.1). Each movie was uploaded into the software individually. Before the analysis, the software was calibrated to set the spatial scale to 14 $\mu\text{m}/\text{pixel}$.

To ensure the accurate recognition of all the animals within the image, the software was configured to detect dark nematodes against a light background. Then, the image parameters (i.e. brightness and contrast) were manually adjusted to ensure a clear contrast between the nematodes in the image and the background (**Figure 2.2B**). Following this, the “Detect worms” option was selected, enabling the software to automatically recognise all the animals in the image based on the applied settings. In instances where a nematode was not automatically detected, the software allows manual identification by selecting the silhouette of the animal with the cursor, training the software to recognise that silhouette as a nematode. Importantly, animals that are colliding (i.e. in contact with each other) are not recognised by the software and should not be selected, as this would lead to the erroneous identification of both animals as a single individual. At this point, the video was advanced to a different timeframe, and the “Detect worm” option was selected again, to ensure that the software had learnt to accurately recognise the nematodes. This procedure was

repeated at various timeframes of the video to ensure consistent recognition of all the animals throughout the locomotion movie (**Figure 2.2C**).

Following the detection process, each movie was saved as a WormLab project file. Subsequently, all videos were selected for tracking under the "Batch tracking" option to facilitate the automatic tracking of nematode movement.

2.17.3. Evaluation of automatic tracking quality

During the automatic tracking process, each nematode was assigned a unique tracking number. WormLab quantifies the locomotory movement of each animal using various parameters displayed under each tracking number. However, automatic tracking can introduce errors, such as a) incorrect head/tail orientation or b) tracking interruptions when animals collide. To address this, WormLab allows users to 'repair' tracks by manually correcting head/tail orientation or merging split trajectories. At the end each animal's tracking was reviewed and errors were manually rectified (**Figure 2.2D**).

2.17.4. WormLab[®] data processing

WormLab provides a quantitative data for each animal tracked under the 'Track Summary' tab. This data was exported into Microsoft Excel for statistical analysis. To ensure a robust analysis, data were manually filtered based on the "Track Duration" parameter, excluding animals tracked for less than 285 seconds (95% of the 5 min video). Parameters of interest were exported to GraphPad for statistical analysis and data visualisation (**Figure 2.2E**).

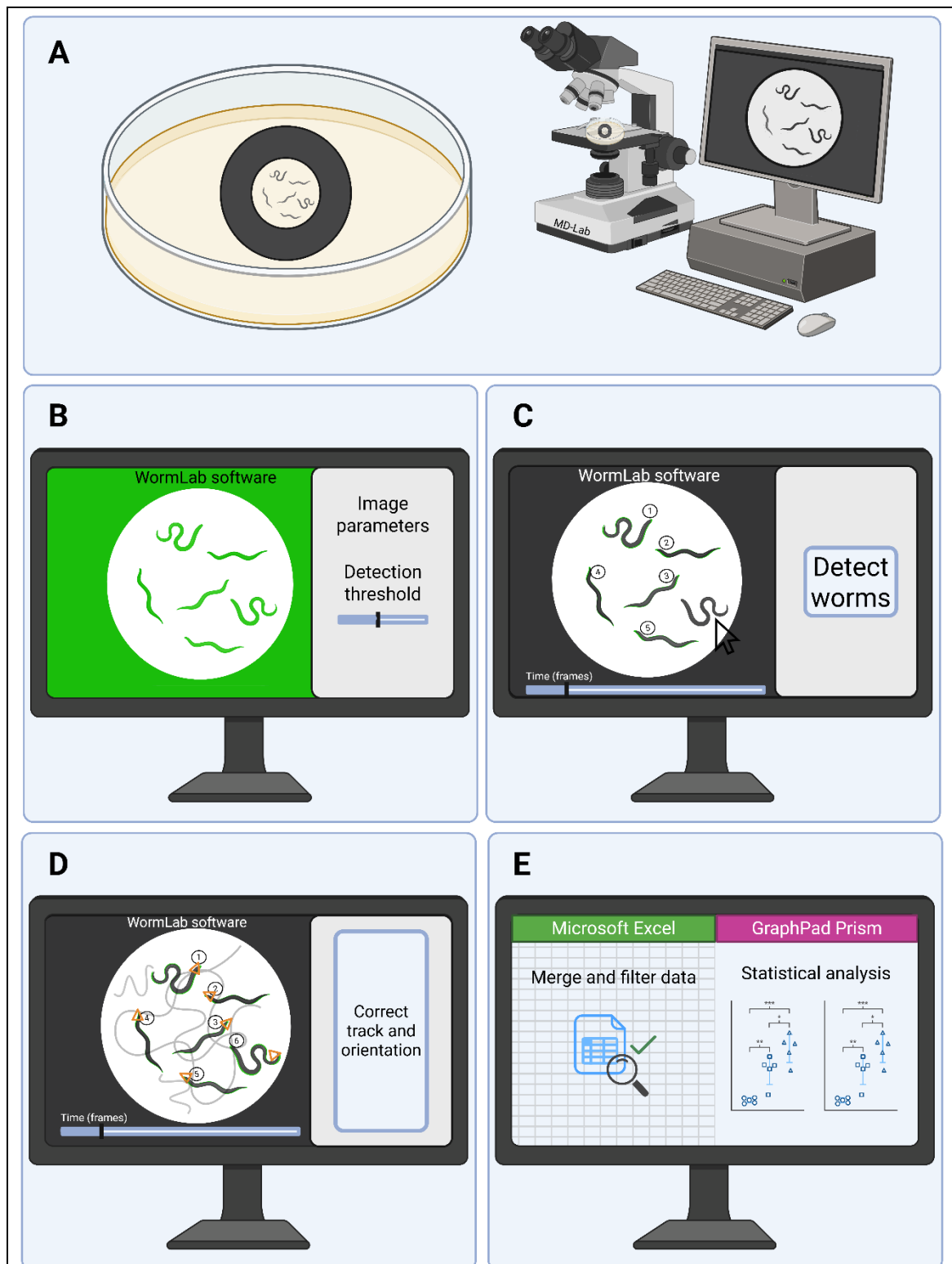


Figure 2.2. Experimental workflow utilised to quantify nematode locomotion using the WormLab® software

(A) Animals were placed within a metallic ring embedded on unseeded NGM plates, to limit the movement of the animals within the field of view. Videos were captured using a Discovery.V8 SteREO microscope equipped with an AxioCam ICc5 camera.

- (B) Locomotion movies were imported into WormLab® software, where image parameters and detection thresholds were adjusted to optimise contrast between animals and background.
- (C) Animals were detected automatically by the software, or selected manually when automatic recognition was unsuccessful.
- (D) Locomotion tracks were reviewed and corrected for head/tail orientation and trajectory continuity.
- (E) Tracking results were exported to Excel for data merging and filtering. Processed datasets were subjected to statistical analysis in GraphPad Prism to compare locomotion metrics across different experimental conditions.

2.18. Antioxidant treatment

C. elegans were cultured on NGM plates containing the desired antioxidant drug. Compounds were purchased from Sigma-Aldrich and were stored according to manufacturer's recommendations. Three concentrations per drug treatment were selected for each *C. elegans* genotype assessed. Each antioxidant compound was dissolved in either autoclaved dH₂O or DMSO before adding it to unsolidified NGM agar solution. It should be noted that the maximum DMSO concentration used herein was set to 0.7% since previous studies indicated that DMSO concentrations greater than 1% can alter *C. elegans* developmental stage and behaviour (AIOkda and Van Raamsdonk, 2022). Drug plates were prepared to maintain a constant percentage of the solvent across the different concentrations selected for each drug. Vehicle plates were prepared by adding only the solvent (autoclaved dH₂O or DMSO) to the media. Each antioxidant treatment was completed within a week, otherwise, plates were stored at 4°C wrapped in parafilm till further use. Table 2.7 summarises the antioxidants used, including information on store stability, solvents, and concentrations.

Table 2.7. Antioxidant compounds used for *C. elegans* drug treatment

Antioxidant compounds, storage conditions, drug solubility and drug concentrations (low, medium, high) are listed below. Storage conditions provide information on temperature and light sensitivity; solubility indicates the recommended solvent to be used; the three drug concentrations tested are also depicted in mM.

| Antioxidant | Sigma-Aldrich catalogue no | Store stability | Solubility | Concentration | | |
|-------------------------------------|----------------------------|-------------------------------------|---|---------------|--------|---------|
| | | | | Low | Medium | High |
| L-Ascorbic acid | A4403 | Room temperature Light sensitive | H ₂ O: 10 mg/mL | 0.1 mM | 1 mM | 10 mM |
| N-Acetyl-L-cysteine | A9165 | 4°C | H ₂ O: 100 mg/mL (with heating) | 3 mM | 6 mM | 9 mM |
| (-)-Epigallocatechin gallate | E4143 | 4°C Light sensitive | H ₂ O: 5 mg/mL | 50 µM | 100 µM | 200 µM |
| Melatonin | M5250 | -20°C Light sensitive | DMSO: 30 mg/mL | 10 µM | 100 µM | 1000 µM |
| Curcumin | C1386 | -20°C | DMSO: 11 mg/mL | 5 µM | 10 µM | 20 µM |

2.19. RNA isolation

RNA isolation was performed by a previous member of the Dimitriadi Lab (Amy Yong). Prior to RNA isolation, the entire working surface was sprayed with industrial methylated spirit (IMS) and RNase Decontamination Solution (RNaseZap RNase Decontamination Solution; Invitrogen #12122000). Approximately 1000 stage-matched nematodes were picked for each biological replicate and washed three times with sterile dH₂O to remove bacterial debris. Total RNA was extracted by adding Trizol (Invitrogen™) into the nematode-containing Eppendorf tubes in a 5:1 ratio. Animals were subjected to at least five cycles that involved freezing-thawing in liquid nitrogen followed by a 37°C incubation. RNA was subsequently isolated with chloroform and ethanol. Eppendorf tubes containing 20 ng/μL RNA were prepared and shipped on dry ice to Novogene (Cambridge Science Park, UK) for sequencing.

2.20. RNA sequencing

RNA sequencing was outsourced to Novogene, where it was performed using Illumina platforms based on the sequencing by synthesis (SBS) mechanism, following the next steps:

1. Data Acquisition: raw data was generated by high-throughput sequencing processed by CASAVA base recognition (Base Calling) and stored in FASTQ format files. These files contain the sequences of reads and corresponding base quality scores.
2. Quality Control: to ensure high quality data, Novogene filtered the raw reads to remove low-quality reads and adaptor sequences, resulting in clean reads suitable for further analysis.
3. Alignment and gene expression quantification: the clean reads were aligned to the reference genome using the HISAT2 algorithm. Gene expression levels were then quantified based on the number of mapped reads.

2.21. Bioinformatic analysis

A detailed summary of the software, packages, and specific parameters used for each step in the analysis is provided in **Table 2.8**.

Table 2.8. List of software packages and parameters utilised for transcriptomic analysis.

| Analysis | Software | Package | Function | Parameters |
|-------------------------------------|-------------------------------|-----------------------------------|-----------------|--|
| Exploratory analysis (pca) | R (R-studio) version 4.3.2 | DESeq2 version 1.42.0 | plotPCA | ntop = nrow(assay(vsd)) |
| Differential expression analysis | | DESeq2 version 1.42.0 | DESeq | Default |
| Functional Analysis | | clusterProfiler version 4.10.1 | enrichGO | pAdjustMethod = "BH" qvalueCutoff = 0.01 |
| | | | enrichKEGG G | |
| | | AnnotationDbi version 1.64.1 | org.Ce.eg | WORMBASE |
| GSEA | | clusterProfiler version 4.10.1 | gseGO | minGSSize = 15 exponent = 1 pAdjustMethod = "BH" pvalueCutoff = 0.05 seed = 149 by = "fgsea" nPermSimple = 1000 |
| | | AnnotationDbi version 1.64.1 | org.Ce.eg | WORMBASE |
| Protein-Protein Interaction Network | STRING version 12.0 | - | - | medium confidence (0.4) |
| | Cytoscape version 3.10.1 | MCODE version 2.0.3 | - | Degree Cutoff: 2 Node Score Cutoff: 0.2 K-Core: 2 Max. Depth: 100 |
| Transcriptor factor network | Ortholist2 | - | - | Default |
| | NetworkAnalyst | JASPAR version 10 | - | Default |
| | Cytoscape version 3.10.1 | - | - | Default |
| Plot | R (R-studio) version 4.3.2 | ggplot2 version 3.5.1 | ggplot | geom_bar geom_point |
| | | enrichplot version 1.22.0 | gseaplot2 | Default |

| | | | | |
|--|--|------------------------|----------|---------|
| | | stats version 4.3.2 | pheatmap | Default |
|--|--|------------------------|----------|---------|

2.21.1. Principal component analysis

Principal component analysis (PCA) was performed to visualise differences in gene expression profiles between samples, projecting the data into two dimensions that highlight the main sources of variance in the raw RNA-seq data. RNA-seq data variance typically increases with the mean, resulting in plots that highlight genes with high counts due to large absolute differences between samples (Love et al., 2015). To mitigate this effect and obtain a more balanced representation of gene expression, we applied a variance-stabilising transformation (VST) using the DESeq2 package in R, as previously described (Anders and Huber, 2010). A PCA plot was then constructed and visualised using the DESeq2 and ggplot2 packages in R.

2.21.2. Differentially expressed genes analysis.

Differentially expressed genes (DEG) analysis was performed to assess individual differences in gene expression between two samples. For each gene, the change in expression between samples was expressed as a log2 fold change ($|\log_2FC|$). The statistical significance of each change was determined by calculating the p-value, which was adjusted using the Benjamini and Hochberg (BH) method to control the False Discovery Rate (FDR). The threshold for significant differential expression was set at an adjusted p-value (P_{adj}) of less than 0.001 and an absolute $|\log_2FC|$ greater than 1. DEG analysis and visualisation were performed using the DESeq function from the DESeq2 package and ggplot function from ggplot2 package, respectively.

2.21.3. Functional analysis

Functional analysis was performed to investigate the biological functions and pathways associated with the identified DEGs. The DEGs were categorised into functional terms obtained from the Gene Ontology (GO) and Kyoto Encyclopedia of Genes and Genomes (KEGG) datasets

(Ashburner et al., 2000; Kanehisa et al., 2007; Aleksander et al., 2023). The *C. elegans* gene annotation database was obtained from the AnnotationDbi package in R, which is updated every six months to ensure accurate and up-to-date mapping of gene identifiers (Carlson, 2024).

Functional analysis was performed using the enrichGO and enrichKEGG functions included in the clusterProfiler R package (Wu et al., 2021; Yu et al., 2012), with a significance threshold of $\text{padj} < 0.01$, adjusted by BH method. Upregulated and downregulated genes from the DGE list were analysed separately. Enriched functional terms were ranked according to their Padj value, and the top 10 enriched terms were plotted using ggplot2.

2.21.4. Gene Set Expression analysis

Gene Set Enrichment Analysis (GSEA) was performed on the complete RNA-seq dataset to evaluate the correlation between genes groups that shared common biological functions with a specific phenotype (i.e. *smn-1(+)* or *smn-1(ok355)*) (Mootha et al., 2003; Subramanian et al., 2005). GSEA was performed on a gene list ranked by a signal-to-noise metric, which allows to establish a correlation between gene expression levels and the two phenotypes under study. This ranked gene list is then compared against reference gene sets from the GO and KEGG databases to assess whether genes from these sets are randomly distributed or concentrated at the top or bottom of the ranked list. Concentration at either end indicates this gene set is strongly correlated with a phenotype, measured by an Enrichment Score (ES) value.

GSEA was performed using the gseGO and gseKEGG functions included in the clusterProfiler R package, with a significance threshold of $\text{padj} < 0.01$, adjusted by BH method. Analysis parameters were set to 1000 permutations and 149 seed value to assure reproducibility, as recommended by GSEA (MSigDB 2024). Enriched terms were ranked by their Normalised Enrichment Score (NES), and the top 10 enriched terms were plotted using ggplot2. Running enrichment score for the most significant terms from each genotype were plotted using the gseaplot2 function included on the enrichplot package.

2.21.5. Identification of oxidative stress hub genes in SMA

Candidate genes potentially influencing the oxidative stress (OS) response in SMA were identified as previously described (Zhang & Kiryu, 2023). A list of SMA-oxidative stress-related genes (SMA-OSRGs) was constructed by the intersecting DEGs with oxidative stress-related genes (OSRGs) obtained from the GO database (GO:0006979). Then, the resulting SMA-OSRGs list was uploaded to STRING database to construct a protein-protein interaction (PPI) network, with an interaction score threshold > 0.4 for confident interactions. This network was exported to Cytoscape and filtered using the molecular complex detection technology (MCODE) plug-in to identify the most densely connected cluster. Gene expression levels for these clustered genes were visualised in a heatmap generated using the R package stats (version 4_4.3.2).

To further investigate gene regulation, a gene-transcription factor (TF) regulatory network was constructed using the JASPAR database in NetworkAnalyst. *C. elegans* genes were first converted to predicted human orthologs via OrthoList 2 (OL2). The TF network was exported to Cytoscape for visualization, where only TFs targeting at least two hub genes were included to enhance clarity.

2.22. Statistical analysis

The statistical analysis of the data was performed in GraphPad Prism (version 10.1.2). Statistical tests were applied only to biological replicates once outliers were identified and excluded via Grubb's test ($\alpha = 0.05$).

For experiments involving one experimental variable across more than two groups (i.e., four *C. elegans* genotypes under the same conditions), one-way ANOVA was employed. Dunnett's post hoc test was performed to compare the mean of multiple genotypes against a control group, while Sidak's post hoc test was utilised for specific comparisons among experimental groups. When only two genotypes were assessed (*smn-1(+)* versus *smn-1(ok355)*), data were analysed using the nonparametric Mann-Whitney test. This approach was chosen instead of a t-test because no

normality testing was performed, and the Mann-Whitney test does not require the assumption of normally distributed data.

For experiments with two independent variables (i.e., genotype and drug concentration), two-way ANOVA was applied, followed by Dunnett's post hoc test to compare the mean of multiple genotypes against a control group. The overall interaction *P* value, which reflects whether the effect of a given treatment differs across genotypes, was reported in figure legends.

To analyse the survival rate over time of a population of nematodes under standard conditions or exposed to drug treatments (i.e., lifespan and juglone/paraquat), a Kaplan-Meier survival curve was constructed and analysed using log-rank test. Individual comparisons between genotypes were performed with separated log-rank tests applied to the two genotypes compared. Survival rate at a specific time point of a population of nematodes exposed to heat or osmotic stress was evaluated with one-way ANOVA, followed by Dunnett's post hoc test to compare multiple genotypes against the control group.

All graphs display mean values from biological replicates with error bars representing SEM. Statistical significance is indicated as follows: ns = not significant, **P* < 0.05; ***P* < 0.01; ****P* < 0.001; *****P* < 0.0001). Specific *n* values for each experiment are noted in figure legends.

**Chapter III. Investigating oxidative stress
involvement in the *Caenorhabditis elegans* spinal
muscular atrophy model.**

3.1. Introduction.

As discussed in Chapter I, oxidative stress is perturbed in SMA patients and mammalian models of SMA. This study aimed to investigate the potential involvement of oxidative stress in SMA pathophysiology by utilising the *smn-1(ok355)* *C. elegans* SMA model. However, prior to exploring the effects of oxidative stress on SMA, it is imperative to ascertain whether the oxidative stress indicators observed in other SMA models are also evident in *C. elegans*.

3.1.1. ROS induction in *Caenorhabditis elegans*

The induction of ROS in *C. elegans* serves as a powerful experimental approach for investigating the organism's capacity to maintain homeostasis between ROS generation, detoxification, and cellular response mechanisms (Senchuk et al., 2017). When applied to *C. elegans* disease models, this methodology facilitates the determination of whether oxidative stress actively contributes to disease progression or is merely a byproduct of cellular dysfunction and metabolic imbalance (Van Raamsdonk & Hekimi, 2010). For example, in a *C. elegans* model of amyotrophic lateral sclerosis (ALS), exposure to ROS-inducing agents exacerbates neuronal degeneration, thus highlighting the pathogenic role of oxidative stress in the disease progression (Baskoylu et al., 2018a).

To elucidate the contribution of oxidative stress to SMA pathology, we investigated the sensitivity of SMN-depleted *C. elegans* to oxidative stress utilising paraquat (1,1'-dimethyl-4,4'-bipyridinium dichloride) and juglone (5-hydroxy-1,4-naphthoquinone), two widely employed chemical agents for ROS induction in *C. elegans* (Keith et al., 2014).

Paraquat and juglone are widely studied compounds known for their capacity to induce cytotoxicity via ROS generation. Both compounds differ in their origin and application. While paraquat is a synthetically produced di-cation used worldwide as an herbicide (Sharma et al., 2019), juglone is a natural compound studied for its therapeutic potential as an antimicrobial agent (Clark, Jurgens and Hufford, 1990) and promising anticarcinogenic properties (Fang et al., 2018;

Sugie et al., 1998; Zhang et al., 2012). However, both compounds share a common mechanism of toxicity involving redox cycling, which results in the excessive production of ROS and subsequent oxidative stress induction (Bus and Gibson, 1984; Dinis-Oliveira et al., 2008; Ahmad and Suzuki, 2019).

Upon cellular entry, paraquat and juglone undergo one-electron reduction by enzymatic systems, resulting in highly reactive intermediate radicals. In the presence of oxygen, these intermediates are rapidly re-oxidised, generating superoxide anions ($O_2^{\cdot-}$) and restoring the parent compound to its original state, allowing for continuous cycles of ROS production (Bus and Gibson, 1984; Ollinger and Brunmark, 1991; Dinis-Oliveira et al., 2008). For paraquat, enzymatic systems such as NADPH cytochrome P450 reductase (Reczek et al., 2017), mitochondrial complex I (Fukushima et al., 1993), xanthine oxidase (Winterbourn, 1981), and thioredoxin reductase (Gray et al., 2007), play key roles in its reduction, suggesting that ROS can be generated in both the cytoplasm and mitochondria. Similarly, juglone relies on systems such as NADPH cytochrome P450 reductase (Muto et al., 1987), mitochondrial complex I (Anderson et al., 1993), xanthine oxidase (Lewis and Shibamoto, 1989), glutathione, and Fe^{2+} ions (Zhang et al., 1994) for its reduction, with ROS formation consequently occurring in both cytoplasm and mitochondria.

Although both compounds induce oxidative stress via redox cycling, they also have additional distinct indirect mechanisms of ROS production that contribute to their cytotoxicity. Paraquat can indirectly increase ROS by critically consuming cellular reductants such as NADPH, which have their own relevance within the cell (Keeling and Smith, 1982). In addition, juglone exhibits nucleophilic reactivity, forming covalent bonds with thiol-containing molecules such as glutathione (GSH). This depletes intracellular antioxidants, exacerbating oxidative stress and cytotoxicity (Doherty, Rodgers and Cohen, 1987).

The ROS generated by paraquat and juglone lead to a variety of cellular damages, including lipid peroxidation (Kappus and Sies, 1981; Kumbhar et al., 1997), protein carbonylation or inhibition (Doherty, Rodgers and Cohen, 1987; Chao, Greenleaf and Price, 2001; Suyal et al., 2024), DNA damage (Paulsen and Ljungman, 2005; Kwiecinski et al., 2012), mitochondrial dysfunction, and

apoptosis (Mesalam et al., 2020; Erkoc-Kaya et al., 2024). Both chemicals are known to modulate oxidative stress response pathways, although this encompasses some of the critical differences between the two compounds. Paraquat activates signalling cascades such as MAPK (Cui et al., 2019), PI3K/Akt/mTOR (Jiang et al., 2021; Liu et al., 2019), and Wnt/ β -catenin (Sun et al., 2020) signalling among others (Liu et al., 2022). Juglone also induces changes in several pathways (Ahmad and Suzuki, 2019; Tang et al., 2022). For example, it activates MAPK signalling (Liu et al., 2017; Wang et al., 2018; Wu et al., 2017), while downregulating the PI3K/Akt/mTOR pathway (Fang et al., 2018; El-Sheikh et al., 2023), among others.

Interestingly, the effects of antioxidants on paraquat and juglone toxicity are not entirely consistent. For paraquat, antioxidants such as superoxide dismutase (SOD) enzymes mitigate toxicity and improve survival rates (Krall et al., 1988; Da Silva et al., 2018; Hu et al., 2018) in cell culture and preclinical models. Juglone, however, interacts with antioxidants in a more complex manner. Although certain antioxidants, such as *N*-acetyl cysteine (NAC), can reverse its cytotoxic effects (Sun et al., 2020), others, such as ascorbate (Vitamin C), may enhance ROS production and apoptosis when combined with juglone (Sajadimajd, Yazdanparast and Roshanzamir, 2016; Erkoc-Kaya et al., 2024). Interestingly, juglone itself possesses the capacity to neutralise free radicals and functions as an antioxidant at low concentrations (Leopoldini et al., 2004; Chobot and Hadacek, 2009), although its antioxidant properties are reportedly weak (Olszowy-Tomczyk and Wianowska, 2024).

Another critical difference between the two compounds lies in their application when used to induce oxidative stress in research settings. While paraquat is used for chronic studies, juglone is usually utilised for acute increases of oxidative stress, owing to its loss of toxicity over time (Cooper et al., 2016). Wild-type *C. elegans* chronically exposed to high concentrations of paraquat (4 mM) exhibited a severely decreased lifespan (Dues et al., 2016). Similarly, acute exposure of *C. elegans* to high concentrations of juglone (300 μ M) resulted in significantly decreased lifespan (Baskoylu et al., 2022).

Despite the fact that both compounds induce ROS production, paraquat and juglone are molecules with distinct chemical properties, resulting in differential effects beyond ROS production, which may provide additional insights into the disease mechanism. For example, although *clk-1* mutants exhibit resistance to chronic oxidative stress induced by 4 mM paraquat, they demonstrate sensitivity to acute oxidative stress induced by 180 μ M juglone (Schaar et al., 2015). Consequently, some researchers advocate for the use of both compounds to obtain a more comprehensive understanding of ROS effects in the mutants under investigation (Senchuk et al., 2017).

3.1.2. ROS detection in *Caenorhabditis elegans*

ROS are highly reactive and short-lived molecules, which makes measuring ROS levels *in vivo* extremely challenging. Nevertheless, several indirect methodologies have been developed to estimate ROS levels, each with their own advantages and limitations (Labuschagne and Brenkman, 2013). In this study, we measured cytoplasmic and mitochondrial ROS levels in *C. elegans* utilising dihydroethidium (DHE) and MitoSOX, respectively, two small-molecule fluorescent probes commonly used for the detection of superoxide.

Dihydroethidium (DHE) and its mitochondria-targeted derivative, MitoSOX Red, are fluorescent probes that are extensively used for the detection of superoxide anions ($O_2^{\cdot-}$) within cells. Both probes share the same chemical core, a blue non-fluorescent dihydroethidium molecule (Ross et al., 2005; Robinson et al., 2006). Upon interaction with $O_2^{\cdot-}$, DHE and MitoSOX undergo one-electron oxidation, resulting in the formation of 2-hydroxyethidium (2-OH-E⁺), which emits red fluorescence. Notably, 2-OH-E⁺ is specific for superoxide anion oxidation and is not generated by any other biologically relevant oxidant (Zhao et al., 2003; Zielonka et al., 2008).

Due to its neutral charge, DHE is a membrane-permeable dye that enables it to distribute uniformly across cellular membranes and accumulate in the cytoplasm (Bucana, Saiki and Nayar, 1986; Zielonka and Kalyanaraman, 2018). Conversely, MitoSOX possesses a

triphenylphosphonium (TPP) cation attached to its core, facilitating its selective accumulation within the mitochondria, which is substantially more negative than other cellular compartments. Under physiological conditions, this results in several hundred-fold enrichment of MitoSOX in the mitochondrial matrix, thus enabling targeted detection of mitochondrial superoxide (Ross et al., 2005; Funk and Scholkmann, 2023).

However, oxidation of DHE is not limited to superoxide anions. In the presence of metal catalysts, such as peroxidases or cytochrome c, DHE and MitoSOX can react with H_2O_2 to form ethidium (E^+) and its dimeric product E^+-E^+ (Zielonka et al., 2008). Importantly, while E^+-E^+ is non-fluorescent, E^+ emits red fluorescence with a spectrum similar to that of 2-OH- E^+ . Furthermore, DHE and MitoSOX oxidation products intercalate into the nucleus and react with DNA, further increasing their fluorescence intensity (Michalski et al., 2012). Consequently, non-specific oxidation products and DNA interactions complicate the identification of 2-OH- E^+ . Some studies have reported that excitation at 396 nm (Robinson et al., 2006) or 405 nm (Nazarewicz, Bikineyeva and Dikalov, 2012) allows for the distinction between 2-OH- E^+ and E^+ ; however, these approaches are limited to cell-free systems and intact cells and fail to capture the complexity of reactions occurring *in vivo*. Therefore, analytical techniques, such as high-performance liquid chromatography (HPLC) and liquid chromatography–mass spectrometry (LC-MS), are considered the only techniques for distinguishing different DHE and MitoSOX oxidation products, with the limitation that those are not feasible for real-time imaging (Murphy et al., 2022; Zielonka & Kalyanaraman, 2018).

Altogether, although DHE and MitoSOX are versatile tools for visualising superoxide in *C. elegans*, their results must be interpreted with caution. Although these probes were designed for the quantification of superoxide anions, in practice, when utilised for the *in vivo* visualisation of ROS in *C. elegans*, they are more suitable for providing an indication of the redox status within cells. Consequently, the results should be interpreted qualitatively, rather than quantitatively.

3.1.3. Research Objectives

The specific objectives of Chapter III were as following:

1. To evaluate whether dysregulated pathways in *smn-1(ok355)* contribute to the hypothesis that oxidative stress plays a significant role in SMA pathophysiology.
2. To assess the ability of *smn-1(ok355)* animals to maintain redox homeostasis under oxidative stress.
3. To assess the ability of *smn-1(ok355)* animals to maintain cellular homeostasis in response to various stressors.
4. To investigate the production and distribution of reactive oxygen species in the *smn-1(ok355)* SMA model.

Altogether, the primary objective of this chapter was to characterise oxidative stress in the *smn-1(ok355)* *C. elegans* SMA model, providing initial insights into its relevance to SMA pathology. To facilitate interpretation of the results presented in this chapter, we first delineated the key assays employed to assess oxidative stress during this project.

3.2. Results

3.2.1. SMN-1 depletion induces changes in gene expression in *Caenorhabditis elegans*

To identify dysregulated pathways in SMA, we investigated variations in gene expression between the *smn-1(ok355)* *C. elegans* SMA model and control nematodes by performing RNA sequencing on three biological replicates per condition.

We initially conducted Principal Component Analysis (PCA) to identify clusters of samples with similar gene expression profiles and to detect outliers. The PCA plot demonstrated a clear separation between the *smn-1(ok355)* and control groups along the first principal component (PC1) (**Figure 3.1A**) accounting for 95% of the variance in the data. This distinct clustering indicated substantial differences in the overall gene expression profiles between control and SMA

nematodes. Notably, the three biological replicates within each group (SMN and control) clustered in close proximity, with only 2% variation along the second principal component (PC2), reflecting the consistency and reliability of our RNA-seq data.

Using a threshold of $P_{adj} < 0.01$ and $|\log_2\text{fold-change}| > 1$, we identified a total of 7358 differentially expressed genes (DEGs), including 2774 downregulated and 4584 upregulated (**Figure 3.1B**) genes, demonstrating widespread alterations in gene expression in *smn-1(ok355)* mutants. These findings suggest further investigation of the specific genes and pathways affected in the *smn-1(ok355)* *C. elegans* SMA model.

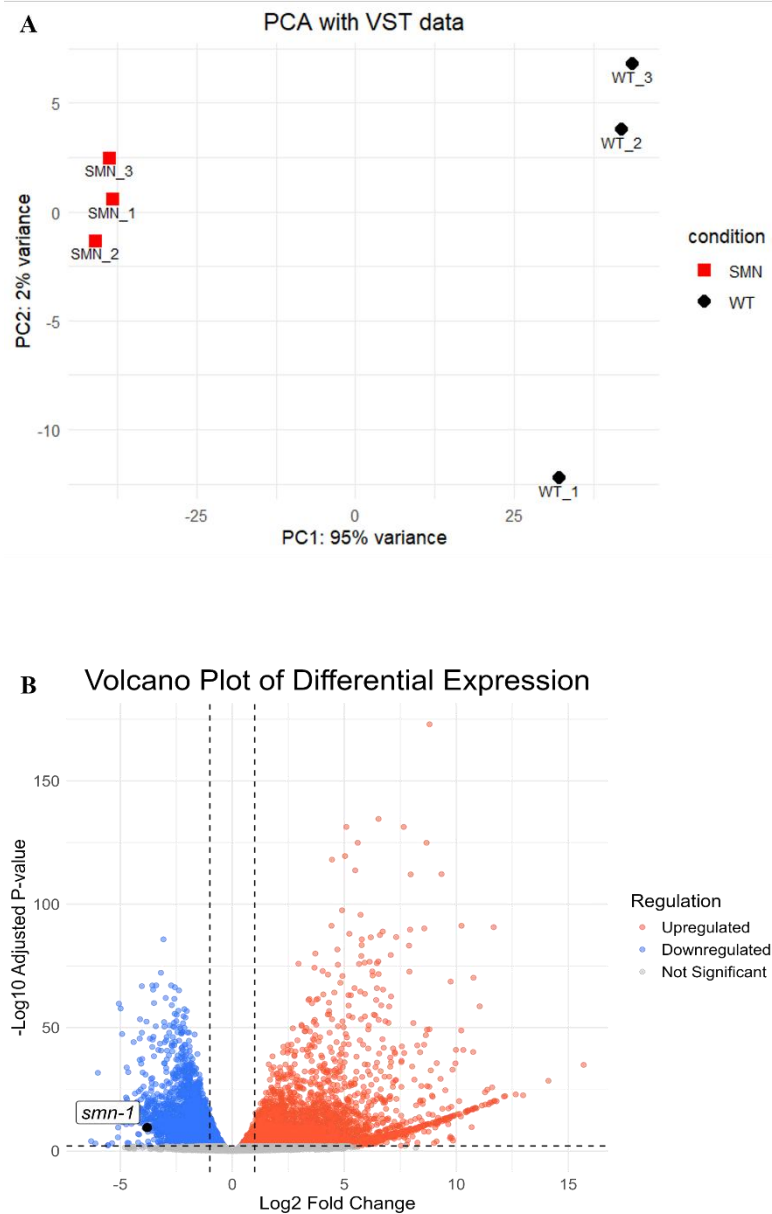


Figure 3.1. SMN-1 depletion induces widespread changes in gene expression of the *smn-1(ok355)* *C. elegans* SMA model

(A) PCA of VST RNA-seq data from three biological replicates of *smn-1(ok355)* animals (SMN_1, SMN_2, SMN_3) and *smn-1(+)* controls (WT_1, WT_2, WT_3) are plotted on the first two PCs and coloured according to their genotype. Samples that cluster together indicate similar gene expression.

(B) Volcano plot showing differential gene expression analysis between *smn-1(+)* and *smn-1(ok355)* animals. Genes significantly upregulated (red) and downregulated (blue) were identified based on a threshold of an adjusted P -value ≤ 0.05 and log2 fold change $\geq |1|$. Non-significant genes are shown in grey. The *smn-1* gene, which was downregulated in our analysis, is highlighted as a black circle and labelled.

We next aimed to identify which specific functional categories and biological pathways are significantly altered in response to the *smn-1(ok355)* mutation to gain a comprehensive understanding of the molecular mechanisms driving SMA pathology. To achieve this, we performed Gene Set Enrichment Analysis (GSEA), a powerful method that captures subtle coordinated changes in expression across predefined gene sets.

Our analysis revealed that SMN depletion in *smn-1(ok355)* animals led to significant dysregulation of enzymatic activities associated with tRNA catalytic activity and ribosome structure (**Figure 3.2**). Specifically, we observed strong negative enrichment scores (NES) for "structural constituent of ribosome" (NES = -2.52, Padj = 1.82e-15), "catalytic activity, acting on a tRNA" (NES = -2.45, Padj = 3.05e-10), and "aminoacyl-tRNA ligase activity" (NES = -2.20, Padj = 2.89e-05). These findings highlight the complex relationship between the SMN protein and various aspects of RNA metabolism, such as the biogenesis of snoRNPs (Wehner et al., 2002) and rRNA processing (Singh et al., 2017). Notably, recent evidence indicates that SMN directly associates with ribosomes, forming tissue-specific SMN-ribosome complexes that positively regulate translation (Lauria et al., 2020). Collectively, these findings suggest that SMN deficiency may compromise translation both indirectly, through impaired RNA metabolism, and directly, by altering ribosome composition and function, ultimately disrupting protein homeostasis.

While our analysis revealed significant dysregulation in RNA-related processes, we also observed intriguing changes in DNA-associated functions (**Figure 3.2**). The overexpression of the term "structural constituent of chromatin" (NES = 1.99, Padj = 2.87e-11) suggests a shift in the cellular focus from RNA metabolism to DNA stability. These alterations may indicate a broader cellular stress response triggered by SMN depletion, as changes in chromatin structure often occur in response to various cellular stresses including hypoxia, DNA damage, and oxidative stress (Johnson and Barton, 2007). Furthermore, we identified upregulation in "non-membrane spanning protein tyrosine kinase activity" (NES = 1.65, Padj = 0.00136). This term encompasses a group of proteins that play crucial roles in regulating numerous signalling pathways that govern cell proliferation, migration, differentiation, and apoptosis (Östman and Böhmer, 2001). Notably, the

"protein tyrosine phosphatase activity" category, which inhibits tyrosine kinases, also showed increased activity ($NES = 1.65$, $Padj = 0.00021$). Although both processes can be modulated by various stimuli, their simultaneous upregulation may suggest that the cells are experiencing an internal conflict between adapting to the changes in their environment due to SMN reduction and the risk of undergoing apoptosis.

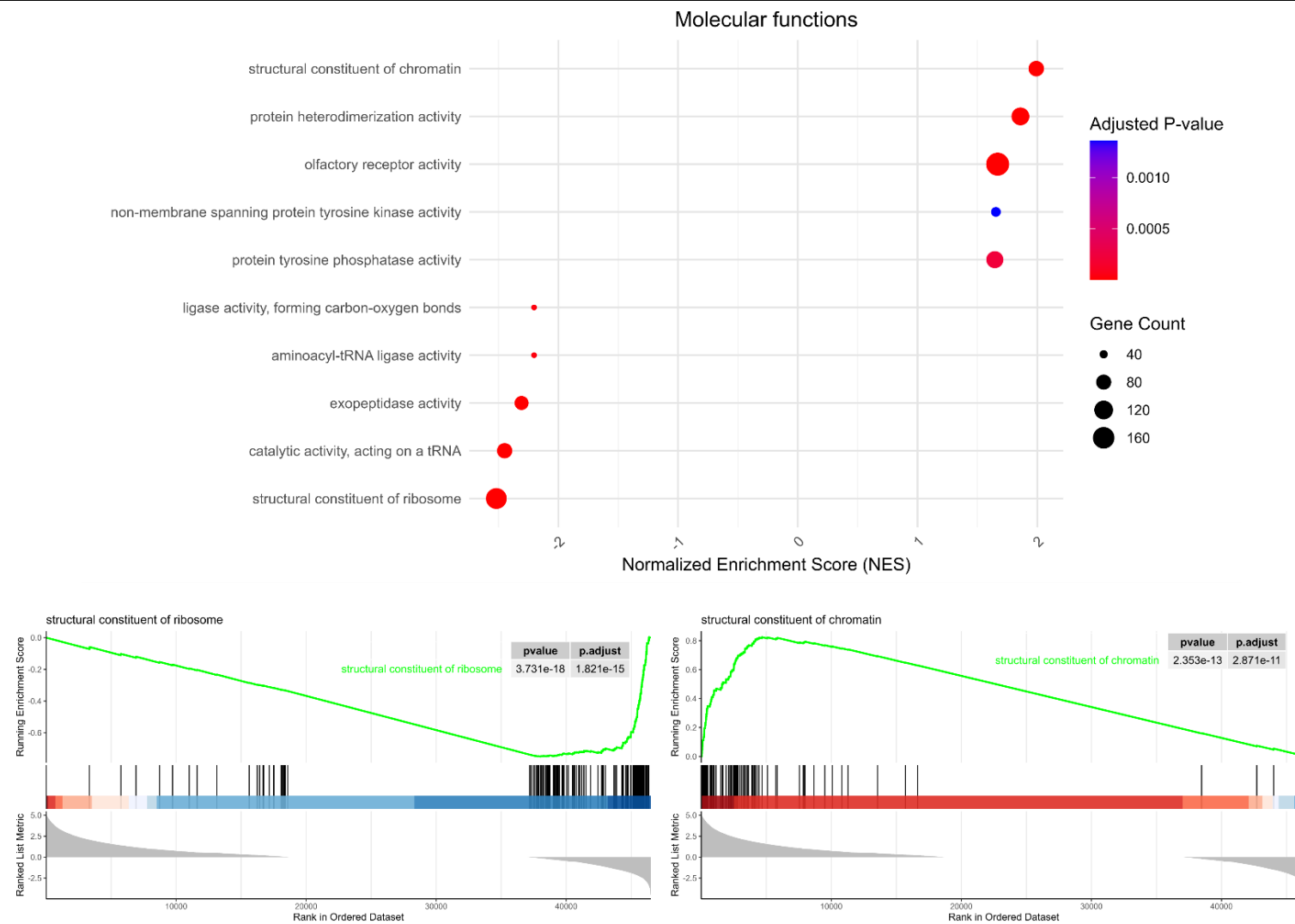


Figure 3.2. Gene Ontology (GO) molecular function enrichment analysis of the *smn-1(ok355)* *C. elegans* SMA model

- (A) Dot plot illustrating the five most upregulated and five most downregulated molecular function terms in *smn-1(ok355)* animals. The x-axis represents the normalised enrichment score (NES), and the y-axis represents the nomenclature of the enriched GO terms. The size of each dot indicates the number of dysregulated genes in each category, and the dot colour represents the adjusted p-value (P_{adj}) of the enrichment analysis.
- (B) Running enrichment score plot for the most upregulated GO molecular function term in *smn-1(ok355)*.
- (C) Running enrichment score plot for the most downregulated GO molecular function term in *smn-1(ok355)*.

Considering the cellular processes that could be contributing towards this 'stressed' cellular state, we found that *smn-1(ok355)* animals are immersed in a profound energetic crisis (**Figure 3.3**). Main biological processes controlling energy production, including “cellular respiration” (NES = -2.76, Padj = 1.27e-16), “aerobic respiration” (NES = -2.72, Padj = 2.67e-16) and "electron transport chain" (NES = -2.64, Padj = 2.17e-12), were strongly inhibited in our *C. elegans* SMA model. Collectively, these findings indicate a severe impairment in energy production pathways, which could ultimately lead to a significant reduction in ATP synthesis in *smn-1(ok355)* animals, as has been observed in other SMA models (Acsadi et al., 2009).

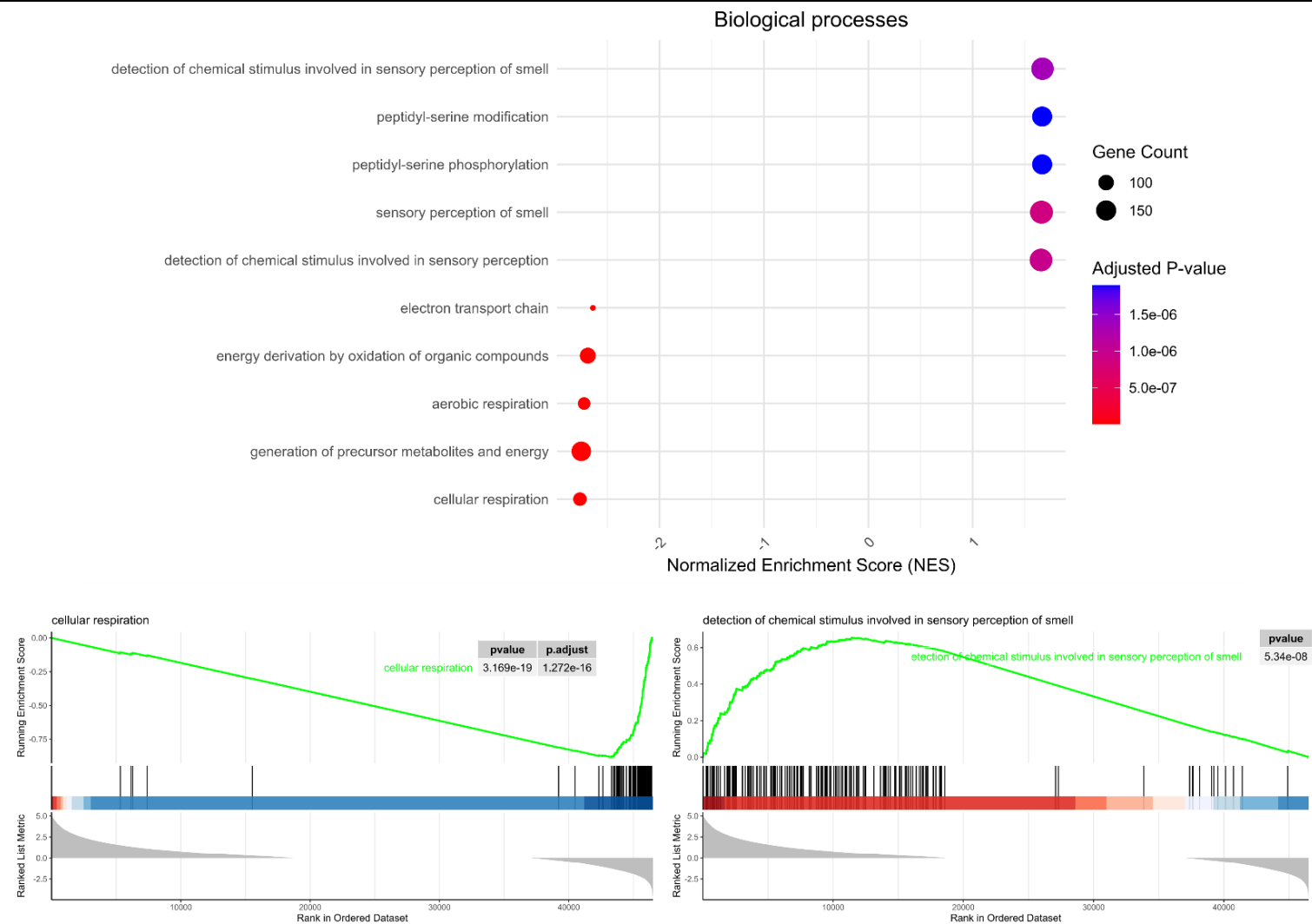


Figure 3.3. Gene Ontology (GO) biological processes enrichment analysis of the *smn-1(ok355)* *C. elegans* SMA model

- (A) Dot plot illustrating the five most upregulated and five most downregulated biological process terms in *smn-1(ok355)* animals. The x-axis represents the normalised enrichment score (NES), and the y-axis represents the nomenclature of the enriched GO terms. The size of each dot indicates the number of dysregulated genes in each category, and the dot colour represents the adjusted p-value (P_{adj}) of the enrichment analysis.
- (B) Running enrichment score plot for the most upregulated GO biological process term in *smn-1(ok355)*.
- (C) Running enrichment score plot for the most downregulated GO biological process term in *smn-1(ok355)*.

Not unexpectedly, upon examination of the major cellular components affected in *smn-1(ok355)* animals, mitochondria emerged as the most significantly affected (**Figure 3.4**). The five most downregulated cellular component terms in SMN-1 depleted animals belonged to mitochondrial protein categories, including "mitochondrial protein-containing complex" (NES = -3.04, Padj = 6.76e-40), "inner mitochondrial membrane protein complex" (NES = -2.87, Padj = 1.12e-23), "mitochondrial inner membrane" (NES = -2.86, Padj = 8.08e-31), "mitochondrial envelope" (NES = -2.78, Padj = 1.91e-33), and "mitochondrial matrix" (NES = -2.78, Padj = 1.12e-24). The extent of mitochondrial involvement aligns with previous studies that have identified mitochondrial defects as critical elements in SMA pathogenesis (Acsadi et al., 2009; Chemello et al., 2023; Miller et al., 2016; Thelen et al., 2020; Xu et al., 2016; Zilio et al., 2022). Moreover, the scarcity of mitochondrial proteins, particularly in the inner mitochondrial membrane, could impair the meticulous transfer of electrons between mitochondrial complexes during the electron transport chain (ETC) agrees with our previous findings. Prior research has shown that electron leakage in ETC complexes is a recognised source of ROS generation (Henderson et al., 2009; Zhang et al., 1998). If this is the case in our model, the overproduction of ROS in the mitochondria could account for the activation of stress signalling cascades, as observed in our analysis.

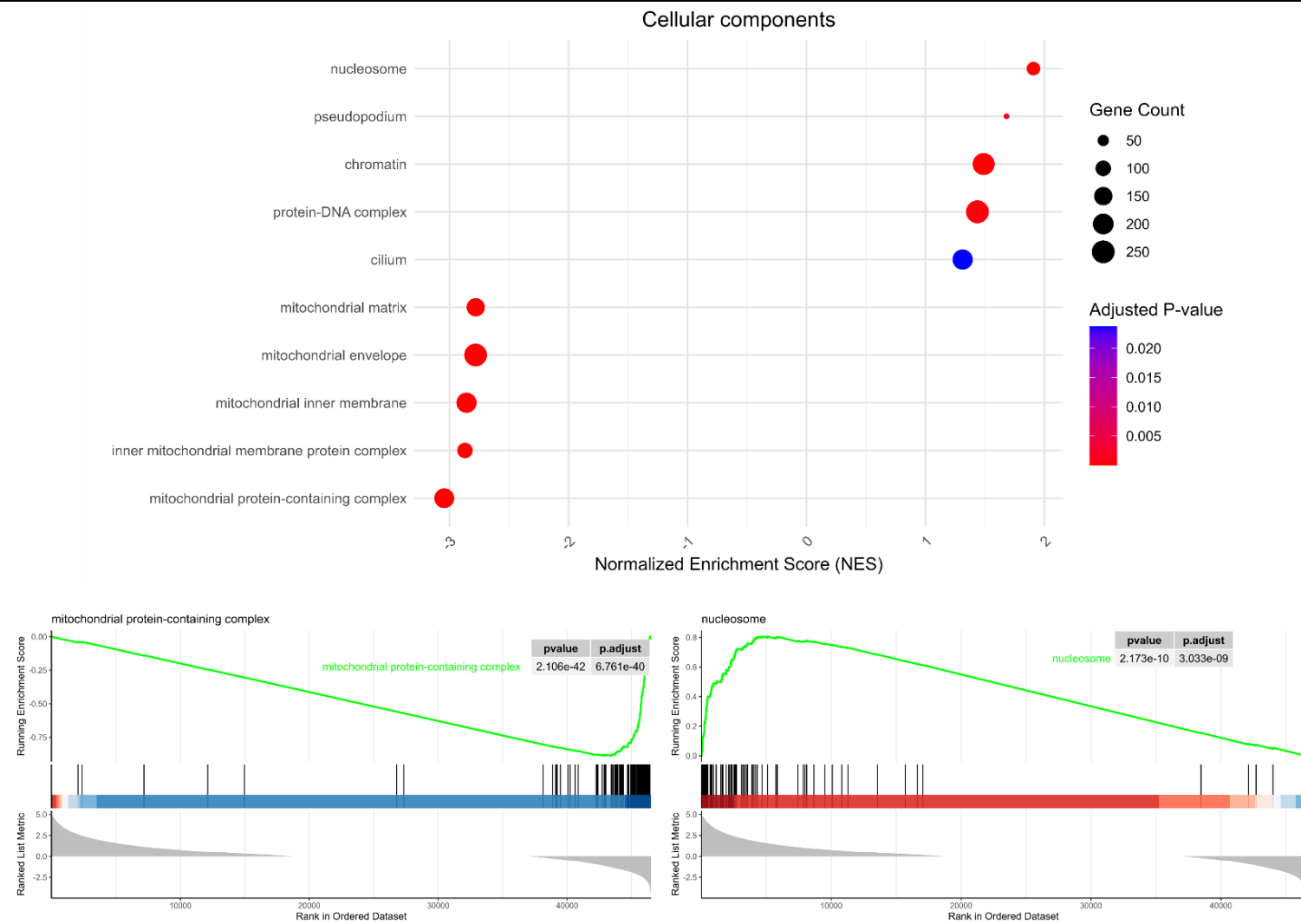


Figure 3.4. Gene Ontology (GO) cellular components enrichment analysis of the *smn-1(ok355)* *C. elegans* SMA model

- (A) Dot plot illustrating the five most upregulated and five most downregulated biological process terms in *smn-1(ok355)* animals. The x-axis represents the normalised enrichment score (NES), and the y-axis represents the nomenclature of the enriched GO terms. The size of each dot indicates the number of dysregulated genes in each category, and the dot colour represents the adjusted p-value (P_{adj}) of the enrichment analysis.
- (B) Running enrichment score plot for the most upregulated GO biological process term in *smn-1(ok355)*.
- (C) Running enrichment score plot for the most downregulated GO biological process term in *smn-1(ok355)*.

Building on previous observations, we investigated the specific metabolic pathways affected in our *C. elegans* SMA model. We found that *smn-1(ok355)* animals exhibited significant downregulation of catabolic and anabolic pathways, indicating a widespread metabolic shutdown (**Figure 3.5**). This extensive metabolic disruption was evidenced by the downregulation of terms such as "carbon metabolism" (NES = -2.51, Padj = 1.68e-14) and the mitochondrial "citrate cycle (TCA cycle)" (NES = -2.30, Padj = 1.49e-06). The most pronounced negative enrichment was observed in the "oxidative phosphorylation" pathway (NES = -2.79, Padj = 3.71e-21), the final step of aerobic respiration following ETC, and a major source of cellular ATP. These findings highlight the severe impairment in energy production in the *smn-1(ok355)* SMA model.

Notably, in the cellular context of SMA where neurons undergo neurodegeneration, there is a notable disruption in protein homeostasis and overall metabolic deficiency, the terms "erbb signalling pathway" (NES = -1.42, Padj = 0.048) and its downstream target "mtor signalling pathway" (NES = -1.46, Padj = 0.011) were found downregulated in *smn-1(ok355)* animals (**Figure 3.5**). These pathways are known to enhance lipid metabolism, protein synthesis, and cell survival (Wang & Proud, 2006), which are disrupted in SMA. Interestingly, although evidence suggests that oxidative stress can stimulate the ErbB signalling pathway (Savino et al., 2022), another study found that chronic oxidative stress exposure can inhibit ErbB2 activation (Dang et al., 2016). Furthermore, oxidative stress often inhibits the downstream mTor signalling pathway (Rieker et al., 2011).

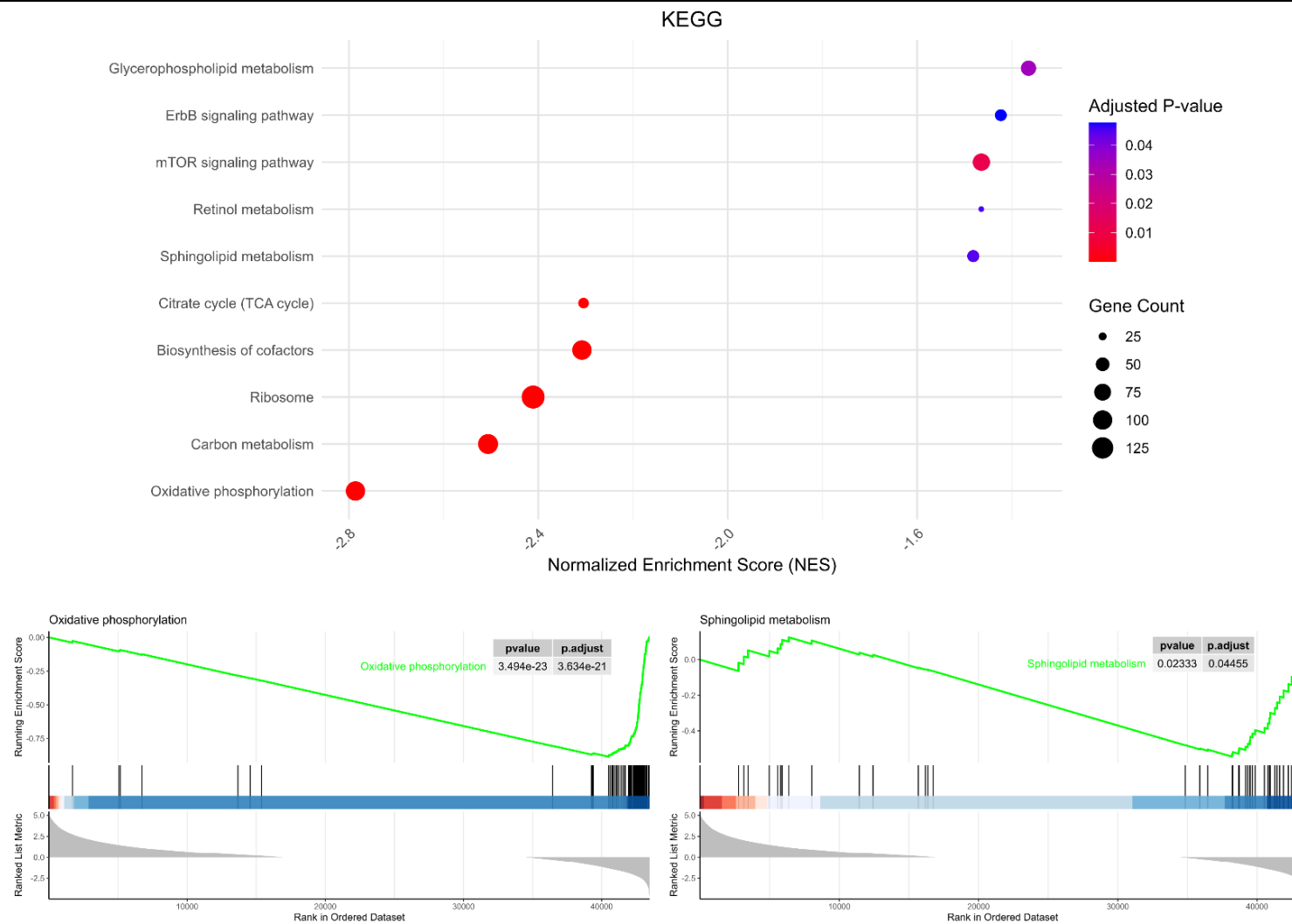


Figure 3.5. Kyoto Encyclopedia of Genes and Genomes (KEGG) pathways enrichment analysis of *smn-1(ok355)* *C. elegans* SMA model

- (A) Dot plot illustrating the five most upregulated and five most downregulated KEGG pathways terms in *smn-1(ok355)* animals. The x-axis represents the normalised enrichment score (NES), and the y-axis represents the nomenclature of the enriched KEGG terms. The size of each dot indicates the number of dysregulated genes in each category, and the dot colour represents the adjusted p-value (padj) of the enrichment analysis.
- (B) Running enrichment score plot for the most upregulated KEGG pathway term in *smn-1(ok355)*.
- (C) Running enrichment score plot for the most downregulated KEGG pathway term in *smn-1(ok355)*.

In conclusion, our comprehensive evaluation of gene expression in the *smn-1(ok355)* *C. elegans* SMA model revealed widespread alterations in gene expression and cellular pathways, underscoring the diverse functions of the SMN-1 protein across various cellular processes. The observed downregulation of key mitochondrial proteins suggests an increased ROS generation, implying that oxidative stress may be a critical factor in the observed metabolic disruptions and activation of stress signalling cascades. These findings highlight the necessity for further research on the potential involvement of oxidative stress in SMA.

3.2.2. SMN-1 depletion increases oxidative stress sensitivity in *Caenorhabditis elegans*

Elevated ROS levels have been associated with various neurodegenerative diseases, including SMA, suggesting that disrupted oxidative stress homeostasis may contribute to the progression of this disorder (El Khoury et al., 2023; Köstel et al., 2012; Thelen et al., 2020; Wang et al., 2013). Evaluating the sensitivity of *smn-1(ok355)* animals to oxidative stress can provide valuable insights into the role of the SMN-1 protein in maintaining the cellular equilibrium between baseline ROS levels, ROS detoxification capacity and the ability to repair ROS-induced damage (Senchuk et al., 2017). To validate and extend our findings beyond a single genetic model, we used an additional SMN-1 loss-of-function allele, the *smn-1(rt248)* mutation (Dimitriadi et al., 2016). This approach allowed us to assess whether the observed results were due to the loss of the SMN-1 protein. Furthermore, we employed the *smn-1(ok355);[smn-1(+)]* rescue strain, previously generated by reintroducing one wild-type copy of the *smn-1* gene into the *smn-1(ok355)* background (Dimitriadi et al., 2016), to elucidate whether defects associated to SMN-1 depletion could be rescued when SMN-1 protein levels are restored.

To gain a comprehensive understanding of the involvement of the SMN-1 protein on ROS homeostasis, we evaluated the sensitivity to oxidative stress of SMN-1-depleted animals and respective controls by exposing day-3 adult animals to well-known ROS generators and assessing the impact on survival. To address this, we first examined the lifespan of SMN-1-depleted animals

under normal conditions. We observed that upon SMN-1 depletion, *smn-1(ok355)* nematodes exhibited a markedly decreased lifespan in comparison to healthy controls, in agreement with findings from previous studies (Briese et al., 2008) (**Figure 3.6A**, $P < 0.0001$). Analogous to their *smn-1(ok355)* counterparts, *smn-1(rt248)* mutants exhibited a significantly reduced lifespan (**Figure 3.6A**, $P < 0.0001$). Notably, introducing a wild type copy of *smn-1* in *smn-1(ok355);[smn-1(+)]* nematodes significantly increased the lifespan of *smn-1(ok355)* mutants (**Figure 3.6A**, $P < 0.0001$), although it remained substantially lower than that of the *smn-1(+)* control animals (**Figure 3.6A**, $P < 0.0001$).

Having established baseline lifespan differences, we investigated the response of these nematodes to chronic oxidative stress induced by 4 mM paraquat. We observed that the survival of healthy *smn-1(+)* animals drastically decreased from over 20 days, in normal conditions, to 7 days upon paraquat exposure, highlighting the detrimental effects of elevated ROS levels on *C. elegans* lifespan (**Figure 3.6B**, $P < 0.0001$). The survival of *smn-1(ok355)* animals was more severely affected, with only 27% of the initial population surviving by day 2 and a maximum lifespan of only 5 days, which was significantly lower than that of control animals (**Figure 3.6B**, $P < 0.0001$). To confirm that these effects were not specific to the *ok355* allele only, we examined the survival of *smn-1(rt248)* mutants in paraquat and found that these animals also exhibited a significant decline in survival compared to controls (**Figure 3.6B**, $P < 0.0001$), further indicating that the increased ROS sensitivity is attributable to the depletion loss of the SMN-1 protein. The introduction of a single copy of the *smn-1* gene in *smn-1(ok355);[smn-1(+)]* animals partially rescued oxidative stress sensitivity, as these animals survived better than their *smn-1(ok355)* counterparts (**Figure 3.6B**, $P < 0.0001$). However, their survival did not fully return to control levels (**Figure 3.6B**, $P = 0.0019$).

To gain a better understanding of the sensitivity of the *smn-1(ok355)* *C. elegans* SMA model to oxidative stress, we modified the experimental design from a chronic to an acute assay, exposing the animals to 60 μ M juglone for 4 h. We observed that *smn-1(+)* animals remained unaffected for the duration of the assay, indicating that this concentration of juglone was insufficient to

disrupt their internal ROS homeostasis. However, the response of *smn-1(ok355)* animals was markedly different, with a progressive decrease in survival throughout the experiment (**Figure 3.6C**, $P < 0.0001$). Similarly, *smn-1(rt248)* mutants also exhibited a significant decline in survival (**Figure 3.6C**, $P < 0.0001$), indicating that sensitivity to acute oxidative stress was likely caused by SMN depletion. Notably, the upregulation of SMN-1 protein levels in *smn-1(ok355);[smn-1(+)]* animals fully rescued the sensitivity of *smn-1(ok355)* nematodes to that of control levels (**Figure 3.6C**, $P > 0.9999$).

Overall, our findings demonstrate that SMN-1 depletion in *C. elegans* significantly increases its sensitivity to oxidative stress, as evidenced by reduced survival in both chronic and acute ROS exposure. This heightened vulnerability was consistently observed across different SMN-1 loss-of-function alleles, confirming that the observed effects are attributable to the depletion of the SMN-1 protein. The partial rescue of oxidative stress resistance in *smn-1(ok355);[smn-1(+)]* animals further supports the critical role of the SMN-1 in maintaining cellular redox homeostasis.

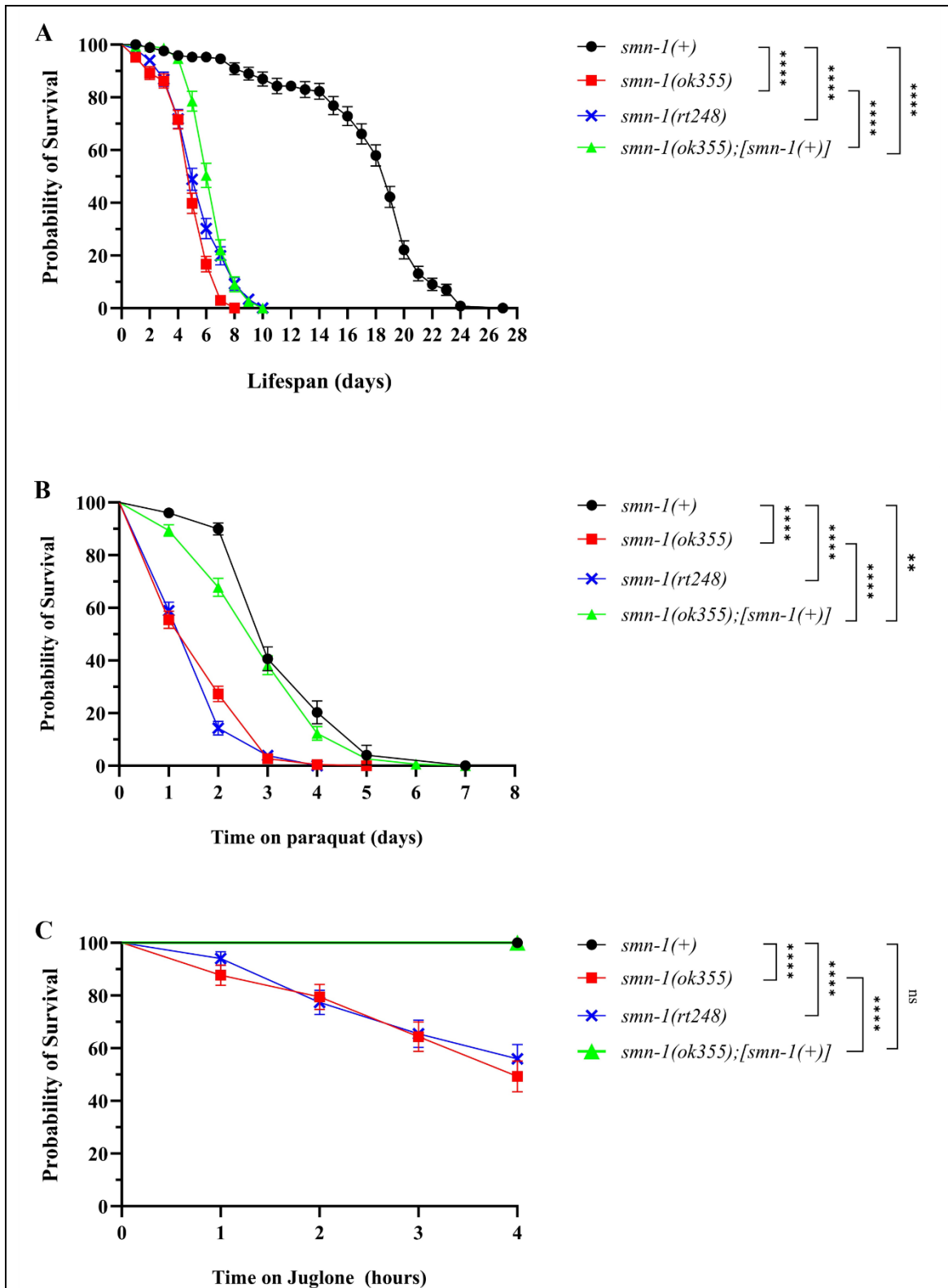


Figure 3.6. Depletion of the SMN-1 protein increases sensitivity to oxidative stress in *C. elegans*

(A) The lifespan of *C. elegans* is reduced in the SMN-1-depleted strains *smn-1(ok355)* (red) and *smn-1(rt248)* (blue). An extrachromosomal single-copy insertion of the *smn-1* gene markedly extended the lifespan of *smn-1(ok355);[smn-1(+)]* mutants (green), yet failed to fully restore it

to the level of *smn-1(+)* controls (black). *smn-1(+)* (n = 147), *smn-1(ok355)* (n = 151), *smn-1(rt248)* (n = 139), *smn-1(ok355);[smn-1(+)]* (n = 111).

(B) Depletion of the SMN-1 protein increased sensitivity to chronic oxidative stress induced by 4 mM paraquat in both *smn-1(ok355)* and *smn-1(rt248)* mutants. The *smn-1(ok355);[smn-1(+)]* strain showed a significant improvement in resistance to chronic oxidative stress compared to *smn-1(ok355)*, yet to the extent observed in *smn-1(+)* controls. *smn-1(+)* (n = 95), *smn-1(ok355)* (n = 231), *smn-1(rt248)* (n = 193), *smn-1(ok355);[smn-1(+)]* (n = 171).

(C) Depletion of the SMN-1 protein increased sensitivity to acute oxidative stress induced by 60 μ M juglone in both *smn-1(ok355)* and *smn-1(rt248)* mutants. The reintroduction of the *smn-1* gene in *smn-1(ok355);[smn-1(+)]* animals completely rescued their sensitivity to acute oxidative stress to *smn-1(+)* control levels. *smn-1(+)* (n = 81), *smn-1(ok355)* (n = 73), *smn-1(rt248)* (n = 84), *smn-1(ok355);[smn-1(+)]* (n = 85).

(A-C) All assays were performed utilising synchronised day-3 *C. elegans* populations. Probability of survival over time is presented in a Kaplan-Meier survival curve. Each time point represents the mean \pm SEM of three independent trials. Statistical significance was determined using separate log-rank test applied to pairwise genotype comparisons. ns $P > 0.05$, ** $P < 0.01$ and **** $P < 0.0001$.

To determine whether the increased oxidative stress sensitivity in the *smn-1(ok355)* *C. elegans* SMA model was specific to oxidative stress or whether these organisms exhibited a generalised heightened sensitivity to various types of stressors, we evaluated their ability to withstand two additional types of stress: heat stress and osmotic stress. If the increased sensitivity of *smn-1(ok355)* animals to oxidative stress was caused by an overall inability to cope with stress, we would anticipate that *smn-1(ok355)* animals would also display enhanced sensitivity to heat and osmotic stress.

Prior to assessing the sensitivity of *smn-1(ok355)* animals to heat stress, we sought to determine the appropriate exposure time to heat that would yield a balanced survival-to-death ratio, enabling us to observe differences in survival between strains more effectively. Young adult wildtype (N2) nematodes were incubated at 35°C for 3, 4, 5, 6, and 7 h and, after 24h of recovery at 20°C, their survival rates were evaluated. The results indicated that exposure to 35°C for 3, 4, or 5 h did not significantly affect the survival of wildtype animals (**Figure 3.7A**, $P = 0.9902$, $P = 0.6683$, $P = 0.5167$, respectively). However, survival rates significantly decreased to 71% after 6 h of exposure (**Figure 3.7A**, $P = 0.0034$) and further declined to 10% after 7 h of exposure (**Figure 3.7A**, $P < 0.0001$). Based on these findings, a 6-hour exposure at 35°C was selected for subsequent experiments.

To our surprise, we observed that *smn-1(ok355)* animals not only failed to exhibit increased heat stress sensitivity but also demonstrated enhanced resistance to heat stress compared to *smn-1(+)* control animals (**Figure 3.7B**, $P = 0.0058$). Notably, the survival rate of *smn-1(rt248)* mutants was not significantly different from that of control animals (**Figure 3.7B**, $P = 0.1642$). Moreover, following osmotic stress induction with 450mM NaCl, while the survival rate of control animals substantially decreased, *smn-1(ok355)* animals again exhibited partial resistance to osmotic stress, with a significantly higher survival rate than control nematodes (**Figure 3.7C**, $P = 0.0219$). In contrast, *smn-1(rt248)* animals showed a survival rate that was not significantly different from that of *smn-1(+)* controls (**Figure 3.7C**, $P = 0.5739$). While these findings revealed unexpected stress response patterns in different SMN-1 depleted mutants, they demonstrated that the

increased oxidative stress sensitivity exhibited after SMN-1 depletion did not extend to other forms of stress.

Overall, our findings suggest that SMN-1 depletion in *C. elegans* selectively impairs pathways related to ROS regulation, without affecting other stress responses. These results underscore the essential role of the SMN-1 protein in maintaining cellular redox homeostasis and highlight the need for further investigation of oxidative stress as a crucial factor in SMA progression.

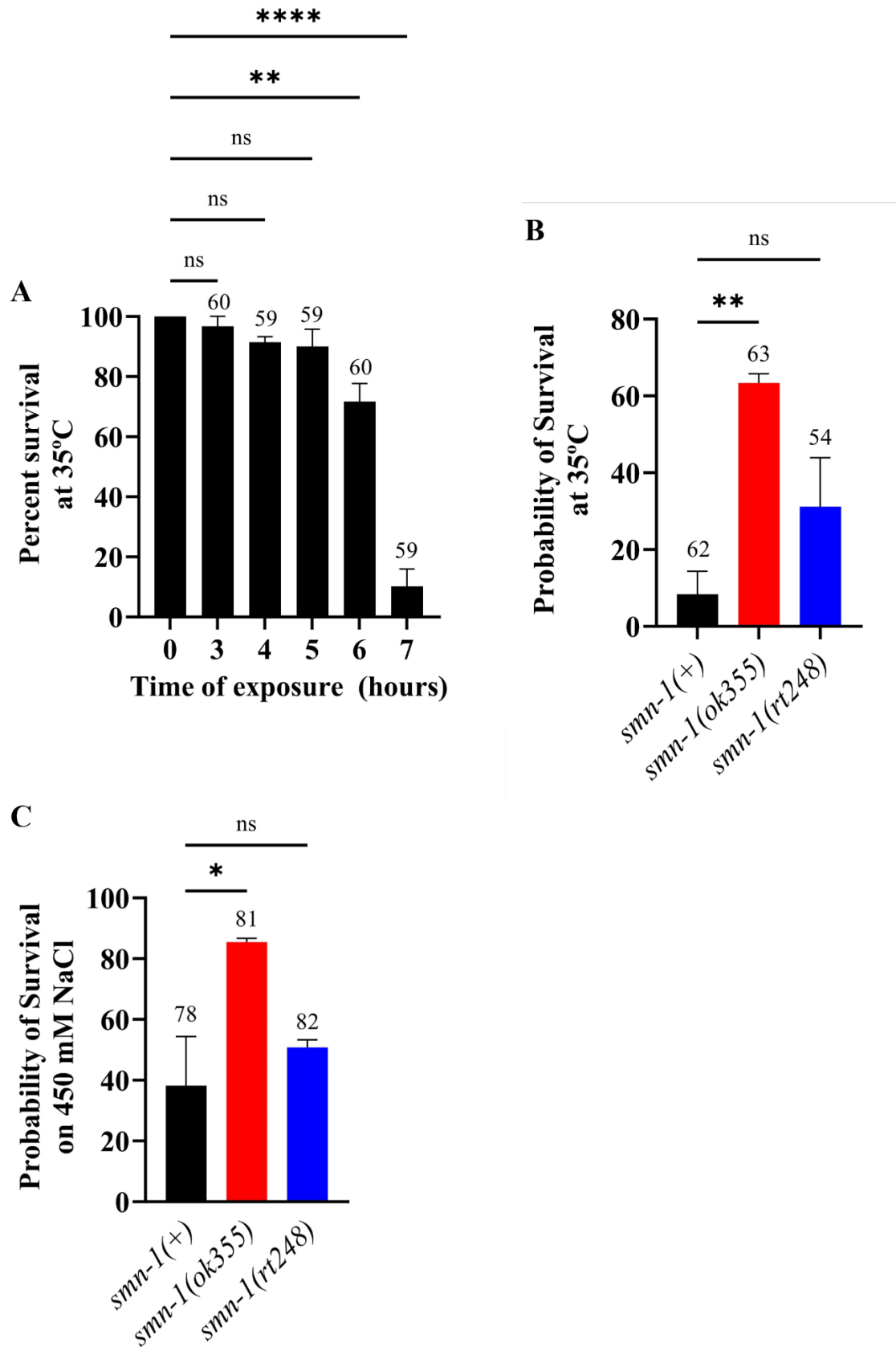


Figure 3.7. SMN-1 depletion modifies the stress response in the *smn-1(ok355)* *C. elegans* SMA model following exposure to heat and osmotic stress

(A) The probability of survival of *C. elegans* wildtype animals in the young adult state exposed to 35°C decreases as the duration of heat exposure increases. Notably, animals exhibited significantly different survival rates compared to non-exposed controls after 6 and 7 h at 35°C.

(B) The *smn-1(ok355)* *C. elegans* SMA model exhibited increased resistance to heat stress induced by exposure to 35°C for 6 h, while their SMN-1 depleted *smn-1(rt248)* counterparts showed no significant difference compared to *smn-1(+)* controls.

(C) The *smn-1(ok355)* *C. elegans* SMA model exhibited increased resistance to osmotic stress induced by exposure to 450 mM NaCl for 24h, while their SMN-1 depleted *smn-1(rt248)* counterparts showed no significant difference compared to *smn-1(+)* controls.

(A-C) Data are presented as the mean \pm SEM from three independent trials. Statistical significance was determined using one-way ANOVA test ($P < 0.0001$, $P = 0.0093$, and $P = 0.0298$, for figures A, B and C, respectively), followed by Dunnett's multiple comparison test. ns $P > 0.05$, ** $P < 0.01$ and **** $P < 0.0001$. The total number of nematodes assessed for each condition is shown above of the corresponding error bar.

3.2.3. SMN-1 depletion increases cytoplasmic ROS in *Caenorhabditis elegans*

Having established that the *smn-1(ok355)* *C. elegans* SMA model exhibits altered stress response pathways and increased sensitivity to oxidative stress, we next aim to investigate the underlying cause of this phenotype. Since mitochondria are a major source of cellular ROS, and considering the notable disruption of proteins involved in mitochondrial structure and function in *smn-1(ok355)* animals (**Figure 3.4**), we hypothesised that elevated mitochondrial ROS levels may contribute to the observed oxidative stress susceptibility. To examine this hypothesis, we utilised MitoSOX, a mitochondrial-specific blue dye that emits red fluorescence upon encountering oxidised products, allowing for a direct measure of mitochondrial ROS (Murphy et al., 2022).

Unexpectedly, our analysis revealed no significant difference in mitochondrial ROS levels in *smn-1(ok355)* mutants in comparison with those in controls after 2 h of incubation with 5 μ M MitoSOX (**Figure 3.8A-D**, $P = 0.9999$). Likewise, introduction of a wildtype copy of the *smn-1* gene in *smn-1(ok355);[smn-1(+)]* animals did not alter ROS production (**Figure 3.8A-B,G-H**, $P = 0.5904$). However, the additional *smn-1* loss-of-function allele, *smn-1(rt248)*, resulted in significantly elevated mitochondrial ROS levels compared to controls (**Figure 3.8A-B, E-F**, $P < 0.0001$), highlighting the differences between the SMN-1 depleted *C. elegans* strains. We included *sod-1(tm776)* mutants as a positive control in our experimental design, which lack the primary cytoplasmic and intermembrane space superoxide dismutase enzyme in *C. elegans*. As expected, *sod-1(tm776)* mutants exhibited significantly elevated MitoSOX fluorescence intensities (**Figure 3.8A-B, I-J**, $P = 0.0002$), validating the reliability of our assay.

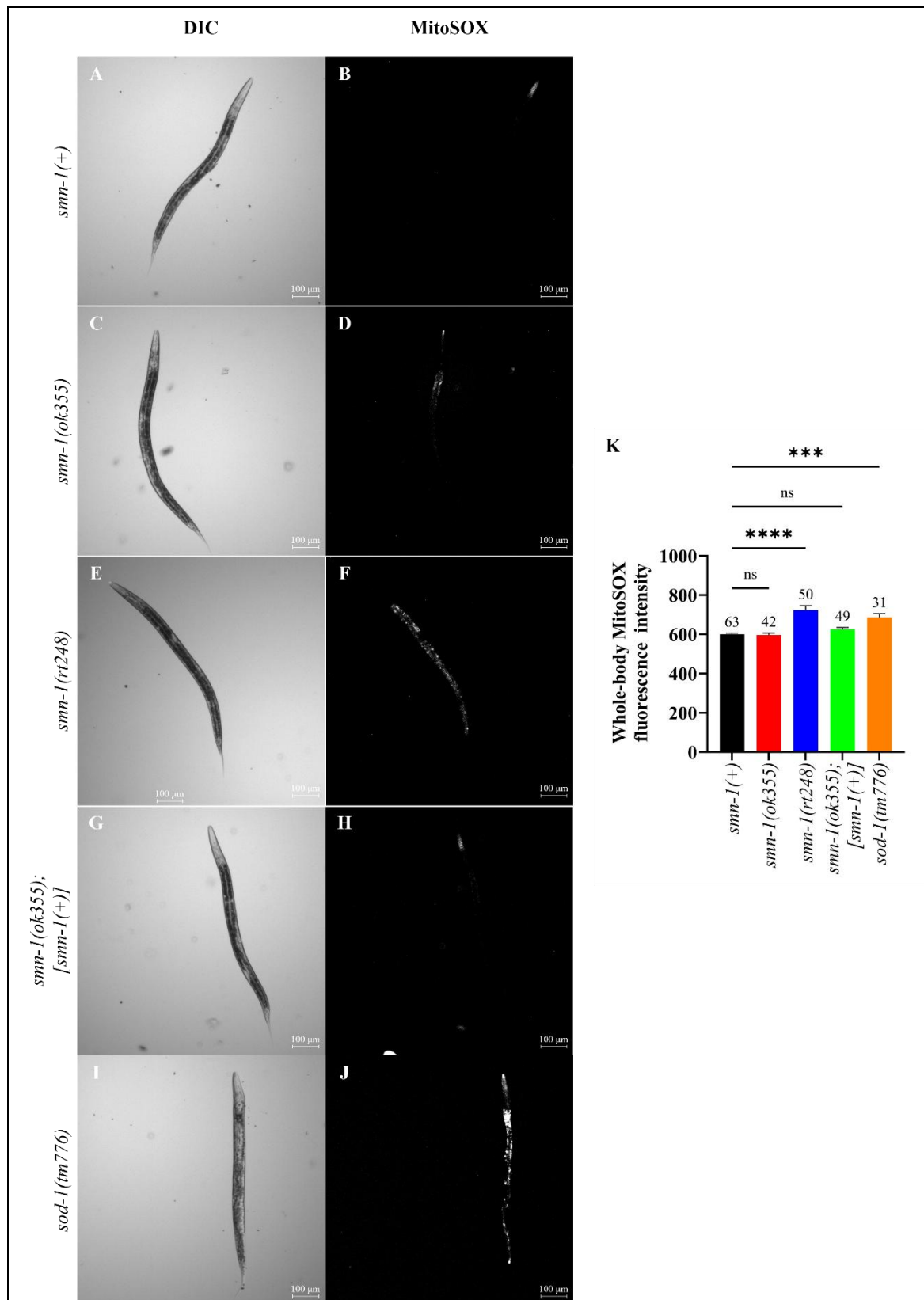


Figure 3.8. Depletion of the SMN-1 protein does not alter whole-body MitoSOX fluorescence in the *smn-1(ok355)* *C. elegans* SMA model

(A–H) Differential interference contrast (DIC) (A, C, E, G, and I) and fluorescence (B, D, F, H, and J) representative images of *C. elegans* stained with 5 μ M MitoSOX for 2 h. *smn-1(rt248)*

mutants (E and F) exhibited elevated mitochondrial ROS levels, whereas *smn-1(ok355)* (C and D) and *smn-1(ok355);[smn-1(+)]* (G and H) animals showed no significant difference compared to *smn-1(+)* controls (A and B). The positive control *sod-1(tm776)* (I and J) displayed significantly elevated mitochondrial ROS levels. Scale bars: 100 μ m.

(I) Quantification of the MitoSOX fluorescence signal. Data are presented as the mean \pm SEM of three independent trials. Statistical significance was determined using one-way ANOVA ($P < 0.0001$) followed by Šídák's multiple comparisons test. ns $P > 0.05$, *** $P < 0.001$ and **** $P < 0.0001$. The sample size (n) for each condition is shown above of the corresponding error bar.

Notably, previous studies have shown that the head of *C. elegans* is particularly rich in mitochondria (Altun and Hall, 2009), suggesting that examining this region may enhance the sensitivity of the MitoSOX assay to detect mitochondrial ROS (Dingley et al., 2010). Thereby, to refine our analysis, we decided to focus on the MitoSOX fluorescence emitted specifically in the head region of animals. However, similar to the whole-body fluorescence analysis, this approach did not reveal any significant changes in the fluorescence emitted by the head region of *smn-1(ok355)* (**Figure 3.9A-B, C-D**, $P = 0.0567$) or *smn-1(ok355);[smn-1(+)]* (**Figure 3.9A-B, G-H**, $P = 0.9462$) nematodes in comparison to *smn-1(+)* controls. Interestingly, while *smn-1(rt248)* animals exhibited elevated mitochondrial ROS in comparison to *smn-1(+)* controls under whole-body fluorescence, they did not display elevated ROS in the head region (**Figure 3.9A-B, E-F**, $P = 0.8692$). Notably, the internal control *sod-1(tm776)* exhibited elevated mitochondrial ROS fluorescence in their head-region (**Figure 3.9A-B, I-J**, $P = 0.0122$), consistently with the previous whole-body analysis, validating the sensitivity of the assay.

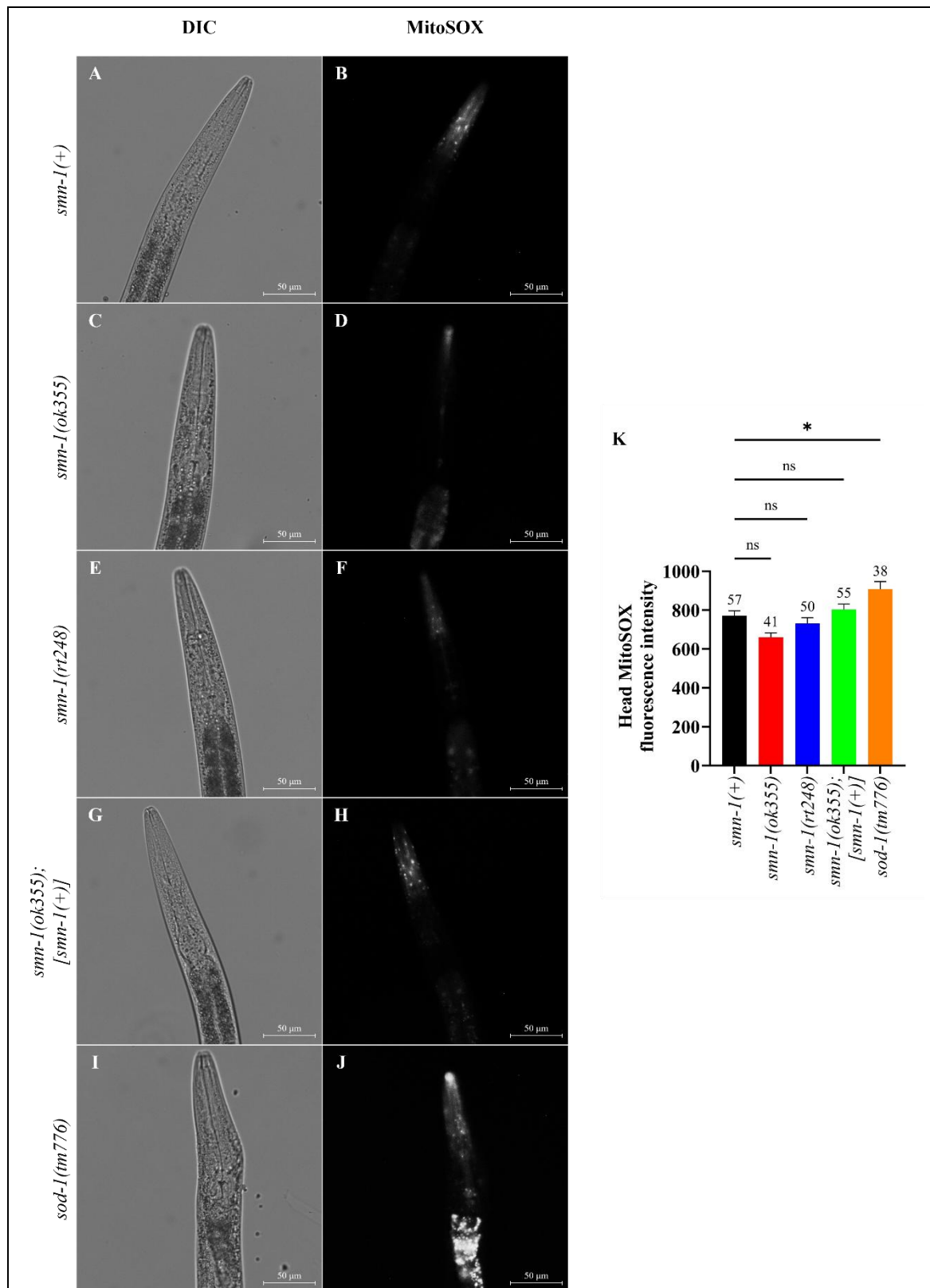


Figure 3.9. Depletion of the SMN-1 protein does not alter head-specific mitochondrial MitoSOX fluorescence in the *smn-1(ok355)* *C. elegans* SMA model.

(A–H) Differential interference contrast (DIC) (A, C, E, G, and I) and fluorescence (B, D, F, H, and J) representative images of the head region in *C. elegans* stained with 5 μ M MitoSOX for 2 h. None of the SMN-1 depleted mutants, *smn-1(ok355)* (C and D) and *smn-1(rt248)* (E and F), or the *smn-1* rescue strain *smn-1(ok355);[smn-1(+)]* (G and H) displayed elevated mitochondrial

ROS levels. The positive control *sod-1(tm776)* (I and J) demonstrated significantly elevated mitochondrial ROS levels. Scale bars: 50 μm

(K) Quantification of MitoSOX fluorescence signal in the head region. Data are presented as the mean \pm SEM of three independent trials. Statistical significance was determined using one-way ANOVA ($P < 0.0001$) followed by Šídák's multiple comparisons test. ns $P > 0.05$, * $P < 0.05$. The sample size (n) for each condition is shown above of the corresponding error bar.

While our findings suggest that mitochondrial ROS levels are not elevated in SMN-1 depleted *C. elegans*, previous studies have indicated that the effectiveness of MitoSOX staining can be affected by mitochondrial membrane potential (Robinson et al., 2006). Considering that our previous analysis revealed a downregulation of electron transport chain proteins in *smn-1(ok355)* nematodes, it is plausible that *C. elegans* SMA animals might experience decreased mitochondrial membrane potential, which could lead to inaccuracies when comparing their MitoSOX fluorescence intensity with that of *smn-1(+)* animals. To address this limitation and to gain a more comprehensive understanding of ROS regulation in the *smn-1(ok355)* *C. elegans* SMA model, we measured their levels of cytoplasmic ROS using dihydroethidium (DHE).

Our results demonstrated, for the first time, that ROS accumulate in the cytoplasm of *smn-1(ok355)* *C. elegans* (**Figure 3.10A-B, C-D**, $P < 0.0001$). To further confirm that the elevated ROS levels displayed by *smn-1(ok355)* mutants were due to SMN-1 depletion, we examined another *smn-1* loss-of-function allele, *smn-1(rt248)*. We found that, similar to *smn-1(ok355)*, cytoplasmic ROS levels were also elevated in *smn-1(rt248)* mutants (**Figure 3.10A-B, E-F**, $P < 0.0001$). Importantly, a single wildtype copy of *smn-1* in *smn-1(ok355);[smn-1(+)]* completely ameliorated the ROS burden in *smn-1(ok355)* mutants (**Figure 3.10A-B, G-H**, $P = 0.2132$).

Overall, our results establish a relationship between SMN-1 depletion and oxidative stress burden in *C. elegans* SMA. In this context, the dysregulation of stress pathways and the heightened oxidative stress sensitivity observed in the *smn-1(ok355)* *C. elegans* SMA model appears to be primarily driven by ROS accumulation. These findings support the utilisation of *smn-1(ok355)* *C. elegans* as a model for studying oxidative stress-related mechanisms dysregulated in SMA and highlights the potential of targeting those pathways as a promising therapeutic strategy.

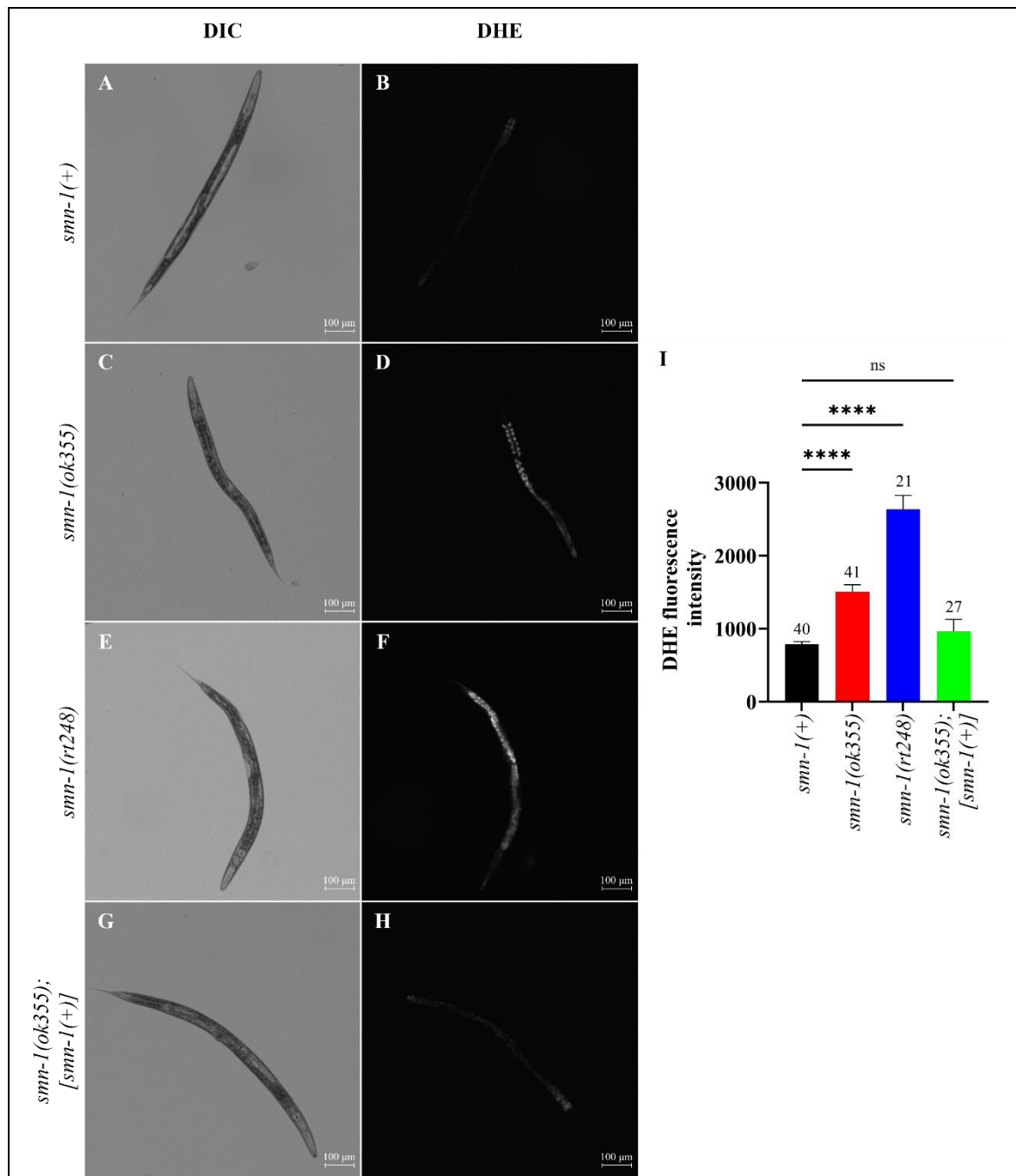


Figure 3.10. The SMN-1 protein prevents the cytoplasmic accumulation of ROS in *C. elegans*

(A–H) Differential interference contrast (DIC) (A, C, E, and G) and fluorescence (B, D, F, and H) representative images of *C. elegans* stained with 10 μ M DHE for 2 h. Depletion of SMN-1 protein levels in *smn-1(ok355)* (C and D) and *smn-1(rt248)* (E and F) induced the cytoplasmic accumulation of ROS in *C. elegans*. A single copy of the *smn-1* gene in *smn-1(ok355); [smn-1(+)]* (G and H) was sufficient to sustain normal cytoplasmic ROS levels. Scale bars: 100 μ m.

(I) Quantification of the DHE fluorescence signal. Data are presented as mean \pm SEM of four independent trials. Statistical significance was determined using one-way ANOVA ($P < 0.0001$) followed by Šidák's multiple comparisons test. ns $P > 0.05$ and **** $P < 0.0001$. The sample size (n) for each condition is shown above of the corresponding error bar.

3.3. Discussion

This chapter investigates the molecular and physiological consequences of SMN-1 depletion in the *C. elegans* SMA model. Through transcriptomic analysis, survival assays under various stress conditions, and ROS detection techniques, we aimed to characterise changes in gene expression, response to oxidative stress and ROS levels following SMN-1 depletion in *C. elegans*, with the goal to determine to whether *smn-1(ok355)* *C. elegans* constitute a suitable model for studying oxidative stress in SMA.

3.3.1. Gene expression changes in the *Caenorhabditis elegans* spinal muscular atrophy model

Our RNA sequencing analysis revealed significant gene expression changes in the *smn-1(ok355)* *C. elegans* SMA model, highlighting the broad molecular and cellular effects upon SMN-1 depletion. The genetic profile of *smn-1(ok355)* animals was consistent with a complex cellular stress response. We found that, in *smn-1(ok355)* nematodes, there was upregulation of chromatin remodelling, non-receptor protein tyrosine kinases and protein tyrosine phosphatase activities, processes that has been associated with cellular stress responses (Johnson and Barton, 2007; Solouki, August and Huang, 2019). These results are consistent with RNA-seq studies conducted in cell culture and SMA mouse models, which demonstrated upregulation of histones and DNA binding transcription factors (i.e. proteins that regulate cellular responses under stress) following SMN depletion (Gao et al., 2019; Kumar et al., 2024; Ren et al., 2024).

Additionally, our analysis revealed downregulation of the mTOR pathway, which could be indicative of overall protein synthesis defects (Wang & Proud, 2006), a finding previously observed in severe SMA mouse models (Bernabò et al., 2017b; Thelen et al., 2020). Notably, the literature contains conflicting findings regarding the activation or deactivation of mTOR in SMA. For example, Sansa et al., (2021) reported decreased mTOR phosphorylation in SMA patients' fibroblasts and in protein extracts from spinal cord and muscle of a severe SMA mouse model. Conversely, the same study observed increased mTOR phosphorylation in human iPCS-derived

MNs and isolated mouse MNs. Under normal conditions, the mTOR pathway is activated during energetic stress conditions, such as that induced by the inactivation of mitochondrial complexes, leading to the activation of pro-survival cellular signals (Kazyken et al., 2019). Given the extensive dysregulation of mitochondrial proteins observed in our analysis (**Figure 3.4**), as well as the evidence of mitochondrial dysfunction and reduced ATP levels found in various SMA models (Acsadi et al., 2009; Miller et al., 2016; Thelen, Wirth and Kye, 2020), it appears that the activation of the mTOR pathway could be crucial for stimulating cell survival in SMA pathological conditions. The downregulation of mTOR in our *C. elegans* SMA model may suggest defects in critical upstream pathways, what demands further investigation.

Our analysis further identified that *smn-1(ok355)* animals are experiencing a profound energetic crisis. This was evidenced by the strong downregulation of processes controlling cellular respiration and ATP production, such as proteins of the ETC, and further emphasised by the significant downregulation of terms related to mitochondrial structure and function. These findings are consistent with previous studies identifying mitochondrial gene dysregulation along with mitochondrial dysfunction (**Table 1.6. Evidence of mitochondrial defects on spinal muscular atrophy**) as a critical features of SMA.

Overall, our findings suggest that mitochondrial dysfunction, combined with impaired energy production provides an ideal environment for ROS accumulation. The overproduction of ROS likely triggers the activated stress responses observed, creating a feedback loop that exacerbates cellular damage.

3.3.2. Dissecting stress vulnerabilities in spinal muscular atrophy

The role of the SMN-1 protein in oxidative stress sensitivity was investigated by utilising oxidative stress-induction assays, wherein ROS levels are chemically elevated to assess the organism's capacity to maintain redox balance, detoxify ROS, and repair ROS-induced damage (Senchuk et al., 2017). Under normal conditions, both *smn-1(ok355)* and *smn-1(rt248)* loss-of-

function alleles exhibited significantly reduced lifespan (**Figure 3.6**). The partial rescue of lifespan observed in *smn-1(ok355);[smn-1(+)]* mutants, which harbours a single copy insertion of the *smn-1* gene, suggests that increasing SMN-1 protein levels can mitigate, though not fully restore, organismal survival. Although the *smn-1* plasmid inserted in *smn-1(ok355);[smn-1(+)]* animals comprised the *smn-1* promoter, coding region and 3' untranslated region (Dimitriadi et al., 2016), it might be possible that other regulatory unknown elements of the *smn-1* gene are missing, which may be critical for proper SMN-1 expression and function.

Notably, our results demonstrate that SMN-1 depletion significantly increases sensitivity to oxidative stress under both chronic (paraquat) and acute (juglone) ROS exposure. The consistent findings across two independent loss-of-function alleles (*ok355* and *rt248*) confirm that the heightened ROS sensitivity is a direct consequence of SMN-1 depletion. Notably, introducing a single wildtype copy of *smn-1* in *smn-1(ok355);[smn-1(+)]* animals partially rescued survival under chronic oxidative stress conditions and fully restored survival under acute stress, suggesting that SMN-1 is particularly critical for responding to short-term oxidative insults. However, prolonged oxidative stress may induce cumulative cellular damage that cannot be completely mitigated, even with SMN-1 restoration.

Interestingly, SMN-1 depleted animals did not show sensitivity to either heat or osmotic stress, revealing that their heightened sensitivity to juglone and paraquat was oxidative stress specific. Notably, both *smn-1* loss-of-function alleles behaved differently under heat and osmotic stresses.

After heat and osmotic stress induction, *smn-1(ok355)* mutants showed increased survival rates compared to control animals. This unexpected resistance suggests that the heightened sensitivity of *smn-1(ok355)* animals to oxidative stress is not due to a general defect in cellular stress responses, but to an oxidative stress-specific vulnerability. A consideration that could explain that differential response is that SMN-1 depletion results in elevated ROS levels, a finding that we have confirmed (**Figure 3.10**). Elevated ROS levels in *smn-1(ok355)* animals would make them more vulnerable to further increases in ROS, but not necessarily to other stressors. This case is exemplified by the *C. elegans* mitochondrial mutant *sod-2*, which lacks the enzyme SOD-2, the

primary responsible for superoxide detoxification in mitochondria (Gems and Doonan, 2008; Suthammarak et al., 2013; Dues et al., 2017). Research has demonstrated that these mutants display increased sensitivity to chronic and acute oxidative stress induction, but not to heat or osmotic stress (Van Raamsdonk & Hekimi, 2009). This finding highlights that while the responses to oxidative, heat and osmotic stress share some molecular components, they are also partly independent from one another (**Supplementary Figure 1**). Notably, studies in *C. elegans* have shown that different stress responses cannot be activated simultaneously to the same extent (Crombie et al., 2016; Deng et al., 2020). For instance, the activation of SKN-1, a key regulator of the oxidative stress response in *C. elegans*, have been shown to impair the response to heat stress. Conversely, reduced SKN-1 activity, enhance heat stress resistance (Crombie et al., 2016). Therefore, if SKN-1 activity is reduced in *smn-1(ok355)* animals, which would explain their increased sensitivity to oxidative stress, those animals might also exhibit enhanced resistance to other stressors, as observed in our results.

Interestingly, under heat and osmotic stress conditions *smn-1(rt248)* mutants exhibited survival rates that were comparable to those of control animals. This distinct behaviour compared to *smn-1(ok355)* mutants could be due to differences in the genetic nature of their mutations. The *ok355* allele is a complete deletion of the *smn-1* gene, which may remove important regulatory sequences upstream of the gene, potentially affecting the differential expression of other genes involved in stress management. By contrast, the *rt248* allele is a point mutation that introduces a premature stop codon in exon 2, resulting in a truncated SMN-1 protein. Although this protein isoform is expected to be rapidly degraded by the proteasome, this has not been experimentally confirmed, which means that *smn-1(rt248)* mutants may retain residual SMN-1 protein or partially preserve regulatory elements required for specific stress responses. This difference may explain why *smn-1(rt248)* mutants do not show enhanced resistance to heat or osmotic stress like *smn-1(ok355)* animals. Despite these differences, both *smn-1(ok355)* and *smn-1(rt248)* mutants did not exhibit increased sensitivity to heat or osmotic stress relative to controls, which strengthens the conclusion that the SMN-1 depletion selectively impairs pathways that manage ROS production,

clearance, and defence mechanisms without broadly compromising other cellular stress responses.

3.3.3. ROS imbalance in the *Caenorhabditis elegans* spinal muscular atrophy model

To further investigate the potential link between SMN-1 depletion and oxidative stress, we directly visualised ROS levels in SMN-1 depleted mutants, *smn-1(ok355)* and *smn-1(rt248)* animals, using small fluorescence probes for superoxide detection in cytoplasm and mitochondria (DHE and MitoSOX, respectively). Our results revealed significantly increased cytoplasmic ROS levels, supporting the hypothesis of elevated baseline ROS levels in SMN-1 deficient animals. These findings are consistent with previous studies that have reported ROS levels in patient-derived cell lines and SMA mouse models (Acsadi et al., 2009; Köstel, Bora-Tatar and Erdem-Yurter, 2012; Ando et al., 2017; El Khoury et al., 2023). The alignment between our findings in *C. elegans* and results from mammalian systems indicates that the association between SMN depletion and increased ROS is evolutionary conserved across different species, highlighting the suitability of *C. elegans* to study the relationship between oxidative stress and SMA pathogenesis.

However, attempts to visualise mitochondrial ROS using MitoSOX, a mitochondria-targeted probe, did not yield detectable signals in SMN-1 depleted mutants. This raises intriguing questions about the specific cellular compartments contributing to ROS production in SMN-1 depleted mutants. One possibility is that the observed ROS increase does not originate from mitochondria. While this interpretation is difficult to reconcile given the previous evidence implicating mitochondria as a source of ROS in SMA patient-derived cell and SMA mouse models (Ando et al., 2017; Miller et al., 2016; Wang et al., 2013), it remains a consideration. Another possible explanation is that increased ROS levels in SMN-1 depleted mutants did stem from mitochondria but MitoSOX staining just failed to target mitochondrial ROS in SMA-like *C. elegans* models. Previous studies have shown that the ability to visualise mitochondrial ROS with MitoSOX depends heavily on the mitochondrial membrane potential ($\Delta\Psi_m$) (Ross et al., 2005).

Numerous studies have shown that mitochondria of SMA patients and SMA mouse models exhibit several defects, including abnormal morphology and reduced $\Delta\Psi_m$ (**Table 1.6. Evidence of mitochondrial defects on spinal muscular atrophy**). Although $\Delta\Psi_m$ has not been directly evaluated in *smn-1(ok355)* animals, research indicates that, similar to mammalian SMA models, *smn-1(ok355)* mitochondria exhibit abnormal morphology (Schultz et al., 2017). Additionally, our RNA-seq analysis has uncovered extensive dysregulation of mitochondrial proteins and processes (**Figure 3.4** and **Figure 3.5**), which might be indicative of decreased $\Delta\Psi_m$. It should also be noted that MitoSOX is not specifically targeted to mitochondria, but to the cellular compartment with the most negative electric charge. In normal conditions, this would be mitochondria, but in case of heavily reduced $\Delta\Psi_m$, MitoSoX would target the endoplasmic reticulum or nucleus (Funk and Scholkmann, 2023). Therefore, the functional state of mitochondria, especially the extent of mitochondrial membrane potential loss, may vary between *C. elegans* and mammalian SMA models, potentially explaining the discrepancies in our results.

While we cannot conclusively confirm mitochondria as the primary source of elevated ROS in SMN-1 depleted *C. elegans*, our results clearly demonstrate a significant increase in overall ROS levels. Taken together, our findings indicate that increased ROS is an evolutionarily conserved hallmark of SMN depletion, and that further elevation of ROS levels has detrimental effects on SMA-like *C. elegans*. This establishes a robust foundation for elucidating the interplay between oxidative stress and SMA pathogenesis in the *smn-1(ok355)* *C. elegans* SMA model.

Chapter IV. Therapeutic potential of antioxidant treatment in spinal muscular atrophy

4.1. Introduction

In Chapter III it was established that SMN-1 depletion in *C. elegans* leads to increased oxidative stress sensitivity and elevated cytoplasmic ROS levels. These findings are consistent with previous observations in SMA pre-clinical models and patient-derived cell lines, as discussed in Chapter I, reinforcing the hypothesis that oxidative stress plays an active role in SMA pathogenesis. Building on this evidence, in Chapter IV we explore whether targeting oxidative stress could serve as a viable therapeutic strategy for SMA.

In this study, we evaluated the therapeutic potential of five antioxidants, *N*-acetylcysteine (NAC), curcumin (CUR), vitamin C (VITC), epigallocatechin gallate (EGCG), and melatonin (MEL), in ameliorating neuromuscular defects in the *smn-1(ok355)* *C. elegans* SMA model. These compounds were selected based on their established antioxidant efficacy and extensive research evidence, highlighting their beneficial effects in neurodegenerative diseases. Furthermore, we measured the efficacy of each of the antioxidants tested in decreasing the ROS levels in *smn-1(ok355)* animals, with the aim of establishing a relationship between oxidative stress burden and neuromuscular dysfunction in SMA.

It is noteworthy that while these compounds are widely recognised for their antioxidant properties, their effect on cellular physiology extend beyond ROS modulation and is, in many cases, highly context dependent. For example, melatonin promotes apoptosis in human colorectal cancer cell lines (Yun et al., 2018), while it inhibits apoptosis in Alzheimer's Disease mouse models (Feng and Zhang, 2004; Feng et al., 2004). Thus, to better understand the mechanism(s) of action of these antioxidants and their relevance as potential therapeutic agents for SMA, this chapter focuses on elucidating the physiological effects of these compounds in the context of neurodegenerative diseases, discussing when available, their beneficial effects associated with improved neuromuscular function.

4.1.1. Antioxidant treatment in neurodegenerative diseases: mechanisms of action and therapeutic potential

N-acetylcysteine

N-acetylcysteine (NAC) is a potent antioxidant with a broad therapeutic potential. NAC can exert its antioxidant properties through direct ROS scavenging via electron or hydrogen subtraction (Winterbourn and Metodiewa, 1999; Trujillo, Alvarez and Radi, 2016). However, studies *in vitro* indicate that NAC does not demonstrate specificity to react with ROS at a higher rate than other endogenous antioxidant enzymes or molecules present in the environment. For instance, NAC can react with superoxide anions, albeit not as rapidly as superoxide dismutase (SOD), peroxiredoxin (Prxs), or glutathione peroxidase (GPxs) (Winterbourn and Metodiewa, 1999; Benrahmoune, Thérond and Abedinzadeh, 2000). Consequently, although this mechanism is expected to occur *in vivo* and contribute to natural antioxidant processes in cells, it is not considered to be the primary source of NAC's antioxidant efficacy.

The principal mechanism responsible for NAC's antioxidant properties is the replenishment of intracellular glutathione (GSH) reserves (Aldini et al., 2018; Pedre et al., 2021; Tenório et al., 2021), which are often downregulated in pathologies with increased oxidative stress, such as diabetes, cancer, and neurodegenerative diseases (Ballatori et al., 2009). GSH is synthesised through the combination of its precursors glutamate, cysteine, and glycine (Deponte, 2013). NAC possesses the intrinsic ability to break disulfide bonds, a mechanism that increases the amount of free cysteine, which in turn enhances the synthesis of GSH (Radtke et al., 2012). This mechanism is particularly relevant to the therapeutic effect of NAC in neurodegenerative diseases, as cystine has been identified as a limiting factor in the synthesis of GSH in neurons (Aoyama, Watabe and Nakaki, 2012). For example, in a Parkinson's Disease-like cell culture, NAC treatment led to reduced DNA fragmentation and apoptosis, which was associated with the antioxidant effect mediated by the increase in GSH biosynthesis (Offen et al., 1996b). Similarly, in mice models of Alzheimer's Disease (AD), NAC improved cognitive function and memory retention by increasing GSH levels, preventing oxidative damage, and reducing neuronal loss (Tchantchou et al., 2005; Fu, Dong and Sun, 2006).

Importantly, some of the most notable therapeutic physiological effects of NAC in cells are also mediated through its effect on the GSH reserve pool. In a rat model of Huntington's disease (HD), NAC contributed to the restoration of endogenous antioxidants, including GSH and mitochondrial SOD, which led to reduced mitochondrial ROS generation and mitochondrial swelling, reduced mitochondrial release of apoptotic factors, such as cytochrome c, and prevention of apoptosis. This enhanced mitochondrial health is believed to be responsible for the improvements observed in the disease phenotype, such as reduced neuronal degeneration and improved motor and cognitive deficits (Sandhir et al., 2012).

In addition to its direct interaction with cellular physiology, NAC has been shown to influence several cellular signalling pathways. For example, in pre-clinical models of PD and focal cerebral ischaemia, NAC inhibits the NF- κ B pathway, thereby reducing the expression of pro-inflammatory genes (Sekhon et al., 2003; Aoki et al., 2009; Sha, Chin and Li, 2009). Furthermore, NAC can activate the Ras-ERK pathway in neuron-like cell cultures, thereby inhibiting apoptosis (Yan and Greene, 1998). Notably, a recent study conducted on motor neurons using an SMA mouse model highlighted the ability of NAC to reduce mitochondrial ROS and increase protein synthesis, specifically SMN, through activation of the mTOR pathway (Thelen, Wirth and Kye, 2020).

Overall, NAC regulates oxidative stress, improves mitochondrial function, and influences key cellular pathways, making it a promising therapeutic agent for oxidative stress-related diseases such as SMA.

Curcumin

Curcumin, a polyphenolic compound belonging to the ginger family, exhibits potent antioxidant and neuroprotective properties across various cellular and animal models. Its antioxidant activity is attributed to both electron transfer and hydrogen atom donation mechanisms, making it highly effective against intracellular free radicals including hydrogen peroxide, hydroxyl radicals, and peroxyl radicals (Barzegar and Moosavi-Movahedi, 2011). These antioxidant properties are

evident in *C. elegans*, where curcumin reduced juglone-induced intracellular ROS accumulation in a concentration-dependent manner (Yu et al., 2014).

Nevertheless, in whole-cell or organismal contexts, the antioxidant effects of curcumin cannot be solely attributed to direct free-radical scavenging, as it also modulates intracellular antioxidant responses through key molecular pathways. For instance, curcumin administration increased the expression of oxidative stress response genes in *C. elegans*, suggesting activation of the SKN-1 pathway, the *C. elegans* ortholog of the NRF2 transcription factor (Yu et al., 2014). Furthermore, curcumin mitigates 1,2-diacetylbenzene (DAB)-induced oxidative stress and neuroinflammation in microglial cells by stimulating the NRF2 antioxidant pathway and inhibiting the pro-inflammatory NF- κ B pathway (Nguyen et al., 2022). Moreover, studies in mouse models of Multiple Sclerosis (MS) and AD have reported reductions in neuroinflammatory markers, such as TNF- α , IL-1, and IL-6, as well as suppression of NF- κ B signalling. These effects contributed to lower oxidative stress levels, delayed disease onset, and improved neuronal function, which are reflected in enhanced cognitive performance and locomotor activity (Boyao et al., 2019; Kawamoto et al., 2012; Lim et al., 2001; Liu et al., 2016; Shao et al., 2023). Another significant molecular target of curcumin is the PI3K/Akt/mTOR signalling pathway, which regulates autophagy and cell survival. In *in vitro* and *in vivo* models of AD, PD, and MS, curcumin treatment inhibits the expression and phosphorylation of PI3K, Akt, and mTOR, resulting in increased autophagy, reduced protein aggregation, lower cell death rates, and enhanced neuronal function (Boyao et al., 2019; He et al., 2022; Wang et al., 2014).

In addition to its role in reducing oxidative stress and inflammation, curcumin plays a crucial role in the regulation of mitochondrial homeostasis and apoptosis. In an MPP⁺-induced PD cell model, where MPP⁺ inhibited mitochondrial complex I, characterised by elevated ROS levels, impaired metabolism, and reduced cell viability, curcumin treatment partially restored mitochondrial function and improved cell survival (Chakraborty et al., 2017). Furthermore, in motor neuron-like cell cultures, curcumin enhanced mitochondrial membrane potential, preserved

mitochondrial function, and reduced cytoplasmic levels of pro-apoptotic proteins, including cytochrome c and caspase-3 (Chang et al., 2014; Dong et al., 2014).

In summary, curcumin's capacity to mitigate oxidative stress, modulate stress-response pathways, maintain mitochondrial function, and regulate apoptosis renders it as a promising antioxidant candidate for investigating its therapeutic potential in SMA.

Vitamin C

Vitamin C (VITC) is a potent water-soluble antioxidant, whose capacity to scavenge ROS depends on its ability to undergo one-electron oxidation (Beyer, 1994; Njus et al., 2020). Upon ROS encounter, VITC is oxidised to a relatively stable ascorbate radical, which can be recycled back to VITC by cellular reductants such as GSH and thioredoxin (Trx) in an NADPH-dependent manner (Li et al., 2004). This redox cycle is also responsible for its ability to regenerate vitamin E (tocopherol), an efficient radical scavenger in membranes, demonstrating the importance of VITC's synergistic effect with other antioxidants in enhancing its antioxidant capacity (Niki, 1987; Ruiz-Ramos et al., 2010; Im et al., 2014). VITC antioxidant effects are evident in a mouse model of AD; VITC administration reduced hallmarks of the disease such as AB oligomer formation and tau phosphorylation while decreased oxidative stress markers, such as protein carbonylation, and increased the levels of GSH, which altogether led to AD behavioural improvements (Murakami et al., 2011).

This redox recycling also elucidates the relationship between VITC and mitochondria. In isolated mitochondria derived from kidney, fibroblast, myeloid, and liver human cell lines, it was demonstrated that VITC can enter the mitochondria via the glucose transporter Glut1 localised in the mitochondrial membrane. Following this, VITC mediated its protective effect in mitochondria by reducing mitochondrial ROS, protecting mitochondrial DNA from oxidative damage and preserving mitochondrial membrane potential (KC, Càrcamo and Golde, 2005). This mechanism is often associated with VITC's anti-apoptotic effects. For instance, in an AD study performed using neuroblastoma cells, VITC significantly reduced the aggregation of β -amyloid-induced apoptosis, as reflected by the depletion of mitochondrial caspase-3 activity. This was related to

the ability of VITC to protect against oxidative stress (Huang and May, 2006). However, the efficacy of VITC as an antioxidant is dependent on its recycling, and some of the reductants involved in this process are within the mitochondria, such as thioredoxin reductase or mitochondrial complex III (Li et al., 2002). Therefore, this could indicate that defects in those elements have the potential to limit VITC's mitochondrial antioxidant capacity. For example, in a *C. elegans* mitochondrial complex I mutant, *gas-1*, characterised by a reduced lifespan and increased mitochondrial ROS, VITC ameliorated the reduced lifespan, while increasing the already elevated mitochondrial burden (Polyak et al., 2018), challenging the relationship between ROS levels and aging/lifespan.

VITC has also been demonstrated to have beneficial effects on motor performance and cognitive function in pre-clinical models of neurodegenerative diseases, such as HD, MS, and ALS (Nagano et al., 2003; Rebec, Conroy and Barton, 2006; Babri et al., 2015). Notably, VITC exhibited capacity in regulating neuroinflammation through inhibition of the NF- κ B pathway in astrocytes (Zeng et al., 2020) and in mouse models of AD (Frontiñán-Rubio et al., 2018), and PD (De Nuccio et al., 2021), resulting in improvements in behavioural and locomotor deficits that were associated with these neurodegenerative diseases. Although interactions with other known oxidative stress pathways have also been reported, notably the stimulation of the antioxidant NRF2 pathway (Li et al., 2019; Somade et al., 2022; Xu et al., 2016) and the inhibition of the autophagy regulator mTOR (Somade et al., 2022; Xu et al., 2016; Yang et al., 2018; Zhang et al., 2022), these have not yet been demonstrated in the context of neurodegenerative diseases.

In conclusion, vitamin C exhibits diverse biological effects through its antioxidant properties, redox recycling mechanisms, mitochondrial health, and regulation of key signalling pathways.

Epigallocatechin gallate

Epigallocatechin gallate (EGCG), the most abundant catechin in green tea, is recognised for its potent antioxidant effects and neuroprotective properties. EGCG directly scavenges ROS via electron or hydrogen donation, such as superoxide anions and hydroxyl radicals, and exhibits the

capacity to chelate metal ions, thereby preventing oxidative damage to biological membranes (Anderson et al., 2001; Nanjo et al., 1999; Procházková et al., 2011). Notably, in a mouse model of PD, EGCG demonstrated neuroprotective properties by inhibiting 1-methyl-4-phenyl-1,2,3,6-tetrahydropyridine (MPTP)-induced neurodegeneration, restoring dopamine levels, and upregulating ferroportin expression to mitigate iron accumulation (Levites et al., 2001; Xu et al., 2017).

EGCG plays a crucial role in regulating mitochondrial function and apoptosis. In an *in vitro* model of PD, EGCG increased the mitochondrial membrane potential and decreased the activation of mitochondrial pro-apoptotic proteins such as caspase-3 and Smac (Hou et al., 2008). Moreover, in an *in vivo* rat model of PD, EGCG reduced oxidative stress markers, including lipid peroxidation and NO, and increased the activity of mitochondrial enzymes such as ATPase. These effects contributed to the prevention of mitochondrial dysfunction and motor function decline associated with the disease (Tseng et al., 2020).

The protective effect of EGCG in neurodegenerative diseases is not solely mediated by the maintenance of mitochondrial health and reduction of ROS, but also by the regulation of key molecular pathways. Specifically, EGCG activates the nuclear translocation of NRF2, upregulating the expression of antioxidants, and modulates the phosphorylation of upstream targets, such as AKT and ERK1/2 (Na and Surh, 2008; Na et al., 2008), contributing to the observed protective effect against protein aggregation in animal models. For example, in a *C. elegans* model of AD, EGCG treatment upregulated the nuclear translocation of DAF-16 (*C. elegans* ortholog of human FOXO), which is downstream of AGE-1/AKT-1/2 (*C. elegans* orthologs of human PI3K/AKT), thereby decreasing A β amyloid aggregates and increasing lifespan (Abbas and Wink, 2010). Furthermore, EGCG demonstrated efficacy in preventing the formation of huntingtin protein aggregates in *in vitro* and *in vivo* models of HD, which elucidated the improvement of locomotor activity in a *Drosophila melanogaster* model of HD (Ehrnhoefer et al., 2006). Moreover, in a transgenic mouse model of ALS, treatment with EGCG led to the downregulation of the inflammatory transcription factor NF- κ B and decreased oxidative stress-

induced apoptosis markers, which were associated with motor neuron preservation, improved motor function, and extended lifespan (Xu et al., 2006).

Overall, EGCG represents a promising therapeutic candidate for SMA because of its well-documented neuroprotective effects in neurodegenerative diseases, driven by its antioxidant properties, regulation of mitochondrial function, and modulation of key stress-response pathways.

Melatonin

Melatonin (MEL), a hormone naturally produced in humans, is a potent antioxidant effective in scavenging a wide range of ROS via electron donation, including superoxide anions, hydroxyl radicals, peroxyl radicals and peroxynitrite anions (Reiter et al., 1998, 2000). Notably, through the donation of electrons, MEL initiates a process known as the melatonin free radical scavenging cascade. In each step of this series of reactions, a melatonin derivate with substantial antioxidant capacity is produced. This phenomenon accounts for a considerable share of MEL's antioxidant power (López-Burillo et al., 2003; Tan et al., 2005).

MEL's ROS scavenging activities have been demonstrated to enhance mitochondrial health. In a study conducted utilising *in vitro* and *in vivo* mouse brain tissue, MEL administration prevented lipid peroxidation, thereby protecting mitochondrial DNA from oxidative damage (Yamamoto & Mohanan, 2002). Moreover, melatonin was effective in stimulating mitochondrial complex I activity in a rat model of PD, which was associated with the amelioration of the animals' neuromuscular defects (Dabbeni-Sala et al., 2001b). Additionally, in *C. elegans* Duchenne muscular dystrophy (DMD) and PD models, MEL treatment significantly improved mitochondrial network integrity and decreased oxidative stress burden, while improving the animal's locomotion (He et al., 2022; Hewitt et al., 2018).

Closely associated with its amelioration of oxidative stress and mitochondrial function conservation properties, MEL has demonstrated efficacy as a modulator of apoptosis. For instance, in a rat-derived cell line model of PD, melatonin reduced oxidative stress and apoptosis

(Mayo et al., 1998). Moreover, in an AD pre-clinical model, melatonin treatment decreased β -amyloid aggregates, while increasing choline acetyltransferase activity, resulting in a reduced number of apoptotic neurons (Feng and Zhang, 2004; Feng et al., 2004).

Beyond its direct effects on ROS and mitochondria, melatonin's antioxidant properties are enhanced by its capacity to modulate key molecular pathways. For example, in AD and PD pre-clinical derived cell culture lines, MEL therapeutic effects included decreased oxidative stress and reduced protein aggregation and these were associated with NRF2 increased activity and consequently endogenous antioxidant defences (Li et al., 2005; Mayo et al., 1998). This activation is hypothesised to occur through the PI3K/AKT axis (Reddy et al., 2015; Wen et al., 2024). For example, in a neuron cell culture, MEL was able to stimulate mTOR activation, reduce autophagy and protect from neurotoxicity (Kongsuphol et al., 2009). MEL has also shown to play a crucial role in regulating neuroinflammation and, thereby decreasing oxidative stress burden, through the inhibition of the NF- κ B pathway, which has been confirmed in various studies using AD pre-clinical models (Rosales-Corral et al., 2003; Shen et al., 2007).

Overall, MEL's antioxidant properties and therapeutic potential in neurodegenerative diseases, through preservation of mitochondrial function and regulation of apoptosis, render MEL as promising candidate to determine whether ROS amelioration can serve as a therapeutic target for complementary therapies in SMA.

4.1.2. Research objectives

In this chapter, the therapeutic potential of each antioxidant compound in SMA was evaluated using two primary outcome measures in the *smn-1(ok355)* *C. elegans* SMA model: neuromuscular function and ROS levels. Neuromuscular function was assessed using the pharyngeal pumping and WormLab locomotion assays, both well-established methods for assessing motor-function in *C. elegans*. Furthermore, intracellular ROS levels in *C. elegans* were quantified using the dihydroethidium (DHE) staining assay described in Chapter III. Moreover, as previous *in vitro*

studies have shown that increased ROS can diminish the levels of functional SMN, we also explored the impact of ROS on SMN protein levels *in vivo*.

The specific objectives of chapter IV were as following:

1. To determine whether treatment with antioxidant compounds can ameliorate the neuromuscular defects observed in *smn-1(ok355)* mutants.
2. To assess the efficacy of the antioxidant compounds tested on reducing the cytoplasmic ROS levels in *smn-1(ok355)* nematodes.
3. To investigate the relationship between intracellular ROS, endogenous SMN-1 protein levels and neuromuscular function in *smn-1(ok355)* animals.

Overall, we aim to elucidate whether there is a direct correlation between oxidative stress and neuromuscular function in the *smn-1(ok355)* *C. elegans* SMA model, opening the avenue for new therapeutic strategies in other pre-clinical SMA models and ultimately in patients.

4.2. Results

4.2.1. Characterisation of the *Caenorhabditis elegans* locomotion.

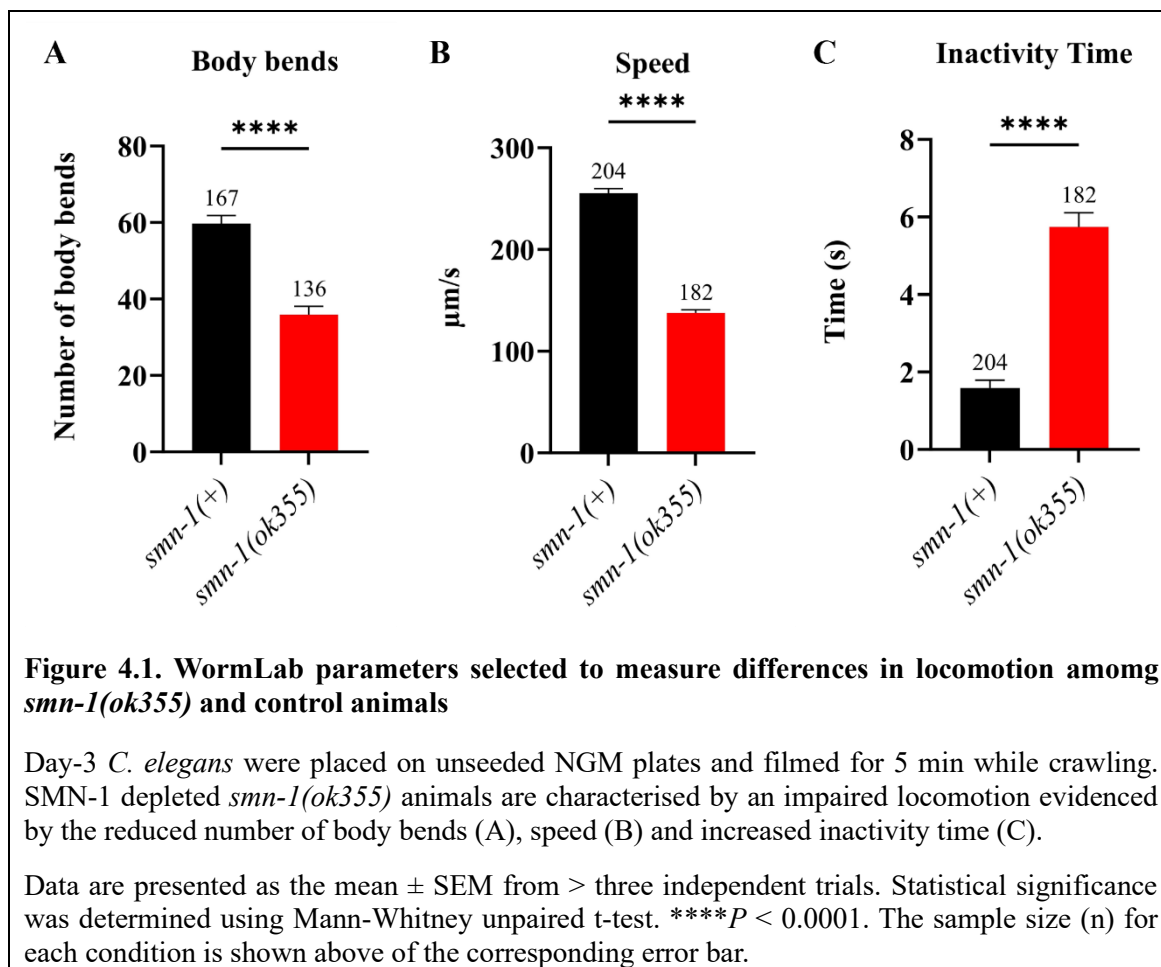
To evaluate the impact of SMN-1 depletion on the neuromuscular function of the *smn-1(ok355)* *C. elegans* SMA model, we utilised the WormLab© software, a multi-worm tracker system that characterises and quantifies *C. elegans* locomotion. Among the 24 parameters generated by the software, 23 were significantly altered in *smn-1(ok355)* animals, reflecting the profound impact of SMN-1 depletion on *C. elegans* locomotion (detailed statistical analyses of all parameters are shown in **Supplementary Figures 2-6**).

However, analysing all parameters under various experimental conditions (i.e. assessing different drug treatments or specific mutations) generates a large dataset that make it difficult to detect meaningful changes in animal movement. To simplify further analyses, we initially examined

each parameter individually and categorised them into five groups: shape-based (**Supplementary Figure 2**), movement-behaviour (**Supplementary Figure 3**), distance-travelled **Supplementary Figure 4**), time-based (**Supplementary Figure 5**), and speed-measurements (**Supplementary Figure 6**). Based on their connection to neuromuscular function and minimal redundancy with other parameters, we identified a set of three key parameters that could be utilised as a reflection of *C. elegans* locomotion for posterior analysis. In this selection, we omitted shape-based parameters, as they are not directly related to neuromuscular function, and distance-travelled parameters, as these are already accounted for in speed calculations.

From the movement-behaviour parameters, we selected the number of body bends because prior research has shown a direct relationship between this measure and the effort exerted by *C. elegans* during movement (Hart, 2006). Our results indicated that the number of body bends in *smn-1(ok355)* animals was significantly lower than those of healthy *smn-1(+)* nematodes (**Figure 4.1A**; $P < 0.0001$). Among the time-based parameters we chose the inactivity time, which measures the total amount of time that the animals spent inactive during the five-minute recording, as it serves as a reliable indicator of inactivity pertinent to neuromuscular diseases such as SMA. As expected, *smn-1(ok355)* animals spent a significantly higher time inactive than healthy *smn-1(+)* nematodes (**Figure 4.1C**; $P < 0.0001$). The final parameter examined was speed the later calculates the total distance travelled by the nematodes during the duration of the film, which was again significantly reduced in *smn-1(ok355)* animals (**Figure 4.1B**; $P < 0.0001$).

This refined approach allowed us to focus on the parameters most relevant to locomotion in the *smn-1(ok355)* *C. elegans* SMA model, thereby establishing a robust framework for assessing neuromuscular function in subsequent analyses.



4.2.2. Evaluation of antioxidant treatment efficacy in modulating neuromuscular activity in SMA

To investigate the therapeutic potential of different antioxidant treatments in ameliorating *smn-1(ok355)* neuromuscular defects, the *smn-1(ok355)* *C. elegans* SMA model and *smn-1(ok355)/hT2* corresponding control animals were cultivated for three days on plates containing the pertinent drug (**Table 2.7. Antioxidant compounds used for *C. elegans* drug treatment**). Neuromuscular function was assessed using the pharyngeal pumping and WormLab locomotion assays, while intracellular ROS levels were quantified using the DHE staining assay.

4.2.2.1. *N*-acetyl cysteine

Our results indicated that NAC did not alter the pharyngeal pumping rates of control animals at any of the concentrations utilised (**Figure 4.2A**; $P = 0.9224$, $P = 0.7917$, $P = 0.9389$, for 3 mM, 6 mM and 9 mM, respectively). However, it significantly increased the pharyngeal pumping rate of *smn-1(ok355)* animals at 6 mM, although not at 3 mM or 9 mM (**Figure 4.2A**; $P = 0.2804$, $P = 0.0110$, $P = 0.0541$, for 3 mM, 6mM and 9 mM, respectively).

In terms of locomotion, NAC significantly reduced the rate of body bends in control animals at 3 mM but not at higher concentrations (**Figure 4.2B**; $P = 0.0016$, $P = 0.7256$, $P = 0.0857$, for 3, 6 and 9 mM respectively). However, no significant differences were found in the rate of body bends in *smn-1(ok355)* animals treated with NAC (**Figure 4.2B**; $P = 0.8531$, $P = 0.7504$, $P = 0.9701$, for 3, 6 and 9 mM, respectively). Furthermore, NAC significantly reduced speed of control animals at 3 mM ($P = 0.0276$) and 9 mM ($P = 0.0147$), but not at 6 mM (**Figure 4.2C**; $P = 0.4120$). Conversely, no differences were observed in the speed of *smn-1(ok355)* animals at any NAC concentration (**Figure 4.2C**; $P = 0.4545$, $P = 0.7681$, $P = 0.5573$, for 3, 6 and 9 mM, respectively). Moreover, analysis of the inactivity time revealed no significant differences between control animals (**Figure 4.2D**; $P = 0.9974$, $P = 0.9998$, $P = 0.8748$, for 3, 6 and 9 mM, respectively) nor *smn-1(ok355)* mutants (**Figure 4.2D**; $P = 0.9528$, $P = 0.0558$, $P = 0.9347$, for 3, 6 and 9 mM, respectively) at any of NAC concentrations tested.

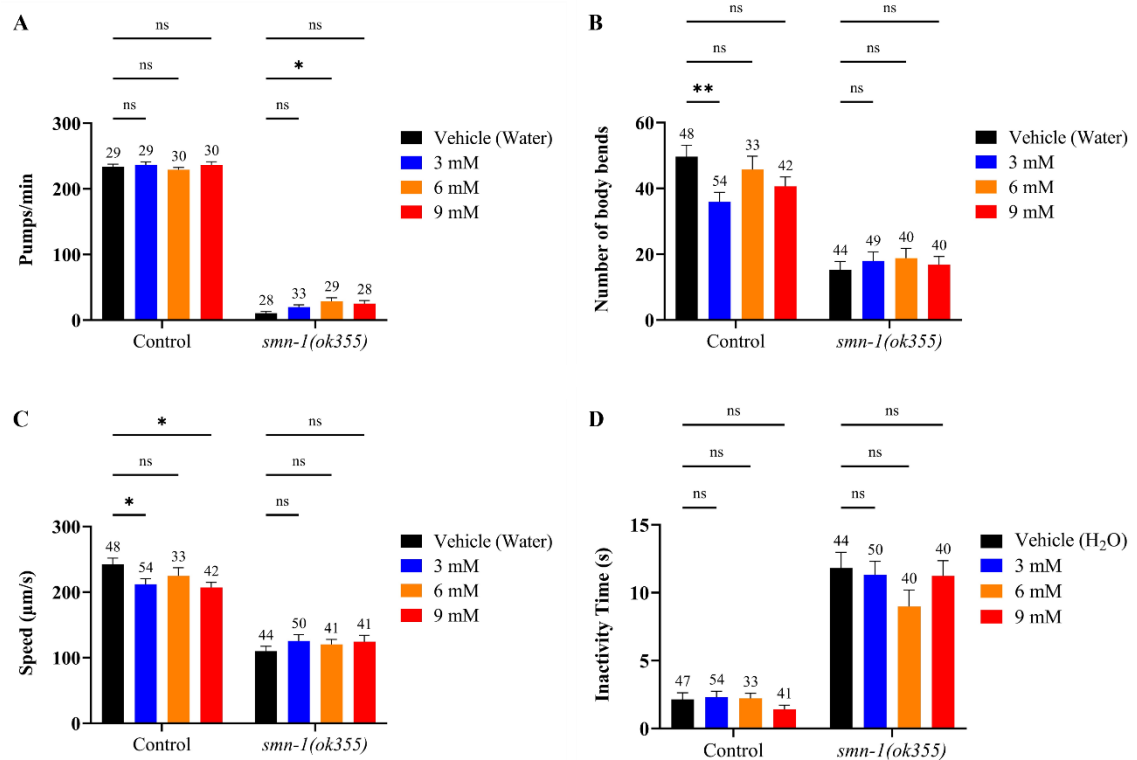


Figure 4.2. N-acetylcysteine partially ameliorates neuromuscular defects in the *smn-1(ok355)* *C. elegans* SMA model

C. elegans were cultivated on plates containing 0 mM (vehicle dH₂O), 3 mM, 6 mM or 9 mM NAC, and neuromuscular function was assessed through pharyngeal pumping (A), body bends (B), crawling speed (C) and inactivity time (D). In control animals, NAC treatment significantly reduced the number of body bends (B; 3 mM) and speed (C; 3 mM and 9 mM). In *smn-1(ok355)*, NAC significantly increased the pharyngeal pumping rate (A; 6 mM).

Data are presented as the mean \pm SEM from at least two independent trials. Statistical significance was determined using two-way ANOVA ($P = 0.0634$, $P = 0.0374$, $P = 0.0204$, and $P = 0.3026$ for figures A, B, C, and D, respectively) followed by Dunnett's multiple comparison test. ns $P > 0.05$; $*P \leq 0.05$; $**P < 0.01$. The sample size (n) for each condition is shown above of the corresponding error bar.

Next, we evaluated the efficacy of NAC in reducing intracellular cytoplasmic ROS levels in control and *smn-1(ok355)* animals. While NAC treatment did not modify intracellular ROS content in control animals (**Figure 4.3Q**; $P = 0.8651$, $P = 0.7695$, $P = 0.5747$, for 3, 6, and 9 mM, respectively), it demonstrated the ability to decrease ROS in *smn-1(ok355)* mutants at all concentrations tested (**Figure 4.3Q**; $P = 0.8651$, $P = 0.7695$, $P = 0.5747$, for 3, 6 and 9 mM, respectively).

In summary, evaluation of *smn-1(ok355)* neuromuscular defects and ROS content after NAC administration revealed that NAC improved *smn-1(ok355)* pharyngeal pumping defects at 6 mM, while it effectively decreased intracellular ROS content at all concentrations tested.

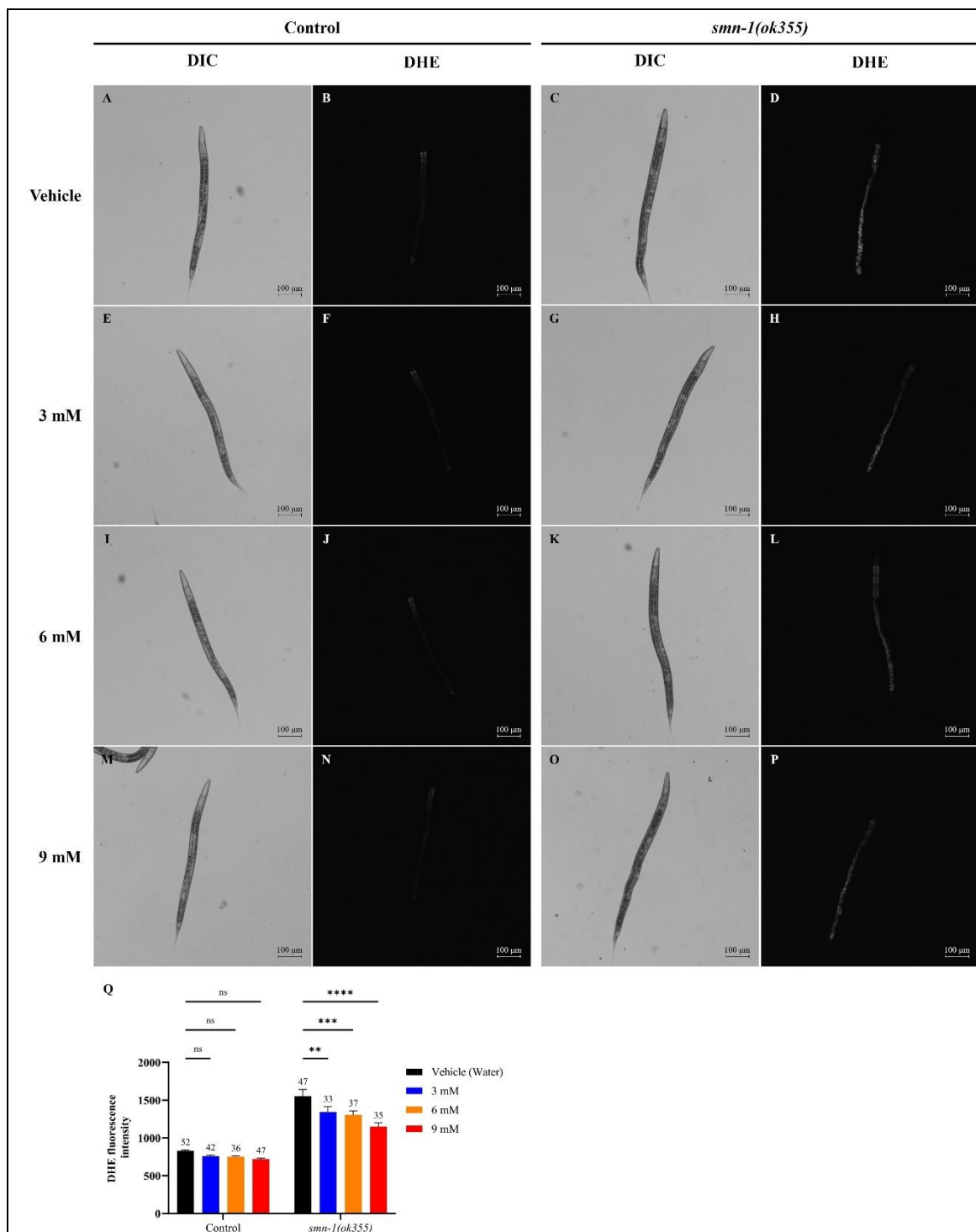


Figure 4.3. N-acetyl cysteine prevents the accumulation of cytoplasmic ROS in the *smn-1(ok355)* *C. elegans* SMA model

(A-P) Differential interference contrast (DIC) and fluorescence (DHE) representative images of control and *smn-1(ok355)* *C. elegans* stained with 10 μ M DHE for 2 h. Animals were cultivated on plates containing 0 mM (vehicle) (A-D), 3 mM (E-H), 6 mM (I-L) and 9 mM (M-P) NAC. Scale bars: 100 μ m.

(Q) Quantification of the DHE fluorescence intensity in control and *smn-1(ok355)* nematodes across all NAC concentrations tested. NAC treatment did not significantly alter DHE fluorescence

intensity in control animals at any of the concentrations utilised, but significantly reduced DHE fluorescence intensity in *smn-1(ok355)* mutants at 3 mM, 6 mM and 9 mM. Data are presented as mean \pm SEM from at least two independent trials. Statistical significance was determined using two-way ANOVA ($P = 0.0168$) followed by Dunnett's multiple comparisons test. ns $P > 0.05$; ** $P < 0.01$; *** $P < 0.001$; **** $P < 0.0001$. The sample size (n) for each condition is shown above of the corresponding error bar.

4.2.2.2. Curcumin

Our results indicated that CUR did not modify the pharyngeal pumping rate of control animals at any of the concentrations utilised (**Figure 4.4A**; $P = 0.5524$, $P = 0.8569$, $P = 0.4671$, for 5, 10 and 20 μM , respectively). Similarly, no differences were observed in the pharyngeal pumping rates of *smn-1(ok355)* mutants after CUR administration (**Figure 4.4A**; $P = 0.9711$, $P = 0.4081$, $P = 0.5607$, for 5, 10 and 20 μM , respectively).

In terms of locomotion, CUR treatment significantly reduced the number of body bends in control animals at 10 μM , although these remained unaffected at 5 and 20 μM (**Figure 4.4B**; $P = 0.4357$, $P = 0.0124$, $P = 0.1234$, for 5, 10 and 20 μM , respectively). However, no significant differences were found in the rate of body bends in *smn-1(ok355)* animals treated with CUR at any of the concentrations utilised (**Figure 4.4B**; $P = 0.7268$, $P = 0.1164$, $P = 0.9409$, for 5, 10 and 20 μM , respectively). Furthermore, CUR significantly reduced the speed at which control animals moved throughout the five-minutes recording, particularly at 10 μM and 20 μM (**Figure 4.4C**; $P = 0.0564$, $P = 0.0001$, $P = 0.0046$, for 5, 10 and 20 μM , respectively). Conversely, no significant differences were found in the speed of *smn-1(ok355)* animals treated with CUR (**Figure 4.4C**; $P = 0.1947$, $P = 0.9373$, $P = 0.1562$, for 5, 10 and 20 μM , respectively). Moreover, our results demonstrated that CUR treatment did not affect the inactivity time of control animals (**Figure 4.4D**, $P = 0.9998$, $P = 0.9992$, $P = 0.9999$, for 5 μM , 10 μM and 20 μM , respectively) nor *smn-1(ok355)* mutants (**Figure 4.4D**, $P = 0.1414$, $P = 0.5401$, $P = 0.4947$, for 5, 10 and 20 μM , respectively) at any of the concentrations tested.

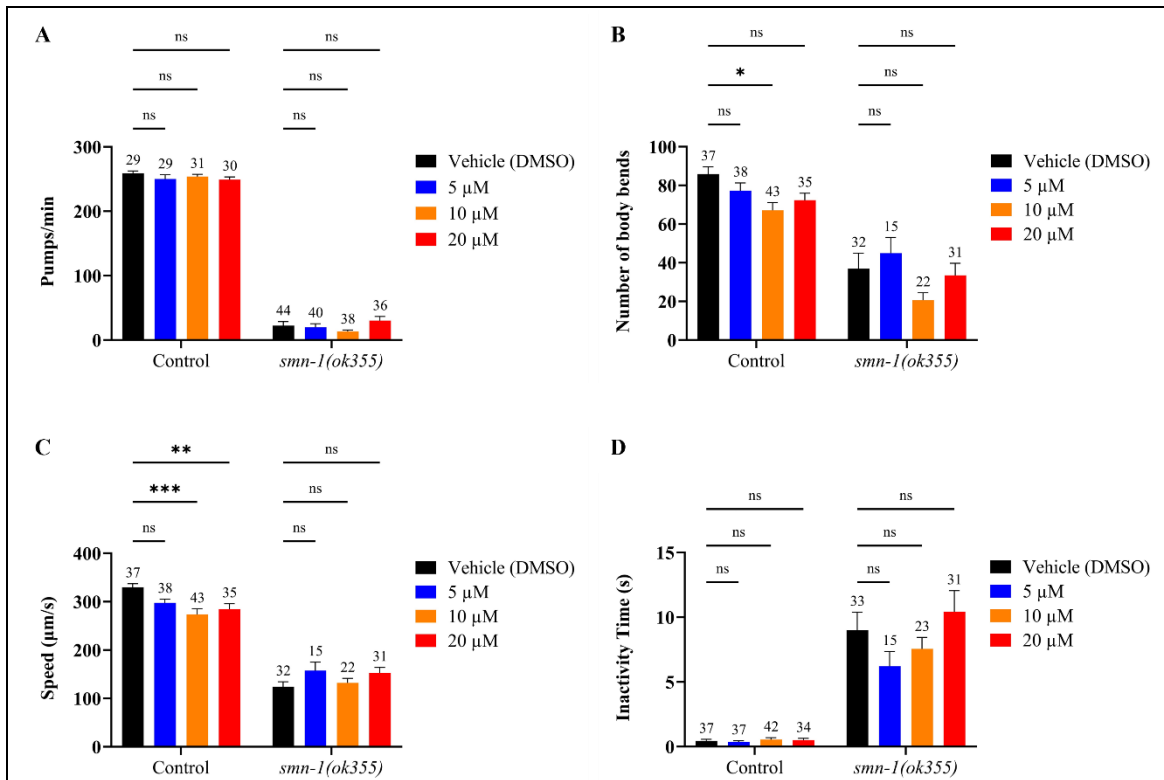


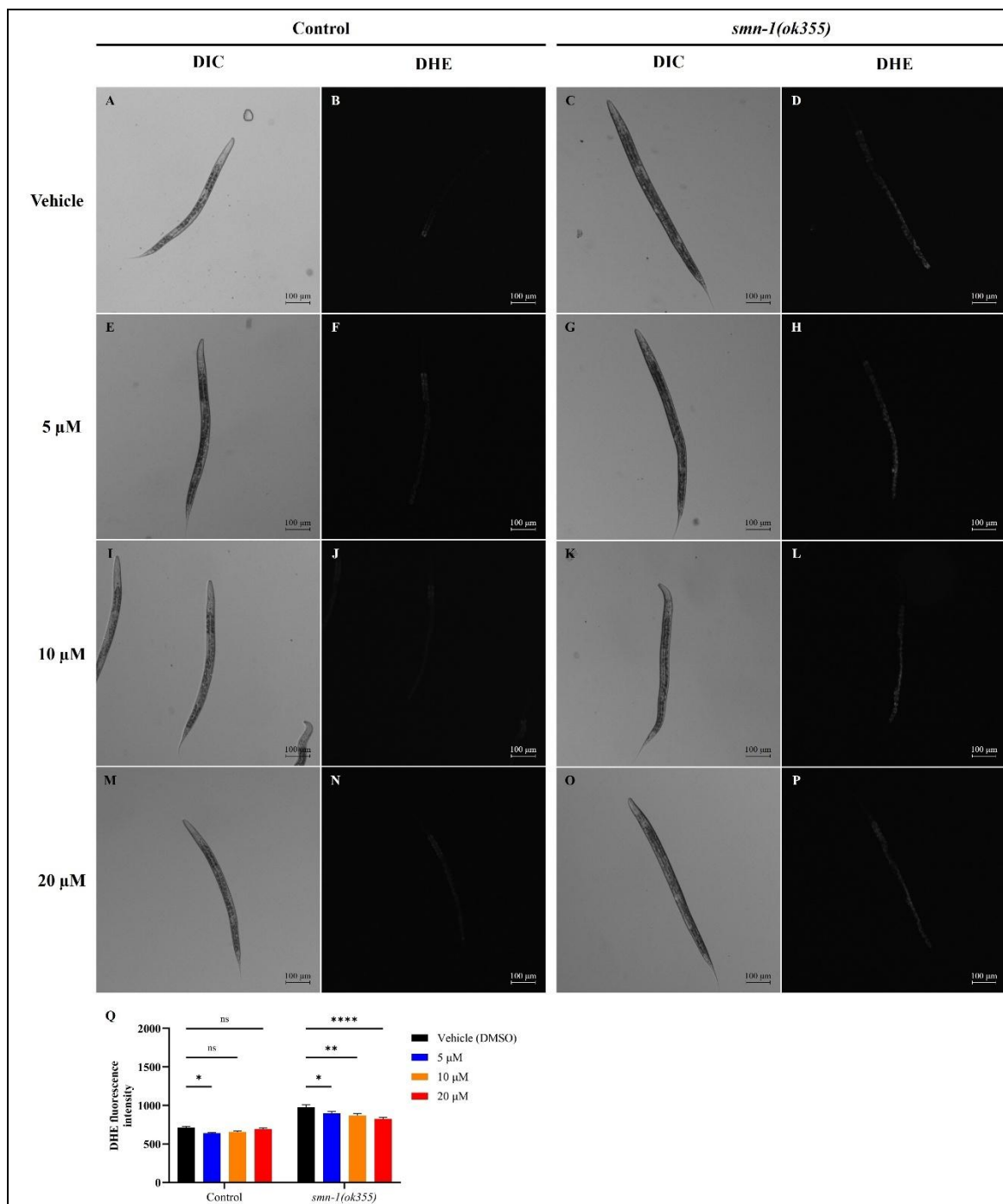
Figure 4.4. Curcumin does not ameliorate neuromuscular defects in the *smn-1(ok355)* *C. elegans* SMA model

C. elegans were cultivated on plates containing 0 mM (vehicle DMSO), 5 μM, 10 μM or 20 μM CUR, and neuromuscular function was assessed through pharyngeal pumping (A), body bends (B), crawling speed (C) and inactivity time (D). In control animals, CUR treatment significantly reduced the number of body bends (B; 10 μM) and speed (C; 10 μM and 20 μM). However, no significant differences were observed in pharyngeal pumping, body bends, crawling speed, or inactivity time in *smn-1(ok355)* mutants at any CUR concentration tested.

Data are presented as mean ± SEM from at least two independent trials. Statistical significance was determined using two-way ANOVA ($P = 0.2023$, $P = 0.4446$, $P = 0.0014$, and $P = 0.1135$ for figures A, B, C, and D, respectively) followed by Dunnett's multiple comparisons test. ns $P > 0.05$; * $P < 0.05$; ** $P < 0.01$; *** $P < 0.001$. The sample size (n) for each condition is shown above of the corresponding error bar.

We next evaluated CUR's efficacy to reduce intracellular ROS levels in control and *smn-1(ok355)* animals. CUR treatment marginally reduced cytoplasmic ROS content in control animals when administered at 5 μ M, the lowest concentration tested but showed no significant effect at higher concentrations (**Figure 4.5Q**; $P = 0.0432$, $P = 0.1527$, $P = 0.8488$, for 5 μ M, 10 μ M and 20 μ M, respectively). Conversely, CUR demonstrated the ability to mitigate oxidative stress in *smn-1(ok355)* mutants at all concentrations utilised (**Figure 4.5Q**; $P = 0.0237$, $P = 0.0011$, $P < 0.0001$, for 5 μ M, 10 μ M and 20 μ M, respectively).

In summary, evaluation of *smn-1(ok355)* neuromuscular defects and ROS content after CUR administration revealed that CUR did not modify *smn-1(ok355)* neuromuscular pathology at any of the concentrations utilised. However, its antioxidant properties were highlighted, as it effectively ameliorated *smn-1(ok355)* ROS burden at all concentrations tested.



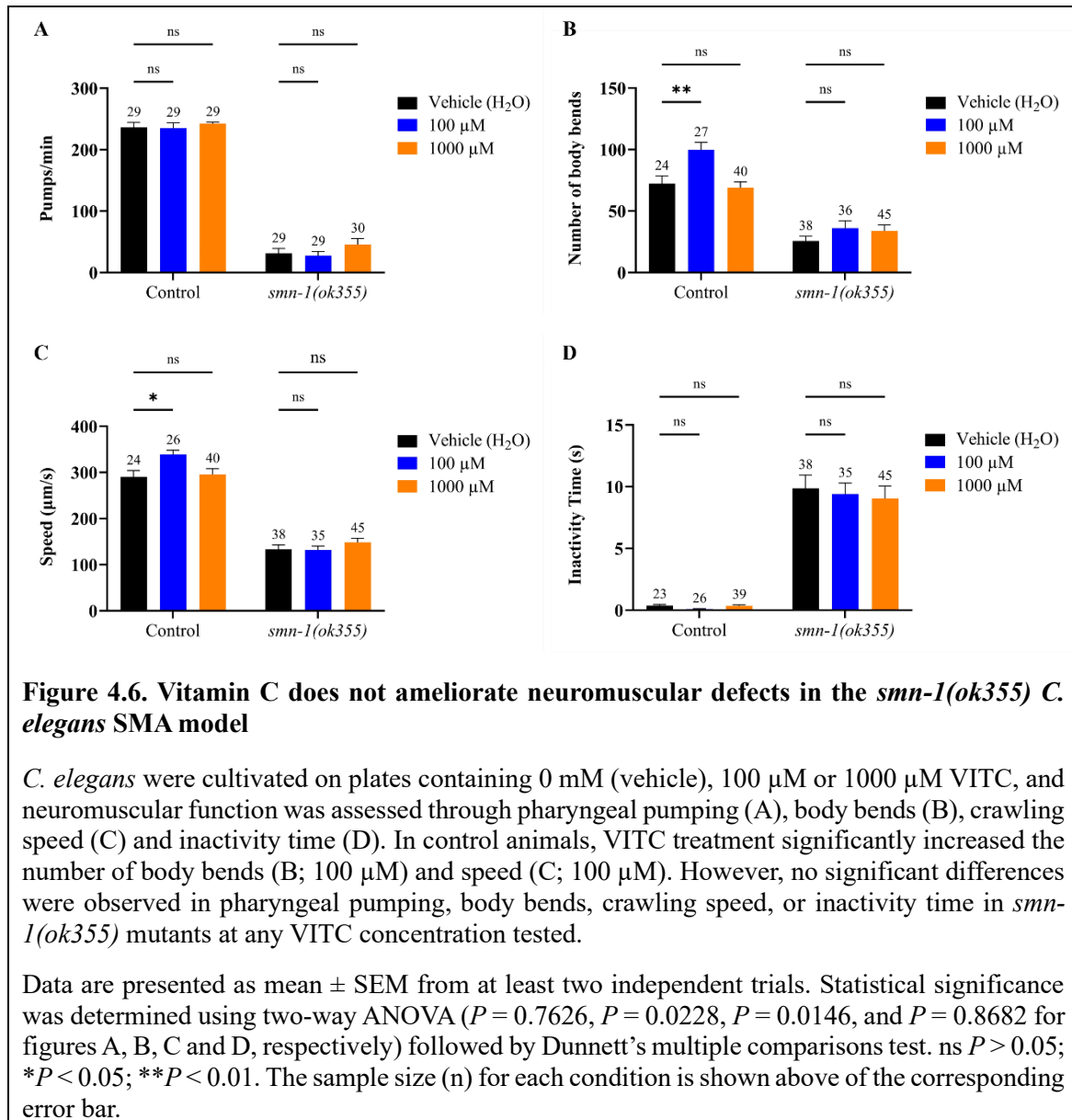
significance was determined using two-way ANOVA ($P = 0.0044$) followed by Dunnett's multiple comparisons test. ns $P > 0.05$; * $P < 0.05$; ** $P < 0.01$; **** $P < 0.0001$. The sample size (n) for each condition is shown above of the corresponding error bar.

4.2.2.3. Vitamin C

To investigate the therapeutic potential of VITC in ameliorating neuromuscular defects and oxidative stress in the *C. elegans* SMA model, *smn-1(ok355)* mutants and *smn-1(ok355)/hT2* control animals were cultivated for three days on plates containing 0 μM (vehicle H_2O), 100 μM , 1000 μM or 10000 μM of VITC. However, as control animals reared at 10000 μM presented a significant developmental delay compared to those cultivated on vehicle plates, this concentration was excluded from further analysis.

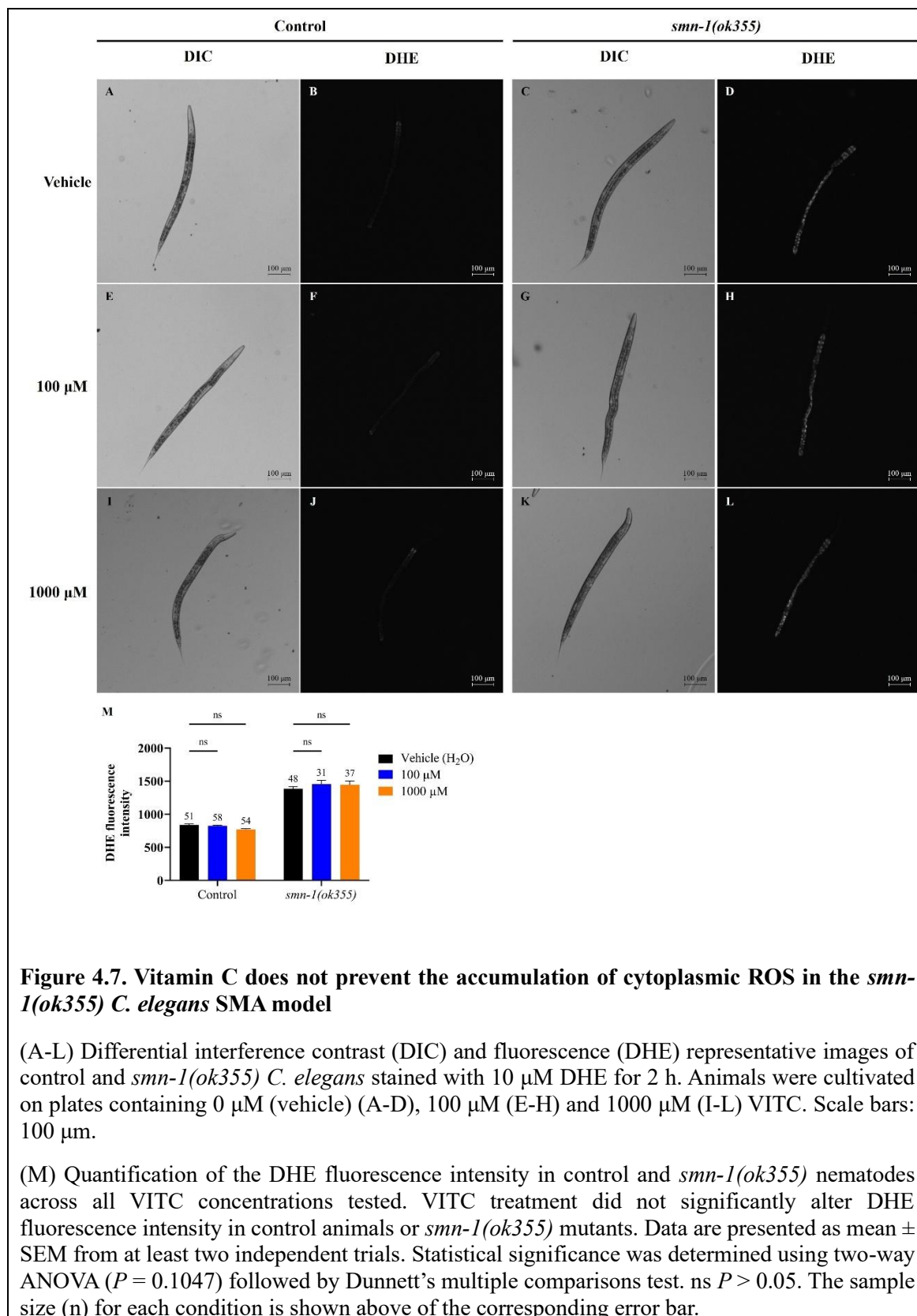
Our results indicated that VITC did not affect the pharyngeal pumping rate of control animals at any of the concentrations utilised (**Figure 4.6A**; $P = 0.9829$ and $P = 0.8134$, for 100 μM and 1000 μM , respectively). Similarly, no changes were observed in the pharyngeal pumping rate of *smn-1(ok355)* mutants after VITC treatment (**Figure 4.6A**; $P = 0.9080$ and $P = 0.3153$ for 100 μM and 1000 μM , respectively).

In terms of locomotion, VITC significantly increased the number of body bends in control animals at 100 μM , although it had no significant effect at 1000 μM (**Figure 4.6B**; $P = 0.0031$, $P = 0.8799$, for 100 and 1000 μM , respectively). No significant differences were observed in the rate of body bends in *smn-1(ok355)* animals treated with VITC at any of the concentrations utilised (**Figure 4.6B**. $P = 0.2527$, $P = 0.3804$, for 100 and 1000 μM , respectively). Furthermore, VITC significantly increased the speed of control animals at 100 μM , although not at 1000 μM (**Figure 4.6C**; $P = 0.0126$, $P = 0.9254$ for 100 and 1000 μM , respectively). Conversely, no significant differences in speed were observed in *smn-1(ok355)* animals after VITC administration (**Figure 4.6C**; $P = 0.9948$ and $P = 0.4265$ for 100 μM and 1000 μM , respectively). Moreover, our analysis revealed that VITC did not affect the inactivity time of control animals (**Figure 4.6D**; $P = 0.9680$, $P > 0.9999$, for 100 and 1000 μM , respectively) nor *smn-1(ok355)* mutants (**Figure 4.6D**; $P = 0.8791$, $P = 0.6537$, for 100 and 1000 μM , respectively) at any of the concentrations utilised.



We next evaluated the efficacy of VITC in reducing intracellular ROS levels in control and *smn-1(ok355)* animals. Interestingly, VITC treatment did not reduce cytoplasmic ROS content in either control nematodes (**Figure 4.7Q**; $P = 0.9360$ and $P = 0.1801$, for 100 and 1000 μM , respectively) or *smn-1(ok355)* animals (**Figure 4.7Q**; $P = 0.2438$ and $P = 0.3092$, for 100 and 1000 μM , respectively) at any concentration tested.

In summary, VITC administration did not modify *smn-1(ok355)* neuromuscular defects nor intracellular ROS burden at any of the concentrations utilised.



4.2.2.4. Epigallocatechin gallate

Our results indicated that treatment with EGCG did not significantly affect the pharyngeal pumping rate of control animals at any of the concentrations utilised (**Figure 4.8A**; $P = 0.9732$, $P = 0.7447$, $P = 0.4481$, for 50, 100 and 200 μM , respectively). Similarly, no changes were observed in the pharyngeal pumping rate of *smn-1(ok355)* mutants after EGCG administration (**Figure 4.8A**; $P = 0.9997$, $P = 0.1391$, $P = 0.4619$, for 50, 100 and 200 μM , respectively).

In terms of locomotion, EGCG did not affect the number of body bends in either control animals (**Figure 4.8B**; $P = 0.5015$, $P = 0.0506$, $P = 0.7645$, for 50, 100 and 200 μM , respectively) or *smn-1(ok355)* mutants (**Figure 4.8B**; $P = 0.4167$, $P = 0.9778$, $P = 0.5304$, for 50, 100 and 200 μM , respectively) at any of the concentrations utilised. Furthermore, EGCG significantly increased the speed at which control animals crawled during the five-minutes recording at the second concentration administered (100 μM), but not at the lower or higher concentrations (50 or 200 μM) (**Figure 4.8C**; $P = 0.0679$, $P = 0.0013$, $P = 0.1225$, for 50, 100 and 200 μM , respectively). Conversely, no differences were found in the speed of *smn-1(ok355)* animals after EGCG treatment at any concentration (**Figure 4.8C**; $P = 0.5075$, $P = 0.2338$, $P = 0.8848$, for 50, 100 and 200 μM , respectively). Moreover, our analysis revealed that while EGCG treatment did not modify the inactivity time of control animals (**Figure 4.8D**; $P > 0.9999$, $P = 0.9981$, $P = 0.9986$, for 50, 100, and 200 μM , respectively), it significantly decreased the time that *smn-1(ok355)* mutants remained inactive when EGCG was administered at 200 μM (**Figure 4.8D**; $P = 0.0759$, $P = 0.4003$, $P = 0.0240$, for 50, 100 and 200 μM , respectively).

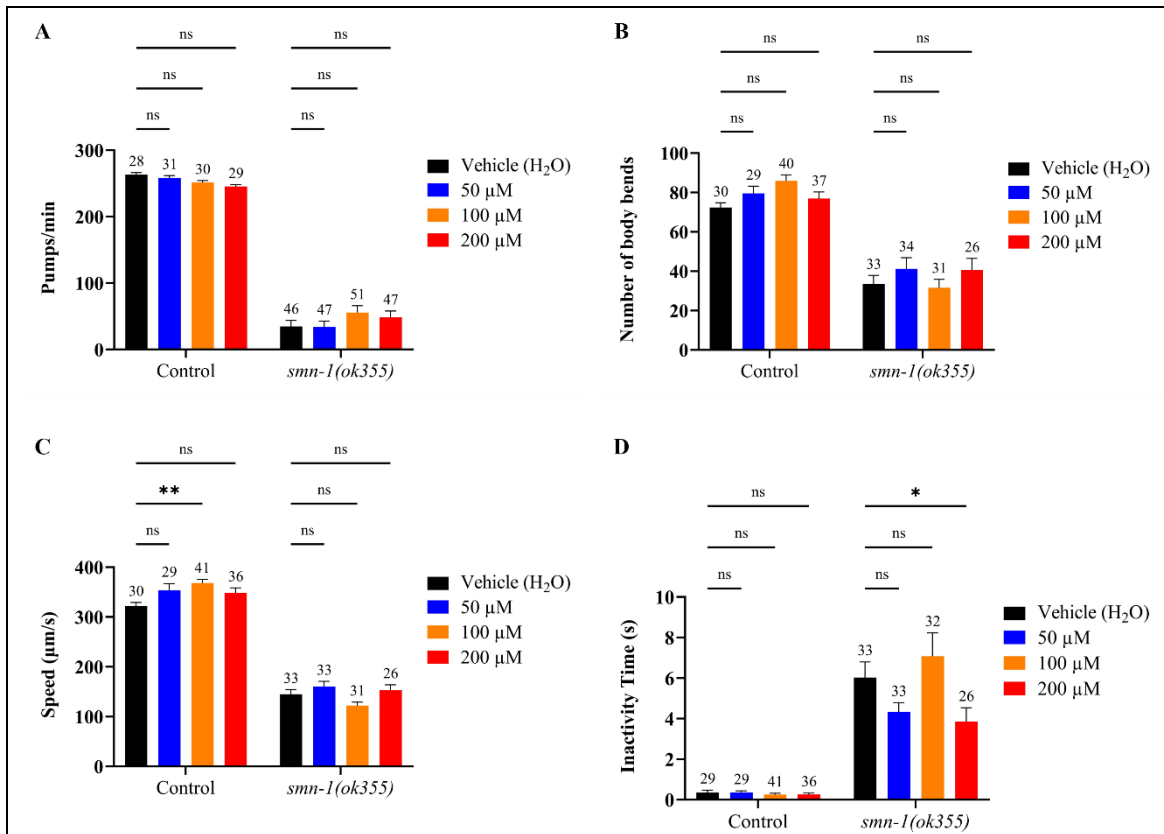


Figure 4.8. Epigallocatechin gallate partially ameliorates neuromuscular defects in the *smn-1(ok355)* *C. elegans* SMA model

C. elegans were cultivated on plates containing 0 μM (vehicle), 50 μM, 100 μM or 200 μM EGCG, and neuromuscular function was assessed through pharyngeal pumping (A), body bends (B), crawling speed (C) and inactivity time (D). In control animals, EGCG treatment significantly increased the crawling speed (C; 100 μM). In *smn-1(ok355)* mutants, EGCG significantly decreased the inactivity time (D; 200 μM).

Data are presented as mean ± SEM from at least two independent trials. Statistical significance was determined using two-way ANOVA ($P = 0.1270$, $P = 0.1070$, $P = 0.0018$, and $P = 0.0108$ for figures A, B, C and D, respectively) followed by Dunnett's multiple comparisons test. ns $P > 0.05$; * $P < 0.05$; ** $P < 0.01$. The sample size (n) for each condition is shown above of the corresponding error bar.

We next evaluated the efficacy of EGCG in reducing intracellular ROS levels in control and *smn-1(ok355)* animals. We found that EGCG administration did not modify the ROS content in control animals (**Figure 4.9Q**; $P = 0.9343$, $P = 0.4568$, $P = 0.9083$, for 50, 100 and 200 μM , respectively). Interestingly, after EGCG administration, *smn-1(ok355)* intracellular ROS levels were increased at 50 μM , although returned to vehicle-treated levels at 100 μM and 200 μM EGCG (**Figure 4.9Q**; $P < 0.0001$, $P > 0.9999$, $P = 0.7308$, for 50, 100 and 200 μM , respectively).

Overall, while EGCG did not significantly ameliorate ROS levels in control animals, it slightly increased their locomotion speed at the medium concentration tested. In *smn-1(ok355)* animals, EGCG promoted ROS generation at the lower concentration tested, yet it had minimal impact on neuromuscular function at this concentration. However, higher EGCG levels ameliorated inactivity time in *smn-1(ok355)* mutants.

In summary, evaluation of *smn-1(ok355)* neuromuscular defects and ROS content following EGCG administration revealed that EGCG possessed the ability to partially ameliorate *smn-1(ok355)* neuromuscular defects at high concentrations, however, such improvements did not correlate with a reduction of intracellular ROS levels in *smn-1(ok355)* animals.

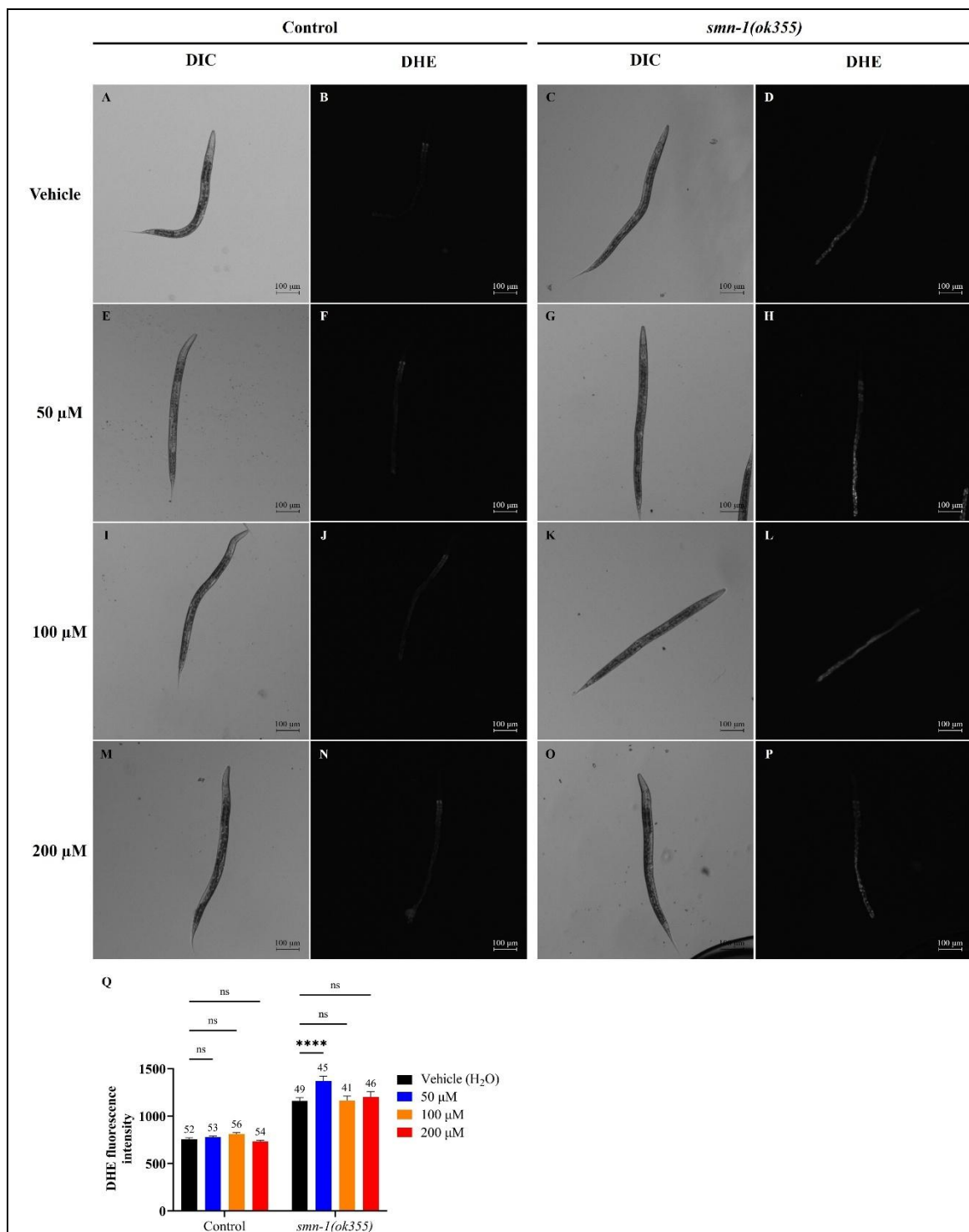


Figure 4.9. Epigallocatechin gallate might induce accumulation of cytoplasmic ROS in the *smn-1(ok355)* *C. elegans* SMA model at low concentrations

(A-P) Differential interference contrast (DIC) and fluorescence (DHE) representative images of control and *smn-1(ok355)* *C. elegans* stained with 10 μM DHE for 2 h. Animals were cultivated on plates containing 0 μM (vehicle) (A-D), 50 μM (E-H), 100 μM (I-L) and 200 μM (M-P) EGCG. Scale bars: 100 μm.

(Q) Quantification of the DHE fluorescence intensity in control and *smn-1(ok355)* nematodes across all EGCG concentrations tested. EGCG treatment did not significantly alter DHE fluorescence intensity in control animals. In *smn-1(ok355)* mutants EGCG treatment significantly

increased DHE fluorescence intensity at 50 μ M, although it did not have any significant effect at 100 μ M and 200 μ M. Data are presented as mean \pm SEM from at least two independent trials. Statistical significance was determined using two-way ANOVA ($P = 0.0023$) followed by Dunnett's multiple comparisons test. ns $P > 0.05$; **** $P < 0.0001$. The sample size (n) for each condition is shown above of the corresponding error bar.

4.2.2.5. Melatonin

Our results indicated that MEL did not significantly affect the pharyngeal pumping rate of control animals at any of the concentration utilised (**Figure 4.10A**; $P = 0.6359$, $P = 0.9996$, $P = 0.9990$, for 10 μM , 100 μM and 1000 μM , respectively). However, it significantly ameliorated *smn-1(ok355)* pharyngeal pumping defects at 100 and 1000 μM (**Figure 4.10A**; $P = 0.0896$, $P = 0.0150$, $P = 0.0114$, for 10 μM , 100 μM and 1000 μM , respectively).

In terms of locomotion, MEL significantly reduced the number of body bends in control animals at 100 μM but had no effect at 10 and 1000 μM (**Figure 4.10B**; $P = 0.4696$, $P = 0.0005$, $P = 0.5054$, for 10, 100 and 1000 μM , respectively). However, no significant differences were found in the number of body bends of *smn-1(ok355)* animals treated with MEL at any concentration (**Figure 4.10B**; $P = 0.9590$, $P = 0.5842$, $P = 0.7774$, for 10, 100 and 1000 μM , respectively). Furthermore, our results revealed that MEL significantly reduced the speed of control animals at 100 μM , although not at 10 or 1000 μM (**Figure 4.10C**; $P = 0.2188$, $P < 0.0001$, $P = 0.0718$, for 10, 100 and 1000 μM , respectively). Conversely, no differences were observed in the speed of *smn-1(ok355)* mutants at any of the MEL concentration utilised (**Figure 4.10C**; $P = 0.1769$, $P = 0.4885$, $P = 0.4169$, for 10, 100 and 1000 μM , respectively). Moreover, analysis of the inactivity time revealed that MEL increased the inactivity time of control animals at 100 μM but had no effect at 10 μM and 1000 μM (**Figure 4.10D**, $P = 0.9300$, $P = 0.0122$, $P = 0.6362$, for 10, 100 and 1000 μM , respectively). In contrast, MEL did not significantly alter the inactivity time of *smn-1(ok355)* mutants at any concentration tested (**Figure 4.10D**; $P = 0.6376$, $P = 0.9974$, $P = 0.3976$, for 10 μM , 100 μM and 1000 μM , respectively).

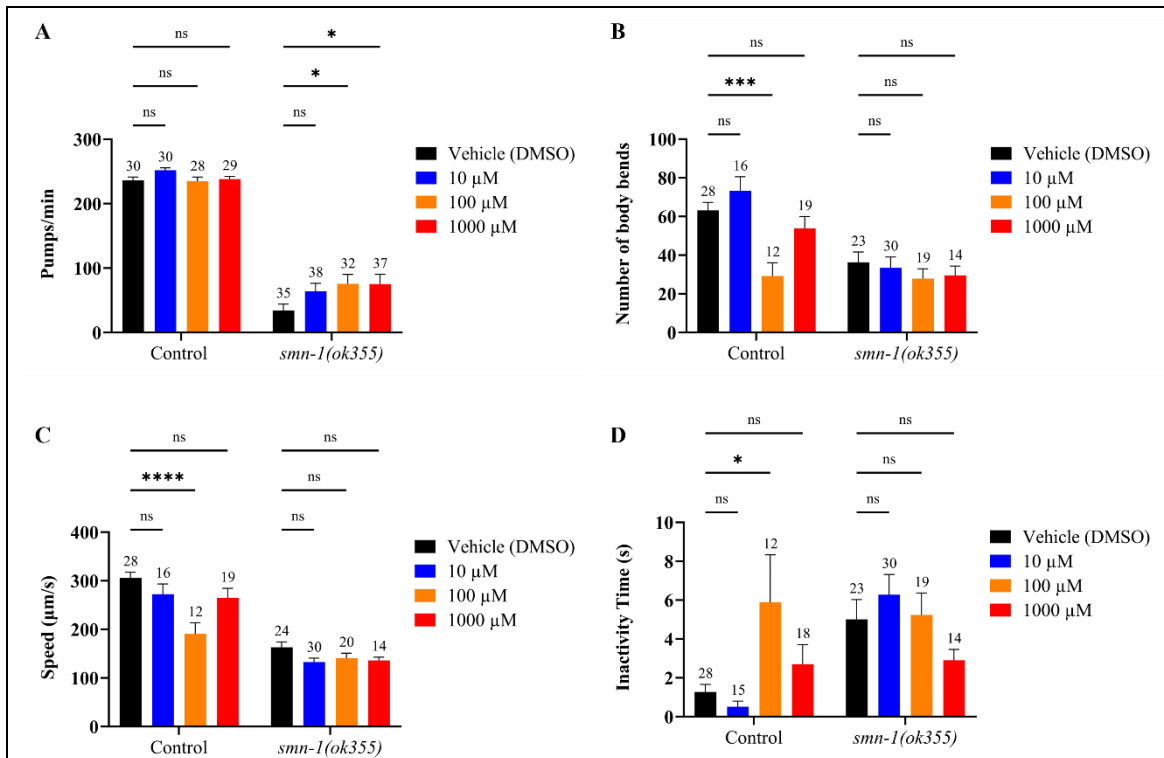


Figure 4.10. Melatonin partially ameliorates neuromuscular defects in the *smn-1(ok355)* *C. elegans* SMA model

C. elegans were cultivated on plates containing 0 μ M (vehicle DMSO), 10 μ M, 100 μ M or 1000 μ M MEL, and neuromuscular function was assessed through pharyngeal pumping (A), body bends (B), crawling speed (C) and inactivity time (D). In control animals, MEL treatment significantly reduced the number of body bends (B; 100 μ M) and crawling speed (C; 100 μ M), while increasing the inactivity time (D; 100 μ M). In *smn-1(ok355)* mutants, MEL significantly increased pharyngeal pumping rate (A; 100 μ M and 1000 μ M).

Data are presented as mean \pm SEM of from at least two independent trials. Statistical significance was determined using two-way ANOVA ($P = 0.1429$, $P = 0.0219$, $P = 0.0057$, and $P = 0.8282$ for figures A, B, C, and D, respectively) followed by Dunnett's multiple comparisons test. ns $P > 0.05$; * $P < 0.05$; *** $P < 0.001$; **** $P < 0.0001$. The sample size (n) for each condition is shown above of the corresponding error bar.

We next evaluated MEL's efficacy to reduce intracellular ROS levels in control and *smn-1(ok355)* animals. We found that while MEL did not significantly modify intracellular ROS content in control animals at any of the concentration utilised (**Figure 4.11Q**; $P = 0.9671$, $P = 0.2411$, $P = 0.0959$, for 10 μM , 100 μM and 1000 μM , respectively), MEL treatment significantly increased ROS levels in *smn-1(ok355)* mutants at 10 μM and 100 μM . Notably, ROS levels returned to baseline vehicle-treated levels at 1000 μM MEL (**Figure 4.11Q**; $P = 0.0020$, $P < 0.0001$, and $P = 0.9927$ for 10 μM , 100 μM , and 1000 μM , respectively).

In summary, evaluation of *smn-1(ok355)* neuromuscular defects and ROS content after MEL administration revealed that MEL possessed the ability to partially ameliorate *smn-1(ok355)* neuromuscular defects at 100 μM and 1000 μM . However, such improvements did not correlate with an amelioration of *smn-1(ok355)* intracellular ROS burden.

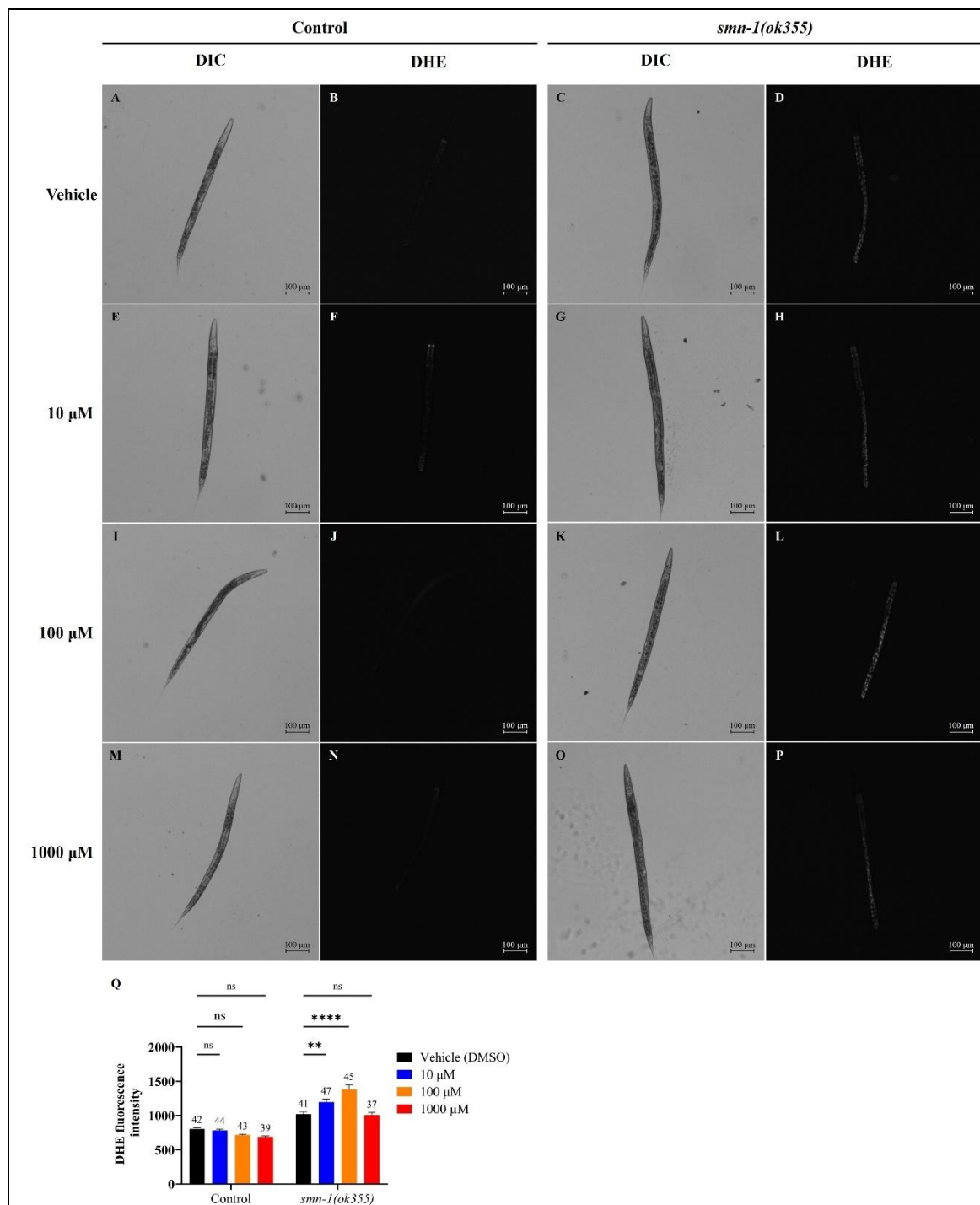


Figure 4.11. Melatonin induces the accumulation of cytoplasmic ROS in the *smn-1(ok355)* *C. elegans* SMA model

(A-P) Differential interference contrast (DIC) and fluorescence (DHE) representative images of control and *smn-1(ok355)* *C. elegans* stained with 10 μM DHE for 2 h. Animals were cultivated on plates containing 0 μM (vehicle DMSO) (A-D), 10 μM (E-H), 100 μM (I-L) and 1000 μM (M-P) MEL. Scale bars: 100 μm.

(Q) Quantification of the DHE fluorescence intensity in control and *smn-1(ok355)* nematodes across all MEL concentrations tested. MEL treatment did not significantly alter DHE fluorescence intensity in control animals. However, in *smn-1(ok355)* mutants MEL treatment significantly

increased DHE fluorescence intensity at 10 μ M and 100 μ M, although did not have any significant effect at 1000 μ M. Data are presented as mean \pm SEM from at least two independent trials. Statistical significance was determined using two-way ANOVA ($P < 0.0001$) followed by Dunnett's multiple comparisons test. ns $P > 0.05$; ** $P < 0.01$; **** $P < 0.0001$. The sample size (n) for each condition is shown above of the corresponding error bar.

Overall, the antioxidant agents evaluated in this study demonstrated variable degrees of efficacy in modulating *smn-1(ok355)* neuromuscular defects and intracellular ROS levels (**Figures 4.2-4.11**). Although NAC, EGCG, and MEL treatments partially ameliorated *smn-1(ok355)* neuromuscular defects, CUR and VITC administration did not led to any beneficial effects. Notably, neuromuscular improvements following NAC, EGCG and MEL treatments did not directly correlate with a reduction in cytoplasmic ROS levels, which challenged our initial hypothesis where increased ROS levels had a deleterious effect on the *smn-1(ok355)* SMA phenotype.

Table 4.1. Differential effects of antioxidant treatment on *smn-1(ok355)* neuromuscular function and intracellular ROS levels

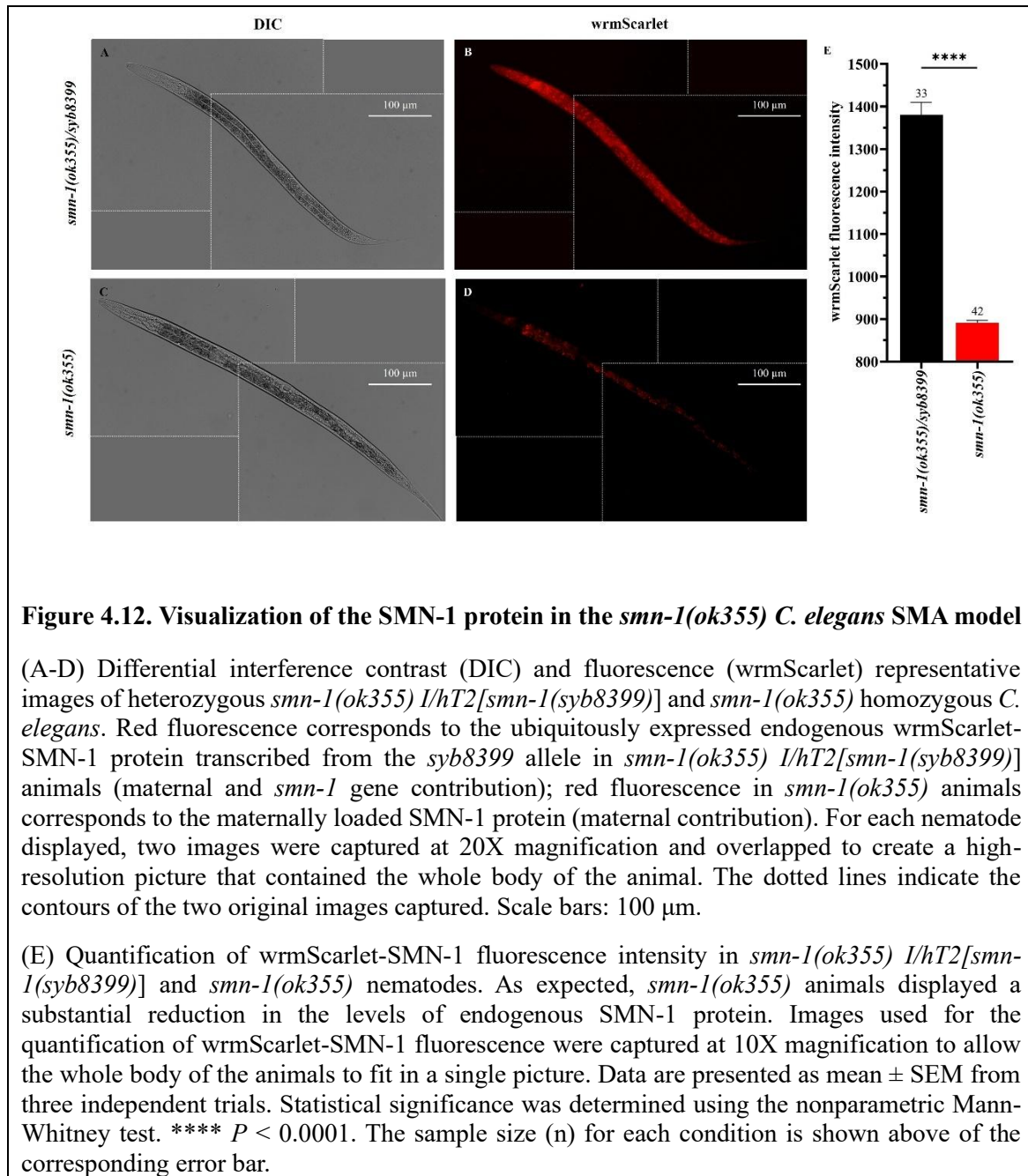
| Antioxidant | ROS reduction in <i>smn-1(ok355)</i> | Neuromuscular improvement in <i>smn-1(ok355)</i> | Correlation neuromuscular improvement / ROS reduction |
|--------------------------|---|--|---|
| N-Acetyl cysteine | Yes, across all concentrations | Yes, at medium concentration | Partial, only at medium concentration |
| Curcumin | Yes, across all concentrations | No | No |
| Vitamin C | No | No | NA |
| Epigallocatechin gallate | No, it increased ROS at lower concentration | Yes, at higher concentration | No |
| Melatonin | No, it increased ROS at lower and medium concentrations | Yes, at medium and higher concentrations | No |

4.2.3. Impact of ROS on SMN-1 protein levels

To investigate the relationship between intracellular ROS levels and SMN-1 protein levels *in vivo*, we utilised the strain PHX8399 *smn-1(ok355) I/hT2[smn-1(syb8399)]*. In these animals, the fluorescent tag wrmScarlet was inserted at the C-terminus of the endogenous wildtype copy of

the *smn-1* gene (*smn-1::wrmScarlet*) in the *smn-1(ok355)/hT2* background (referred herein as *syb8399*). Thereby, the *smn-1::wrmScarlet* tag is transmitted through the *hT2* balancer chromosome. Consequently, *smn-1(ok355)* mutants produce *smn-1(ok355)* homozygous offspring that lack any functional *smn-1* copy and rely solely on the maternally loaded wrmScarlet SMN-1 protein.

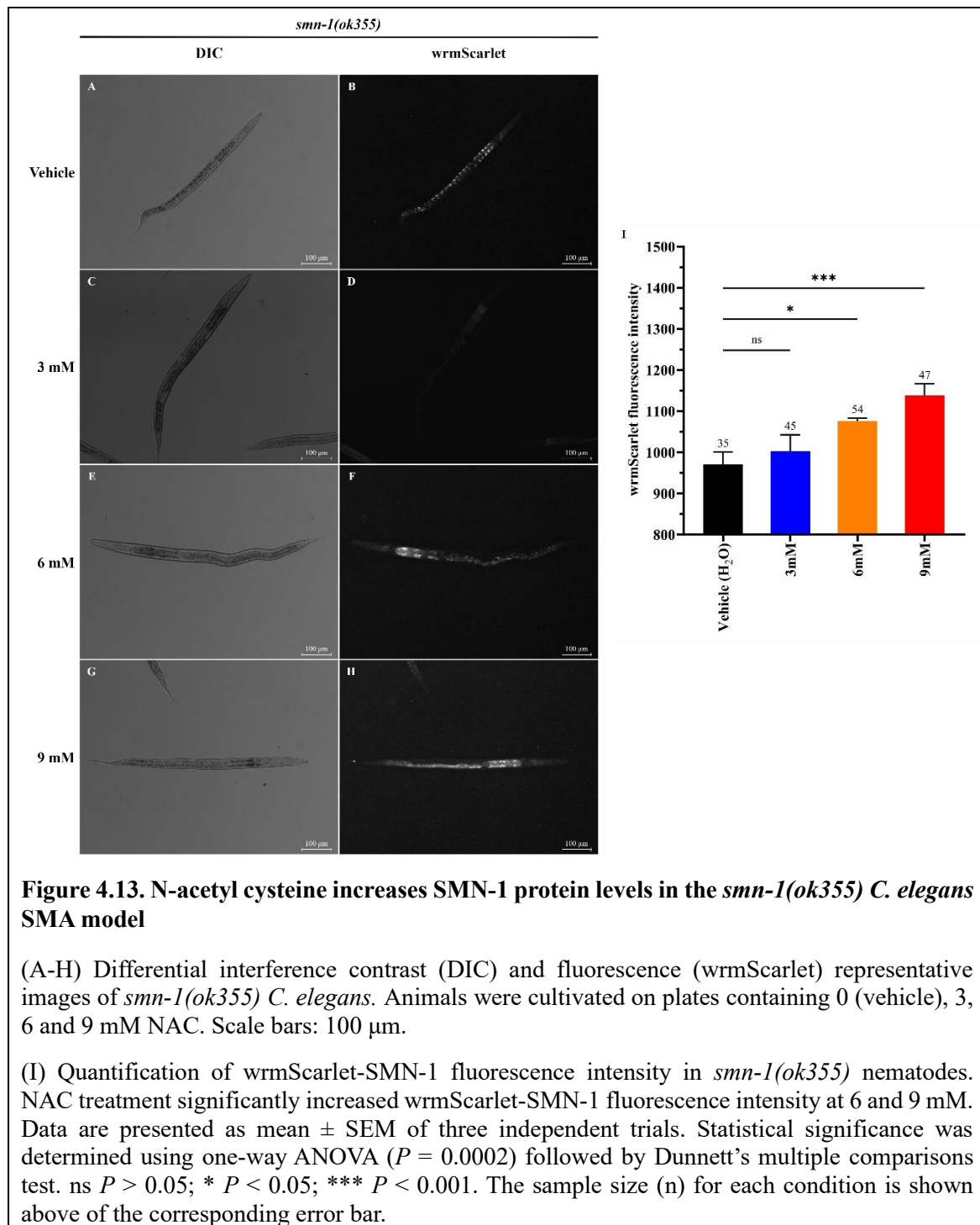
When maintained at standard conditions *smn-1(ok355) I/hT2[smn-1(syb8399)]* heterozygous mutants exhibited normal embryonic viability and a visible phenotype similar to that of *smn-1(ok355)/hT2* and wild-type animals. Furthermore, using fluorescent microscopy, we observed that the SMN-1 protein was ubiquitously expressed across the body in these animals, as previously suggested (Briese et al., 2008) (**Figure 4.12A, B**). We also noticed that their *smn-1(ok355)* offspring, loaded with maternal wrmScarlet-SMN-1 protein, exhibited larval arrest at L4 stage, similar to the *smn-1(ok355)* mutant progeny of *smn-1(ok355)/hT2* heterozygous parents. In addition, under fluorescence microscopy, we observed that the SMN-1 protein was also ubiquitously distributed throughout the body of *smn-1(ok355)* animals (**Figure 4.12C, D**), although expression was considerably less than those from *smn-1(ok355) I/hT2[smn-1(syb8399)]* (maternal contribution *versus* maternal and *smn-1* gene contribution) (**Figure 4.12E; $P < 0.0001$**). These findings suggest that the *smn-1::wrmScarlet* tag did not impair SMN-1 protein expression and therefore, it that can be used in further experimental procedures to evaluate whether oxidative stress affects SMN-1 protein levels *in vivo*.

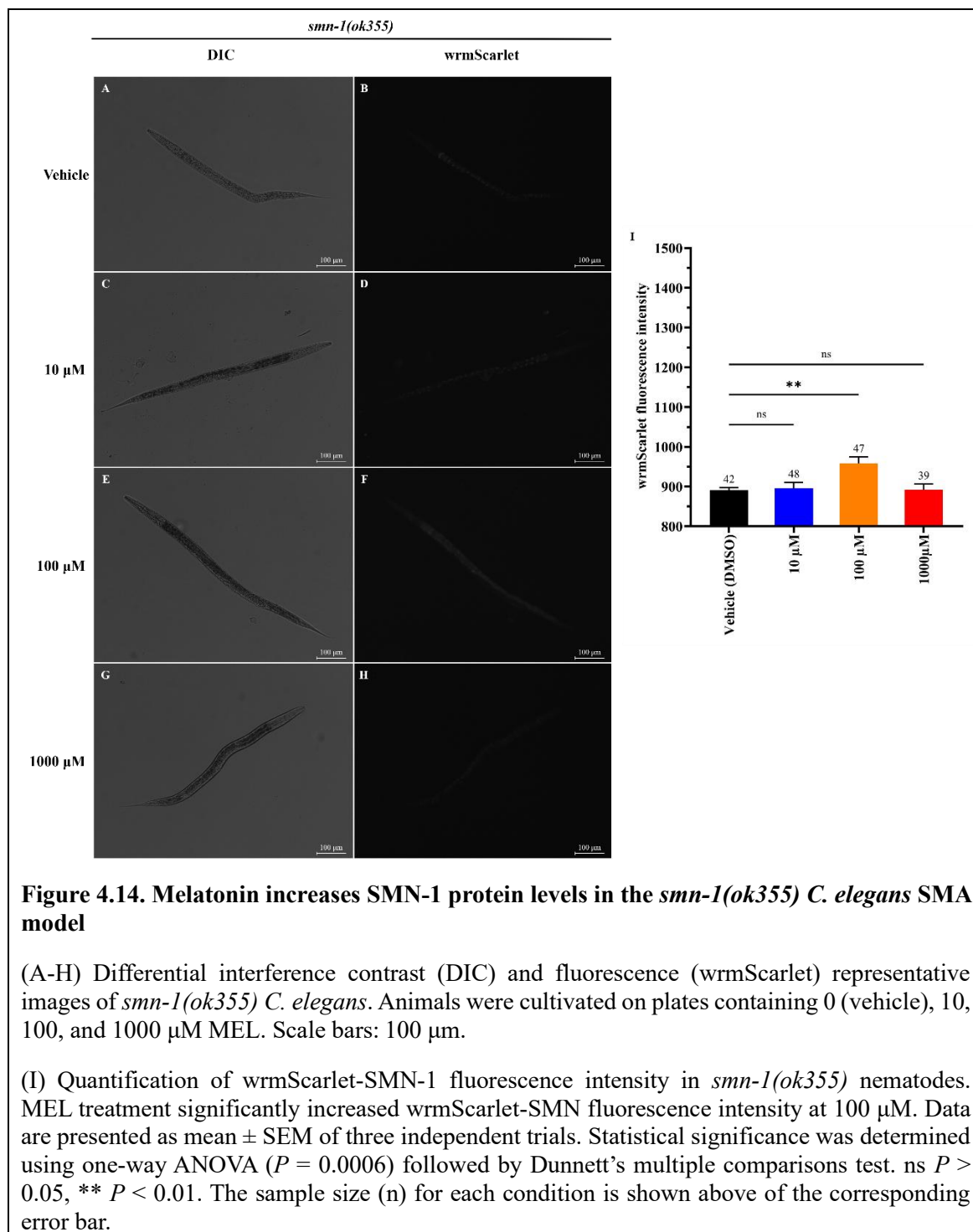


Among the antioxidants evaluated in this study, NAC and MEL emerged as promising SMA therapeutic agents because of their capacity to ameliorate *smn-1(ok355)* neuromuscular defects. Additionally, their opposite effect on regulating *smn-1(ok355)* intracellular ROS content make them interesting candidates to elucidate the impact of ROS in SMN-1 protein levels.

To evaluate whether NAC and MEL can regulate SMN-1 protein levels *in vivo*, *smn-1(ok355)* mutants that derive from heterozygous *smn-1(ok355) I/hT2[smn-1(syb8399)]* parents were cultivated for three days on plates containing 0 mM (vehicle water), 3 mM, 6 mM, or 9 mM NAC; or 0 μ M (vehicle DMSO), 10 μ M, 100 μ M, or 1000 μ M MEL. Then, endogenous *smn-1(ok355)* SMN-1 protein levels were visualised by fluorescence microscopy. Quantification of wrmScarlet-SMN-1 fluorescence revealed that NAC increased SMN-1 protein levels in the *smn-1(ok355)* *C. elegans* SMA model. While treatment with 3 mM NAC did not significantly change the levels of the SMN-1 protein, 6 and 9 mM NAC administration significantly increased *smn-1(ok355)* SMN-1 levels compared to vehicle-treated animals (**Figure 4.13A-I**; $P = 0.8297$, $P = 0.0283$, $P = 0.0002$, for 3, 6 and 9 mM NAC, respectively). Furthermore, fluorescence quantification revealed that MEL treatment significantly increased SMN-1 protein levels at 100 μ M MEL only, whereas no differences with vehicle-treated animals were observed at 10 μ M or 1000 μ M (**Figure 4.14A-I**; $P = 0.9866$, $P = 0.0015$, $P = 0.9998$, for 10, 100, or 1000 μ M MEL, respectively).

Overall, these results demonstrate that treatment with NAC and MEL increased maternally loaded SMN-1 protein levels. However, the levels of SMN-1 protein did not directly correspond to the levels at which the drug proved more effective in ameliorating *smn-1* neuromuscular defects.





4.3. Discussion

The central aim of this thesis is to elucidate whether oxidative stress contributes to SMA progression and/or severity. This chapter examines two derivative hypotheses: firstly, that mitigating oxidative stress might ameliorate SMA pathogenesis; and secondly, that oxidative stress directly impacts SMN-1 protein levels. We administered five different antioxidant treatments to the *C. elegans* SMA model and evaluated their individual efficacy in ameliorating neuromuscular function decline, a primary hallmark central to the pathophysiology of SMA. Furthermore, we explored the mechanistic insights into how oxidative stress might influence SMA, by investigating the relationship between oxidative stress and SMN-1 endogenous protein levels in *smn-1(ok355)* animals.

4.3.1. Neuromuscular function and ROS levels

Our analysis did not reveal a direct correlation between oxidative stress modulation and neuromuscular function in SMA. The secondary hypothesis underlying the use of antioxidants in the *smn-1(ok355)* SMA model was suggesting that ROS reduction would ameliorate SMA phenotypes, which in this study is correlated with the alleviation of the neuromuscular defects. The set of antioxidants compounds selected for this study proved to have a beneficial effect on neurodegenerative diseases in which the role of oxidative stress has been well established, such as Alzheimer's disease (AD) and Parkinson's disease (PD) (Houldsworth, 2024). A wide range of studies using different models of AD and PD have found that antioxidant treatment decreases oxidative stress markers, reduces protein aggregation, prevents apoptosis, and improves cognitive and motor function following treatment with NAC, CUR, VITC, EGCG, and MEL (**Table 1.3. Effect of antioxidant treatment in Alzheimer's Disease and Parkinson's Disease pre-clinical models**). However, our results demonstrate that the relationship between oxidative stress and neuromuscular function in the *smn-1(ok355)* *C. elegans* SMA model is not straightforward. For clarity, the results are discussed here in three separate groups, depending on the effect of the specific antioxidant treatment on endogenous ROS levels in *smn-1(ok355)* animals.

NAC reduced ROS burden in *smn-1(ok355)* animals in a concentration-dependent manner. Although our analysis revealed significant improvements in the neuromuscular function of these animals, they appeared solely at the medium concentration utilised, and did not correlate with ROS amelioration in *smn-1(ok355)* animals. Moreover, while CUR treatment also decreased ROS levels in a concentration-dependent manner in *smn-1(ok355)* animals, these animals did not experience any significant improvement in neuromuscular function.

Interestingly, VITC treatment did not modify intracellular ROS levels or neuromuscular function in *smn-1(ok355)* animals. One possible explanation for this could be that VITC is not bioavailable in *C. elegans* at the concentrations utilised. Some studies have reported that *C. elegans* impermeable cuticle can constitute an obstacle for proper pharmacological absorption, leading to reduced drug bioavailability (Xiong, Pears and Woollard, 2017; Giunti et al., 2021). However, previous research has shown that even at the lower concentration utilised in this study (1 mM), VITC is able to modulate different phenotypes in *C. elegans*, which proves its bioavailability (Desjardins et al., 2017; Polyak et al., 2018). Furthermore, although we did not observe any changes in the neuromuscular function or intracellular ROS levels of *smn-1(ok355)* animals, VITC treatment modulated the neuromuscular function of control animals. Therefore, a more plausible explanation is that the concentrations administered in this study were not sufficient to modulate ROS levels nor induce any changes in the neuromuscular phenotype in *smn-1(ok355)* animals.

Notably, EGCG and MEL increased the intracellular ROS levels in *smn-1(ok355)* animals. Although initially unexpected, the prooxidant effects of MEL and EGCG in the *smn-1(ok355)* *C. elegans* SMA model are not atypical. The impact of a drug, or more specifically, an antioxidant, is highly dependent on previous factors in the cellular environment, such as glucose levels, oxidative stress, or pH levels (Moldasheva et al., 2023). Several studies have demonstrated that MEL can increase mitochondrial ROS production in cancerous cells (Bejarano et al., 2011; Chen et al., 2021; Florido et al., 2022; Yun et al., 2016), whereas it can generally reduce oxidative stress in non-tumorous cells (Deng et al., 2023; Ding et al., 2014; Zavodnik et al., 2006). Similarly,

EGCG exhibits both antioxidant and prooxidant effects depending on its concentration, cell type, and experimental conditions (Lecumberri et al., 2013). Particularly, the prooxidant effects of EGCG have been well documented in cancer research, where they are associated with its antitumour activity (Della Via et al., 2021; Kuriya et al., 2023). Despite exacerbating oxidative stress burden in *smn-1(ok355)* animals, these drugs still led to improvements in neuromuscular function.

Overall, our results do not support a direct correlation between ROS reduction and neuromuscular improvement in SMA. Instead, our data suggest that ROS levels alone do not determine neuromuscular function in *smn-1(ok355)* animals, at least within the range of the endogenous ROS levels observed.

4.3.2. SMN-1 protein and ROS levels

Next, we aimed to gain a deeper understanding into of mechanism that connects oxidative stress with SMA pathology. Previous research has demonstrated that inducing oxidative stress can reduce the levels of functional SMN-1 protein via exon skipping during mRNA translation (Seo et al., 2016) or via redox-induced dysfunctional SMN-1 protein complexes (Wan et al., 2008). Furthermore, the use of pharmacological agents, such as CUR, EGCG, and NAC, utilised for their antioxidant properties in this study, have been reported to counteract these effects by promoting correct *SMN2* splicing (Dayangac-Erden et al., 2011b; Sakla & Lorson, 2008b) and increase SMN protein levels (Thelen, Wirth and Kye, 2020). If oxidative stress has the potential to influence SMN-1 protein stability *in vivo*, *smn-1(ok355)* animals might be particularly susceptible to increased SMN-1 degradation because of their increased ROS levels, thereby exacerbating their neuromuscular defects. To investigate whether ROS levels influence SMN-1 protein stability in *C. elegans* we quantified SMN-1 endogenous protein levels following NAC and MEL treatments, which, despite exerting opposing effects on ROS levels, modified *smn-1(ok355)* neuromuscular function.

Our results demonstrated that NAC treatment decreased ROS levels in *smn-1(ok355)* animals while increasing SMN-1 protein levels in a concentration-dependent manner. In addition, MEL treatment increased SMN-1 protein levels in *smn-1(ok355)* animals when administered at medium concentrations, despite exacerbating their intracellular ROS levels at medium and high concentrations. As both depletion of ROS following NAC treatment and exacerbation of ROS following MEL treatment resulted in an increase in SMN-1, it can be concluded that the effect of these drugs on SMN-1 was not directly mediated by ROS. Although we cannot entirely reject the hypothesis that ROS-induced protein modifications influence SMN protein stability *in vivo*, as postulated by Wan et al., (2008), our findings suggest that the ROS levels observed in *smn-1(ok355)* animals do not seem to directly affect endogenous SMN-1 protein levels.

4.3.3. Neuromuscular function and SMN-1 protein levels

Furthermore, we examined whether the neuromuscular improvements observed after NAC and MEL administration could be attributed to the elevated SMN-1 protein levels detected after antioxidant treatment. Although NAC treatment resulted in a concentration-dependent increase in SMN-1 protein levels, neuromuscular function did not consistently improve at all concentrations, but only at the medium concentration of NAC. Furthermore, MEL treatment increased SMN-1 levels only at the medium concentration administered, whereas neuromuscular improvements were observed at both medium and high concentrations. Our findings indicate that the neuromuscular improvements observed in *smn-1(ok355)* animals do not directly correlate with the observed increase in SMN-1 protein levels. Notably, previous studies have demonstrated that even a modest increase in SMN protein levels can lead to significant phenotypic rescue in SMA models (Bowerman et al., 2012; Kwon et al., 2011; Naryshkin et al., 2014), which appears to contradict the findings of our experiments in the nematode model. Nevertheless, there are several possible explanations for our results.

Previous research has emphasised that an increase in total SMN levels, without considering the temporal and spatial distribution where the protein is increased, may not achieve comprehensive

therapeutic effects (Groen et al., 2018). For instance, while an increase in SMN protein in the central nervous system has been shown to improve neuromuscular function in SMA mouse models, it does not necessarily correlate with an increase in lifespan. Instead, it has been proposed that restoration of SMN in both the central and peripheral nervous systems is required for a full phenotypic rescue (Hua et al., 2011; Kwon et al., 2011). This idea was also observed in the *smn-1(ok355)* *C. elegans* SMA model. In *C. elegans*, pan-neuronal expression of *smn-1* has been shown to partially rescue the SMA phenotype of *smn-1(ok355)* mutants, including body size, lifespan, and neuromuscular defects. Conversely, muscle-directed expression of *smn-1* did not rescue body size and neuromuscular defects, and only exhibited a modest increase in lifespan, suggesting that neuronal SMN-1 expression is critical for overall fitness and survival in *C. elegans* (Briese et al., 2008). In our study, we did not differentiate the SMN-1 protein levels in specific tissues. This differential distribution may explain the absence of a correlation between SMN-1 protein levels and neuromuscular improvement in *smn-1(ok355)* animals.

Overall, our results demonstrate that in the *smn-1(ok355)* *C. elegans* SMA model, ROS amelioration did not directly influence neuromuscular function, nor SMN-1 protein levels.

4.3.4. Relationship between ROS, neuromuscular function and SMN-1 protein levels

Given that neither ROS amelioration nor SMN-1 protein increase can fully explain the neuromuscular improvement observed in *smn-1(ok355)* animals, we explored alternative pathways that may be responsible for the therapeutic effects observed following NAC, EGCG, and MEL administration. The research question that we aim to address in this section was: what distinguishes the group of antioxidants that demonstrated efficacy in ameliorating *smn-1(ok355)* neuromuscular defects (NAC, EGCG, and MEL) from the group that did not (CUR and VITC)?

Some of the therapeutic properties associated with the pharmacological agents utilised in this study were not directly associated with the amelioration of ROS, but rather to the modulation of specific molecular pathways. **Table 4.2** summarises the most relevant pathways modulated by

these antioxidants in the context neurodegenerative diseases. All five antioxidants examined in this study have been reported to modulate the NF- κ B inflammatory pathway and the NRF2 antioxidant response pathway. Notably, a significant difference between the "effective" (NAC, EGCG, and MEL) and "ineffective" (CUR and VITC) antioxidants in our model was their differential regulation of the ERK and PI3K/AKT pathways and their downstream target mTOR. NAC has been reported to activate the Ras-ERK pathway and its downstream effector mTOR in neuronal cell cultures (Yan and Greene, 1998; Thelen, Wirth and Kye, 2020). Similarly, EGCG has been demonstrated to stimulate AKT and ERK signalling in various biological systems (Na and Surh, 2008; Na et al., 2008; Abbas and Wink, 2010). Moreover, MEL has also been found to enhance mTOR activation in neuronal cultures, resulting in reduced autophagy and neuroprotection (Kongsuphol et al., 2009). Conversely, CUR has been reported to suppress PI3K, AKT, and mTOR activity in neuronal cell models (Boyao et al., 2019; He et al., 2022; Wang et al., 2014). Although the specific effect of VITC on these pathways in the nervous system remains unclear, existing evidence suggests that VITC induces autophagy via mTOR inhibition (Somade et al., 2022; Xu et al., 2016; Yang et al., 2018; Zhang et al., 2022).

Table 4.2. Modulation of molecular pathways by antioxidants utilised in this study

| Antioxidant | NF- κ B | Ras/ERK | NRF2 | PI3K/Akt | mTOR |
|-------------|----------------|------------|------------|------------|------------|
| NAC | Inhibition | Activation | | No effect | Activation |
| CUR | Inhibition | | Activation | Inhibition | Inhibition |
| VITC | Inhibition | | Activation | - | - |
| EGCG | Inhibition | Activation | Activation | Activation | - |
| MEL | Inhibition | | Activation | - | Activation |

Interestingly, mTOR pathway was found to be downregulated in our bioinformatic analysis presented in Chapter III, suggesting that this pathway warrants further investigation as a potential therapeutic target in SMA. While these findings remain hypothetical and require experimental validation, they offer new avenues for future research aimed at elucidating molecular targets for new therapeutic approaches in SMA.

**Chapter V. Investigating the oxidative stress
response in the *Caenorhabditis elegans* spinal
muscular atrophy model**

5.1. Introduction

In Chapter IV, we demonstrated that simply reducing ROS levels was not sufficient to ameliorate the neuromuscular defects detected in *smn-1(ok355)* *C. elegans* SMA animals. It is important to emphasise that the impact of oxidant molecules on physiological processes is not exclusively detrimental; rather, they can also serve as critical signalling agents in various cellular pathways. (Bardaweel et al., 2018; Sies and Jones, 2020; Kozlov, Javadov and Sommer, 2024).

Based on this understanding, in Chapter V we adopted a more targeted approach by examining specific components of the *C. elegans* stress response that are dysregulated in SMA. In *C. elegans* there is not a unique pathway dedicated to oxidative stress protection. Instead, mechanisms that mitigate oxidative stress are typically integrated within broader, environment-responsive pathways. Among these pathways, the insulin/IGF-1 signalling (IIS) pathway and the p38 mitogen-activated protein kinase (MAPK) pathway, regulated in *C. elegans* by DAF-16 and SKN-1 transcription factors, respectively, are especially relevant (Back et al., 2012; Lin et al., 2023; Liu et al., 2022; Priya Dharshini et al., 2020; Teichman et al., 2021). In this introduction, we provide a comprehensive overview of oxidative stress-related pathways and antioxidants that could shed light on the impact of ROS imbalance detected in SMA.

5.1.1. Transcription factors that regulate the oxidative stress response

5.1.1.1. DAF-16

In *C. elegans*, DAF-16, the functional orthologue of the mammalian transcription factor FOXO, functions as the central transcription factor that regulates the IIS signalling pathway (Murphy & Hu, 2013; Ogg et al., 1997). Consequently, DAF-16 plays a crucial role in regulating metabolism, lifespan, protein homeostasis and stress resilience by controlling the transcription of numerous genes in response to environmental and cellular cues (Murphy & Hu, 2013; Zhang et al., 2022).

The IIS pathway is initiated when insulin-like peptides (ILPs) bind to DAF-2, a receptor tyrosine kinase analogous to mammalian insulin/IGF-1 receptors (Kimura et al., 1997). *C. elegans* encodes

approximately forty ILPs, some of which function as agonists (activating DAF-2) while others act as antagonist (inhibiting DAF-2) (Zheng et al., 2019). Upon ILP binding, DAF-2 undergoes autophosphorylation and subsequently phosphorylates AGE-1, the ortholog of the mammalian PI3K (Morris, Tissenbaum and Ruvkun, 1996; Wolkow et al., 2002). AGE-1 catalyses the conversion of PIP₂ to PIP₃, thereby recruiting PDK-1, which in turn activates the serine/threonine kinases AKT-1 and AKT-2 (Paradis et al., 1999; Toker and Newton, 2000). These kinases phosphorylate DAF-16 (FOXO), retaining it in the cytoplasm and thus preventing its translocation to the nucleus, where it would induce gene expression changes associated with stress resistance and enhanced longevity (Henderson & Johnson, 2001; Padmanabhan et al., 2009). Conversely, DAF-18, the ortholog of the mammalian PTEN, functions as a negative regulator of the IIS signalling cascade, dephosphorylating PIP₃ and thus promoting DAF-16 activity (Rouault et al., 1999) (**Figure 5.1**).

Overall, under normal favourable conditions (i.e. sufficient nutrients and minimal stress), signalling through the *C. elegans* insulin receptor DAF-2 remains active, inhibiting DAF-16 translocation to the nucleus. Conversely, in unfavourable conditions (i.e. nutrient deprivation or oxidative stress), IIS signalling is attenuated, allowing DAF-16 to translocate into the nucleus and activate the transcription of target genes that fortify the organism response against adverse conditions (Henderson & Johnson, 2001). These include antioxidant enzymes such as superoxide dismutases and catalases, heat-shock proteins, and other regulators of cellular protein homeostasis, and immune response (Honda et al., 2008; Hsu et al., 2003; McElwee et al., 2003; Meléndez et al., 2003; Yanase et al., 2002, 2020).

Notably, different studies have demonstrated that many DAF-16 target genes may differ based on developmental stage, the nature of the stress, and interactions with other pathways. For example, JNK and AMPK pathways, which are activated under stress conditions, can regulate DAF-16 by either promoting its nuclear translocation or by enhancing its transcriptional activity on stress-responsive genes, respectively (Oh et al., 2005; Greer et al., 2007). Consequently, the precise

subset of genes upregulated after DAF-16 induction can vary among different experiments, explaining some of the inconsistencies found in the literature (C. T. Murphy, 2006).

5.1.1.2. SKN-1

Skinhead-1 (SKN-1) is the *C. elegans* functional orthologue of human transcription factor NRF2 (Walker et al., 2000). Although it is best known for its involvement in tissue specification during embryonic development (Bowerman et al., 1992), SKN-1 is involved in multiple regulatory processes in the cells, including protein homeostasis, stress resistance and longevity (An & Blackwell, 2003; Inoue et al., 2005; Li et al., 2011; Tullet et al., 2008).

SKN-1 expression and location vary across different cell types and specific cellular environments. For example, SKN-1 is abundant in the nuclei of ASI sensory neurons under normal conditions, but not in the nuclei of intestinal cells, suggesting that in the absence of stressors SKN-1 plays a role in preventing the entry of *C. elegans* in the dauer diapause state (An and Blackwell, 2003), a stress-resistant, developmentally arrested larval stage that promotes survival under unfavourable environmental conditions (Corsi, Wightman and Chalfie, 2015). Conversely, under exposure to stressors such as oxidative stress, SKN-1 becomes activated and migrates to the nuclei in intestinal cells, but not in neurons, via phosphorylation by the p38 MAPK cascade (An and Blackwell, 2003; Inoue et al., 2005). Importantly, recent studies have highlighted that genetic changes induced in intestinal cells are sufficient to initiate a systemic protective response in other cell types, including neurons, where they enhance synaptic transmission at the neuromuscular junction. (Staab et al., 2013, 2014). Another example of specific regulation among different tissues is that starvation triggers nuclear translocation of SKN-1 in ASI sensory neurons, but not in intestinal cells (Bishop and Guarente, 2007), highlighting that increased SKN-1 activation must be interpreted carefully in specific contexts.

SKN-1 activation in oxidative stress conditions occurs through phosphorylation via the p38 MAPK cascade. Specifically, oxidative stress triggers the activation of SEK-1 (MAPKK), which

phosphorylates PMK-1 (MAPK), which in return phosphorylates SKN-1, facilitating its translocation to the nucleus (Inoue et al., 2005) (**Figure 5.1**). Once in the nucleus, SKN-1 binds to specific DNA sequences to activate the transcription of genes involved in stress-response, detoxification and metabolism, including glutathione S-transferases (GST), thioredoxin, cytochrome P450 and mitochondrial genes among others (Oliveira et al., 2009; Park, Tedesco and Johnson, 2009; Staab et al., 2014). Notably, although the cellular response activated by SKN-1 does not specifically focus on increasing antioxidant defences, its activation enhances cellular integrity through detoxification and cellular repair, that consequently results in increased oxidative stress resistance (Tullet et al., 2008; Oliveira et al., 2009).

SKN-1 is regulated by the integration of multiple cellular signals which allow for fine tune regulation of the cellular response to different cues. For example, recent studies have shown that a pool of cytoplasmic SKN-1 is bound to the outer mitochondrial membrane, where it functions as a mitochondrial sensor, activating genes related with metabolism and adaptation to starvation when mitochondria function is compromised (Paek et al., 2012; Sheng et al., 2021). Additionally, several studies have highlighted the complex relationship between elements from the IIS pathway (such as AKT-1/2 and DAF-16) and SKN-1. For instance, intestinal cell kinases from the insulin/IGF-1 signalling (IIS) pathway, such as AKT-1/2 and SGK-1, not only inhibited the activation of DAF-16 but also directly suppressed SKN-1 activity, demonstrating that stress responses mediated by both transcription factors are regulated in parallel by IIS signalling (Tullet et al., 2008). In line with this evidence, further research from the same group (Tullet et al., 2017), demonstrated that under conditions of IIS signalling deactivation, SKN-1 expression is upregulated in response to DAF-16 overexpression, possibly due to DAF-16's ability to bind to SKN-1 promoter regions (Schuster et al., 2010). This parallel activity could explain why the activation of both transcription factors can regulate similar processes (i.e. response to oxidative stress and longevity).

Importantly, the responses elicited following DAF-16 and SKN-1 activation are not stationary and can vary depending on specific contexts (i.e. specific tissues or specific stress responses). For

example, although activation of DAF-16 is known to confer protection against oxidative stress (Li et al., 2008), in contexts where mitochondrial ROS levels were elevated, DAF-16 activation was insufficient to prevent increased sensitivity to oxidative stress (Senchuk et al., 2018). Other examples illustrate how SKN-1 was necessary for lifespan extension independently of IIS signalling in some contexts (studies on whole body or neuronal tissues) (Houthoofd et al., 2003; Bishop and Guarente, 2007), while it was not required for IIS mediated longevity in others (study on intestinal cells) (Tullet et al., 2017).

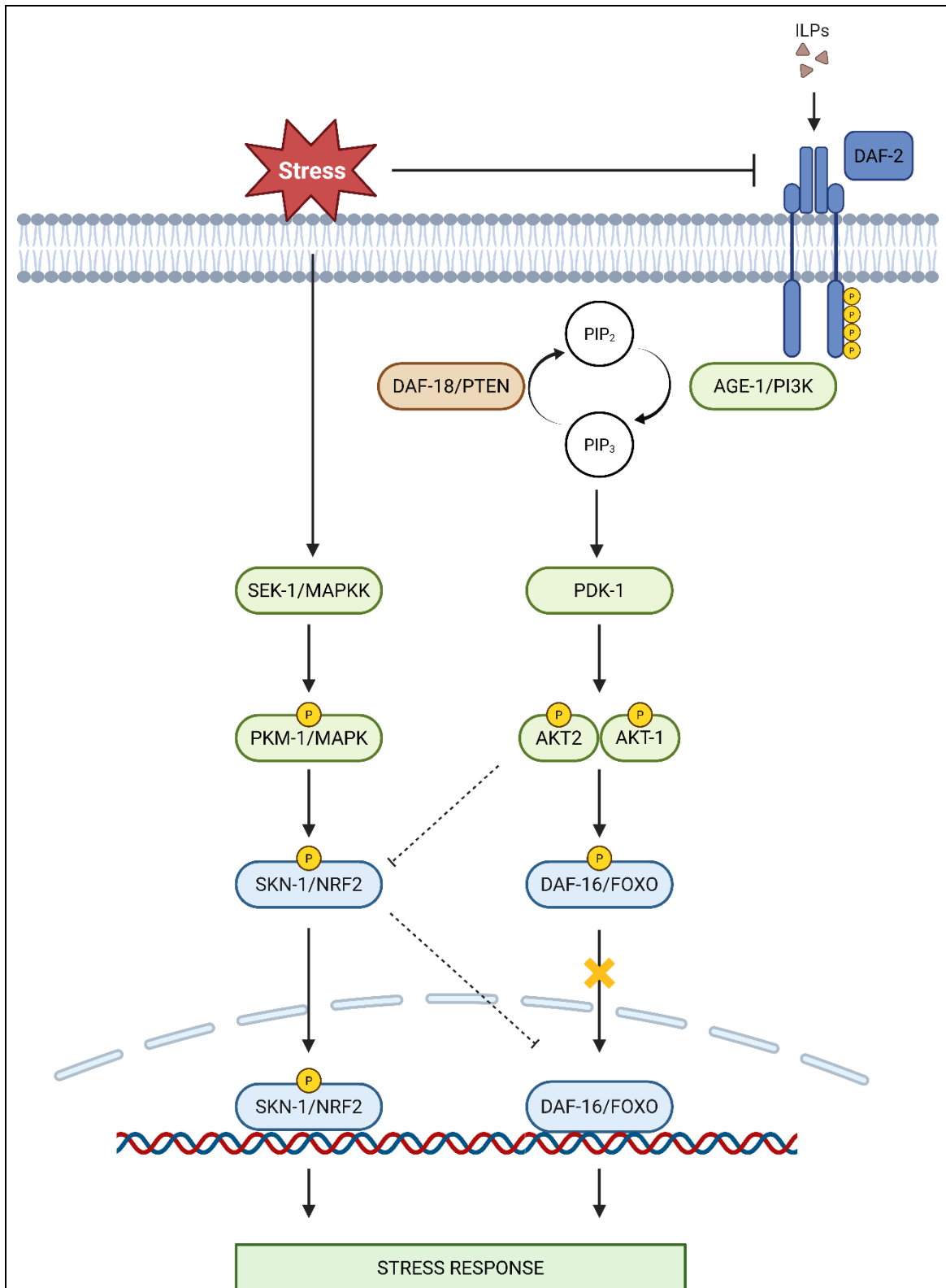


Figure 5.1. Regulatory pathways controlling the activation of the transcription factors DAF-16 and SKN-1 in *Caenorhabditis elegans*

Insulin-like peptides (ILPs) activate the *C. elegans* insulin receptor DAF-2, which triggers a signalling cascade through AGE-1/PI3K that facilitates the conversion of PIP₂ to PIP₃. PIP₃ activates PDK-1, which phosphorylates AKT-1 and AKT-2. Phosphorylated AKTs, in turn, phosphorylate DAF-16, sequestering it in the cytoplasm and thereby inhibiting the transcription

of stress response genes. DAF-18/PTEN functions antagonistically to AGE-1 by converting PIP_3 back to PIP_2 , thereby inhibiting the phosphorylation of DAF-16 and allowing its translocation to the nucleus. In parallel, cellular stress, such as oxidative stress, inhibits IIS signalling and activates the MAPK pathway via SEK-1 and PKM-1, resulting in SKN-1 phosphorylation and its translocation to the nucleus. SKN-1 and DAF-16 can function independently or in parallel to induce expression of genes that activate cellular stress responses. Dashed lines indicate regulatory interactions between these pathways.

5.1.2. Endogenous antioxidant enzymes

5.1.2.1. Superoxide dismutase

Superoxide dismutases (SOD) catalyse the conversion of superoxide anion into hydrogen peroxide. The *C. elegans* genome encodes five SOD enzymes: SOD-1, SOD-2, SOD-3, SOD-4, and SOD-5. SOD-1 (Cu,Zn-SOD) is ubiquitously expressed in the cytoplasm and mitochondrial intermembrane space of cells, and it accounts for the majority of cellular SOD activity under both normal and stress conditions (Gems and Doonan, 2008; Yanase et al., 2009). Loss of SOD-1 in *C. elegans* reduced lifespan and increased sensitivity to stressors such as oxidative and heat stress (Gems & Doonan, 2008; Van Raamsdonk & Hekimi, 2009; Yanase et al., 2009). SOD-2 (Mn-SOD) is primary responsible for superoxide detoxification in mitochondria across different tissues (Gems and Doonan, 2008; Suthammarak et al., 2013; Dues et al., 2017). Deletion of SOD-2 reduced *C. elegans* developmental rate and egg laying behaviour and increased oxidative stress vulnerability without influencing other stress responses (i.e. heat or osmotic stress) (Gems & Doonan, 2008; Suthammarak et al., 2013; Van Raamsdonk & Hekimi, 2009). Interestingly, despite increasing endogenous ROS levels, SOD-2 depletion could extend *C. elegans* lifespan (Dingley et al., 2010; Gems & Doonan, 2008; Van Raamsdonk & Hekimi, 2009). SOD-3 (Mn-SOD) localises to the mitochondrial matrix, predominantly in non-neuronal tissues (Gems and Doonan, 2008; Honda, Tanaka and Honda, 2008; Suthammarak et al., 2013). Under normal conditions the expression levels of SOD-3 remain low, which could explain the minimal phenotypic effects in *C. elegans* upon *sod-3* deletion (Libina, Berman and Kenyon, 2003; Gems and Doonan, 2008; Dues et al., 2017). SOD-4 (Cu,Zn-SOD) is a low-expressed SOD isoform, which is anchored to the membrane of intestinal cells under normal conditions (Gems and Doonan, 2008; Paavanen-Huhtala et al., 2023). Studies have shown that loss of *sod-4* has minimal effects on *C. elegans*' phenotype, with no changes on oxidative stress resistance or longevity in comparison to wildtype animals (Gems & Doonan, 2008; Honda et al., 2008; Van Raamsdonk & Hekimi, 2009). SOD-5 (Cu,Zn-SOD) represents a minor SOD isoform, expressed at low levels in a limited set of neurons (Gems and Doonan, 2008; Dues et al., 2017). Similar to other minor SOD isoforms, the loss of SOD-5 did not result in significant phenotypic changes under normal

conditions (Gems & Doonan, 2008; Van Raamsdonk & Hekimi, 2009). SOD enzymes can be upregulated upon stress conditions such as starvation or oxidative stress (Panowski et al., 2007; Gems and Doonan, 2008; Yanase et al., 2009; Meng et al., 2016; Dues et al., 2017). Interestingly, increased SOD activity did not necessarily correlate with reduced ROS levels or increased lifespan (Cabreiro et al., 2011), illustrating a complex interplay among the five SOD isoforms, ROS levels and lifespan in *C. elegans*.

5.1.2.2. Catalase

Catalases (CTL) are essential to the maintenance of intracellular redox homeostasis by catalysing the decomposition of hydrogen peroxide (H_2O_2) into water and oxygen. The *C. elegans* genome encodes three CTL enzymes: CTL-1, CTL-2 and CTL-3. CTL-1 is a cytosolic catalase found predominantly in intestinal cells (Hamaguchi et al., 2019), yet its absence has minimal impact on *C. elegans* phenotypes such as survival or reproduction (Petriv and Rachubinski, 2004). Conversely, deletion of CTL-2, which localise to peroxisomes and constitutes the majority of catalase activity in the cells, resulted in shortened lifespan, reduced reproduction, and abnormal peroxisome morphology (Petriv and Rachubinski, 2004). CTL-3 remains understudied due to challenges in producing viable knockout mutants; however, studies suggested that it might play a relevant role in neurons and muscles of the *C. elegans* pharynx, as its expression was limited to those tissues (Petriv and Rachubinski, 2004). Similar to other endogenous antioxidants, the regulation of catalase expression within cells is complex, with studies emphasising its upregulation by SKN-1 and DAF-16 under oxidative stress conditions or in long-lived mutants (Hekimi et al., 2001; Yanase, Yasuda and Ishii, 2002; Petriv and Rachubinski, 2004; Park, Tedesco and Johnson, 2009). Notably, research has shown that while overexpression of catalases enhances the tolerance of *C. elegans* to H_2O_2 exposure, excessive catalase activity resulted in detrimental phenotypes (i.e. reduced lifespan and reproductive defects) (Cabreiro et al., 2011), underscoring the necessity for a precise balance of intracellular H_2O_2 within cells.

5.1.2.3. Glutathione peroxidase

Glutathione peroxidases (GPx) reduce hydrogen peroxide (H_2O_2) and lipid hydroperoxides to water and corresponding alcohols, using glutathione (GSH) as a reducing agent. In *C. elegans* there are eight putative GPx isoforms. From those, four isoforms (GPx-1, GPx-2, GPx-6 and GPx-7) are homologous to human GPX4 and are predominantly expressed in the intestine (Sakamoto et al., 2014). Deletion of the four GPX4 homologous in *C. elegans* did not yield changes in the developmental rate or neuromuscular function, although it resulted in a reduced lifespan (Sakamoto et al., 2014, 2020). On the other hand, the remaining four isoforms (GPx-3, GPx-4, GPx-5, *(gpx-3, gpx-4, gpx-5, gpx-8)*) are homologous to human GPX3 or GPX5 (Sakamoto et al., 2014) and have been less extensively studied, with no reported direct phenotype following single knockouts in *C. elegans* (Sternberg et al., 2024). The expression of GPx genes in *C. elegans* is upregulated in response to metal exposure, suggesting that they might play an important role during detoxification (Song et al., 2014). During dietary restriction, only expression of *gpx-6* was enhanced (Sakamoto et al., 2014). Although GPx deletion increased the levels of lipid peroxidation (Sakamoto et al., 2020), it did not significantly alter *C. elegans* sensitivity to H_2O_2 exposure (Sakamoto et al., 2014). These findings, along with the lack of significant phenotypic changes following gene knockouts, suggest functional redundancy of GPx with other antioxidant mechanisms specialized in the reduction of H_2O_2 , such as catalases and peroxiredoxins.

5.1.2.4. Peroxiredoxin

Peroxiredoxins (PRDXs) are thiol-based peroxidases that reduce hydrogen peroxide (H_2O_2) and organic hydroperoxides using thioredoxin as a reducing agent. The *C. elegans* genome encodes three peroxiredoxins: PRDX-2, PRDX-3, and PRDX-6. PRDX-3 is predicted to be localised to mitochondria where it associates with respiratory chain complexes (Ferguson and Bridge, 2019). Early studies demonstrated that knockout of *prdx-3* did not modify *C. elegans* sensitivity to H_2O_2 and did not lead to phenotypic alterations (Isermann et al., 2004; Oláhová et al., 2008), possibly due to upregulation of other antioxidant genes. However, PRDX-3 depletion during adulthood did modify the *C. elegans* phenotype, resulting in reduced ATP levels and impaired neuromuscular

function, although their lifespan remained unaffected (Ranjan et al., 2013). PRDX-2, is the most extensively studied isoform, is highly expressed across multiple tissues, including the intestine, muscles and neurons in head and tail (Isermann et al., 2004; Bhatla and Horvitz, 2015). Depletion of PRDX-2 reduces *C. elegans* brood size, decreases lifespan and increases susceptibility to hydrogen peroxide exposure (Isermann et al., 2004; Oláhová et al., 2008). Notably, PRDX-6 remains less characterised, possibly due to early reports indicating the lack of any characteristic phenotypes in its absence (Isermann et al., 2004; Sternberg et al., 2024). Beyond direct H₂O₂ decomposition, PRDX-2 has also been associated with redox modulation of signalling pathways, particularly inhibiting DAF-16 and SKN-1 through activation of IIS signalling in normal conditions (Olahova and Veal, 2015), and increasing p38 MAPK signalling cascade in response to H₂O₂.

5.1.3. Research objectives

In this this chapter, we utilise bioinformatic approaches to determine central elements of the oxidative stress response dysregulated in SMA, with the objective of determining whether these genes can modulate oxidative stress and neuromuscular phenotypes associated with SMA. Oxidative stress sensitivity was assessed exposing *C. elegans* to pro-oxidant compounds (paraquat and juglone). *C. elegans* neuromuscular function was assessed using the pharyngeal pumping and WormLab locomotion assays as described in Chapter IV.

The specific objectives of Chapter V were as following:

1. To identify central oxidative stress-related genes dysregulated in *smn-1(ok355)* animals.
2. To investigate the impact of selected genes in modulating oxidative stress sensitivity in *smn-1(ok355)* animals.
3. To assess the capacity of selected genes in modulating the neuromuscular defects observed in *smn-1(ok355)* nematodes.

Overall, we aim to determine whether the precise targeting of ROS signals within cells can deepen our understanding of the impact of oxidative stress in SMA. This research could hold the potential to identify novel redox therapeutic targets specifically relevant to SMA.

5.2. Results

5.2.1. Dysregulated genes controlling the oxidative stress response in spinal muscular atrophy

The results obtained in Chapter IV demonstrated that although ROS levels were elevated in the *smn-1(ok355)* *C. elegans* SMA model, modulation of ROS alone was insufficient to ameliorate SMA-associated neuromuscular defects. These findings suggest a complex relationship between ROS and SMA pathology. Therefore, we sought to identify key regulatory genes within the oxidative stress response pathways that might contribute to SMA pathogenesis beyond the mere alteration of ROS levels.

We obtained a list of genes implicated in the oxidative stress response (OxSR) in *C. elegans* utilising the GO database (GO:0006979). From this dataset, we identified 13 genes that were significantly upregulated (**Figure 5.2A**) and 34 genes that were significantly downregulated (**Figure 5.2B**), yielding a total of 47 oxidative stress related genes differentially expressed (OxSR-DE) in *smn-1(ok355)* *C. elegans* SMA. Among these, gene targets of DAF-16 and SKN-1 transcription factors were also observed, including GSH enzymes, antioxidants, and mitochondrial genes.

To gain a better understanding of the precise role that our candidate OxSR-DE genes play in SMA, we performed GO and KEGG functional annotations. The identified OxSR-DE genes were significantly enriched in 59 different GO terms: 65 BP, 13 MF and 11 CC. Among the biological processes terms, we observed enrichment for “Response to oxidative stress”, “Response to toxic substance” and “Response to reactive oxygen species” (**Figure 5.2C**). Among the molecular function (MF) terms, we observed enrichment for “Antioxidant activity”, “Peroxidase activity”

and “chondroitin 4-sulfotransferase activity” (**Figure 5.2D**). Finally, within the cellular component terms, we observed enrichment for “Mitochondrion”, “Mitochondrial prohibitin complex” and “inner mitochondrial membrane protein complex” (**Figure 5.2E**). Additionally, KEGG pathway analysis identified seven significantly enriched pathways, including “Glutathione metabolism”, “Peroxisome” and “Longevity regulating pathway-multiple species” (**Figure 5.2F**).

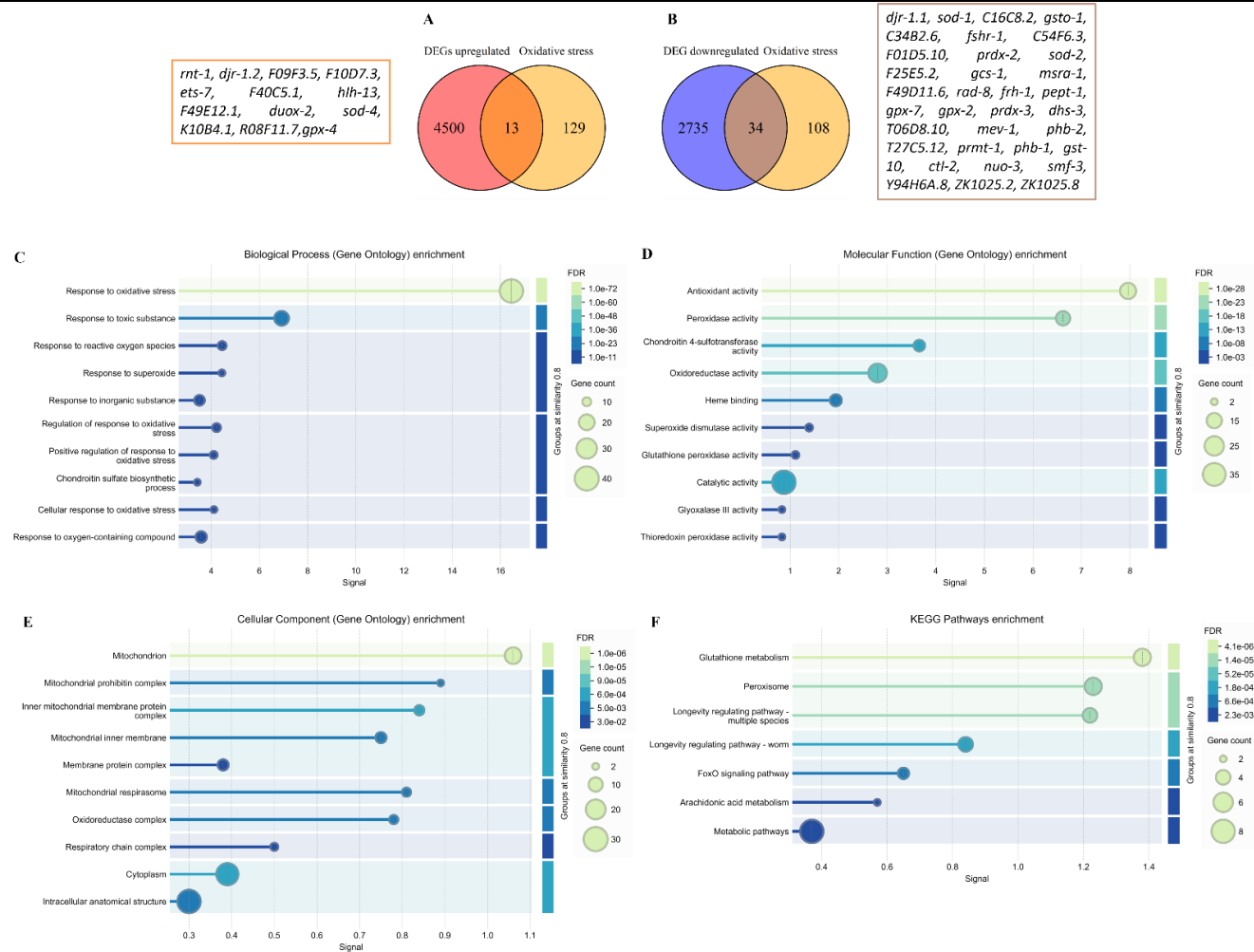


Figure 5.2. Oxidative stress-response genes differentially expressed (OxSR-DE) in the *smn-1(ok355)* *C. elegans* SMA model

(A-B) OxSR-DE genes were found in the intersection between DEGs that were upregulated (A) and downregulated (B) in transcriptomic analysis, and genes belonging to the GO dataset “response to oxidative stress” (GO:0006979). The specific 13 upregulated genes (A) and 34 downregulated gene (B) that were yield by the analysis are shown next to each diagram.

(C-F) Functional annotations for OxSR-DE genes in categories biological process (C), molecular function (B), cellular component (E), and KEGG pathways (F). The size of each dot indicates the number of dysregulated genes in each category, and the dot colour represents the adjusted p-value (FDR) of the analysis.

To identify the key regulatory genes in our dataset, we first constructed a protein-protein interaction (PPI) network using the online database STRING. This software allows us to visualise how the protein products of the OxSR-DE genes connect functionally, with lines between proteins representing jointly contributions to a shared function (**Figure 5.3A**). We next analysed the topology of this network using the Molecular Complex Detection (MCODE) plug in Cytoscape. This software enables a deeper understanding of the organisation within the PPI network and the relationships between its components, assigning a “centrality score” value that reflects the influence of specific genes within relevant clusters. Utilising this method, two sub-networks with high centrality scores were detected. The first sub-network contained seven genes, each with a centrality score of 5 (**Figure 5.3B**), while the second sub-network consisted of six genes, each with a centrality score of 3 (**Figure 5.3C**). By integrating these findings, we refined our candidate gene list to 13 oxidative stress response “hub” genes that were differentially expressed in *smn-1(ok355)* animals compared to *smn-1(+)* controls.

Among these 13 hub genes, there were key members of antioxidant defence systems, including three genes belonging to the superoxide dismutase (SOD) family (*sod-1*, *sod-2*, *sod-4*), three genes belonging to the glutathione peroxidase (GPX) family (*gpx-2*, *gpx-4*, *gpx-7*), two genes belonging to the peroxiredoxin (PRDX) family (*prdx-2*, *prdx-3*), two genes belonging to the glutathione-independent glyoxalase enzymes (*djr-1.1*, *djr-1.2*), one catalase (CTL) enzyme (*ctl-2*) and one methionine sulfoxide reductase (*msra-1*). From those, only *djr-1.2*, *sod-4* and *gpx-4* were found upregulated in *smn-1(ok355)* in comparison to *smn-1(+)* controls, while the rest were significantly downregulated (**Figure 5.3D**).

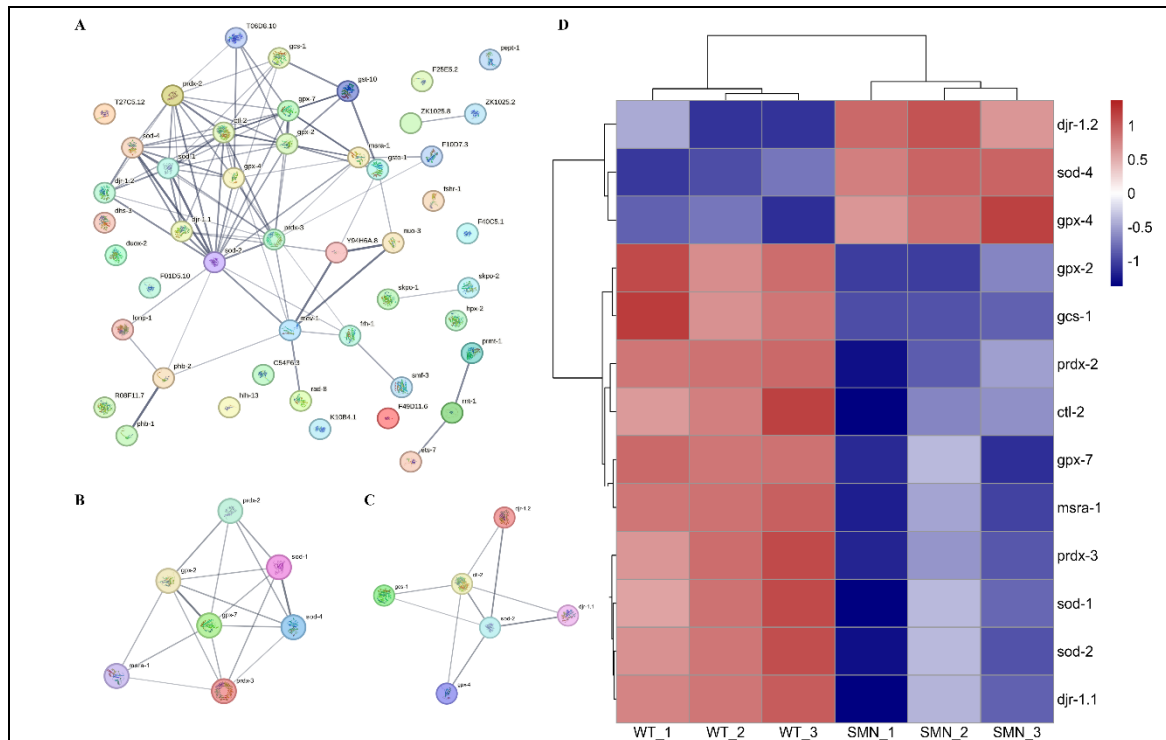


Figure 5.3. Identification of oxidative stress hub genes in the *smn-1(ok355)* *C. elegans* SMA model using protein-protein interaction (PPI) network analysis

(A) PPI network of OxSR-DE genes was generated using the STRING database. Edges represent functional interactions between proteins based on experimental evidence, co-expression data, and curated databases.

(B-C) Highly interconnected clusters identified from the main PPI network using the MCODE plugin in Cytoscape. The first cluster (B) contains seven genes, each with a centrality score of 5. The second cluster (C) contains six genes, each with a centrality score of 3.

(D) Heat map illustrating the differential gene expression (log2 fold-change) between *smn-1(+)* (WT_1, WT_2, WT_3) controls and *smn-1(ok355)* (SMN_1, SMN_2, SMN_3). Among the final 13 hub genes identified from the integrated MCODE clusters, three genes were significantly upregulated (red) in *smn-1(ok355)*, while ten were significantly downregulated (blue).

To identify the transcriptional factors (TF) regulating the expression of the 13 hub genes we utilised the JASPAR database via NetworkAnalyst. Importantly, this online tool does not recognise *C. elegans* identifiers, thus, prior to the analysis, each *C. elegans* gene was mapped to its closest human ortholog using the OrthoList2 (**Table 5.1**).

Table 5.1. Conversion of candidate *C. elegans* OxSR-DE genes to their closest human ortholog

| <i>C. elegans</i> gene | Wormbase ID | Human ortholog | Ensembl ID |
|------------------------|----------------|----------------|-----------------|
| <i>sod-4</i> | WBGene00004933 | <i>SOD1</i> | ENSG00000142168 |
| <i>phb-2</i> | WBGene00004015 | <i>PHB2</i> | ENSG00000215021 |
| <i>phb-1</i> | WBGene00004014 | <i>PHB</i> | ENSG00000167085 |
| <i>mev-1</i> | WBGene00003225 | <i>SDHC</i> | ENSG00000143252 |
| <i>gpx-2</i> | WBGene00011045 | <i>GPX7</i> | ENSG00000116157 |
| | | <i>GPX4</i> | ENSG00000167468 |
| | | <i>GPX8</i> | ENSG00000164294 |
| <i>gpx-7</i> | WBGene00019846 | <i>GPX8</i> | ENSG00000164294 |
| | | <i>GPX4</i> | ENSG00000167468 |
| | | <i>GPX7</i> | ENSG00000116157 |
| <i>sod-1</i> | WBGene00004930 | <i>CCS</i> | ENSG00000173992 |
| | | <i>SOD1</i> | ENSG00000142168 |
| <i>nuo-3</i> | WBGene00013308 | <i>NDUFA6</i> | ENSG00000184983 |
| | | <i>NDUFA6</i> | ENSG00000272765 |
| | | <i>NDUFA6</i> | ENSG00000273397 |
| | | <i>NDUFA6</i> | ENSG00000277365 |
| | | <i>NDUFA6</i> | ENSG00000281013 |
| | | <i>BRK1</i> | ENSG00000254999 |
| <i>Y94H6A.8</i> | WBGene00022380 | <i>NDUFA12</i> | ENSG00000184752 |
| <i>sod-2</i> | WBGene00004931 | <i>SOD2</i> | ENSG00000112096 |

The resultant TF network is shown in **Figure 5.4**. The details of the analysis have been compiled in **Table 5.2**, where only nodes (input genes or predicted TFs) that exhibit five or more connections within the network have been included. Among the input hub genes, *gpx-2*, *gpx-7*, *nuo-3*, *phb-2* and *sod-2* demonstrated the highest number of connections within the cluster, implying that their transcription is modulated by multiple TFs predicted by the analysis. Notably, all five genes are downregulated in *smn-1(ok355)* animals (**Figure 5.3D**). The five TFs with more

connections within the network were FOXC1, GATA2, RELA, PPARG, and HOXA5. *C. elegans* possess orthologues for four of these: DAF-16 (FOXO), PHA-4 (FOXA, a paralogue of FOXC1), ETL-2 (GATA), and DAF-12 (PPARG). In *C. elegans*, these TFs are associated with stress responses and development (Ogg et al., 1997; Gaudet and Mango, 2002; Dowell et al., 2003; Zárte-Potes et al., 2020). The remaining TF, RELA, which is part of the NF- κ B pathway, lacks a direct equivalent in *C. elegans* (Brena et al., 2020). It is important to note that, while this transcription factor network offers valuable insights for generating hypotheses regarding the regulatory control of our hub genes, the cross-species approach employed means that the results should be regarded as approximations rather than a definitive transcriptional regulatory map.

Table 5.2. Transcription factor analysis of hub oxidative stress hub genes identified in *smn-1(ok355)* animals

| Node type | Human ID | <i>C. elegans</i> ID | Connections |
|-----------|----------------|----------------------|-------------|
| Gene | <i>GPX4</i> | <i>gpx-2/gpx-7</i> | 19 |
| Gene | <i>NDUFA12</i> | <i>nuo-3</i> | 11 |
| Gene | <i>BRK1</i> | <i>nuo-3</i> | 11 |
| Gene | <i>PHB2</i> | <i>phb-2</i> | 11 |
| TF | FOXC1 | DAF-16/PHA-4 | 10 |
| TF | GATA2 | ELT-2 | 9 |
| Gene | <i>SOD2</i> | <i>sod-2</i> | 9 |
| Gene | <i>NDUFA6</i> | <i>Y94H6A.8</i> | 8 |
| Gene | <i>PHB</i> | <i>phb-1</i> | 7 |
| Gene | <i>GPX7</i> | <i>gpx-2/gpx-7</i> | 7 |
| Gene | <i>CCS</i> | <i>sod-1</i> | 6 |
| TF | RELA | NA | 6 |
| Gene | <i>SOD1</i> | <i>sod-1/sod-4</i> | 6 |
| Gene | <i>SDHC</i> | <i>mev-1</i> | 5 |
| TF | PPARG | DAF-12 | 5 |
| TF | HOXA5 | LIN-39 | 5 |
| Gene | <i>GPX8</i> | <i>gpx-2/gpx-7</i> | 5 |

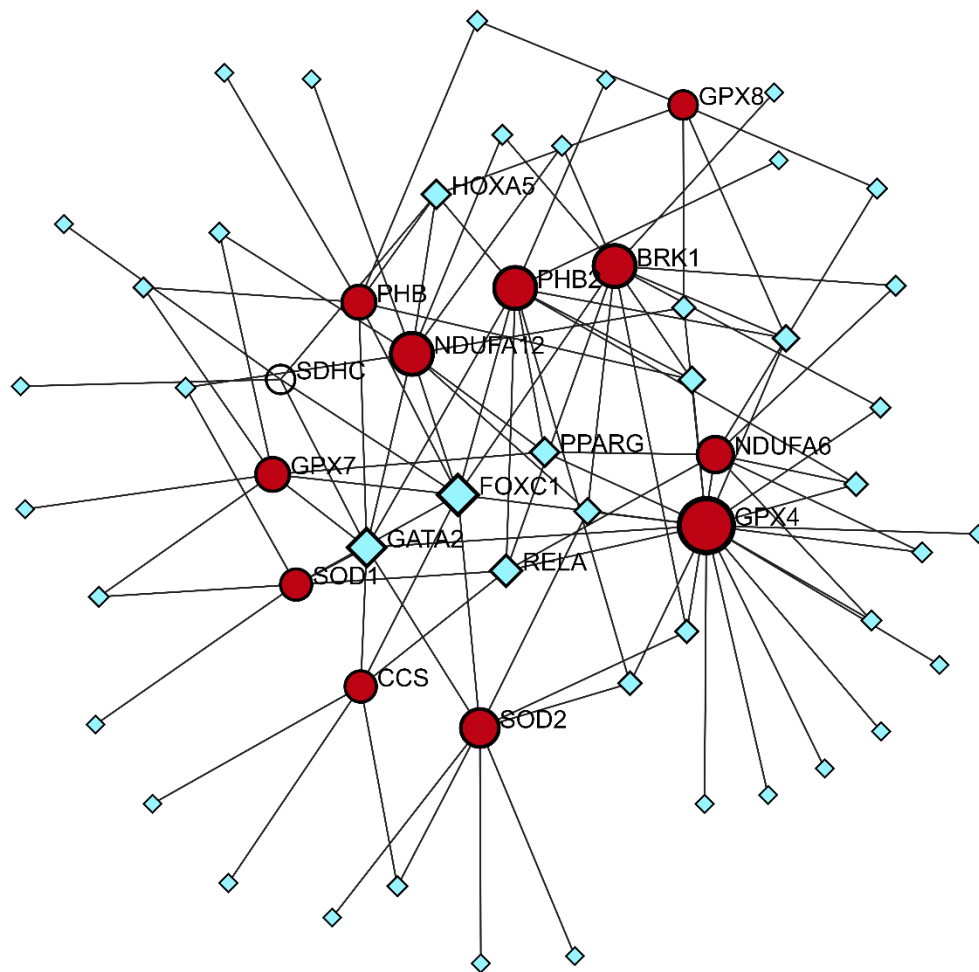


Figure 5.4. Transcription-factor (TF) network of oxidative stress hub genes identified in *smn-1(ok355)* animals

Transcriptional regulatory map predicted by NetworkAnalyst (JASPAR database) employing human orthologs for our 13 oxidative stress hub genes. The input genes are represented by red circles, while TFs are depicted as blue diamonds.

5.2.2. Evaluation of the impact of *sod* knockouts on neuromuscular function

The identification of 13 hub genes enriched in oxidative stress-related pathways highlight their significant role in modulating the ROS imbalance observed in SMA pathology. Among those genes, the SOD family emerged as a key candidate due to its central presence in both PPI and TF networks. Furthermore, unlike other antioxidant enzyme families, whose function may overlap (i.e., CTL, GPX, and PRDX catalyse similar reactions converting H_2O_2 into H_2O), the SOD family performs a specialised and non-redundant role within cells catalysing the conversion of $\text{O}_2^{\bullet-}$ into H_2O_2 .

To determine whether SOD activity can modulate *smn-1(ok355)* SMA phenotypes, we introduced the available *sod* null alleles into *smn-1(ok355)* animals by genetic crossing, generating *smn-1(ok355);sod* double mutant strains. We included all five members of the SOD family in our analysis, leveraging their distinct subcellular compartmentalisation to investigate how the fine modulation of ROS influences SMA-related phenotypes.

5.2.2.1. Superoxide dismutase 1

To elucidate the impact of SOD-1 depletion in the oxidative stress response of *C. elegans*, *smn-1(+)*, *sod-1(tm776)*, *smn-1(ok355)*, and *smn-1(ok355);sod-1(tm776)* animals were assessed under chronic (4 mM paraquat) and acute (60 μM juglone) oxidative stress conditions.

Our analysis indicated that *sod-1(tm776)* animals exhibit increased sensitivity to chronic oxidative stress conditions relative to *smn-1(+)* controls (**Figure 5.5A**; $P < 0.0001$). Similarly, *smn-1(ok355);sod-1(tm776)* double mutants demonstrated increased sensitivity to chronic oxidative stress exposure in comparison to *smn-1(ok355)* animals (**Figure 5.5A**; $P < 0.0001$). Previous unpublished work from our group has shown that the sensitivity of *sod-1(tm776)* animals to low levels of acute oxidative conditions did not differ from that of *smn-1(+)* animals (**Supplementary Figure 7A**; $P = 0.1556$). Likewise, *smn-1(ok355);sod-1(tm776)* double mutants exhibited the same sensitivity to acute oxidative stress exposure as *smn-1(ok355)* animals

(**Supplementary Figure 7A**; $P = 0.2114$). Combined, these findings highlight the significant role of SOD-1 in conferring protection against chronic oxidative stress conditions, while its role in acute oxidative stress protection appears less relevant at the concentrations tested in this study.

Next, we investigated whether SOD-1 depletion can modulate *C. elegans* neuromuscular behaviour using the pharyngeal pumping and locomotion assays. Previous unpublished work from our group demonstrated that the pharyngeal pumping rate of *sod-1(tm776)* animals did not significantly differ from that of *smn-1(+)* animals (**Supplementary Figure 8A**; $P > 0.9999$). In addition, *smn-1(ok355);sod-1(tm776)* double mutants did not exhibit significant change in their pharyngeal pumping rate in comparison to *smn-1(ok355)* animals (**Supplementary Figure 8A**; $P = 0.0001$). We then further evaluated the influence of SOD-1 depletion in *C. elegans* neuromuscular performance and observed no statistically significant difference in the number of body bends during locomotion assays between *sod-1(tm776)* and *smn-1(+)* animals (**Figure 5.5B**; $P = 0.4240$). Similarly, we found no differences in the number of body bends between *smn-1(ok355);sod-1(tm776)* double mutants and *smn-1(ok355)* animals (**Figure 5.5B**; $P = 0.1434$). Furthermore, assessment of the speed during locomotion revealed no significant differences between *sod-1(tm776)* and *smn-1(+)* animals (**Figure 5.5C**; $P = 0.9396$). Likewise, the speed of *smn-1(ok355);sod-1(tm776)* remained similar to that exhibited by *smn-1(ok355)* animals alone (**Figure 5.5C**; $P = 0.3458$). Moreover, the time that the animals spent inactive during the assay was similar for both *sod-1(tm776)* and *smn-1(+)* animals (**Figure 5.5D**; $P = 0.9838$). Notably, the time that *smn-1(ok355);sod-1(tm776)* animals remained inactive during the assay was significantly increased in comparison to *smn-1(ok355)* animals (**Figure 5.5D**; $P = 0.0037$). Overall, deletion of *sod-1* increases sensitivity to oxidative stress under chronic conditions and exacerbates the neuromuscular defects of *smn-1(ok355)* animals.

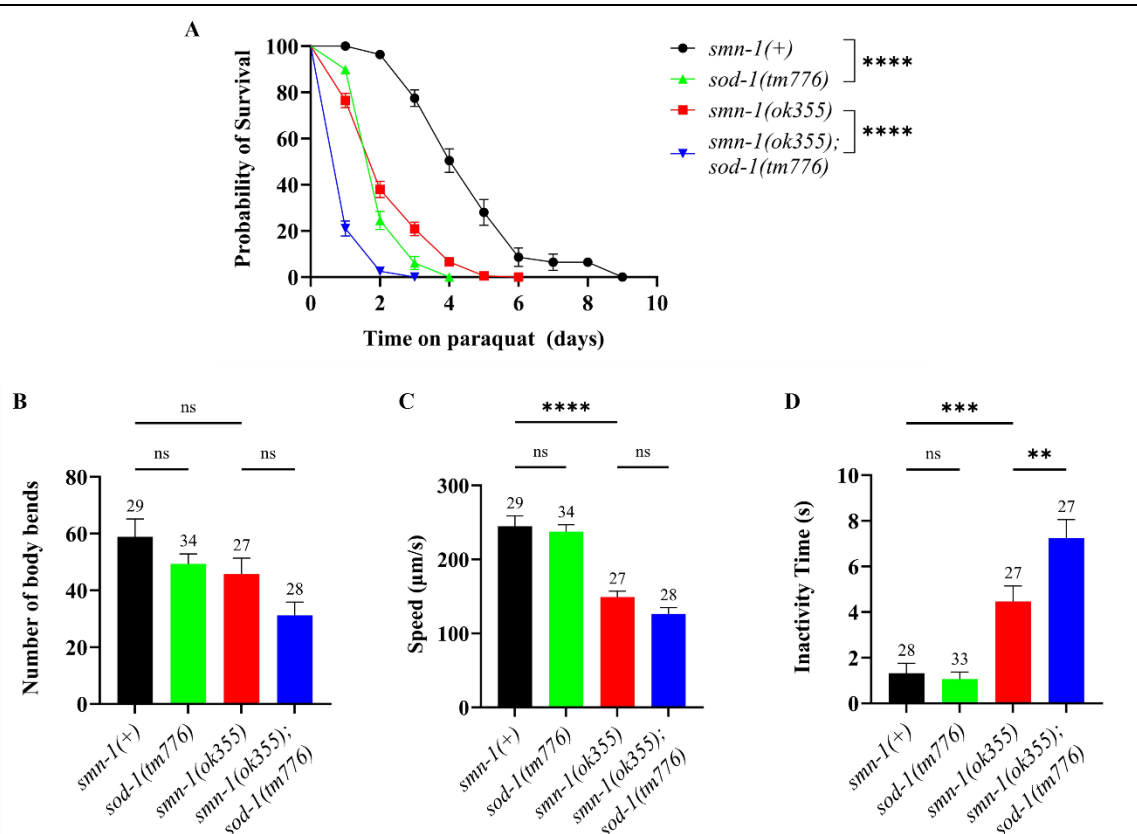


Figure 5.5. Deletion of *sod-1* increases sensitivity to oxidative stress and exacerbates neuromuscular defects in the *smn-1(ok355)* *C. elegans* SMA model

(A) Deletion of *sod-1(tm776)* increased sensitivity to chronic oxidative stress induced by 4 mM paraquat; this was also evident when *sod-1* was deleted in *smn-1(ok355)* mutants. Probability of survival over time is presented in a Kaplan-Meier survival curve. Each time point represents the mean \pm SEM of three independent trials. Statistical significance was determined using separate log-rank test applied to pairwise genotype comparisons. **** $P < 0.0001$. *smn-1(+)* ($n = 77$), *sod-1(tm776)* ($n = 118$), *smn-1(ok355)* ($n = 186$), and *smn-1(ok355);sod-1(tm776)* ($n = 157$).

(B-D) *C. elegans* neuromuscular function was assessed in a locomotion assay and evaluated through number of body bends (B), speed (C) and inactivity time (D). Deletion of *sod-1(tm776)* did not affect the animal's neuromuscular function. However, deletion of *sod-1(tm776)* in *smn-1(ok355)* mutants significantly exacerbated their neuromuscular defects, reflected as an increase in the time that the animals spent inactive (D). Data are presented as the mean \pm SEM from at least two independent trials. Statistical significance was determined using one-way ANOVA ($P = 0.0024$, $P < 0.0001$, and $P < 0.0001$, for figures B, C, and D, respectively), followed by Sidak's multiple comparison test. ns $P > 0.05$; ** $P < 0.01$; *** $P < 0.001$; **** $P < 0.0001$. The sample size (n) for each condition is shown above of the corresponding error bar.

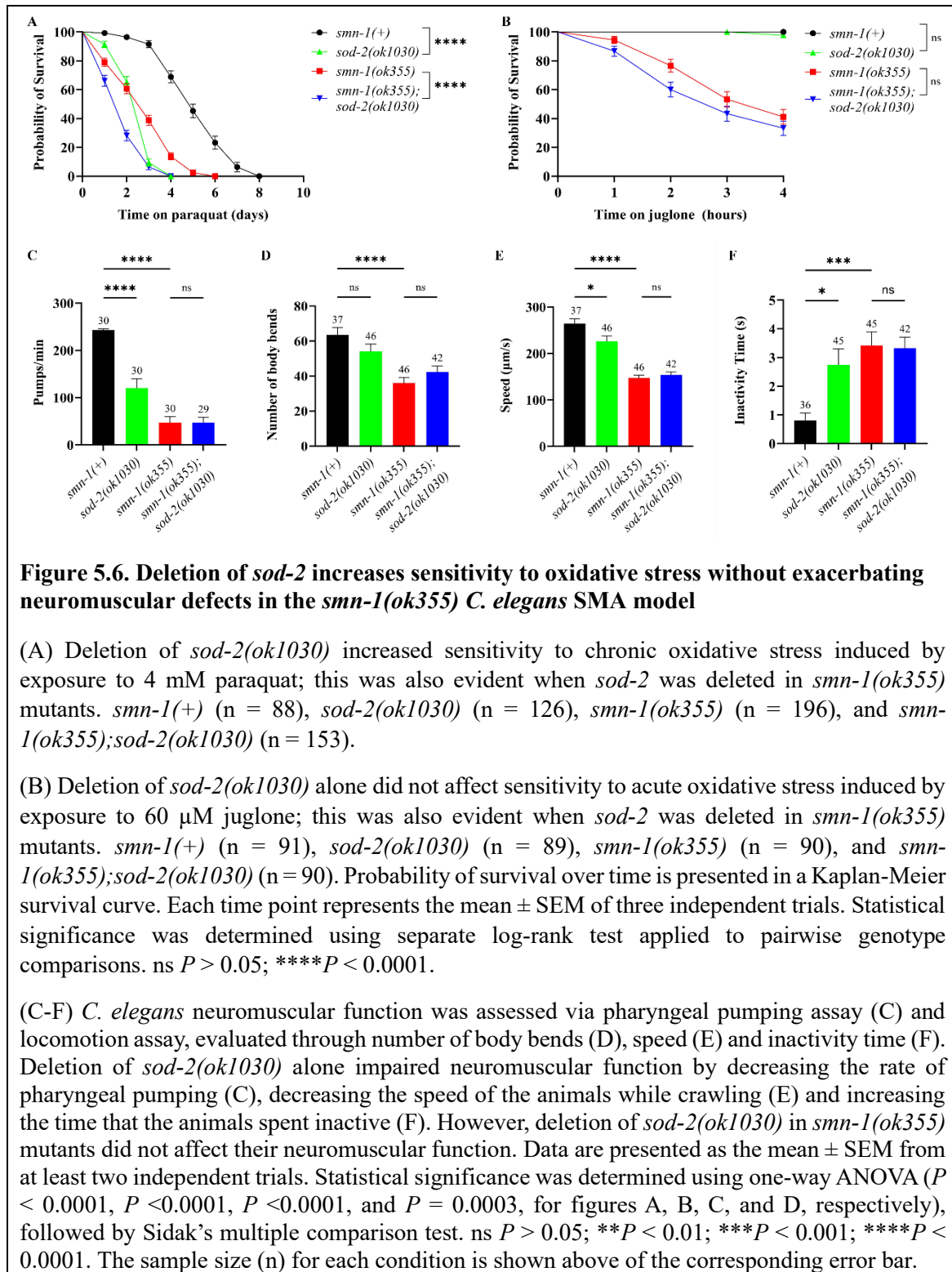
5.2.2.2. Superoxide dismutase 2

To elucidate the impact of SOD-2 depletion in the oxidative stress response of *C. elegans*, *smn-1(+)*, *sod-2(ok1030)*, *smn-1(ok355)*, and *smn-1(ok355);sod-2(ok1030)*, animals were assessed under chronic (4 mM paraquat) and acute (60 μ M juglone) oxidative stress conditions.

Our analysis indicated that *sod-2(ok1030)* animals exhibited increased sensitivity to chronic oxidative stress conditions relative to *smn-1(+)* controls (**Figure 5.6A**; $P < 0.0001$). Similarly, *smn-1(ok355);sod-2(ok1030)* double mutants demonstrated increased sensitivity to chronic oxidative stress exposure in comparison to *smn-1(ok355)* animals alone (**Figure 5.6A**; $P < 0.0001$). In contrast, the sensitivity of *sod-2(ok1030)* animals to acute oxidative conditions did not differ from that of *smn-1(+)* animals (**Figure 5.6B**; $P = 0.1493$). Likewise, *smn-1(ok355);sod-2(ok1030)* double mutants exhibited the same sensitivity to acute oxidative stress exposure as *smn-1(ok355)* animals (**Figure 5.6B**; $P = 0.1027$). Combined, these findings highlight the significant role of SOD-2 in conferring protection against chronic oxidative stress conditions, while its role in acute oxidative stress protection appears less relevant at the concentrations tested in this study.

Next, we investigated whether SOD-2 depletion modulate *C. elegans* neuromuscular behaviours using the pharyngeal pumping and locomotion assays. Our findings demonstrated that the pharyngeal pumping rates of *sod-2(ok1030)* animals were significantly reduced in comparison to *smn-1(+)* animals (**Figure 5.6C**; $P < 0.0001$). In contrast, the pharyngeal pumping rate of *smn-1(ok355);sod-2(ok1030)* double mutants was not statistically significantly different from *smn-1(ok355)* animals (**Figure 5.6C**; $P > 0.9999$). Building upon those findings, we further evaluated the influence of SOD-2 depletion in *C. elegans* neuromuscular performance and observed no statistically significant difference in the number of body bends during locomotion between *sod-2(ok1030)* and *smn-1(+)* animals (**Figure 5.6D**; $P = 0.2396$). Similarly, we found no differences in the number of body bends between *smn-1(ok355);sod-2(ok1030)* double mutants and *smn-1(ok355)* single mutant animals (**Figure 5.6D**; $P = 0.5390$). Furthermore, assessment of the animal's speed during locomotion revealed that the speed of *sod-2(ok1030)* animals was

significantly reduced in comparison to *smn-1(+)* animals (**Figure 5.6E**; $P = 0.0141$). Conversely, the speed of *smn-1(ok355);sod-2(ok1030)* double mutants remained similar to that exhibited by *smn-1(ok355)* animals (**Figure 5.6E**; $P = 0.9433$). Moreover, the time that *sod-2(ok1030)* animals remained inactive during the assay was significantly increased in comparison to *smn-1(+)* animals (**Figure 5.6F**; $P = 0.0101$). However, no significant differences were found in the time that *smn-1(ok355);sod-2(ok1030)* double mutants remained inactive in comparison to *smn-1(ok355)* animals (**Figure 5.6F**; $P = 0.9982$). Collectively, these findings highlight a role for SOD-2 in neuromuscular function; however, SOD-2 does not seem to act as a genetic modifier of *smn-1(ok355)* neuromuscular defects.



5.2.2.3. Superoxide dismutase 3

To elucidate the impact of SOD-3 depletion in the oxidative stress response of *C. elegans*, *smn-1(+)*, *sod-3(tm760)*, *smn-1(ok355)*, and *smn-1(ok355);sod-3(tm760)*, animals were assessed under chronic (4 mM paraquat) and acute (60 μ M juglone) oxidative stress conditions.

Our analysis indicated that *sod-3(tm760)* animals exhibited increased sensitivity to chronic oxidative stress conditions relative to *smn-1(+)* controls (**Figure 5.7A**; $P < 0.0001$). In contrast, *smn-1(ok355);sod-3(tm760)* double mutants exhibited the same sensitivity to chronic oxidative stress exposure as *smn-1(ok355)* animals (**Figure 5.7A**; $P = 0.5107$). In addition, previous unpublished work from our group has shown that the sensitivity of *sod-3(tm760)* animals to acute oxidative conditions did not differ from that of *smn-1(+)* animals (**Supplementary Figure 7B**; $P = 0.3085$). Likewise, *smn-1(ok355);sod-3(tm760)* double mutants exhibited the same sensitivity to acute oxidative stress exposure as *smn-1(ok355)* animals (**Supplementary Figure 7B**; $P = 0.1569$). Despite SOD-3 having a role in chronic oxidative stress, its absence did not modify *smn-1(ok355)* oxidative stress sensitivity.

Next, we investigated whether SOD-3 depletion modulated *C. elegans* neuromuscular behaviours using the pharyngeal pumping and locomotion assays. Previous unpublished work from our group demonstrated that the pharyngeal pumping rate of *sod-3(tm760)* animals did not significantly differ from that of *smn-1(+)* animals (**Supplementary Figure 8A**; $P = 0.2913$). Likewise, there was no statistically significant difference in the pharyngeal pumping rate of *smn-1(ok355);sod-3(tm760)* double mutants and *smn-1(ok355)* animals (**Supplementary Figure 8A**; $P = 0.9914$). Building upon those findings, we further evaluated the influence of SOD-3 depletion in *C. elegans* neuromuscular performance and observed no statistically significant difference in the number of body bends during locomotion in *sod-3(tm760)* versus *smn-1(+)* animals (**Figure 5.7B**; $P = 0.8342$). Similarly, we found no differences in the number of body bends between *smn-1(ok355);sod-3(tm760)* double mutants and *smn-1(ok355)* animals (**Figure 5.7B**; $P = 0.8045$). Furthermore, assessment of the animals' speed during locomotion revealed no significant differences between *sod-3(tm760)* and *smn-1(+)* animals (**Figure 5.7C**; $P = 0.9997$). Likewise,

the speed of *smn-1(ok355);sod-3(tm760)* double mutants remained similar to that exhibited by *smn-1(ok355)* animals (**Figure 5.7C**; $P = 0.8868$). Moreover, the time that the animals spent inactive during the assay was similar for both *sod-3(tm760)* and *smn-1(+)* animals (**Figure 5.7D**; $P = 0.8876$). Similarly, there was no difference in the time that *smn-1(ok355);sod-3(tm760)* double mutants and *smn-1(ok355)* animals remained inactive (**Figure 5.7D**; $P = 0.3351$). Collectively, these findings suggest that SOD-3 depletion does not significantly modulate *C. elegans* neuromuscular function.

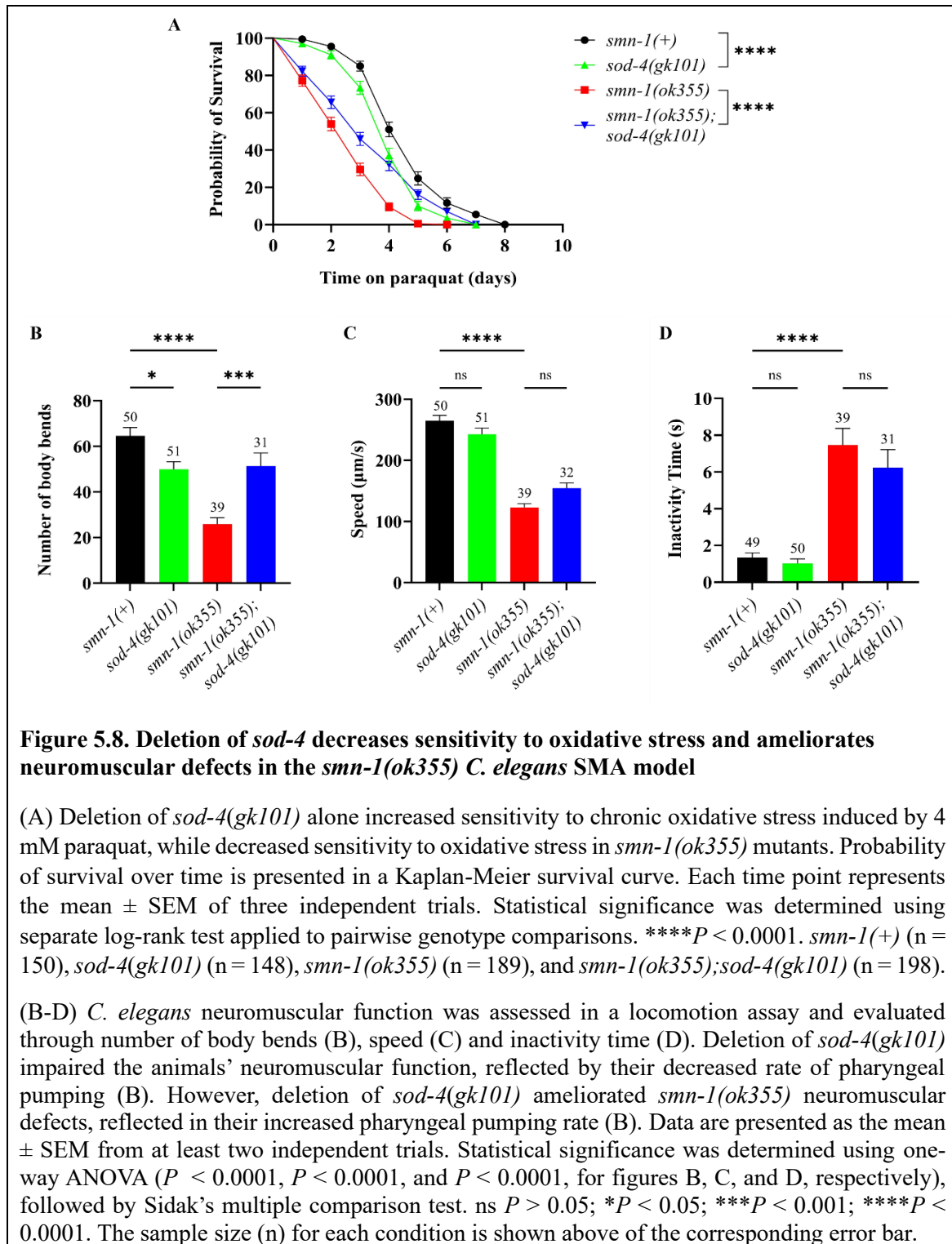
5.2.2.4. *Superoxide dismutase 4*

To elucidate the impact of SOD-4 depletion in the oxidative stress response of *C. elegans*, *smn-1(+)*, *sod-4(gk101)*, *smn-1(ok355)*, and *smn-1(ok355);sod-4(gk101)*, animals were assessed under chronic (4 mM paraquat) and acute (60 μ M juglone) oxidative stress conditions.

Our analysis indicated that *sod-4(gk101)* animals exhibited increased sensitivity to chronic oxidative stress conditions relative to *smn-1(+)* controls (**Figure 5.8A**; $P = 0.0004$). Interestingly, *smn-1(ok355);sod-4(gk101)* double mutants demonstrated decreased sensitivity (i.e. increased tolerance) to chronic oxidative stress exposure in comparison to *smn-1(ok355)* animals (**Figure 5.8A**; $P < 0.0001$). In contrast, previous unpublished work from our group has shown that the sensitivity of *sod-4(gk101)* animals to acute oxidative conditions did not differ from that of *smn-1(+)* animals at low juglone concentration (**Supplementary Figure 7C**; $P = 0.3297$). Notably, *smn-1(ok355);sod-4(gk101)* double mutants exhibited decreased sensitivity (i.e. increased tolerance) to acute oxidative stress exposure in comparison to *smn-1(ok355)* animals (**Supplementary Figure 7C**; $P < 0.0001$). Combined, these findings highlight that although SOD-4 is required for protection against chronic oxidative stress, its absence in *smn-1(ok355)* animals unexpectedly conferred resistance to oxidative stress insults.

Next, we investigated whether SOD-4 depletion can modulate *C. elegans* neuromuscular behaviours using the pharyngeal pumping and locomotion assays. Previous unpublished work from our group demonstrated that the pharyngeal pumping rate of *sod-4(gk101)* animals did not significantly differ from that of *smn-1(+)* animals (**Supplementary Figure 8C**; $P = 0.2374$). In contrast, *smn-1(ok355);sod-4(gk101)* double mutants exhibited significantly increased pharyngeal pumping rates in comparison to *smn-1(ok355)* animals (**Supplementary Figure 8CA**; $P = 0.0003$). Building upon those findings, we further evaluated the influence of SOD-4 depletion in *C. elegans* neuromuscular performance and observed that the number of body bends during locomotion was significantly reduced in *sod-4(gk101)* animals in comparison to *smn-1(+)* control animals (**Figure 5.8B**; $P = 0.0115$). In contrast, *smn-1(ok355);sod-4(gk101)* double mutants exhibited increased number of body bends in comparison to *smn-1(ok355)* animals (**Figure 5.8B**;

$P = 0.0001$). Furthermore, assessment of speed during locomotion revealed no significant differences between *sod-4(gk101)* and *smn-1(+)* animals (**Figure 5.8C**; $P = 0.1616$). Likewise, the speed of *smn-1(ok355);sod-4(gk101)* remained similar to that exhibited by *smn-1(ok355)* animals (**Figure 5.8C**; $P = 0.0753$). Moreover, the time that the animals spent inactive during the assay was similar for both *sod-4(gk101)* and *smn-1(+)* animals (**Figure 5.8D**; $P = 0.9652$). Similarly, we found no differences in the time that *smn-1(ok355);sod-4(gk101)* and *smn-1(ok355)* animals remained inactive (**Figure 5.8D**; $P < 0.0001$). Collectively, these findings suggest that depletion of SOD-4 could be acting as a protective genetic modifier of *smn-1(ok355)* defects since deletion of *sod-4* decreased sensitivity to oxidative stress and ameliorated neuromuscular defects in the *smn-1(ok355)* *C. elegans* SMA model.



5.2.2.5. *Superoxide dismutase 5*

To elucidate the impact of SOD-5 depletion in the oxidative stress response of *C. elegans*, *smn-1(+)*, *sod-5(tm1146)*, *smn-1(ok355)*, and *smn-1(ok355);sod-5(tm1146)*, animals were assessed under chronic (4 mM paraquat) and acute (60 μ M juglone) oxidative stress conditions.

Our analysis indicated that the sensitivity of *sod-5(tm1146)* animals to chronic oxidative stress conditions did not differ from that of *smn-1(+)* animals (**Figure 5.9A**; $P = 0.8583$). Interestingly, *smn-1(ok355);sod-5(tm1146)* double mutants demonstrated decreased sensitivity (i.e. increased tolerance) to chronic oxidative stress exposure in comparison to *smn-1(ok355)* animals (**Figure 5.9A**; $P < 0.0001$). Likewise, previous unpublished work from our group has shown that the sensitivity of *sod-5(tm1146)* animals to acute oxidative stress conditions did not differ from that of *smn-1(+)* animals (**Supplementary Figure 7D**; $P > 0.9999$). Notably, *smn-1(ok355);sod-5(tm1146)* double mutants exhibited decreased sensitivity (i.e. increased tolerance) to acute oxidative stress exposure in comparison to *smn-1(ok355)* animals (**Supplementary Figure 7D**; $P < 0.0001$). Combined, these findings highlight the differential impact of SOD-5 in *smn-1(+)* animals and *smn-1(ok355)*. While it is not required for oxidative stress protection in *smn-1(+)* animals, its absence in *smn-1(ok355)* animals conferred protection against oxidative stress insults.

Next, we investigated whether SOD-5 depletion modulated *C. elegans* neuromuscular behaviours using the pharyngeal pumping and locomotion assays. Previous unpublished work from our group demonstrated that the pharyngeal pumping rate of *sod-5(tm1146)* animals did not significantly differ from that of *smn-1(+)* animals (**Supplementary Figure 8D**; $P = 0.6155$). Likewise, there was no statistically significant difference in the pharyngeal pumping rate of *smn-1(ok355);sod-5(tm1146)* double mutants and *smn-1(ok355)* animals (**Supplementary Figure 8D**; $P = 0.0838$). Building upon those findings, we further evaluated the influence of SOD-5 depletion in *C. elegans* neuromuscular performance and observed that the number of body bends during locomotion was significantly increased in *sod-5(tm1146)* animals in comparison to *smn-1(+)* animals (**Figure 5.9B**; $P = 0.0060$). In contrast, we found no differences in the number of body bends between *smn-1(ok355);sod-5(tm1146)* double mutants and *smn-1(ok355)* animals (**Figure 5.9B**; $P =$

0.1605). Furthermore, assessment of the speed during locomotion revealed that the speed of *sod-5(tm1146)* animals was significantly increased in comparison to that of *smn-1(+)* animals (**Figure 5.9C**; $P = 0.0188$). Conversely, the speed of *smn-1(ok355);sod-5(tm1146)* double mutants remained similar to that exhibited by *smn-1(ok355)* animals (**Figure 5.9C**; $P = 0.0525$). Moreover, the time that the animals spent inactive during the assay was similar for both *sod-5(tm1146)* and *smn-1(+)* animals (**Figure 5.9D**; $P = 0.9545$). Notably, the time that *smn-1(ok355);sod-5(tm1146)* animals remained inactive during the assay was significantly reduced in comparison to *smn-1(ok355)* animals (**Figure 5.9D**; $P = 0.0325$). Collectively, these findings suggest that deletion of *sod-5* decreased sensitivity to oxidative stress and ameliorated neuromuscular defects in the *smn-1(ok355)* *C. elegans* SMA model.

Altogether, these findings highlight the distinct contributions of each SOD isoform to oxidative stress sensitivity and neuromuscular function in SMA, as summarized in **Table 5.3**, whose significance is discussed in the following section.

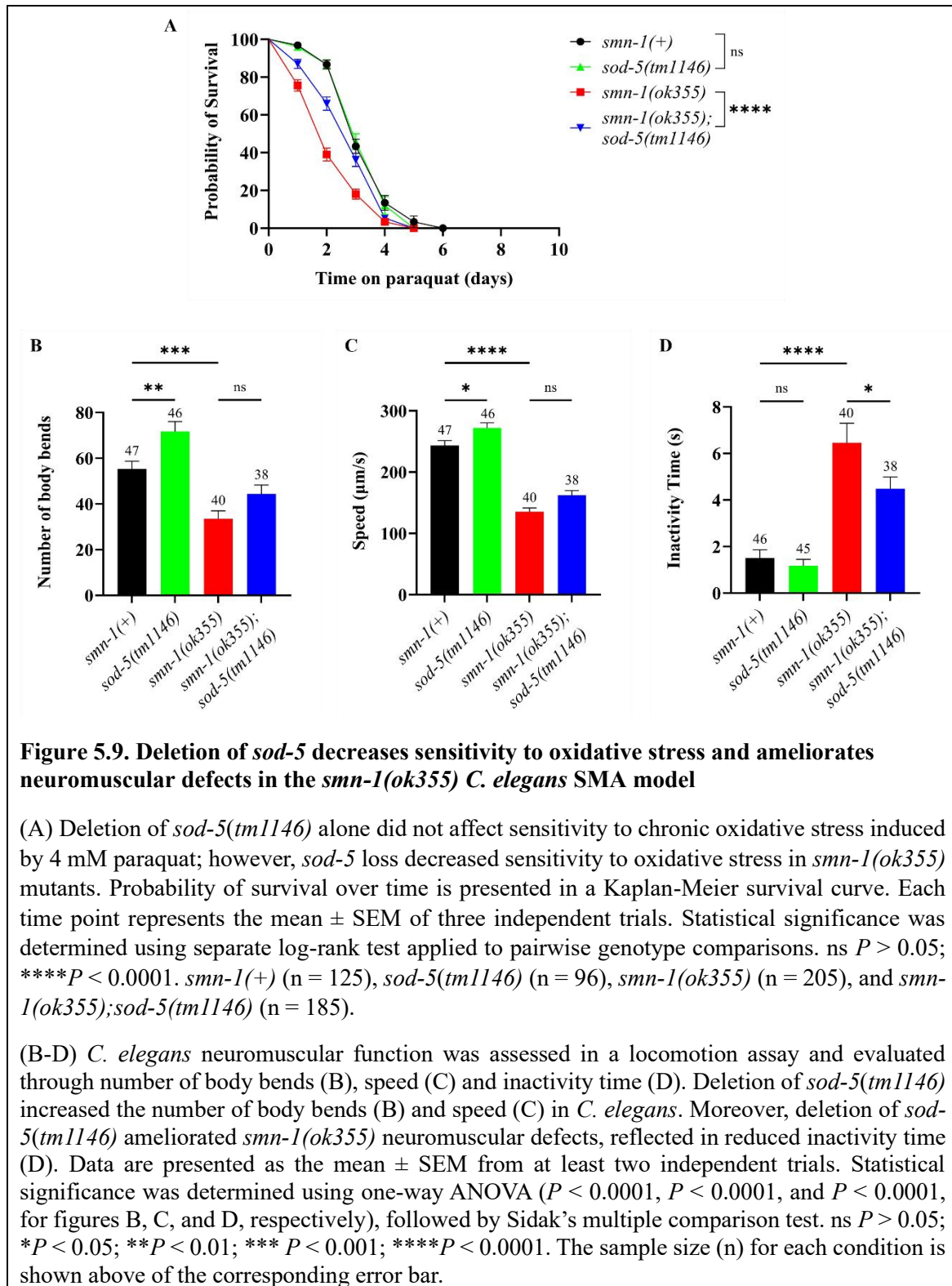


Table 5.3. Summary of phenotypic outcomes observed in *C. elegans* single *sod* mutants and *smn-1(ok355);sod* double mutants across oxidative stress and neuromuscular function assays.

| | Paraquat | Juglone | Pumping | Body Bends | Speed | Inactivity Time |
|---|---------------|---------------|-------------|--------------|---------|-----------------|
| <i>sod-1(tm776)</i> vs. <i>smn-1(+)</i> | ↑ Sensitivity | ns | ns | ns | ns | ns |
| <i>smn-1(ok355);sod-1(tm776)</i> vs. <i>smn-1(ok355)</i> | ↑ Sensitivity | ns | ns | ns | ns | ↑ Inactive time |
| <i>sod-2(ok1030)</i> vs. <i>smn-1(+)</i> | ↑ Sensitivity | ns | ↓ Pumps/min | ns | ↓ Speed | ↑ Inactive time |
| <i>smn-1(ok355);sod-2(ok1030)</i> vs. <i>smn-1(ok355)</i> | ↑ Sensitivity | ns | ns | ns | ns | ns |
| <i>sod-3(tm760)</i> vs. <i>smn-1(+)</i> | ↑ Sensitivity | ns | ns | ns | ns | ns |
| <i>smn-1(ok355);sod-3(tm760)</i> vs. <i>smn-1(ok355)</i> | ns | ns | ns | ns | ns | ns |
| <i>sod-4(gk101)</i> vs. <i>smn-1(+)</i> | ↑ Sensitivity | ns | ns | ↓ Body Bends | ns | ns |
| <i>smn-1(ok355);sod-4(gk101)</i> vs. <i>smn-1(ok355)</i> | ↓ Sensitivity | ↓ Sensitivity | ↑ Pumps/min | ↑ Body bends | ns | ns |
| <i>sod-5(tm1146)</i> vs. <i>smn-1(+)</i> | ns | ns | ns | ↑ Body Bends | ↑ Speed | ns |
| <i>smn-1(ok355);sod-5(tm1146)</i> vs. <i>smn-1(ok355)</i> | ↓ Sensitivity | ↓ Sensitivity | ns | ns | ns | ↓ Inactive time |

5.3. Discussion

Accumulating evidence indicates that SMA patients exhibit elevated ROS levels (**Table 1.4. Evidence of elevated reactive oxygen species in spinal muscular atrophy**). Indeed, we have observed elevated ROS levels in the *smn-1(ok355)* *C. elegans* SMA model, reinforcing the notion that increased oxidative stress is consistently present across different SMA models. Furthermore, these animals display increased sensitivity specifically to oxidative stress, but not to other stressors, suggesting a particular vulnerability to oxidative damage (Chapter III). Although it is known that oxidative stress can trigger mitochondrial abnormalities, protein misfolding, synapse dysfunction, and other degenerative processes in neurons (Barnham et al., 2004; Chen et al., 2012; Houldsworth, 2024; Singh et al., 2019) its precise impact on SMA remains poorly understood. In this line, our own findings revealed that modulating ROS levels alone did not always improve neuromuscular function in *C. elegans* SMA (Chapter IV). Thus, understanding how managing ROS levels interacts with SMA phenotypes could provide a deeper understanding into the molecular mechanisms that drive motor neuron loss.

5.3.1. Identification of central oxidative stress related genes differentially expressed

In this context, a central challenge emerges: which oxidative-stress-related genes stand out as crucial regulators of SMA pathology? By identifying oxidative stress-related genes differentially expressed in SMA, we aimed to gain novel insights into the mechanisms driving the disease, ultimately contributing to the identification of new therapeutic targets to mitigate the effects of oxidative stress in SMA.

Multiple studies have identified dysregulated genes associated with mitochondrial bioenergetics, oxidative stress modulation, and antioxidant defence in SMA models (Shababi et al., 2012; Miller et al., 2016; Boyd et al., 2017; Thelen, Wirth and Kye, 2020; El Khoury et al., 2023; Barbo et al., 2024). However, few have investigated the functional significance of these genes in relation to

specific SMA phenotypes. For example, Miller et al., (2016) and Thelen et al., (2020) reported significant alterations in cellular processes related to mitochondrial function, but did not further examine individual targets from the pool of genes identified. Notably, Boyd et al., (2017) reported similar mitochondrial dysregulation and focused on PGK1, a gene linked to ATP production downregulated in SMA. Reducing PGK1 expression in wild-type zebrafish partially replicated the SMA phenotype, while its overexpression ameliorated motor neuron axon phenotypes in cell culture, highlighting the critical role of maintaining mitochondrial integrity in SMA.

Other studies have concentrated on specific modulators of oxidative stress. El Khoury et al., (2023) investigated NADPH oxidases NOX2 and NOX4, while Shababi et al., (2012) assessed differential expression of Nox2, Rac1 and p47-phox. Among these, only NOX4 (upregulated in SMA) was further investigated and emerged as a promising candidate for therapeutic intervention, as researchers observed that NOX4 inactivation prevented motor neuron loss and improved the motor behaviour in severe SMA mice. In a broader examination, Köstel et al., (2012) evaluated the expression of 84 antioxidant-response genes in fibroblasts from SMA patients and healthy controls, identifying five genes whose expression was significantly altered (SEPP1, AOX1, TTN, DHCR24 were upregulated, while COX2 was downregulated), although the study did not examine the effect of those genes in the SMA phenotype. More recently, Barbo and colleagues explored genetic polymorphisms across seven oxidative-stress-related genes and found that variants in SOD2, CAT, NFE2L2, GPX1, and HMOX1 correlated with clinical severity and disease onset (Barbo et al., 2024). These findings further underscore the potential role of specific elements of the oxidative stress-response as modifier of SMA progression.

Nevertheless, the majority of these studies have focused on a limited subset of predetermined genes, potentially overlooking significant yet underrecognized regulators of the oxidative stress response. Recent advancements in the field of bioinformatics facilitate a more comprehensive and unbiased approach to identifying “hub” genes within complex disease networks (Gu et al., 2023; Zhang & Kiryu, 2023; Zhu & Jiang, 2023), enabling the discovery of novel oxidative-stress-associated genes in SMA that may not have been previously prioritised.

In accordance with these methodologies, our study advances previous research by identifying, from an extensive set of oxidative stress-related genes, those that may play a critical role in SMA pathogenesis. This integrative bioinformatics approach identified 13 key hub genes that encompass the four main antioxidant families, superoxide dismutase (SOD), catalase (CAT), glutathione peroxidase (GPx), and peroxiredoxin (PRDx), as well as enzymes of the glutathione-independent glyoxalase system (DJR) and methionine sulfoxide reductase (MSRA), highlighting the complex nature of oxidative stress regulation in SMA. From these, we prioritised the *C. elegans* *sod* family to further evaluate their functional significance experimentally, due to its central presence in both PPI and TF networks, its non-redundant role within cells and their different compartmentalisation within cells, which will allow us to understand how fine modulation of ROS interferes with SMA phenotypes. Among the 13 hub genes yielded by our analysis, three *sod* genes were identified: cytoplasmic *sod-1*, mitochondrial *sod-2* and extracellular *sod-4*. We also included the inducible mitochondrial *sod-3* and cytoplasmic *sod-5* in our analysis for a more comprehensive understanding of how subcellular location and regulatory signalling influence oxidative stress management and regulation in SMA.

5.3.2. SOD isoforms can modulate oxidative stress sensitivity in the *Caenorhabditis elegans* spinal muscular atrophy model

We first assessed the contributions of each of the *sod* genes to ROS management in *C. elegans*. Consistent with previous evidence, our findings demonstrated that individual deletion of *sod-1*, *sod-2* and *sod-3* markedly increased the sensitivity of *C. elegans* to chronic oxidative stress induced by paraquat. In contrast, the sensitivity of *sod-5* mutants remained similar to that of *smn-1(+)* controls (Gems & Doonan, 2008; Van Raamsdonk & Hekimi, 2009; Yanase et al., 2009). Interestingly, contrary to some earlier reports, our data suggest that *sod-4* mutants exhibited greater sensitivity to paraquat-induced oxidative stress than wildtype *C. elegans* (Gems & Doonan, 2008; Van Raamsdonk & Hekimi, 2009). Furthermore, while previous literature has indicated that *sod-1* and *sod-2* mutants display increased sensitivity to acute oxidative stress

conditions induced by juglone (Van Raamsdonk & Hekimi, 2009), our analysis did not reveal differences in juglone sensitivity among any of the *sod* mutants. These subtle yet significant discrepancies between our study and previous ones likely originate from differences in experimental setups. For instance, while Van Raamsdonk & Hekimi (2009) assessed paraquat sensitivity on day-7 *C. elegans*, we utilised day-3 animals. Additionally, the same research group evaluated acute sensitivity to oxidative stress using 240 μ M juglone, whereas we employed a much lower concentration (60 μ M juglone), allowing us to potentially detect differential phenotypes without causing uniformly lethal effects. Notably, differences in lifespan and stress sensitivity of *C. elegans* *sod* mutants, as reported by various research groups, are not uncommon. For instance, we observed inconsistencies regarding whether *sod-1* and *sod-2* mutants decrease or increase *C. elegans* lifespan, or whether *sod-3* mutants present increased sensitivity to paraquat-induced oxidative stress or not (Gems & Doonan, 2008; Honda et al., 2008; Suthammarak et al., 2013; Van Raamsdonk & Hekimi, 2009; Yanase et al., 2009; Yang & Hekimi, 2010). These disagreements provide a theoretical framework to understand the differences in oxidative stress sensitivity found between our work and others. Additionally, they underscore the necessity for careful consideration of even subtle differences in genetic background and experimental conditions when comparing our results, as these factors can significantly influence the phenotypes under study.

Deletion of *sod* genes in the *smn-1(ok355)* *C. elegans* SMA model will deepen our understanding on how each of the *sod* genes contribute to ROS regulation in SMA and ultimately, how they influence the disease phenotype. Our study revealed distinct impacts of individual *sod* gene deletions on oxidative stress sensitivity in the *smn-1(ok355)* *C. elegans* SMA model. Specifically, deletion of *sod-1* and *sod-2* exacerbated sensitivity to chronic oxidative stress induced by paraquat but did not affect acute stress sensitivity to juglone, highlighting the critical role for cytoplasmic SOD-1 and mitochondrial SOD-2 during prolonged stress conditions. Conversely, *sod-3* deletion did not alter the sensitivity of SMA nematodes to either chronic or acute oxidative insults, consistent with its minor, inducible role in mitochondrial ROS handling. Interestingly, deletion of

extracellular *sod-4* and cytoplasmic *sod-5* improved the survival of *smn-1(ok355)* animals under both acute and chronic oxidative stress conditions, suggesting that subtle adjustments in extracellular or cytoplasmic ROS equilibrium may correct deleterious oxidative stress response signalling pathways in the context of SMA.

Collectively, these observations underscore the unique contributions of each SOD isoform to oxidative stress sensitivity in SMA, shaped by their distinct subcellular localisations and specific roles within ROS signalling networks.

5.3.3. SOD isoforms can modulate neuromuscular function in the *Caenorhabditis elegans* spinal muscular atrophy model

Some studies have demonstrated that oxidative stress have potential detrimental effects on *C. elegans* motor function. For example, *C. elegans* exposed to the superoxide generator paraquat exhibited reduced pumping rates, speed and overall motility associated with neurodegeneration (Ji et al., 2022; Taylor et al., 2021; Wu et al., 2018). However, there is not always a direct correlation between the levels of oxidative damage and neuromuscular behaviour in *C. elegans*. For instance, Taylor et al., (2021) evaluated the motility of different mitochondrial mutants and found no association between their lifespan or oxidative stress profiles and their locomotor abilities. Instead, the fine-tuning of ROS levels and compartment-specific redox signalling appears more critical than ROS levels alone. This complexity further highlights the importance of the type, localisation, and intensity of ROS exposure in shaping behavioural phenotypes.

While previous studies have investigated the effects of *sod* knockouts on *C. elegans* lifespan and stress sensitivity, few have explored how SOD activity modulates neuromuscular phenotypes. This gap in the literature presents a challenge for directly comparing our findings with previous work. To facilitate interpretation, we will discuss the impact of each *sod* gene deletion grouped according to the subcellular compartment in which the corresponding isoform is localised.

5.3.3.1. Cytoplasmic *sods*

The current literature indicates that, under normal conditions, *sod-1* mutants do not experience motor neuron loss and exhibit enhanced cholinergic signalling, although their locomotion rates remain unchanged (Baskoylu et al., 2018b). In agreement with those findings, our results demonstrated that the knockout of cytoplasmic *sod-1* did not modify *C. elegans* neuromuscular function under normal conditions. Notably, when *sod-1* is knocked out in the *smn-1(ok355)* background, we observed no change in the pharyngeal pumping rates but diminished locomotion activity. Interestingly, our findings differed regarding the cytoplasmic enzyme SOD-5. Deletion of *sod-5* boosted *C. elegans* locomotor activity. Similarly, deletion of *sod-5* in *smn-1(ok355)* animals led to mild yet significant improvements in motor function.

Interestingly, recent studies have indicated that animals lacking SOD-1 and SOD-5 enzymes display enhanced locomotion behaviour when exposed to conditions that increase their endogenous ROS levels (i.e. paraquat exposure or pathogen infection) (Baskoylu et al., 2018b; Horspool & Chang, 2017). This observation could explain the amelioration of neuromuscular defects observed in *smn-1(ok355);sod-5(tm1146)* animals, but is not consistent with the absence of neuromuscular improvements in *smn-1(ok355);sod-1(tm776)* mutants. However, the differential impact of *sod-1* and *sod-5* deletions in the neuromuscular phenotype of *smn-1(ok355)* animals could be attributed to the differential expression of the SOD-1 and SOD-5 enzymes in *C. elegans*. Although both enzymes are found in the cytoplasm, SOD-1 is ubiquitously expressed and is responsible for the majority of SOD activity within cells, whereas SOD-5 presence is limited to a specific subset of neurons in the pharynx and represented only 0.5% of the total SOD mRNA (Gems and Doonan, 2008). While the experimental conditions utilised by Baskoylu et al., (2018) and Horspool & Chang, (2017), which reported enhanced locomotion behaviour in *sod-1* and *sod-5* mutants when exposed to increased ROS levels, are known for their ability to induce oxidative stress, the specific cellular conditions of *smn-1(ok355)* animals are very likely to be different from those induced in the referenced studies. It is possible that in *smn-1(ok355)* animals, the elimination of SOD-1, one of the primary enzymes responsible for global ROS detoxification in *C. elegans*, may push *smn-1(ok355);sod-1(tm776)* animals beyond a threshold where ROS

induced damage would overcome ROS signalling benefits. The overcoming of this threshold would be particularly evident in behaviours that require significant effort and the coordinated activity of large groups of muscles and neurons, such as crawling behaviour, just as it was observed in *smn-1(ok355);sod-1(tm776)* animals.

Overall, the results presented here suggest that subtle elevations in cytoplasmic superoxide anion within specific neurons may enhance *smn-1(ok355)* locomotor activity. Nonetheless, the underlying mechanisms responsible for this enhanced behaviour remain unidentified.

5.3.3.2. Mitochondrial *sods*

Currently, there is limited evidence of the neuromuscular phenotype of mitochondrial *sod* mutants in *C. elegans*. However, Taylor et al., (2021) reported that the speed of *sod-2* and *sod-3* mutants was not different from that of control animals, suggesting no visible neuromuscular defects. Interestingly, our data suggested that deletion of mitochondrial *sod-2* did not compromise *C. elegans* neuromuscular function. By contrast, no differences in the neuromuscular phenotype of *smn-1(ok355)* animals were observed in our analysis after *sod-3* deletion. Studies using *C. elegans* models have demonstrated that muscles and neurons are highly energy-demanding tissues that rely heavily on mitochondrial ATP production. These studies have also established a strong association between mitochondrial integrity and proper neuronal and muscular function (Scholtes et al., 2018; Byrne et al., 2019; Guha et al., 2022). Thus, despite the limited but significant evidence provided by previous literature, the fact that we found neuromuscular defects in *sod-2* knockout animals did not appear surprising to us.

The differential phenotypes observed in *sod-2* and *sod-3* deletion mutants can be explained by differences in their regulatory profiles. While *sod-2* represents between 18% and 34% of the total *sod* mRNA, *sod-3* accounts for only 1% of the total *sod* mRNA under normal conditions (Gems and Doonan, 2008; Dues et al., 2017). That means that under normal conditions, overall SOD activity does not rely heavily on SOD-3, which could explain the lack of observed effects on *C. elegans* neuromuscular phenotype. For example, while studies have found that *sod-2* deletion

causes developmental delays and reproductive defects, *sod-3* mutants do not exhibit such defects (Gems and Doonan, 2008).

Interestingly, in the *smn-1(ok355)* background, neither *sod-2* nor *sod-3* deletion modify *smn-1(ok355)* neuromuscular performance. Assuming that the effects of *sod-2* and *sod-3* deletion primarily impact mitochondrial function, the lack of observable influence of these genes on the neuromuscular behaviour of *smn-1(ok355)* animals could be explained by the fact that SMN-1 depletion already compromises mitochondrial homeostasis, potentially masking additional effects. For instance, our own bioinformatic analysis showed profound dysregulation of mitochondrial genes (Chapter I). Furthermore, *smn-1(ok355)* animals exhibited abnormal mitochondrial morphology and mislocalisation within muscle cells, which has been associated with neuromuscular defects by previous studies (Schultz et al., 2017).

Overall, our findings highlight the effect of reducing mitochondrial ROS detoxification in *C. elegans*. Although deletion of *sod-2* or *sod-3* did not lead to additional defects in pharyngeal pumping or locomotion, this does not necessarily indicate that muscle or neuronal mitochondria are unaffected. On the contrary, it may suggest that mitochondrial dysfunction in *smn-1(ok355)* animals is already saturated, leaving little room for further impairment by the loss of these mitochondrial SODs. The question here therefore remains if increasing superoxide detoxification in *smn-1(ok355)* would lead to improvements.

5.3.3.3. Extracellular *sod*

Previous reports indicated that, under normal conditions, depletion of the extracellular enzyme SOD-4 alone did not significantly alter the lifespan, development, or reproductive capacity of *C. elegans* (Gems and Doonan, 2008). However, the specific impact of *sod-4* deletion on neuromuscular phenotypes has not yet been explored. Our results demonstrated that animals lacking *sod-4* exhibited subtle neuromuscular defects. Interestingly, deleting *sod-4* in *smn-1(ok355)* mutants resulted in improved pharyngeal pumping rates and locomotion performance.

Beyond their classical antioxidant roles, superoxide dismutases can modulate cellular signalling by balancing the production of superoxide ($O_2^{\bullet-}$) and hydrogen peroxide (H_2O_2). Under normal conditions, SOD enzymes reduce $O_2^{\bullet-}$ levels, concomitantly increasing H_2O_2 ($O_2^{\bullet-} \rightarrow H_2O_2$). Elevated levels of H_2O_2 are known to inhibit protein tyrosine phosphatases (PTPases) (Tanner et al., 2011; Zhou et al., 2011), enzymes that negatively regulate protein-tyrosine kinase activity. Thus, inhibition of PTPases by H_2O_2 indirectly promotes the phosphorylation and activation of tyrosine kinases, such as those involved in the IIS signalling pathway. For instance, studies *in vitro* demonstrated that H_2O_2 exposure significantly activate downstream elements of the insulin signalling (IIS) pathway, such as Akt, by enhancing the phosphorylation of PI3K in muscle cells (Kim et al., 2006). Similarly, in *C. elegans* treatment with H_2O_2 increases PIP3 levels and promotes the cytosolic retention of DAF-16, in a process that is dependent of AGE-1, the PI3K homologue in *C. elegans* (Weinkove et al., 2006) (**Figure 5.10A**).

Deletion of *sod-4* is predicted to cause a reduction of local extracellular or membrane-adjacent intracellular production of H_2O_2 . A decrease in H_2O_2 levels would lead to decreased oxidative inhibition of PTPases, thereby enhancing their activity and reducing the activation of downstream targets of the IIS pathway, such as Akt. Consequently, reduced Akt phosphorylation would promote the nuclear translocation of DAF-16, thereby activating its stress-response and longevity-associated gene targets (**Figure 5.10B**). Consistent with this hypothesis, among the five *sod* genes in *C. elegans*, only the deletion of *sod-4* has been shown to extend the lifespan of long-lived *daf-2* mutants, an effect known to be dependent on DAF-16 nuclear localization (Doonan et al., 2008). Notably, a recent study evaluated the effects of *daf-2* (the *C. elegans* insulin receptor) downregulation in *smn-1(ok355)* animals (Wu et al., 2019). Introduction of the *daf-2(e1368)* mutation in *smn-1(ok355)* animals lead to a significant increase in *smn-1(ok355)* lifespan and rescued their motor performance. Notably, those effects were dependent on the presence of DAF-16.

Ultimately, our results highlight the critical importance of subcellular compartmentalisation of ROS management in SMA and suggest their therapeutic potential of selectively modulating the

activity of specific SOD isoforms. It is important to distinguish between intracellular and extracellular localisation of ROS, as well as the specific signalling roles of $O_2^{\bullet-}$ and H_2O_2 . Indeed, our findings illustrate that not all SOD isoforms uniformly protect against oxidative stress, especially in contexts involving mitochondrial dysfunction or disrupted cellular homeostasis. Hence, elevated ROS levels in SMA should not be regarded merely as indicators of a pathological state, but rather as integral components of cellular signalling.

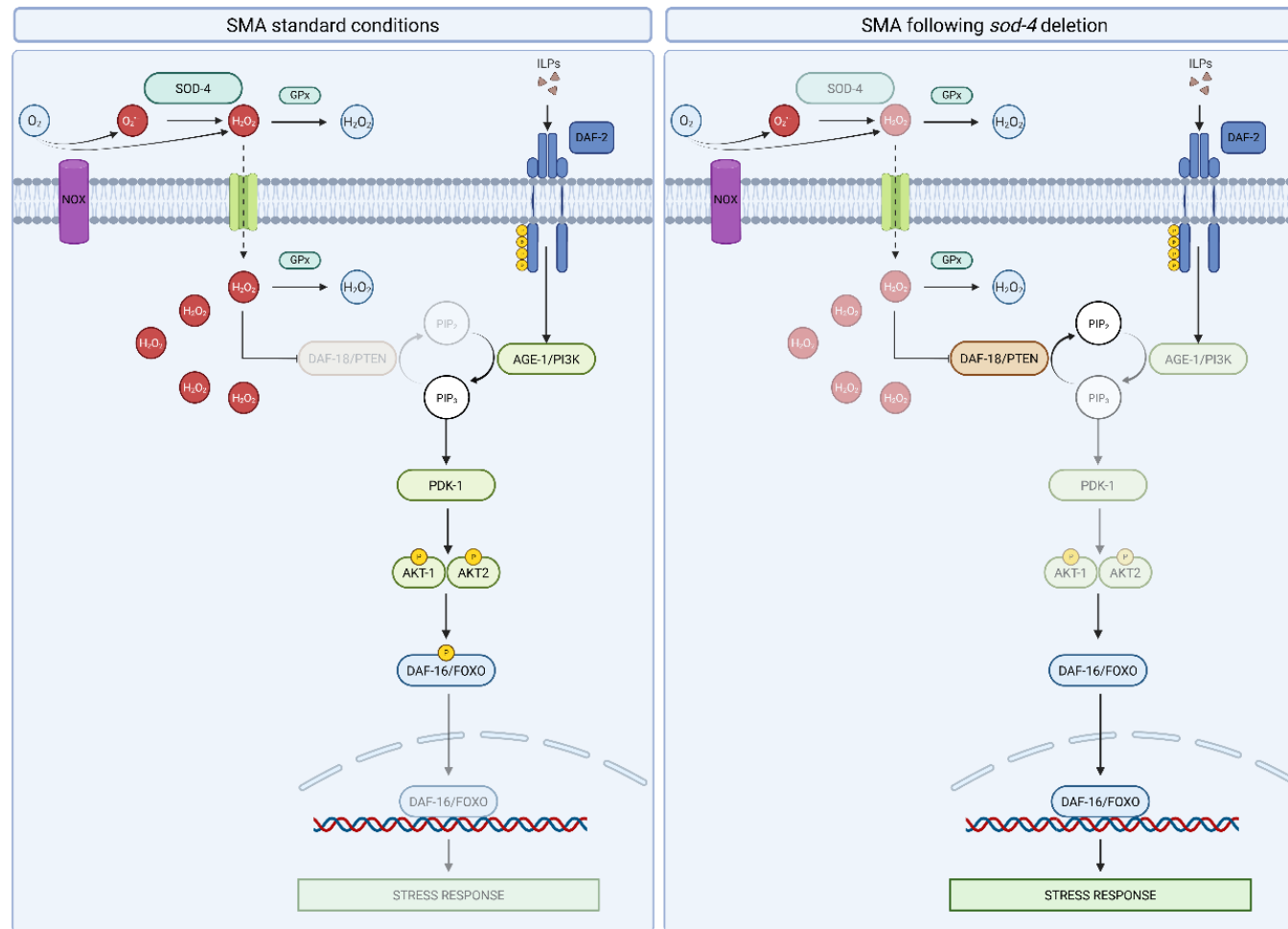


Figure 5.10. Hypothetical model illustrating how loss of *sod-4* modulates IIS signalling and enhances stress responses in the *C. elegans* SMA model

Under SMA conditions (left panel), the conversion of superoxide anion ($O_2^{\bullet-}$) into hydrogen peroxide (H_2O_2) by SOD-4 increases the presence of extracellular and membrane-adjacent H_2O_2 . H_2O_2 inhibits the protein-tyrosine phosphatase DAF-18/PTEN, which allows the accumulation of PIP_3 , resulting in the phosphorylation and activation of (AKT-1/2). Active AKT inhibits nuclear translocation of DAF-16/FOXO, suppressing the expression of genes involved in the stress response.

Following *sod-4* deletion (right panel), reduced local H_2O_2 levels result in increased DAF-18/PTEN activity. DAF-18 activation decreases PIP_3 levels, reducing Akt phosphorylation and promoting nuclear translocation of DAF-16/FOXO. Enhanced DAF-16 nuclear activity consequently increases the expression of genes associated with stress response, potentially explaining the improved neuromuscular function observed in *smn-1(ok355);sod-4(gk101)* double mutants.

Chapter VI. Discussion

6.1 Project outcomes

The presence of elevated markers of oxidative stress (i.e. mitochondrial dysfunction, elevated ROS levels and oxidative damage to proteins and lipids) has been long noted in different SMA models (**1.4 Oxidative stress in spinal muscular atrophy**). Yet, the precise molecular mechanisms by which oxidative damage contributes to neuromuscular degeneration in SMA remains relatively elusive. Recent therapeutic advances, especially gene-replacement strategies, have resulted in significant improvements in SMA patients' lives, increasing their life expectancy and improving their motor function (**1.1.5 Approved therapies**). In the context of ongoing advancements, elucidating the molecular pathways perturbed by SMN deficiency is of critical importance, as it holds the potential to identify novel therapeutic targets and inform the development of more effective intervention strategies. This project was undertaken to address how oxidative stress can be targeted or modulated for therapeutic benefit in SMA, utilising the *smn-1(ok355)* *C. elegans* SMA model.

In Chapter III, we aimed to characterise the molecular features of oxidative stress in the *smn-1(ok355)* *C. elegans* SMA model, thereby establishing its validity for investigating oxidative stress related mechanisms in *C. elegans*. Through transcriptomic analysis, we identified the downregulation of energy production pathways, particularly those involving mitochondrial components (**Figure 3.4**). Alongside these transcriptional alterations we observed an increased sensitivity to oxidative stress in *smn-1(ok355)* nematodes, despite their unexpectedly enhanced resilience to other stressors such as heat or osmotic stress (**Figure 3.6, Figure 3.7**). Finally, utilising *in vivo* fluorescence ROS detection methods, we identified a significant elevation in cytoplasmic ROS levels in *smn-1(ok355)* animals (**Figure 3.10**). Notably, the selective inability to counteract pro-oxidant challenges, while other stress response mechanisms remain relatively intact, suggest that heightened susceptibility to oxidative stress may represent a key pathological feature in spinal muscular atrophy (SMA). Collectively, the results of this chapter underscore oxidative stress as a critical feature of the SMA phenotype and provide the foundation for future research investigating the relationship between ROS management and SMA in *C. elegans*.

In Chapter IV, we investigated whether there is a direct correlation between overall ROS levels and neuromuscular function in the *smn-1(ok355)* *C. elegans* SMA model. We also explored whether oxidative stress directly regulates SMN-1 protein levels, as prior reports have suggested that redox-sensitive post-translational modifications in SMN could lead to its degradation (Wan et al., 2008). We administered five known antioxidant compounds that have been shown to have beneficial effects in other neuromuscular diseases (NAC, CUR, VITC, EGCG, MEL) (**Table 1.3**) and evaluated their effects in *smn-1(ok355)* endogenous ROS levels and neuromuscular phenotypes. Some antioxidants reduced ROS but this did not robustly translate into a functional improvement (i.e. CUR) (**Figure 4.4, Figure 4.5**) or did so only at specific doses (i.e. no positive results were found for NAC at low or high concentration, only at medium concentration) (**Figure 4.2, Figure 4.3**), while others unexpectedly increased ROS levels in *smn-1(ok355)* animals yet still led to partial improvements in neuromuscular function (i.e. EGCG and MEL) (**Figure 4.8, Figure 4.9, Figure 4.10, Figure 4.11**). Additionally, we evaluated whether the modulation of ROS in *C. elegans* SMA resulted in an elevation of SMN-1 protein levels, which could shed light into the mechanism behind the improvements in motor function of *smn-1(ok355)* animals. Surprisingly, both ROS reduction and ROS elevation were compatible with increased SMN-1 levels (**Figure 4.13, Figure 4.14**), indicating that the endogenous levels of ROS observed in *smn-1(ok355)* nematodes do not strictly dictate SMN-1 protein abundance. Furthermore, we underscored the importance of spatiotemporal regulation of SMN-1 within specific tissues (i.e., neuron *versus* muscle) as a critical factor in functional recovery, as increased SMN-1 levels did not strictly dictate motor recovery in *smn-1(ok355)* animals. Collectively, these findings underscore that neuromuscular dysfunction in SMA cannot be fully ameliorated solely through the reduction of endogenous ROS, implying that additional molecular targets modulated by these compounds may exert a more pronounced effect on motor phenotypes than ROS attenuation alone.

In Chapter V, we focused on identifying specific oxidative stress related genes that were dysregulated in *C. elegans* SMA and investigated whether they could contribute to SMA

pathophysiology. By leveraging novel bioinformatic methods, we identified a set of thirteen oxidative stress related genes that were dysregulated in *smn-1(ok355)* animals. Among those, five genes belonging to the *C. elegans* antioxidant *sod* family were selected for further investigation. By individually deleting each of the *sod* genes in the *smn-1(ok355)* background, we evaluated their ability to regulate oxidative stress sensitivity and neuromuscular function in *C. elegans* SMA. Deletion of the main cytoplasmic and mitochondrial *sod* isoforms (*sod-1* and *sod-2*, respectively) exacerbated *smn-1(ok355)* oxidative stress sensitivity (**Figure 5.5**, **Figure 5.6**). However, their impact in neuromuscular function was varied. While *sod-1* deletion led to the deterioration of *smn-1(ok355)* neuromuscular phenotype (**Figure 5.5**), deletion of mitochondrial *sod-2* did not modify *C. elegans* SMA motor function (**Figure 5.6**). Conversely, deletion of mitochondrial *sod-3* did not modify *smn-1(ok355)* oxidative stress sensitivity or motor performance on behavioural assays (**Figure 5.7**). Notably, deletion of extracellular *sod-4* and cytoplasmic *sod-5* increased *smn-1(ok355)* resilience to oxidative stress challenges and improved their motor performance in behavioural assays under normal conditions (**Figure 5.8**, **Figure 5.9**). The diverse outcomes revealed by each SOD isoform are noteworthy. Although reduction of ROS levels was not associated with amelioration of SMA neuromuscular defects (Chapter IV), oxidative stress resilience did correlate with neuromuscular improvements. Overall, this could indicate that subtle manipulation of extracellular or cytoplasmic ROS can modulate redox signalling in SMN-1 deficient animals, which could result in improved neuromuscular health.

6.2. Future directions

This section delineates three major avenues for future research. First, it considers additional methodological advancements that could strengthen the findings presented in this thesis. Second, it explores specific signalling pathways and molecular targets that may shed light into novel treatment strategies. Third, it discusses the direction of therapeutic strategies targeting oxidative

stress in SMA. Overall, this section provides suggestions on how to further validate our results and explored more focused hypotheses on the interplay between ROS regulation and SMN-1 biology, ultimately increasing the translational value of our findings.

6.2.1. Methodological considerations

The extensive dysregulation of oxidative stress-related cellular processes observed in the *C. elegans* SMA model constitute a critical foundation for this thesis, as it strongly points towards oxidative stress as a key contributing factor in the disease pathology (Chapter III). To characterise the transcriptomic profile of *smn-1(ok355)* animals, we utilised bulk RNA sequencing. This methodology involved the analysis of samples composed by hundreds of *C. elegans* animals, thereby encompassing multiple tissues and cell types. A significant advantage of this technique was its ability to identify the molecular pathways that are most relevant to SMA pathology at a global level, which aligned well with the objectives of this thesis. Nevertheless, it is important to note that SMN-1 depletion does not uniformly affect all cell types. For example, in SMA patients, motor neurons are the first cells to undergo degeneration, whereas other cell types and tissues remain largely unaffected until later stages (Burr and Reddivari, 2023). Consequently, by relying on whole-organism analyses, we may have obscured critical cell-specific gene expression changes that could be of critical importance to neuromuscular function. To overcome this limitation, future research should consider gene expression analyses at the tissue or single-cell level, which may reveal more accurate targets. Additionally, validating gene expression through qRT-PCR and protein quantification assays, particularly for the thirteen hub genes identified in Chapter V, would significantly strengthen the validity and reproducibility of our bioinformatic findings.

Another methodological advancement involves the use of genetically encoded ROS fluorescent detectors. In this thesis we have relied on small molecule fluorescence probes, which are advantageous due to their feasibility to provide insights into intracellular ROS levels across a wide range of conditions and genetic backgrounds. However, based on our findings, future research would benefit from focusing on compartment-specific measurements rather than global

ROS assessments. This targeted approach could elucidate the differential role of ROS in SMA based on specific cellular compartments and cell types. For example, although treatments with MEL and EGCG increased overall ROS levels, it remains a possibility that they induced a beneficial redistribution of ROS within specific cellular compartments that led to the improvements in neuromuscular function.

The experimental design of this thesis was developed to investigate the relationship between oxidative stress and neuromuscular function in SMA. As a result, the phenotypic changes observed in *smn-1(ok355)* animals following antioxidant treatments or individual *sod* deletions were discussed from the perspective of changes in oxidative stress. Nevertheless, future research should explore how antioxidant treatment or depletion of a particular SOD isoform affects the expression of other antioxidant genes or relevant pathways. It is plausible that some of the phenotypic outcomes observed resulted from molecular and genetic compensatory adaptations rather than the modulation of ROS levels itself. This is particularly evident in the results presented in Chapter IV, where the behavioural improvements in *C. elegans* SMA could not be directly correlated with ROS modulation. Furthermore, in Chapter V, deletion of *sod-4* and *sod-5* unexpectedly enhanced oxidative stress resistance in *smn-1(ok355)* animals, despite the assumption that SOD deletion would reduce intracellular detoxification capacity. Thus, it is possible that changes induced by the aforementioned *sod* deletions could activate adaptive responses in broader cellular networks, conferring unexpected protective effects. Additionally, future research should expand the range of physiological parameters assessed (i.e. lifespan and reproductive fitness) to provide a more comprehensive understanding of how oxidative stress impacts the overall pathogenesis of SMA.

Ultimately, future research endeavours should focus on validating and expanding the mechanistic insights gained from *smn-1(ok355)* *C. elegans* across additional SMA models. This approach will enhance the translational relevance of the therapeutic targets and strategies identified in this project.

6.2.2. Refine molecular targets modulated by ROS in spinal muscular atrophy

A central consideration that emerged from Chapters III, IV, and V is the possibility that oxidative stress is not that much of a uniform contributor to SMA pathology itself, but more of an active modulator of specific signalling pathways that have an impact on determining neuromuscular health. For instance, through this project, we have presented several lines of evidence to suggest that the IIS signalling pathway and its downstream targets, in particular mTOR, may hold particular significance in SMA.

In Chapter III we observed that the transcriptomic profile of *smn-1(ok355)* animals aligned with the reduction of mTOR activity (**Figure 3.3**), a hypothesis supported by findings in SMN-deficient neurons (Kye et al., 2014). Notably, mTOR regulation in SMA appears to be tissue-specific, with studies pointing towards increased signalling in motor neurons and decreased signalling in skeletal muscle and fibroblasts (Rashid & Dimitriadi, 2024b).

In Chapter IV, we demonstrated that NAC, EGCG and MEL treatments have the potential to ameliorate SMA-associated neuromuscular defects. However, our evidence dictates that their therapeutic effect is not mediated by the modulation of ROS alone. Notably, a review of the existing literature revealed a significant difference between the antioxidants that we found "effective" (NAC, EGCG, and MEL) and "ineffective" (CUR and VITC) in enhancing *C. elegans* SMA motor function. Specifically, NAC, EGCG and MEL have been reported to activate the ERK and PI3K/AKT pathways along with their mTOR downstream target, whereas CUR and VITC demonstrated to suppress them (**Table 4.2**). These findings suggest that the activation of PI3K/AKT/mTOR and ERK pathways may represent a plausible unifying mechanism underlying the beneficial effects observed on *C. elegans* SMA following NAC, EGCG and MEL treatments.

Chapter V suggested an important multifaceted role of the SOD enzymes, functioning not only as detoxifiers of superoxide anions but also as key modulators of redox-sensitive signalling pathways. Importantly, deletion of certain SOD isoforms, *sod-4* and *sod-5*, in *smn-1(ok355)* animals unexpectedly increased their resistance to pro-oxidant compounds. These findings

underline the significant influence of $O_2^{\bullet-}/H_2O_2$ ratios, modulated by SOD activity, on cellular redox signalling. Notably, there is wide evidence in previous research that connect the balance between superoxide and hydrogen peroxide ROS at the cell membrane and the modulation of the IIS signalling pathway through the modification of the phosphorylation sites of key protein tyrosine phosphatases (Tanner et al., 2011; Zhou et al., 2011). In *C. elegans*, IIS is mediated by the insulin receptor DAF-2, leading to the activation of AGE-1/PI3K, PIP_3 generation, phosphorylation of PDK-1 and AKT and, ultimately, the exclusion of DAF-16 from the nucleus, a transcription factor broadly associated with longevity and enhanced cellular protection against cellular and environmental stressors (Murphy & Hu, 2013; Zhang et al., 2022). Conversely, DAF-18/PTEN, a protein tyrosine phosphatase that is inhibited by H_2O_2 , antagonises this pathway by converting PIP_3 back to PIP_2 . Thus, modulating local H_2O_2 concentrations at the plasma membrane can significantly impact IIS pathway activity.

The beneficial effect observed following *sod-4* deletion, a gene that is significantly overexpressed in *smn-1(ok355)* animals, can be explained by a reduction in local extracellular or membrane-proximal H_2O_2 levels. This reduction decreases oxidative inhibition of PTPases, restoring their activity, which in turn decreases PI3K and AKT phosphorylation. Lowered AKT activity promotes DAF-16 nuclear localisation, activating stress-response genes and ultimately enhancing stress resistance and longevity. Indeed, previous research supports this model, demonstrating that *sod-4* deletion uniquely extends the lifespan of *daf-2* long-lived mutants through enhanced DAF-16 nuclear translocation. Additionally, and more specific to our study, previous research in *C. elegans* have shown that *daf-2* inhibition enhances DAF-16 localisation to the nucleus, resulting in increased lifespan and improved motor behaviour (Wu et al., 2019). Although this interaction was not empirically validated in the present study, it remains a plausible hypothesis that the amelioration of neuromuscular defects in *smn-1(ok355)* mutants following *sod-4* deletion may be mediated by reduced H_2O_2 levels and increase DAF-16 activity (**Figure 5.10**).

Notably, other studies in SMA mouse models have suggested that reduced IIS signalling might be beneficial in the context of SMA, reporting increased lifespan and motor behaviour after

inhibition of the insulin-like growth factor-1 receptor (Igf-1r) in muscles (Biondi et al., 2015). Conversely, other researchers have suggested the opposite relation, showing that increased Igf-1r expression in SMA mouse muscles increases myofibers size and increases lifespan (Bosch-Marcé et al., 2011). Interestingly, while IIS inhibition is associated with decreased PI3K/AKT/mTOR signalling in normal conditions, studies have shown that this relationship might be inverted in SMA. For example, a recent study found elevated NOX4 activity in SMA cells (El Khoury et al., 2023). NOX4 is a membrane-bound enzyme that generates H₂O₂ and activates IIS through oxidative inhibition of cellular PTPases (Mahadev et al., 2004). However, in SMA models, increased NOX4 activity was associated with reduced Akt phosphorylation, which is a sign of reduced IIS signalling. Notably, pharmacological inhibition of NOX4 restored Akt phosphorylation to control levels, reduced motor neuron degeneration, and improved motor function (El Khoury et al., 2023). Additionally, Biondi et al., (2015) found that inhibition of Igf-1r in muscle, which led to increased lifespan and motor behaviour, caused activation, and not inhibition, of the AKT/mTOR pathway. These distinctions highlight the critical role that dose, timing and tissue context of IIS activation might play in determining protective versus deleterious outcomes.

Nonetheless, the role of the insulin pathway in regulating neuromuscular function in the *smn-1(ok355) C. elegans* SMA model after *sod-4* deletion remains hypothetical and requires experimental validation. Future studies should include measurements of the phosphorylation state of key signalling proteins, and evaluate downstream processes regulated by this pathway, such as protein synthesis and autophagy. Importantly, the overall outcome of modulating PI3K/AKT signalling depends heavily on the cellular context, thereby, future studies should carefully consider IIS signalling in different tissues and disease stages.

6.3. Therapeutic opportunities

In this thesis, we have demonstrated that despite the extensive evidence indicating elevated oxidative stress in SMA (Chapter III), simply decreasing ROS levels does not consistently translate into beneficial outcomes for SMA pathology (Chapter IV). Surprisingly, the deletion of certain SOD isoforms, enzymes critical for cellular antioxidant defence, led to improved neuromuscular function in the *smn-1(ok355)* *C. elegans* SMA model (Chapter V). Does this suggest that oxidative stress research in SMA should be abandoned in favour of other cellular processes? Not necessarily. Instead, a shift in perspective is needed. A common misconception is that ROS are merely harmful metabolic byproducts. However, recognising ROS as key physiological signalling molecules could explain the limited efficacy of non-selective antioxidants. It is possible that these treatments are failing because while reducing oxidative damage, they also disrupt essential redox signalling pathways. Therefore, future therapeutic approaches should aim to strategically target the mechanisms responsible for oxidative damage while preserving or enhancing beneficial ROS signalling. Although further investigation is required to corroborate relevant points of redox regulation in SMA, our study highlights the potential therapeutic benefits of reducing hydrogen peroxide (H₂O₂) at the membrane level, for example, through the pharmacological inhibition of NADPH oxidase (NOX) or extracellular superoxide dismutase (SOD) enzymes.

6.4. Conclusion

Beginning with a thorough mapping of transcriptome perturbations and increased oxidative stress (Chapter III), moving on to an experimental investigation of the association between ROS levels and neuromuscular function (Chapter IV), and concluding with the identification of key oxidative stress-related genes that are dysregulated in SMA, the findings presented here provide a solid framework for understanding how oxidative stress interacts with SMA pathology. This thesis ultimately demonstrates that while oxidative stress is integral to SMA pathology, novel

therapeutic strategies should focus on achieving a finer spatiotemporal control of redox chemistry and the downstream pathways regulated by ROS, rather than on the global suppression of ROS.

References

1. Burr P, Reddivari AKR. Spinal Muscle Atrophy. *StatPearls*. July 17, 2023. Accessed May 7, 2025. <https://www.ncbi.nlm.nih.gov/books/NBK560687/>
2. Kolb SJ, Kissel JT. Spinal Muscular Atrophy. *Neurol Clin*. 2015;33(4):831. doi:10.1016/J.NCL.2015.07.004
3. Macdonald WK, Hamilton D, Kuhle S. SMA carrier testing: A meta-analysis of differences in test performance by ethnic group. *Prenat Diagn*. 2014;34(12):1219-1226. doi:10.1002/PD.4459;PAGE:STRING:ARTICLE/CHAPTER
4. Hamilton G, Gillingwater TH. Spinal muscular atrophy: going beyond the motor neuron. *Trends Mol Med*. 2013;19(1):40-50. doi:10.1016/J.MOLMED.2012.11.002
5. Zayia LC, Tadi P. Neuroanatomy, Motor Neuron. *StatPearls*. Published online July 24, 2023. Accessed May 8, 2025. <https://www.ncbi.nlm.nih.gov/books/NBK554616/>
6. Stifani N. Motor neurons and the generation of spinal motor neuron diversity. *Front Cell Neurosci*. 2014;8(OCT). doi:10.3389/FNCEL.2014.00293/PDF
7. Simic G, Seso-Simic D, Lucassen PJ, et al. Ultrastructural Analysis and TUNEL Demonstrate Motor Neuron Apoptosis in Werdnig-Hoffmann Disease. *J Neuropathol Exp Neurol*. 2000;59(5):398-407. doi:10.1093/JNEN/59.5.398
8. Murray LM, Comley LH, Thomson D, Parkinson N, Talbot K, Gillingwater TH. Selective vulnerability of motor neurons and dissociation of pre- and post-synaptic pathology at the neuromuscular junction in mouse models of spinal muscular atrophy. *Hum Mol Genet*. 2008;17(7):949-962. doi:10.1093/HMG/DDM367
9. Powis RA, Gillingwater TH. Selective loss of alpha motor neurons with sparing of gamma motor neurons and spinal cord cholinergic neurons in a mouse model of spinal muscular atrophy. *J Anat*. 2016;228(3):443-451. doi:10.1111/JOA.12419,
10. Thomson SR, Nahon JE, Mutsaers CA, et al. Morphological Characteristics of Motor Neurons Do Not Determine Their Relative Susceptibility to Degeneration in a Mouse Model of Severe Spinal Muscular Atrophy. *PLoS One*. 2012;7(12):e52605. doi:10.1371/JOURNAL.PONE.0052605
11. Tu WY, Simpson JE, Highley JR, Heath PR. Spinal muscular atrophy: Factors that modulate motor neurone vulnerability. *Neurobiol Dis*. 2017;102:11-20. doi:10.1016/j.nbd.2017.01.011
12. Boyd PJ, Tu WY, Shorrock HK, et al. Bioenergetic status modulates motor neuron vulnerability and pathogenesis in a zebrafish model of spinal muscular atrophy. *PLoS Genet*. 2017;13(4). doi:10.1371/JOURNAL.PGEN.1006744
13. Rindt H, Feng Z, Mazzasette C, et al. Astrocytes influence the severity of spinal muscular atrophy. *Hum Mol Genet*. 2015;24(14):4094. doi:10.1093/HMG/DDV148
14. Cheng X, Wang J, Sun X, Shao L, Guo Z, Li Y. Morphological and functional alterations of astrocytes responding to traumatic brain injury. *J Integr Neurosci*. 2019;18(2):203-215. doi:10.31083/J.JIN.2019.02.110,
15. Rama Rao K V., Kielian T. Neuron–astrocyte interactions in neurodegenerative diseases: Role of neuroinflammation. *Clin Exp Neuroimmunol*. 2015;6(3):245. doi:10.1111/CEN3.12237

16. Khalil B, Marwaha K, Bollu PC. Physiology, Neuromuscular Junction. *StatPearls*. Published online February 17, 2025. Accessed May 8, 2025. <https://www.ncbi.nlm.nih.gov/books/NBK470413/>
17. Martínez-Hernández R, Bernal S, Also-Rallo E, et al. Synaptic defects in type i spinal muscular atrophy in human development. *Journal of Pathology*. 2013;229(1):49-61. doi:10.1002/PATH.4080,
18. Kariya S, Park GH, Maeno-Hikichi Y, et al. Reduced SMN protein impairs maturation of the neuromuscular junctions in mouse models of spinal muscular atrophy. *Hum Mol Genet*. 2008;17(16):2552-2569. doi:10.1093/HMG/DDN156
19. Rafii S, O'Regan P, Xinarianos G, et al. Neurofilament accumulation at the motor endplate and lack of axonal sprouting in a spinal muscular atrophy mouse model. *Hum Mol Genet*. 2002;11(12):1439-1447. doi:10.1093/HMG/11.12.1439
20. Martínez-Hernández R, Soler-Botija C, Also E, et al. The Developmental Pattern of Myotubes in Spinal Muscular Atrophy Indicates Prenatal Delay of Muscle Maturation. *J Neuropathol Exp Neurol*. 2009;68(5):474-481. doi:10.1097/NEN.0B013E3181A10EA1
21. Mutsaers CA, Wishart TM, Lamont DJ, et al. Reversible molecular pathology of skeletal muscle in spinal muscular atrophy. *Hum Mol Genet*. 2011;20(22):4334-4344. doi:10.1093/HMG/DDR360
22. Kim JK, Jha NN, Feng Z, et al. Muscle-specific SMN reduction reveals motor neuron-independent disease in spinal muscular atrophy models. *Journal of Clinical Investigation*. 2020;130(3):1271-1287. doi:10.1172/JCI131989,
23. Lefebvre S, Bürglen L, Reboullet S, et al. Identification and characterization of a spinal muscular atrophy-determining gene. *Cell*. 1995;80(1):155-165. doi:10.1016/0092-8674(95)90460-3
24. Chen Q, Baird SD, Mahadevan M, et al. Sequence of a 131-kb Region of 5q13.1 Containing the Spinal Muscular Atrophy Candidate Genes SMN and NAIP. *Genomics*. 1998;48(1):121-127. doi:10.1006/GENO.1997.5141
25. Wirth B. An update of the mutation spectrum of the survival motor neuron gene (SMN1) in autosomal recessive spinal muscular atrophy (SMA). *Hum Mutat*. 2000;15(3):228-237. doi:10.1002/(SICI)1098-1004(200003)15:3<228::AID-HUMU3>3.0.CO;2-9,
26. Farrar MA, Kiernan MC. The Genetics of Spinal Muscular Atrophy: Progress and Challenges. *Neurotherapeutics*. 2014;12(2):290. doi:10.1007/S13311-014-0314-X
27. Theodosiou AM, Morrison KE, Nesbit AM, et al. Complex repetitive arrangements of gene sequence in the candidate region of the spinal muscular atrophy gene in 5q13. *Am J Hum Genet*. 1994;55(6):1209. Accessed May 7, 2025. <https://pmc.ncbi.nlm.nih.gov/articles/PMC1918431/>
28. Crawford TO. From enigmatic to problematic: The new molecular genetics of childhood spinal muscular atrophy. *Neurology*. 1996;46(2):335-340. doi:10.1212/WNL.46.2.335/ASSET/E2F39708-71E8-46F7-9BD4-17C4876BDED7/ASSETS/WNL.46.2.335.FP.PNG
29. Lorson CL, Hahnen E, Androphy EJ, Wirth B. A single nucleotide in the SMN gene regulates splicing and is responsible for spinal muscular atrophy. *Proc Natl Acad Sci U S*

- A. 1999;96(11):6307-6311. doi:10.1073/PNAS.96.11.6307/ASSET/55282051-CAEE-40AB-9DF4-038068B6B9F8/ASSETS/GRAPHIC/PQ1190286003.JPEG
30. Monani UR, Lorson CL, Parsons DW, et al. A single nucleotide difference that alters splicing patterns distinguishes the SMA gene SMN1 from the copy gene SMN2. *Hum Mol Genet.* 1999;8(7):1177-1183. doi:10.1093/HMG/8.7.1177,
 31. Blencowe BJ. Exonic splicing enhancers: Mechanism of action, diversity and role in human genetic diseases. *Trends Biochem Sci.* 2000;25(3):106-110. doi:10.1016/S0968-0004(00)01549-8
 32. Kashima T, Manley JL. A negative element in SMN2 exon 7 inhibits splicing in spinal muscular atrophy. *Nat Genet.* 2003;34(4):460-463. doi:10.1038/NG1207;KWRD=BIOMEDICINE
 33. Gray KM, Kaifer KA, Baillat D, et al. Self-oligomerization regulates stability of survival motor neuron protein isoforms by sequestering an SCFS^{lmb} degron. *Mol Biol Cell.* 2018;29(2):96. doi:10.1091/MBC.E17-11-0627
 34. Crawford TO, Paushkin S V., Kobayashi DT, et al. Evaluation of SMN Protein, Transcript, and Copy Number in the Biomarkers for Spinal Muscular Atrophy (BforSMA) Clinical Study. *PLoS One.* 2012;7(4):e33572. doi:10.1371/JOURNAL.PONE.0033572
 35. Wadman RI, Stam M, Jansen MD, et al. A Comparative Study of SMN Protein and mRNA in Blood and Fibroblasts in Patients with Spinal Muscular Atrophy and Healthy Controls. *PLoS One.* 2016;11(11):e0167087. doi:10.1371/JOURNAL.PONE.0167087
 36. Calucho M, Bernal S, Alías L, et al. Correlation between SMA type and SMN2 copy number revisited: An analysis of 625 unrelated Spanish patients and a compilation of 2834 reported cases. *Neuromuscular Disorders.* 2018;28(3):208-215. doi:10.1016/j.nmd.2018.01.003
 37. Singh RN, Howell MD, Ottesen EW, Singh NN. Diverse role of Survival Motor Neuron Protein. *Biochim Biophys Acta.* 2017;1860(3):299. doi:10.1016/J.BBAGRM.2016.12.008
 38. Coover DD, Le TT, McAndrew PE, et al. The survival motor neuron protein in spinal muscular atrophy. *Hum Mol Genet.* 1997;6(8):1205-1214. doi:10.1093/HMG/6.8.1205,
 39. Ramos DM, d'Ydewalle C, Gabbeta V, et al. Age-dependent SMN expression in disease-relevant tissue and implications for SMA treatment. *J Clin Invest.* 2019;129(11):4817-4831. doi:10.1172/JCI124120
 40. Gubitzi AK, Feng W, Dreyfuss G. The SMN complex. *Exp Cell Res.* 2004;296(1):51-56. doi:10.1016/J.YEXCR.2004.03.022
 41. Fallini C, Zhang H, Su Y, et al. The Survival of Motor Neuron (SMN) Protein Interacts with the mRNA-Binding Protein HuD and Regulates Localization of Poly(A) mRNA in Primary Motor Neuron Axons. *The Journal of Neuroscience.* 2011;31(10):3914. doi:10.1523/JNEUROSCI.3631-10.2011
 42. Rossoll W, Jablonka S, Andreassi C, et al. Smn, the spinal muscular atrophy-determining gene product, modulates axon growth and localization of β -actin mRNA in growth cones of motoneurons. *J Cell Biol.* 2003;163(4):801. doi:10.1083/JCB.200304128
 43. Fallini C, Donlin-Asp PG, Rouanet JP, Bassell GJ, Rossoll W. Deficiency of the survival of motor neuron protein impairs mrna localization and local translation in the growth cone

- of motor neurons. *Journal of Neuroscience*. 2016;36(13):3811-3820. doi:10.1523/JNEUROSCI.2396-15.2016,
44. Bernabò P, Tebaldi T, Groen EJN, et al. In Vivo Translatome Profiling in Spinal Muscular Atrophy Reveals a Role for SMN Protein in Ribosome Biology. *Cell Rep*. 2017;21(4):953-965. doi:10.1016/J.CELREP.2017.10.010,
 45. Wishart TM, Mutsaers CA, Riessland M, et al. Dysregulation of ubiquitin homeostasis and β -catenin signaling promote spinal muscular atrophy. *Journal of Clinical Investigation*. 2014;124(4):1821-1834. doi:10.1172/JCI71318,
 46. Dimitriadi M, Derdowski A, Kalloo G, et al. Decreased function of survival motor neuron protein impairs endocytic pathways. *Proc Natl Acad Sci U S A*. 2016;113(30):E4377-4386. doi:10.1073/pnas.1600015113
 47. Rashid S, Dimitriadi M. Autophagy in spinal muscular atrophy: from pathogenic mechanisms to therapeutic approaches. *Front Cell Neurosci*. 2024;17:1307636. doi:10.3389/FNCEL.2023.1307636
 48. James R, Chaytow H, Ledahawsky LM, Gillingwater TH. Revisiting the role of mitochondria in spinal muscular atrophy. *Cell Mol Life Sci*. 2021;78(10):4785. doi:10.1007/S00018-021-03819-5
 49. Chaytow H, Huang YT, Gillingwater TH, Faller KME. The role of survival motor neuron protein (SMN) in protein homeostasis. *Cell Mol Life Sci*. 2018;75(21):3877. doi:10.1007/S00018-018-2849-1
 50. Wirth B. Spinal Muscular Atrophy: In the Challenge Lies a Solution. *Trends Neurosci.Elsevier Ltd*. 2021;44(4):306-322. doi:10.1016/j.tins.2020.11.009
 51. Monani UR. Spinal Muscular Atrophy: A Deficiency in a Ubiquitous Protein; a Motor Neuron-Specific Disease. *Neuron*. 2005;48(6):885-895. doi:10.1016/J.NEURON.2005.12.001
 52. Zhang L, Li X, Zhao R. Structural analyses of the pre-mRNA splicing machinery. *Protein Science*. 2013;22(6):677-692. doi:10.1002/PRO.2266
 53. Gabanella F, Butchbach MER, Saieva L, Carissimi C, Burghes AHM, Pellizzoni L. Ribonucleoprotein Assembly Defects Correlate with Spinal Muscular Atrophy Severity and Preferentially Affect a Subset of Spliceosomal snRNPs. *PLoS One*. 2007;2(9):e921. doi:10.1371/JOURNAL.PONE.0000921
 54. Patel SB, Bellini M. The assembly of a spliceosomal small nuclear ribonucleoprotein particle. *Nucleic Acids Res*. 2008;36(20):6482-6493. doi:10.1093/NAR/GKN658
 55. Narayanan U, Achsel T, Lührmann R, Matera AG. Coupled In Vitro Import of U snRNPs and SMN, the Spinal Muscular Atrophy Protein. *Mol Cell*. 2004;16(2):223-234. doi:10.1016/J.MOLCEL.2004.09.024
 56. Friesen WJ, Paushkin S, Wyce A, et al. The Methylosome, a 20S Complex Containing JBP1 and pICln, Produces Dimethylarginine-Modified Sm Proteins. *Mol Cell Biol*. 2001;21(24):8289-8300. doi:10.1128/MCB.21.24.8289-8300.2001
 57. Henriksson S, Farnebo M. On the road with WRAP53 β : guardian of Cajal bodies and genome integrity. *Front Genet*. 2015;6(FEB):91. doi:10.3389/FGENE.2015.00091

58. So BR, Wan L, Zhang Z, et al. A U1 snRNP-specific assembly pathway reveals the SMN complex as a versatile hub for RNP exchange. *Nat Struct Mol Biol.* 2016;23(3):225-230. doi:10.1038/NSMB.3167;TECHMETA=106,109,13,82,83,89;SUBJMETA=337,45,631; KWRD=BIOCHEMISTRY,MOLECULAR+BIOLOGY
59. Pillai RS, Grimm M, Meister G, et al. Unique Sm core structure of U7 snRNPs: assembly by a specialized SMN complex and the role of a new component, Lsm11, in histone RNA processing. *Genes Dev.* 2003;17(18):2321. doi:10.1101/GAD.274403
60. Zhang Z, Lotti F, Dittmar K, et al. SMN deficiency causes tissue-specific perturbations in the repertoire of snRNAs and widespread defects in splicing. *Cell.* 2008;133(4):585. doi:10.1016/J.CELL.2008.03.031
61. Lotti F, Imlach WL, Saieva L, et al. An SMN-Dependent U12 Splicing Event Essential for Motor Circuit Function. *Cell.* 2012;151(2):440-454. doi:10.1016/J.CELL.2012.09.012
62. See K, Yadav P, Giegerich M, et al. SMN deficiency alters Nrnx2 expression and splicing in zebrafish and mouse models of spinal muscular atrophy. *Hum Mol Genet.* 2014;23(7):1754-1770. doi:10.1093/HMG/DDT567
63. Moradi M, Sivadasan R, Saal L, et al. Differential roles of α -, β -, and γ -actin in axon growth and collateral branch formation in motoneurons. *J Cell Biol.* 2017;216(3):793. doi:10.1083/JCB.201604117
64. Xu CC, Denton KR, Wang ZB, Zhang X, Li XJ. Abnormal mitochondrial transport and morphology as early pathological changes in human models of spinal muscular atrophy. *DMM Disease Models and Mechanisms.* 2016;9(1):39-49. doi:10.1242/DMM.021766/-/DC1
65. Fallini C, Rouanet JP, Donlin-Asp PG, et al. Dynamics of survival of motor neuron (SMN) protein interaction with the mRNA-binding protein IMP1 facilitates its trafficking into motor neuron axons. *Dev Neurobiol.* 2013;74(3):319. doi:10.1002/DNEU.22111
66. Beck R, Ravet M, Wieland FT, Cassel D. The COPI system: Molecular mechanisms and function. *FEBS Lett.* 2009;583(17):2701-2709. doi:10.1016/J.FEBSLET.2009.07.032;WEBSITE:WEBSITE:FEBS;PAGE:STRING:ARTICLE/CHAPTER
67. Peter CJ, Evans M, Thayanithy V, et al. The COPI vesicle complex binds and moves with survival motor neuron within axons. *Hum Mol Genet.* 2011;20(9):1701-1711. doi:10.1093/HMG/DDR046,
68. Kevenaar JT, Hoogenraad CC. The axonal cytoskeleton: From organization to function. *Front Mol Neurosci.* 2015;8(AUGUST):156502. doi:10.3389/FNMOL.2015.00044/XML/NLM
69. Nölle A, Zeug A, Van bergeijk J, et al. The spinal muscular atrophy disease protein SMN is linked to the Rho-kinase pathway via profilin. *Hum Mol Genet.* 2011;20(24):4865-4878. doi:10.1093/HMG/DDR425,
70. Sanchez G, Dury AY, Murray LM, et al. A novel function for the survival motoneuron protein as a translational regulator. *Hum Mol Genet.* 2013;22(4):668-684. doi:10.1093/HMG/DDS474,

71. Han KJ, Foster DG, Zhang NY, et al. Ubiquitin-specific protease 9x deubiquitinates and stabilizes the spinal muscular atrophy protein-survival motor neuron. *Journal of Biological Chemistry*. 2012;287(52):43741-43752. doi:10.1074/jbc.M112.372318
72. Hsu SH, Lai MC, Er TK, et al. Ubiquitin carboxyl-terminal hydrolase L1 (UCHL1) regulates the level of SMN expression through ubiquitination in primary spinal muscular atrophy fibroblasts. *Clinica Chimica Acta*. 2010;411(23-24):1920-1928. doi:10.1016/j.cca.2010.07.035
73. Hosseinibarkooie S, Peters M, Torres-Benito L, et al. The Power of Human Protective Modifiers: PLS3 and CORO1C Unravel Impaired Endocytosis in Spinal Muscular Atrophy and Rescue SMA Phenotype. *Am J Hum Genet*. 2016;99(3):647-665. doi:10.1016/j.ajhg.2016.07.014
74. Acsadi G, Lee I, Li X, et al. Mitochondrial dysfunction in a neural cell model of spinal muscular atrophy. *J Neurosci Res*. 2009;87(12):2748-2756. doi:10.1002/JNR.22106
75. Cobben JM, Van der Steege G, Grootsholten P, De Visser M, Scheffer H, Buys CHCM. Deletions of the survival motor neuron gene in unaffected siblings of patients with spinal muscular atrophy. *Am J Hum Genet*. 1995;57(4):805. Accessed May 8, 2025. <https://pmc.ncbi.nlm.nih.gov/articles/PMC1801497/>
76. Hahnen E, Forkert R, Marke C, et al. Molecular analysis of candidate genes on chromosome 5q13 in autosomal recessive spinal muscular atrophy: Evidence of homozygous deletions of the SMN gene in unaffected individuals. *Hum Mol Genet*. 1995;4(10):1927-1933. doi:10.1093/HMG/4.10.1927,
77. Wang CH, Xu J, Carter TA, et al. Characterization of survival motor neuron (SMNT) gene deletions in asymptomatic carriers of spinal muscular atrophy. *Hum Mol Genet*. 1996;5(3):359-365. doi:10.1093/HMG/5.3.359,
78. Lamar KM, McNally EM. Genetic Modifiers for Neuromuscular Diseases. *J Neuromuscul Dis*. 2014;1(1):3. doi:10.3233/JND-140023
79. Monani UR, Sendtner M, Coover DD, et al. The human centromeric survival motor neuron gene (SMN2) rescues embryonic lethality in *Smn*^{-/-} mice and results in a mouse with spinal muscular atrophy. *Hum Mol Genet*. 2000;9(3):333-339. doi:10.1093/HMG/9.3.333
80. Oprea GE, Kröber S, McWhorter ML, et al. Plastin 3 Is a Protective Modifier of Autosomal Recessive Spinal Muscular Atrophy. *Science*. 2008;320(5875):524. doi:10.1126/SCIENCE.1155085
81. Yanyan C, Yujin Q, Jinli B, Yuwei J, Hong W, Fang S. Correlation of PLS3 expression with disease severity in children with spinal muscular atrophy. *Journal of Human Genetics* 2014 59:1. 2013;59(1):24-27. doi:10.1038/jhg.2013.111
82. Delanote V, Vandekerckhove J, Gettemans J. Plastins: Versatile modulators of actin organization in (patho)physiological cellular processes. *Acta Pharmacol Sin*. 2005;26(7):769-779. doi:10.1111/J.1745-7254.2005.00145.X;KWRD=BIOMEDICINE
83. Dent EW, Gertler FB. Cytoskeletal dynamics and transport in growth cone motility and guidance. *Neuron*. 2003;40(2):209-227. doi:10.1016/S0896-6273(03)00633-0

84. Engqvist-Goldstein ÅEY, Drubin DG. Actin Assembly and Endocytosis: From Yeast to Mammals. *Annu Rev Cell Dev Biol.* 2003;19(Volume 19, 2003):287-332. doi:10.1146/ANNUREV.CELLBIO.19.111401.093127/CITE/REFWORKS
85. Ackermann B, Kröber S, Torres-benito L, et al. Plastin 3 ameliorates spinal muscular atrophy via delayed axon pruning and improves neuromuscular junction functionality. *Hum Mol Genet.* 2013;22(7):1328-1347. doi:10.1093/HMG/DDS540
86. Walsh MB, Janzen E, Wingrove E, et al. Genetic modifiers ameliorate endocytic and neuromuscular defects in a model of spinal muscular atrophy. *BMC Biol.* 2020;18(1). doi:10.1186/s12915-020-00845-w
87. Riessland M, Kaczmarek A, Schneider S, et al. Neurocalcin Delta Suppression Protects against Spinal Muscular Atrophy in Humans and across Species by Restoring Impaired Endocytosis. *Am J Hum Genet.* 2017;100(2):297. doi:10.1016/J.AJHG.2017.01.005
88. Braunewell KH, Gundelfinger ED. Intracellular neuronal calcium sensor proteins: A family of EF-hand calcium-binding proteins in search of a function. *Cell Tissue Res.* 1999;295(1):1-12. doi:10.1007/S004410051207/METRICS
89. Iino S, Kobayashi S, Hidaka H. Neurocalcin-immunopositive nerve terminals in the muscle spindle, Golgi tendon organ and motor endplate. *Brain Res.* 1998;808(2):294-299. doi:10.1016/S0006-8993(98)00750-1
90. Hoareau E, Belley N, Klinker K, Desbat B, Boisselier É. Characterization of neurocalcin delta membrane binding by biophysical methods. *Colloids Surf B Biointerfaces.* 2019;174:291-299. doi:10.1016/J.COLSURFB.2018.11.017
91. Slepnev VI, De Camilli P. Accessory factors in clathrin-dependent synaptic vesicle endocytosis. *Nature Reviews Neuroscience* 2000 1:3. 2000;1(3):161-172. doi:10.1038/35044540
92. Jablonka S, Beck M, Lechner BD, Mayer C, Sendtner M. Defective Ca²⁺ channel clustering in axon terminals disturbs excitability in motoneurons in spinal muscular atrophy. *J Cell Biol.* 2007;179(1):139. doi:10.1083/JCB.200703187
93. Wojcik MH, Schwartz TS, Thiele KE, et al. Infant Mortality: the Contribution of Genetic Disorders. *J Perinatol.* 2019;39(12):1611. doi:10.1038/S41372-019-0451-5
94. Finkel RS, Mercuri E, Darras BT, et al. Nusinersen versus Sham Control in Infantile-Onset Spinal Muscular Atrophy. *New England Journal of Medicine.* 2017;377(18):1723-1732. doi:10.1056/NEJMOA1702752/SUPPL_FILE/NEJMOA1702752_DISCLOSURES.PDF
95. Biliouris K, Gaitonde P, Yin W, et al. A Semi-Mechanistic Population Pharmacokinetic Model of Nusinersen: An Antisense Oligonucleotide for the Treatment of Spinal Muscular Atrophy. *CPT Pharmacometrics Syst Pharmacol.* 2018;7(9):581-592. doi:10.1002/PSP4.12323;JOURNAL:JOURNAL:21638306;REQUESTEDJOURNAL:JOURNAL:21638306;WGROU:STRING:PUBLICATION
96. Singh NN, Seo J, Ottesen EW, Shishimorova M, Bhattacharya D, Singh RN. TIA1 Prevents Skipping of a Critical Exon Associated with Spinal Muscular Atrophy. *Mol Cell Biol.* 2011;31(5):935-954. doi:10.1128/MCB.00945-10,
97. Singh NN, Lee BM, DiDonato CJ, Singh RN. Mechanistic principles of antisense targets for the treatment of Spinal Muscular Atrophy. *Future Med Chem.* 2015;7(13):1793. doi:10.4155/FMC.15.101

98. Rigo F, Chun SJ, Norris DA, et al. Pharmacology of a central nervous system delivered 2'-O-methoxyethyl- modified survival of motor neuron splicing oligonucleotide in mice and nonhuman primates. *Journal of Pharmacology and Experimental Therapeutics*. 2014;350(1):46-55. doi:10.1124/JPET.113.212407,
99. Mercuri E, Darras BT, Chiriboga CA, et al. Nusinersen versus Sham Control in Later-Onset Spinal Muscular Atrophy. *New England Journal of Medicine*. 2018;378(7):625-635. doi:10.1056/NEJMOA1710504,
100. De Vivo DC, Bertini E, Swoboda KJ, et al. Nusinersen initiated in infants during the presymptomatic stage of spinal muscular atrophy: Interim efficacy and safety results from the Phase 2 NURTURE study. *Neuromuscular Disorders*. 2019;29(11):842-856. doi:10.1016/j.nmd.2019.09.007
101. Sivaramakrishnan M, McCarthy KD, Campagne S, et al. Binding to SMN2 pre-mRNA-protein complex elicits specificity for small molecule splicing modifiers. *Nat Commun*. 2017;8(1):1-13. doi:10.1038/S41467-017-01559-4;SUBJMETA=154,1645,1946,337,500,555,631,92;KWRD=ALTERNATIVE+SPLICIN G, RNA, TARGET+IDENTIFICATION
102. Sturm S, Günther A, Jaber B, et al. A phase 1 healthy male volunteer single escalating dose study of the pharmacokinetics and pharmacodynamics of risdiplam (RG7916, RO7034067), a SMN2 splicing modifier. *Br J Clin Pharmacol*. 2019;85(1):181-193. doi:10.1111/BCP.13786,
103. Servais L, Oskoui M, Day J, et al. SUNFISH Parts 1 and 2: 4-year Efficacy and Safety Data of Risdiplam in Types 2 and 3 Spinal Muscular Atrophy (SMA) (S34.009). *Neurology*. 2023;100(17_supplement_2). doi:10.1212/WNL.0000000000203570
104. Baranello G, Darras BT, Day JW, et al. Risdiplam in Type 1 Spinal Muscular Atrophy. *New England Journal of Medicine*. 2021;384(10):915-923. doi:10.1056/NEJMOA2009965,
105. Finkel RS, Farrar MA, Vlodavets D, et al. RAINBOWFISH: Preliminary Efficacy and Safety Data in Risdiplam-Treated Infants with Presymptomatic SMA (P17-5.003). *Neurology*. 2022;98(18_supplement). doi:10.1212/WNL.98.18_SUPPLEMENT.1636
106. Dominguez E, Marais T, Chatauret N, et al. Intravenous scAAV9 delivery of a codon-optimized SMN1 sequence rescues SMA mice. *Hum Mol Genet*. 2011;20(4):681-693. doi:10.1093/HMG/DDQ514,
107. Mendell JR, Al-Zaidy S, Shell R, et al. Single-Dose Gene-Replacement Therapy for Spinal Muscular Atrophy. *New England Journal of Medicine*. 2017;377(18):1713-1722. doi:10.1056/NEJMOA1706198/SUPPL_FILE/NEJMOA1706198_DISCLOSURES.PDF
108. Finkel RS, McDermott MP, Kaufmann P, et al. Observational study of spinal muscular atrophy type I and implications for clinical trials. *Neurology*. 2014;83(9):810. doi:10.1212/WNL.0000000000000741
109. Al-Zaidy S, Pickard AS, Kotha K, et al. Health outcomes in spinal muscular atrophy type 1 following AVXS-101 gene replacement therapy. *Pediatr Pulmonol*. 2019;54(2):179-185. doi:10.1002/PPUL.24203
110. Day JW, Finkel RS, Chiriboga CA, et al. Onasemnogene abeparvovec gene therapy for symptomatic infantile-onset spinal muscular atrophy in patients with two copies of SMN2

- (STRIVE): an open-label, single-arm, multicentre, phase 3 trial. *Lancet Neurol.* 2021;20(4):284-293. doi:10.1016/S1474-4422(21)00001-6
111. Chand D, Mohr F, McMillan H, et al. Hepatotoxicity following administration of onasemnogene abeparvovec (AVXS-101) for the treatment of spinal muscular atrophy. *J Hepatol.* 2021;74(3):560-566. doi:10.1016/j.jhep.2020.11.001
 112. Waldrop MA, Karingada C, Storey MA, et al. Gene therapy for spinal muscular atrophy: Safety and early outcomes. *Pediatrics.* 2020;146(3). doi:10.1542/PEDS.2020-0729/36757
 113. Varone A, Esposito G, Bitetti I. Spinal muscular atrophy in the era of newborn screening: how the classification could change. *Front Neurol.* 2025;16:1542396. doi:10.3389/FNEUR.2025.1542396
 114. Hensel N, Kubinski S, Claus P. The Need for SMN-Independent Treatments of Spinal Muscular Atrophy (SMA) to Complement SMN-Enhancing Drugs. *Front Neurol.* 2020;11:45. doi:10.3389/FNEUR.2020.00045
 115. Cruz R, Lenz M, Belter L, Hobby K, Jarecki J, Smart T. *The Voice of the Patient Report for Spinal Muscular Atrophy.*; 2018.
 116. Hensel N, Stockbrügger I, Rademacher S, et al. Bilateral crosstalk of rho- and extracellular-signal-regulated-kinase (ERK) pathways is confined to an unidirectional mode in spinal muscular atrophy (SMA). *Cell Signal.* 2014;26(3):540-548. doi:10.1016/j.cellsig.2013.11.027
 117. Hensel N, Baskal S, Walter LM, Brinkmann H, Gernert M, Claus P. ERK and ROCK functionally interact in a signaling network that is compensationally upregulated in Spinal Muscular Atrophy. *Neurobiol Dis.* 2017;108:352-361. doi:10.1016/J.NBD.2017.09.005
 118. Proud CM, Mercuri E, Finkel RS, et al. Combination disease-modifying treatment in spinal muscular atrophy: A proposed classification. *Ann Clin Transl Neurol.* 2023;10(11):2155. doi:10.1002/ACN3.51889
 119. Wan L, Ottinger E, Cho S, Dreyfuss G. Inactivation of the SMN complex by oxidative stress. *Mol Cell.* 2008;31(2):244-254. doi:10.1016/J.MOLCEL.2008.06.004
 120. Köstel AS, Bora-Tatar G, Erdem-Yurter H. Spinal muscular atrophy: An oxidative stress response counteracted with curcumin. *Biomedicine & Aging Pathology.* 2012;2(2):61-66. doi:10.1016/J.BIOMAG.2012.03.007
 121. Ng SY, Rubin LL. Cell Culture Models of Spinal Muscular Atrophy. *Spinal Muscular Atrophy: Disease Mechanisms and Therapy.* Published online January 1, 2017:213-220. doi:10.1016/B978-0-12-803685-3.00013-6
 122. Ebert AD, Yu J, Rose FF, et al. Induced pluripotent stem cells from a spinal muscular atrophy patient. *Nature* 2008 457:7227. 2008;457(7227):277-280. doi:10.1038/nature07677
 123. Corti S, Nizzardo M, Simone C, et al. Genetic correction of human induced pluripotent stem cells from patients with spinal muscular atrophy. *Sci Transl Med.* 2012;4(165). doi:10.1126/SCITRANSLMED.3004108
 124. Liu H, Lu J, Chen H, Du Z, Li XJ, Zhang SC. Spinal muscular atrophy patient-derived motor neurons exhibit hyperexcitability. *Sci Rep.* 2015;5. doi:10.1038/SREP12189

125. Schrank B, Götz R, Gunnensen JM, et al. Inactivation of the survival motor neuron gene, a candidate gene for human spinal muscular atrophy, leads to massive cell death in early mouse embryos. *Proc Natl Acad Sci U S A*. 1997;94(18):9920-9925. doi:10.1073/PNAS.94.18.9920/ASSET/37484178-08BD-430F-8F6A-EF72C61F7910/ASSETS/GRAPHIC/PQ1771376003.JPEG
126. Jablonka S, Schrank B, Kralewski M, Rossoll W, Sendtner M. Reduced survival motor neuron (Smn) gene dose in mice leads to motor neuron degeneration: an animal model for spinal muscular atrophy type III. *Hum Mol Genet*. 2000;9(3):341-346. doi:10.1093/HMG/9.3.341
127. Simon CM, Jablonka S, Ruiz R, Tabares L, Sendtner M. Ciliary neurotrophic factor-induced sprouting preserves motor function in a mouse model of mild spinal muscular atrophy. *Hum Mol Genet*. 2010;19(6):973-986. doi:10.1093/HMG/DDP562
128. Bowerman M, Michalski JP, Beauvais A, Murray L, DeRepentigny Y, Kothary R. Defects in pancreatic development and glucose metabolism in SMN-depleted mice independent of canonical spinal muscular atrophy neuromuscular pathology. *Hum Mol Genet*. 2014;23(13):3432-3444. doi:10.1093/HMG/DDU052
129. Hsieh-Li HM, Chang JG, Jong YJ, et al. A mouse model for spinal muscular atrophy. *Nature Genetics* 2000 24:1. 2000;24(1):66-70. doi:10.1038/71709
130. Le TT, Pham LT, Butchbach MER, et al. SMN Δ 7, the major product of the centromeric survival motor neuron (SMN2) gene, extends survival in mice with spinal muscular atrophy and associates with full-length SMN. *Hum Mol Genet*. 2005;14(6):845-857. doi:10.1093/HMG/DDI078
131. Bandmann O, Burton EA. Genetic zebrafish models of neurodegenerative diseases. *Neurobiol Dis*. 2010;40(1):58-65. doi:10.1016/J.NBD.2010.05.017
132. McWhorter ML, Monani UR, Burghes AHM, Beattie CE. Knockdown of the survival motor neuron (Smn) protein in zebrafish causes defects in motor axon outgrowth and pathfinding. *J Cell Biol*. 2003;162(5):919. doi:10.1083/JCB.200303168
133. Nasevicius A, Ekker SC. Effective targeted gene “knockdown” in zebrafish. *Nat Genet*. 2000;26(2):216-220. doi:10.1038/79951
134. Boon KL, Xiao S, McWhorter ML, et al. Zebrafish survival motor neuron mutants exhibit presynaptic neuromuscular junction defects. *Hum Mol Genet*. 2009;18(19):3615-3625. doi:10.1093/HMG/DDP310
135. Tay SH, Ellieyana EN, Le Y, et al. A novel zebrafish model for intermediate type spinal muscular atrophy demonstrates importance of Smn for maintenance of mature motor neurons. *Hum Mol Genet*. 2021;30(24):2488-2502. doi:10.1093/HMG/DDAB212
136. Yamamoto S, Jaiswal M, Charng WL, et al. A drosophila genetic resource of mutants to study mechanisms underlying human genetic diseases. *Cell*. 2014;159(1):200-214. doi:10.1016/J.CELL.2014.09.002
137. Chintapalli VR, Wang J, Dow JAT. Using FlyAtlas to identify better *Drosophila melanogaster* models of human disease. *Nature Genetics* 2007 39:6. 2007;39(6):715-720. doi:10.1038/ng2049

138. Liguori F, Pandey UB, Digilio FA. Editorial: Drosophila as a model to study neurodegenerative diseases. *Front Neurosci.* 2023;17:1275253. doi:10.3389/FNINS.2023.1275253/BIBTEX
139. Miguel-Aliaga I, Chan YB, Davies KE, Van Den Heuvel M. Disruption of SMN function by ectopic expression of the human SMN gene in Drosophila. *FEBS Lett.* 2000;486(2):99-102. doi:10.1016/S0014-5793(00)02243-2
140. Chan YB, Miguel-Aliaga I, Franks C, et al. Neuromuscular defects in a Drosophila survival motor neuron gene mutant. *Hum Mol Genet.* 2003;12(12):1367-1376. doi:10.1093/HMG/DDG157
141. Chang HCH, Dimlich DN, Yokokura T, et al. Modeling Spinal Muscular Atrophy in Drosophila. *PLoS One.* 2008;3(9):e3209. doi:10.1371/JOURNAL.PONE.0003209
142. Rajendra TK, Gonsalvez GB, Walker MP, Shpargel KB, Salz HK, Matera AG. A Drosophila melanogaster model of spinal muscular atrophy reveals a function for SMN in striated muscle. *J Cell Biol.* 2007;176(6):831. doi:10.1083/JCB.200610053
143. Félix MA, Duvéau F. Population dynamics and habitat sharing of natural populations of *Caenorhabditis elegans* and *C. briggsae*. *BMC Biol.* 2012;10(1):1-19. doi:10.1186/1741-7007-10-59/FIGURES/6
144. Brenner S. The genetics of *Caenorhabditis elegans*. *Genetics.* 1974;77(1):71-94. doi:10.1093/GENETICS/77.1.71
145. Corsi AK, Wightman B, Chalfie M. A Transparent window into biology: A primer on *Caenorhabditis elegans*. *WormBook.* Preprint posted online 2015:1-31. doi:10.1895/wormbook.1.177.1
146. Raizen DM, Zimmerman JE, Maycock MH, et al. Lethargus is a *Caenorhabditis elegans* sleep-like state. *Nature.* 2008;451(7178):569-572. doi:10.1038/NATURE06535
147. M C, Y T, G E, WW W, DC P. Green fluorescent protein as a marker for gene expression. *Science.* 1994;263(5148):1766-1767. doi:10.1126/SCIENCE.8303295
148. Fire A, Xu S, Montgomery MK, Kostas SA, Driver SE, Mello CC. Potent and specific genetic interference by double-stranded RNA in *Caenorhabditis elegans*. *Nature.* 1998;391(6669):806-811. doi:10.1038/35888
149. Lee RC, Feinbaum RL, Ambros V. The *C. elegans* heterochronic gene *lin-4* encodes small RNAs with antisense complementarity to *lin-14*. *Cell.* 1993;75(5):843-854. doi:10.1016/0092-8674(93)90529-Y,
150. White JG, Southgate E, Thomson JN, Brenner S. The structure of the nervous system of the nematode *Caenorhabditis elegans*. *Philos Trans R Soc Lond B Biol Sci.* 1986;314(1165):1-340. doi:10.1098/RSTB.1986.0056
151. Smith JJ, Taylor SR, Blum JA, et al. A molecular atlas of adult *C. elegans* motor neurons reveals ancient diversity delineated by conserved transcription factor codes. *Cell Rep.* 2024;43(3):113857. doi:10.1016/J.CELREP.2024.113857
152. Trojanowski NF, Padovan-Merhar O, Raizen DM, Fang-Yen C. Neural and genetic degeneracy underlies *Caenorhabditis elegans* feeding behavior. *J Neurophysiol.* 2014;112(4):951-961. doi:10.1152/jn.00150.2014
153. Hart AC. Behaviour. Published online 2006:1-67. doi:10.1895/wormbook.1.87.1

154. Kaletta T, Hengartner MO. Finding function in novel targets: *C. elegans* as a model organism. *Nature Reviews Drug Discovery* 2006 5:5. 2006;5(5):387-399. doi:10.1038/nrd2031
155. Carrol SB, Grenier JK, Weatherbee SD. From DNA to Diversity: Molecular Genetics and the Evolution of Animal Design. *Heredity* 2002 89:6. 2002;89(6):411-411. doi:10.1038/sj.hdy.6800154
156. Miguel-Aliaga I, Culetto E, Walker DS, Baylis HA, Sattelle DB, Davies KE. *The Caenorhabditis Elegans Orthologue of the Human Gene Responsible for Spinal Muscular Atrophy Is a Maternal Product Critical for Germline Maturation and Embryonic Viability*. Vol 8.; 1999. http://www.ch.embnet.org/software/BOX_form.html
157. Briese M, Esmaili B, Fraboulet S, et al. Deletion of *smn-1*, the *Caenorhabditis elegans* ortholog of the spinal muscular atrophy gene, results in locomotor dysfunction and reduced lifespan. *Hum Mol Genet.* 2008;18(1):97. doi:10.1093/HMG/DDN320
158. Sleight JN, Buckingham SD, Esmaili B, et al. A novel *Caenorhabditis elegans* allele, *smn-1(cb131)*, mimicking a mild form of spinal muscular atrophy, provides a convenient drug screening platform highlighting new and pre-approved compounds. *Hum Mol Genet.* 2011;20(2):245-260. doi:10.1093/HMG/DDQ459
159. Ogawa C, Usui K, Aoki M, et al. Gemin2 plays an important role in stabilizing the survival of motor neuron complex. *Journal of Biological Chemistry.* 2007;282(15):11122-11134. doi:10.1074/jbc.M609297200
160. Sleight JN, Buckingham SD, Esmaili B, et al. A novel *Caenorhabditis elegans* allele, *smn-1(cb131)*, mimicking a mild form of spinal muscular atrophy, provides a convenient drug screening platform highlighting new and pre-approved compounds. *Hum Mol Genet.* 2011;20(2):245-260. doi:10.1093/hmg/ddq459
161. Doyle JJ, Vranckx C, Maios C, Labarre A, Patten SA, Alex Parker J. Modulating the endoplasmic reticulum stress response attenuates neurodegeneration in a *Caenorhabditis elegans* model of spinal muscular atrophy. *DMM Disease Models and Mechanisms.* 2021;13(12). doi:10.1242/DMM.041350/267217/AM/MODULATING-THE-ER-STRESS-RESPONSE-ATTENUATES
162. Cooper (J K), Bloom JR, Roth FE, et al. The GABAergic nervous system of *Caenorhabditis elegans*. *Nature* 1993 364:6435. 1993;364(6435):337-341. doi:10.1038/364337a0
163. Gallotta I, Mazzarella N, Donato A, et al. Neuron-specific knock-down of SMN1 causes neuron degeneration and death through an apoptotic mechanism. *Hum Mol Genet.* 2016;25(12):2564-2577. doi:10.1093/HMG/DDW119
164. Davies KJ. Oxidative stress: the paradox of aerobic life. *Biochem Soc Symp.* 1995;61:1-31. doi:10.1042/BSS0610001
165. De Sequeira C, Hancock JT. A Brief History of Oxygen: 250 Years on. *Oxygen 2022, Vol 2, Pages 31-39.* 2022;2(1):31-39. doi:10.3390/OXYGEN2010004
166. Priestley J. An Account of Further Discoveries in Air. Royal Society. 1775. Accessed October 17, 2024. <https://www.jstor.org/stable/106209?seq=3>
167. Fenton HJH. Oxidation of tartaric acid in presence of iron. *Journal of the Chemical Society, Transactions.* 1894;65(0):899-910. doi:10.1039/CT8946500899

168. Villamena FA. *CHEMISTRY OF REACTIVE SPECIES*.; 2013.
169. Gomberg M. An instance of trivalent carbon: Triphenylmethyl. *J Am Chem Soc.* 1900;22(11):757-771. doi:10.1021/JA02049A006/ASSET/JA02049A006.FP.PNG_V03
170. Haber F, Weiss J, Seph JO, Eiss W. The catalytic decomposition of hydrogen peroxide by iron salts. *Proc R Soc Lond A Math Phys Sci.* 1934;147(861):332-351. doi:10.1098/RSPA.1934.0221
171. Harman D. Aging: a theory based on free radical and radiation chemistry. *J Gerontol.* 1956;11(3):298-300. doi:10.1093/GERONJ/11.3.298
172. Weiss SJ, King GW, LoBuglio AF. Evidence for hydroxyl radical generation by human Monocytes. *Journal of Clinical Investigation.* 1977;60(2):370. doi:10.1172/JCI108785
173. Sies H. *Oxidative Stress*. 1st ed. (Sies H, ed.). San Diego: Academic Press; 1985. Accessed October 18, 2024. <http://p5070-www.sciencedirect.com.ezproxy.herts.ac.uk/book/9780126427608/oxidative-stress>
174. Sies H, Jones DP. Reactive oxygen species (ROS) as pleiotropic physiological signalling agents. *Nat Rev Mol Cell Biol.Nature Research.* 2020;21(7):363-383. doi:10.1038/s41580-020-0230-3
175. Sies H, Berndt C, Jones DP. Oxidative Stress. *Annu Rev Biochem.* 2017;86:715-748. doi:10.1146/annurev-biochem-061516-045037
176. Snezhkina A V., Kudryavtseva A V., Kardymon OL, et al. ROS Generation and Antioxidant Defense Systems in Normal and Malignant Cells. *Oxid Med Cell Longev.* 2019;2019:6175804. doi:10.1155/2019/6175804
177. Mori MP, Penjweini R, Knutson JR, Wang P yuan, Hwang PM. Mitochondria and Oxygen Homeostasis. *FEBS J.* 2021;289(22):6959. doi:10.1111/FEBS.16115
178. Nolfi-Donagan D, Braganza A, Shiva S. Mitochondrial electron transport chain: Oxidative phosphorylation, oxidant production, and methods of measurement. *Redox Biol.* 2020;37:101674. doi:10.1016/J.REDOX.2020.101674
179. Faxén K, Gilderson G, Ädelroth P, Brzezinski P. A mechanistic principle for proton pumping by cytochrome c oxidase. *Nature* 2005 437:7056. 2005;437(7056):286-289. doi:10.1038/nature03921
180. Henderson JR, Swalwell H, Boulton S, Manning P, McNeil CJ, Birch-Machin MA. Direct, real-time monitoring of superoxide generation in isolated mitochondria. *Free Radic Res.* 2009;43(9):796-802. doi:10.1080/10715760903062895
181. Zhang L, Yu L, Yu CA. Generation of superoxide anion by succinate-cytochrome c reductase from bovine heart mitochondria. *J Biol Chem.* 1998;273(51):33972-33976. doi:10.1074/JBC.273.51.33972
182. Zhao RZ, Jiang S, Zhang L, Yu Z Bin. Mitochondrial electron transport chain, ROS generation and uncoupling (Review). *Int J Mol Med.* 2019;44(1):3. doi:10.3892/IJMM.2019.4188
183. Sena LA, Chandel NS. Physiological roles of mitochondrial reactive oxygen species. *Mol Cell.* 2012;48(2):158. doi:10.1016/J.MOLCEL.2012.09.025

184. Zito E. ERO1: A protein disulfide oxidase and H₂O₂ producer. *Free Radic Biol Med*. 2015;83:299-304. doi:10.1016/j.freeradbiomed.2015.01.011
185. Tu BP, Weissman JS. The FAD- and O₂-Dependent Reaction Cycle of Ero1-Mediated Oxidative Protein Folding in the Endoplasmic Reticulum. *Mol Cell*. 2002;10(5):983-994. doi:10.1016/S1097-2765(02)00696-2
186. Roscoe JM, Sevier CS. Pathways for Sensing and Responding to Hydrogen Peroxide at the Endoplasmic Reticulum. *Cells*. 2020;9(10):2314. doi:10.3390/CELLS9102314
187. Zhang IX, Raghavan M, Satin LS. The Endoplasmic Reticulum and Calcium Homeostasis in Pancreatic Beta Cells. *Endocrinology*. 2019;161(2):bqz028. doi:10.1210/ENDOCR/BQZ028
188. Bhattarai KR, Riaz TA, Kim HR, Chae HJ. The aftermath of the interplay between the endoplasmic reticulum stress response and redox signaling. *Experimental & Molecular Medicine 2021 53:2*. 2021;53(2):151-167. doi:10.1038/s12276-021-00560-8
189. Zeeshan HMA, Lee GH, Kim HR, Chae HJ. Endoplasmic Reticulum Stress and Associated ROS. *Int J Mol Sci*. 2016;17(3):327. doi:10.3390/IJMS17030327
190. Del Río LA, López-Huertas E. ROS Generation in Peroxisomes and its Role in Cell Signaling. *Plant Cell Physiol*. 2016;57(7):1364-1376. doi:10.1093/PCP/PCW076
191. Schrader M, Fahimi HD. Peroxisomes and oxidative stress. *Biochimica et Biophysica Acta (BBA) - Molecular Cell Research*. 2006;1763(12):1755-1766. doi:10.1016/J.BBAMCR.2006.09.006
192. Fransen M, Nordgren M, Wang B, Apanasets O. Role of peroxisomes in ROS/RNS-metabolism: Implications for human disease. *Biochimica et Biophysica Acta (BBA) - Molecular Basis of Disease*. 2012;1822(9):1363-1373. doi:10.1016/J.BBADIS.2011.12.001
193. Brandes RP, Weissmann N, Schröder K. Nox family NADPH oxidases: Molecular mechanisms of activation. *Free Radic Biol Med*. 2014;76:208-226. doi:10.1016/J.FREERADBIOMED.2014.07.046
194. Vermot A, Petit-Härtlein I, Smith SME, Fieschi F. NADPH Oxidases (NOX): An Overview from Discovery, Molecular Mechanisms to Physiology and Pathology. *Antioxidants*. 2021;10(6):890. doi:10.3390/ANTIOX10060890
195. Halliwell B, Gutteridge JMC. *Free Radicals in Biology and Medicine*. 4th ed. Oxford University Press; 2007. doi:10.1093/ACPROF:OSO/9780198717478.001.0001
196. Jomova K, Alomar SY, Alwasel SH, Nepovimova E, Kuca K, Valko M. Several lines of antioxidant defense against oxidative stress: antioxidant enzymes, nanomaterials with multiple enzyme-mimicking activities, and low-molecular-weight antioxidants. *Archives of Toxicology 2024 98:5*. 2024;98(5):1323-1367. doi:10.1007/S00204-024-03696-4
197. Fukai T, Ushio-Fukai M. Superoxide Dismutases: Role in Redox Signaling, Vascular Function, and Diseases. *Antioxid Redox Signal*. 2011;15(6):1583. doi:10.1089/ARS.2011.3999
198. Hsu JL, Hsieh Y, Tu C, O'Connor D, Nick HS, Silverman DN. Catalytic Properties of Human Manganese Superoxide Dismutase. *Journal of Biological Chemistry*. 1996;271(30):17687-17691. doi:10.1074/JBC.271.30.17687

199. McCord JM, Fridovich I. Superoxide dismutase. An enzymic function for erythrocuprein (hemocuprein). *J Biol Chem*. Published online June 23, 1969. Accessed May 2, 2025. <https://pubmed.ncbi.nlm.nih.gov/5389100/>
200. Chang LY, Slot JW, Geuze HJ, Crapo JD. Molecular immunocytochemistry of the CuZn superoxide dismutase in rat hepatocytes. *J Cell Biol*. 1988;107(6 Pt 1):2169-2179. doi:10.1083/JCB.107.6.2169
201. Sturtz LA, Diekert K, Jensen LT, Lill R, Culotta VC. A fraction of yeast Cu,Zn-superoxide dismutase and its metallochaperone, CCS, localize to the intermembrane space of mitochondria. A physiological role for SOD1 in guarding against mitochondrial oxidative damage. *J Biol Chem*. 2001;276(41):38084-38089. doi:10.1074/JBC.M105296200
202. Weisiger R, Fridovich I. Mitochondrial superoxide simutase. Site of synthesis and intramitochondrial localization - PubMed. *Journal of Biological Chemistry*. Published online 1973. Accessed May 2, 2025. <https://pubmed.ncbi.nlm.nih.gov/4578091/>
203. Marklund SL. Extracellular superoxide dismutase in human tissues and human cell lines. *Journal of Clinical Investigation*. 1984;74(4):1398. doi:10.1172/JCI111550
204. Karnati S, Lüers G, Pfreimer S, Baumgart-Vogt E. Mammalian SOD2 is exclusively located in mitochondria and not present in peroxisomes. *Histochem Cell Biol*. 2013;140(2):105-117. doi:10.1007/S00418-013-1099-4/METRICS
205. Alfonso-Prieto M, Biarnés X, Vidossich P, Rovira C. The molecular mechanism of the catalase reaction. *J Am Chem Soc*. 2009;131(33):11751-11761. doi:10.1021/JA9018572/SUPPL_FILE/JA9018572_SI_001.PDF
206. Kettle AJ, Winterbourn CC. A kinetic analysis of the catalase activity of myeloperoxidase. *Biochemistry*. 2001;40(34):10204-10212. doi:10.1021/BI010940B/ASSET/IMAGES/MEDIUM/BI010940BE00022.GIF
207. Walton PA, Pizzitelli M. Effects of peroxisomal catalase inhibition on mitochondrial function. *Front Physiol*. 2012;3 APR:23357. doi:10.3389/FPHYS.2012.00108/BIBTEX
208. Maiorino FM, Brigelius-Flohé R, Aumann KD, Roveri A, Schomburg D, Flohé L. Diversity of glutathione peroxidases. *Methods Enzymol*. 1995;252(C):38-48. doi:10.1016/0076-6879(95)52007-4
209. Brigelius-Flohé R, Maiorino M. Glutathione peroxidases. *Biochimica et Biophysica Acta (BBA) - General Subjects*. 2013;1830(5):3289-3303. doi:10.1016/J.BBAGEN.2012.11.020
210. Takebe G, Yarimizu J, Saito Y, et al. A Comparative Study on the Hydroperoxide and Thiol Specificity of the Glutathione Peroxidase Family and Selenoprotein P. *Journal of Biological Chemistry*. 2002;277(43):41254-41258. doi:10.1074/JBC.M202773200
211. Flohà L, Loschen G, Günzler WA, Eichele E. Glutathion Peroxidase, V. *Hoppe Seylers Z Physiol Chem*. 1972;353(1):987-1000. doi:10.1515/BCHM2.1972.353.1.987/PDF/FIRSTPAGE
212. Maiorino M, Ursini F, Bosello V, et al. The Thioredoxin Specificity of Drosophila GPx: A Paradigm for a Peroxiredoxin-like Mechanism of many Glutathione Peroxidases. *J Mol Biol*. 2007;365(4):1033-1046. doi:10.1016/J.JMB.2006.10.033
213. Flohé L, Toppo S, Cozza G, Ursini F. A Comparison of Thiol Peroxidase Mechanisms. <https://home.liebertpub.com/ars>. 2011;15(3):763-780. doi:10.1089/ARS.2010.3397

214. Brigelius-Flohé R, Aumann KD, Blöcker H, et al. Phospholipid-hydroperoxide glutathione peroxidase. Genomic DNA, cDNA, and deduced amino acid sequence. *Journal of Biological Chemistry*. 1994;269(10):7342-7348. doi:10.1016/S0021-9258(17)37290-3
215. Asayama K, Dobashi K, Hayashibe H, Nakazawa S, Yokota S, Kawaoi A. Purification and immunoelectron microscopic localization of cellular glutathione peroxidase in rat hepatocytes: quantitative analysis by postembedding method. *Histochemistry*. 1994;102(3):213-219. doi:10.1007/BF00268898/METRICS
216. Wei Z, Hao C, Radeen KR, et al. Deficiency in glutathione peroxidase 4 (GPX4) results in abnormal lens development and newborn cataract. *Proc Natl Acad Sci U S A*. 2024;121(48):e2407842121. doi:10.1073/PNAS.2407842121/SUPPL_FILE/PNAS.2407842121.SAPP.PDF
217. Nguyen VD, Saaranen MJ, Karala AR, et al. Two Endoplasmic Reticulum PDI Peroxidases Increase the Efficiency of the Use of Peroxide during Disulfide Bond Formation. *J Mol Biol*. 2011;406(3):503-515. doi:10.1016/J.JMB.2010.12.039
218. Zeida A, Reyes AM, Lebrero MCG, Radi R, Trujillo M, Estrin DA. The extraordinary catalytic ability of peroxiredoxins: a combined experimental and QM/MM study on the fast thiol oxidation step. *Chemical Communications*. 2014;50(70):10070-10073. doi:10.1039/C4CC02899F
219. Wood ZA, Schröder E, Harris JR, Poole LB. Structure, mechanism and regulation of peroxiredoxins. *Trends Biochem Sci*. 2003;28(1):32-40. doi:10.1016/S0968-0004(02)00003-8
220. Heo S, Kim S, Kang D. The Role of Hydrogen Peroxide and Peroxiredoxins throughout the Cell Cycle. *Antioxidants* 2020, Vol 9, Page 280. 2020;9(4):280. doi:10.3390/ANTIOX9040280
221. Wood ZA, Poole LB, Hantgan RR, Karplus PA. Dimers to doughnuts: Redox-sensitive oligomerization of 2-cysteine peroxiredoxins. *Biochemistry*. 2002;41(17):5493-5504. doi:10.1021/BI012173M
222. Choi J, Choi S, Choi J, Cha MK, Kim IH, Shin W. Crystal structure of Escherichia coli thiol peroxidase in the oxidized state: insights into intramolecular disulfide formation and substrate binding in atypical 2-Cys peroxiredoxins. *J Biol Chem*. 2003;278(49):49478-49486. doi:10.1074/JBC.M309015200/ASSET/9CE60609-66F5-4EA3-9791-8CC472E53592/MAIN.ASSETS/GR4.JPG
223. Monteiro G, Horta BB, Pimenta DC, Augusto O, Netto LES. Reduction of 1-Cys peroxiredoxins by ascorbate changes the thiol-specific antioxidant paradigm, revealing another function of vitamin C. *Proc Natl Acad Sci U S A*. 2007;104(12):4886-4891. doi:10.1073/PNAS.0700481104/SUPPL_FILE/00481FIG11.PDF
224. Manevich Y, Feinstein SI, Fisher AB. Activation of the antioxidant enzyme 1-CYS peroxiredoxin requires glutathionylation mediated by heterodimerization with π GST. *Proc Natl Acad Sci U S A*. 2004;101(11):3780. doi:10.1073/PNAS.0400181101
225. Montemartini M, Kalisz HM, Hecht HJ, Steinert P, Flohé L. Activation of active-site cysteine residues in the peroxiredoxin-type trypanothione peroxidase of Crithidia fasciculata. *Eur J Biochem*. 1999;264(2):516-524. doi:10.1046/J.1432-1327.1999.00656.X

226. Hyun AW, Jeong W, Chang TS, et al. Reduction of cysteine sulfinic acid by sulfiredoxin is specific to 2-Cys peroxiredoxins. *Journal of Biological Chemistry*. 2005;280(5):3125-3128. doi:10.1074/jbc.C400496200
227. Biteau B, Labarre J, Toledano MB. ATP-dependent reduction of cysteine–sulphinic acid by *S. cerevisiae* sulphiredoxin. *Nature* 2003 425:6961. 2003;425(6961):980-984. doi:10.1038/nature02075
228. Tejero I, González-Lafont Á, Lluch JM, Eriksson LA. Theoretical modeling of hydroxyl-radical-induced lipid peroxidation reactions. *J Phys Chem B*. 2007;111(20):5684-5693. doi:10.1021/JP0650782
229. Ayala A, Muñoz MF, Argüelles S. Lipid Peroxidation: Production, Metabolism, and Signaling Mechanisms of Malondialdehyde and 4-Hydroxy-2-Nonenal. *Oxid Med Cell Longev*. 2014;2014:360438. doi:10.1155/2014/360438
230. Yadav DK, Kumar S, Choi EH, Chaudhary S, Kim MH. Molecular dynamic simulations of oxidized skin lipid bilayer and permeability of reactive oxygen species. *Sci Rep*. 2019;9(1):4496. doi:10.1038/S41598-019-40913-Y
231. Juan CA, de la Lastra JMP, Plou FJ, Pérez-Lebeña E. The Chemistry of Reactive Oxygen Species (ROS) Revisited: Outlining Their Role in Biological Macromolecules (DNA, Lipids and Proteins) and Induced Pathologies. *Int J Mol Sci*. 2021;22(9):4642. doi:10.3390/IJMS22094642
232. Slatter DA, Bolton CH, Bailey AJ. The importance of lipid-derived malondialdehyde in diabetes mellitus. *Diabetologia*. 2000;43(5):550-557. doi:10.1007/S001250051342
233. Uchida K. Role of reactive aldehyde in cardiovascular diseases. *Free Radic Biol Med*. 2000;28(12):1685-1696. doi:10.1016/S0891-5849(00)00226-4
234. Cai F, Dupertuis YM, Pichard C. Role of polyunsaturated fatty acids and lipid peroxidation on colorectal cancer risk and treatments. *Curr Opin Clin Nutr Metab Care*. 2012;15(2):99-106. doi:10.1097/MCO.0B013E32834FEAB4
235. Spickett CM, Pitt AR. Protein oxidation: role in signalling and detection by mass spectrometry. *Amino Acids*. 2012;42(1):5-21. doi:10.1007/S00726-010-0585-4
236. Kehm R, Baldensperger T, Raupbach J, Höhn A. Protein oxidation - Formation mechanisms, detection and relevance as biomarkers in human diseases. *Redox Biol*. 2021;42:101901. doi:10.1016/J.REDOX.2021.101901
237. Smallwood MJ, Nissim A, Knight AR, Whiteman M, Haigh R, Winyard PG. Oxidative stress in autoimmune rheumatic diseases. *Free Radic Biol Med*. 2018;125:3-14. doi:10.1016/J.FREERADBIOMED.2018.05.086
238. Bickers DR, Athar M. Oxidative stress in the pathogenesis of skin disease. *J Invest Dermatol*. 2006;126(12):2565-2575. doi:10.1038/SJ.JID.5700340
239. Uttara B, Singh A V, Zamboni P, Mahajan RT. Oxidative Stress and Neurodegenerative Diseases: A Review of Upstream and Downstream Antioxidant Therapeutic Options. *Curr Neuroparmacol*. 2009;7(1):65. doi:10.2174/157015909787602823
240. Ock CY, Kim EH, Choi DJ, Lee HJ, Hahm KB, Chung MH. 8-Hydroxydeoxyguanosine: Not mere biomarker for oxidative stress, but remedy for oxidative stress-implicated gastrointestinal diseases. *World Journal of Gastroenterology: WJG*. 2012;18(4):302. doi:10.3748/WJG.V18.I4.302

241. Sharma V, Collins LB, Chen TH, et al. Oxidative stress at low levels can induce clustered DNA lesions leading to NHEJ mediated mutations. *Oncotarget*. 2016;7(18):25377. doi:10.18632/ONCOTARGET.8298
242. Kühbacher U, Duxin JP. How to fix DNA-protein crosslinks. *DNA Repair (Amst)*. 2020;94:102924. doi:10.1016/J.DNAREP.2020.102924
243. Van Remmen H, Hamilton ML, Richardson A. Oxidative damage to DNA and aging. *Exerc Sport Sci Rev*. 2003;31(3):149-153. doi:10.1097/00003677-200307000-00009
244. Bashir S, Harris G, Denman MA, Blake DR, Winyard PG. Oxidative DNA damage and cellular sensitivity to oxidative stress in human autoimmune diseases. *Ann Rheum Dis*. 1993;52(9):659-666. doi:10.1136/ARD.52.9.659
245. Tubbs A, Nussenzweig A. Endogenous DNA Damage as a Source of Genomic Instability in Cancer. *Cell*. 2017;168(4):644. doi:10.1016/J.CELL.2017.01.002
246. Redza-Dutordoir M, Averill-Bates DA. Activation of apoptosis signalling pathways by reactive oxygen species. *Biochimica et Biophysica Acta (BBA) - Molecular Cell Research*. 2016;1863(12):2977-2992. doi:10.1016/J.BBAMCR.2016.09.012
247. Petrosillo G, Ruggiero FM, Pistolese M, Paradies G. Reactive oxygen species generated from the mitochondrial electron transport chain induce cytochrome c dissociation from beef-heart submitochondrial particles via cardiolipin peroxidation. Possible role in the apoptosis. *FEBS Lett*. 2001;509(3):435-438. doi:10.1016/S0014-5793(01)03206-9
248. Tabas I, Ron D. Integrating the mechanisms of apoptosis induced by endoplasmic reticulum stress. *Nat Cell Biol*. 2011;13(3):184. doi:10.1038/NCB0311-184
249. Yoshida K, Miki Y. The cell death machinery governed by the p53 tumor suppressor in response to DNA damage. *Cancer Sci*. 2010;101(4):831-835. doi:10.1111/J.1349-7006.2009.01488.X
250. Kruk J, Aboul-Enein HY, Kładna A, Bowser JE. Oxidative stress in biological systems and its relation with pathophysiological functions: the effect of physical activity on cellular redox homeostasis. *Free Radic Res*. 2019;53(5):497-521. doi:10.1080/10715762.2019.1612059
251. Bélanger M, Allaman I, Magistretti PJ. Brain energy metabolism: Focus on Astrocyte-neuron metabolic cooperation. *Cell Metab*. 2011;14(6):724-738. doi:10.1016/J.CMET.2011.08.016/ASSET/CE6E545D-1AC8-4AA8-9AE0-3D4919723C8D/MAIN.ASSETS/GR3.JPG
252. Lundgaard I, Li B, Xie L, et al. Direct neuronal glucose uptake heralds activity-dependent increases in cerebral metabolism. *Nature Communications* 2015 6:1. 2015;6(1):1-12. doi:10.1038/ncomms7807
253. Friedman J. Why Is the Nervous System Vulnerable to Oxidative Stress? *Oxidative Stress and Free Radical Damage in Neurology*. Published online 2011:19-27. doi:10.1007/978-1-60327-514-9_2
254. Shichiri M. The role of lipid peroxidation in neurological disorders. *J Clin Biochem Nutr*. 2014;54(3):151. doi:10.3164/JCBN.14-10
255. Kvistad CE, Kråkenes T, Gavasso S, Bø L. Neural regeneration in the human central nervous system—from understanding the underlying mechanisms to developing

- treatments. Where do we stand today? *Front Neurol.* 2024;15:1398089. doi:10.3389/FNEUR.2024.1398089
256. Mecocci P, MacGarvey U, Kaufman AE, et al. Oxidative damage to mitochondrial DNA shows marked age-dependent increases in human brain. *Ann Neurol.* 1993;34(4):609-616. doi:10.1002/ANA.410340416
 257. Hou Y, Dan X, Babbar M, et al. Ageing as a risk factor for neurodegenerative disease. *Nature Reviews Neurology* 2019 15:10. 2019;15(10):565-581. doi:10.1038/s41582-019-0244-7
 258. Singh A, Kukreti R, Saso L, Kukreti S. Oxidative Stress: A Key Modulator in Neurodegenerative Diseases. *Molecules.* 2019;24(8):1583. doi:10.3390/MOLECULES24081583
 259. Serrano-Pozo A, Frosch MP, Masliah E, Hyman BT. Neuropathological Alterations in Alzheimer Disease. *Cold Spring Harb Perspect Med.* 2011;1(1):a006189. doi:10.1101/CSHPERSPECT.A006189
 260. De-Paula VJ, Radanovic M, Diniz BS, Forlenza O V. Alzheimer's Disease. *Subcell Biochem.* 2012;65:329-352. doi:10.1007/978-94-007-5416-4_14
 261. Zhao Y, Zhao B. Oxidative stress and the pathogenesis of alzheimer's disease. *Oxid Med Cell Longev.* 2013;2013. doi:10.1155/2013/316523,
 262. Wang X, Wang W, Li L, Perry G, Lee H gon, Zhu X. Oxidative stress and mitochondrial dysfunction in Alzheimer's disease. *Biochimica et Biophysica Acta (BBA) - Molecular Basis of Disease.* 2014;1842(8):1240-1247. doi:10.1016/J.BBADIS.2013.10.015
 263. La Penna G, Hureau C, Andreussi O, Faller P. Identifying, by first-principles simulations, Cu[Amyloid- β] species making Fenton-type reactions in Alzheimer's disease. *Journal of Physical Chemistry B.* 2013;117(51):16455-16467. doi:10.1021/JP410046W/SUPPL_FILE/JP410046W_SI_001.PDF
 264. Cai Z, Zhao B, Ratka A. Oxidative Stress and β -Amyloid Protein in Alzheimer's Disease. *NeuroMolecular Medicine* 2011 13:4. 2011;13(4):223-250. doi:10.1007/S12017-011-8155-9
 265. Dias V, Junn E, Mouradian MM. The Role of Oxidative Stress in Parkinson's Disease. *J Parkinsons Dis.* 2013;3(4):461. doi:10.3233/JPD-130230
 266. Muñoz P, Huenchuguala S, Paris I, Segura-Aguilar J. Dopamine Oxidation and Autophagy. *Parkinsons Dis.* 2012;2012:920953. doi:10.1155/2012/920953
 267. Kim GH, Kim JE, Rhie SJ, Yoon S. The Role of Oxidative Stress in Neurodegenerative Diseases. *Exp Neurobiol.* 2015;24(4):325-340. doi:10.5607/EN.2015.24.4.325,
 268. Fu AL, Dong ZH, Sun MJ. Protective effect of N-acetyl-l-cysteine on amyloid β -peptide-induced learning and memory deficits in mice. *Brain Res.* 2006;1109(1):201-206. doi:10.1016/J.BRAINRES.2006.06.042
 269. Tchanchou F, Graves M, Rogers E, Ortiz D, Shea TB. N-acteyl cysteine alleviates oxidative damage to central nervous system of ApoE-deficient mice following folate and vitamin E-deficiency. <https://doi.org/10.3233/JAD-2005-7206>. 2005;7(2):135-138. doi:10.3233/JAD-2005-7206

270. Kawamoto EM, Scavone C, Mattson MP, Camandola S. Curcumin Requires Tumor Necrosis Factor α Signaling to Alleviate Cognitive Impairment Elicited by Lipopolysaccharide. *Neurosignals*. 2012;21(1-2):75. doi:10.1159/000336074
271. Shao S, Ye X, Su W, Wang Y. Curcumin alleviates Alzheimer's disease by inhibiting inflammatory response, oxidative stress and activating the AMPK pathway. *J Chem Neuroanat*. 2023;134:102363. doi:10.1016/J.JCHEMNEU.2023.102363
272. Lim GP, Chu T, Yang F, Beech W, Frautschy SA, Cole GM. The Curry Spice Curcumin Reduces Oxidative Damage and Amyloid Pathology in an Alzheimer Transgenic Mouse. *Journal of Neuroscience*. 2001;21(21):8370-8377. doi:10.1523/JNEUROSCI.21-21-08370.2001
273. Liu ZJ, Li ZH, Liu L, et al. Curcumin Attenuates Beta-Amyloid-Induced Neuroinflammation via Activation of Peroxisome Proliferator-Activated Receptor-Gamma Function in a Rat Model of Alzheimer's Disease. *Front Pharmacol*. 2016;7(AUG):261. doi:10.3389/FPHAR.2016.00261
274. Murakami K, Murata N, Ozawa Y, et al. Vitamin C Restores Behavioral Deficits and Amyloid- β Oligomerization without Affecting Plaque Formation in a Mouse Model of Alzheimer's Disease. <https://doi.org/10.3233/JAD-2011-101971>. 2011;26(1):7-18. doi:10.3233/JAD-2011-101971
275. Rezai-Zadeh K, Shytle D, Sun N, et al. Green Tea Epigallocatechin-3-Gallate (EGCG) Modulates Amyloid Precursor Protein Cleavage and Reduces Cerebral Amyloidosis in Alzheimer Transgenic Mice. *The Journal of Neuroscience*. 2005;25(38):8807. doi:10.1523/JNEUROSCI.1521-05.2005
276. Rezai-Zadeh K, Arendash GW, Hou H, et al. Green tea epigallocatechin-3-gallate (EGCG) reduces β -amyloid mediated cognitive impairment and modulates tau pathology in Alzheimer transgenic mice. *Brain Res*. 2008;1214:177-187. doi:10.1016/J.BRAINRES.2008.02.107
277. Lee YK, Yuk DY, Lee JW, et al. (-)-Epigallocatechin-3-gallate prevents lipopolysaccharide-induced elevation of beta-amyloid generation and memory deficiency. *Brain Res*. 2009;1250:164-174. doi:10.1016/J.BRAINRES.2008.10.012
278. Lee YJ, Choi DY, Yun YP, Han SB, Oh KW, Hong JT. Epigallocatechin-3-gallate prevents systemic inflammation-induced memory deficiency and amyloidogenesis via its anti-neuroinflammatory properties. *J Nutr Biochem*. 2013;24(1):298-310. doi:10.1016/J.JNUTBIO.2012.06.011
279. Li XC, Wang ZF, Zhang JX, Wang Q, Wang JZ. Effect of melatonin on calyculin A-induced tau hyperphosphorylation. *Eur J Pharmacol*. 2005;510(1-2):25-30. doi:10.1016/J.EJPHAR.2005.01.023
280. Feng Z, Zhang JT. Protective effect of melatonin on β -amyloid-induced apoptosis in rat astrogloma c6 cells and its mechanism. *Free Radic Biol Med*. 2004;37(11):1790-1801. doi:10.1016/J.FREERADBIOMED.2004.08.023
281. Matsubara E, Bryant-Thomas T, Quinto JP, et al. Melatonin increases survival and inhibits oxidative and amyloid pathology in a transgenic model of Alzheimer's disease. *J Neurochem*. 2003;85(5):1101-1108. doi:10.1046/J.1471-4159.2003.01654.X;JOURNAL:JOURNAL:14714159;WGROU:STRING:PUBLICATION

282. Feng Z, Chang Y, Cheng Y, et al. Melatonin alleviates behavioral deficits associated with apoptosis and cholinergic system dysfunction in the APP 695 transgenic mouse model of Alzheimer's disease. *J Pineal Res.* 2004;37(2):129-136. doi:10.1111/J.1600-079X.2004.00144.X
283. Rosales-Corral S, Tan DX, Reiter RJ, et al. Orally administered melatonin reduces oxidative stress and proinflammatory cytokines induced by amyloid-beta peptide in rat brain: a comparative, in vivo study versus vitamin C and E. *J Pineal Res.* 2003;35(2):80-84. doi:10.1034/J.1600-079X.2003.00057.X
284. Offen D, Ziv I, Sternin H, Melamed E, Hochman A. Prevention of Dopamine-Induced Cell Death by Thiol Antioxidants: Possible Implications for Treatment of Parkinson's Disease. *Exp Neurol.* 1996;141(1):32-39. doi:10.1006/EXNR.1996.0136
285. Cocco T, Sgobbo P, Clemente M, et al. Tissue-specific changes of mitochondrial functions in aged rats: Effect of a long-term dietary treatment with N-acetylcysteine. *Free Radic Biol Med.* 2005;38(6):796-805. doi:10.1016/J.FREERADBIOMED.2004.11.034
286. Siddique YH, Naz F, Jyoti S. Effect of Curcumin on Lifespan, Activity Pattern, Oxidative Stress, and Apoptosis in the Brains of Transgenic Drosophila Model of Parkinson's Disease. *Biomed Res Int.* 2014;2014(1):606928. doi:10.1155/2014/606928
287. Chakraborty S, Karmenyan A, Tsai JW, Chiou A. Inhibitory effects of curcumin and cyclocurcumin in 1-methyl-4-phenylpyridinium (MPP+) induced neurotoxicity in differentiated PC12 cells. *Sci Rep.* 2017;7(1):16977. doi:10.1038/S41598-017-17268-3
288. He HJ, Xiong X, Zhou S, et al. Neuroprotective effects of curcumin via autophagy induction in 6-hydroxydopamine Parkinson's models. *Neurochem Int.* 2022;155:105297. doi:10.1016/J.NEUINT.2022.105297
289. Sil S, Ghosh T, Gupta P, Ghosh R, Kabir SN, Roy A. Dual Role of Vitamin C on the Neuroinflammation Mediated Neurodegeneration and Memory Impairments in Colchicine Induced Rat Model of Alzheimer Disease. *Journal of Molecular Neuroscience.* 2016;60(4):421-435. doi:10.1007/S12031-016-0817-5/METRICS
290. Levites Y, Weinreb O, Maor G, Youdim MBH, Mandel S. Green tea polyphenol (-)-epigallocatechin-3-gallate prevents N-methyl-4-phenyl- 1,2,3,6-tetrahydropyridine-induced dopaminergic neurodegeneration. *J Neurochem.* 2001;78(5):1073-1082. doi:10.1046/J.1471-4159.2001.00490.X
291. Xu Q, Langley M, Kanthasamy AG, Reddy MB. Epigallocatechin Gallate Has a Neurorescue Effect in a Mouse Model of Parkinson Disease. *J Nutr.* 2017;147(10):1926. doi:10.3945/JN.117.255034
292. Zhou T, Zhu M, Liang Z. (-)-Epigallocatechin-3-gallate modulates peripheral immunity in the MPTP-induced mouse model of Parkinson's disease. *Mol Med Rep.* 2018;17(4):4883. doi:10.3892/MMR.2018.8470
293. Tseng HC, Wang MH, Chang KC, et al. Protective Effect of (-)Epigallocatechin-3-gallate on Rotenone-Induced Parkinsonism-like Symptoms in Rats. *Neurotox Res.* 2020;37(3):669-682. doi:10.1007/S12640-019-00143-6
294. Sharma R, McMillan CR, Tenn CC, Niles LP. Physiological neuroprotection by melatonin in a 6-hydroxydopamine model of Parkinson's disease. *Brain Res.* 2006;1068(1):230-236. doi:10.1016/J.BRAINRES.2005.10.084

295. Dabbeni-Sala F, Santo S, Franceschini D, D. Skaper S, Pietro G. Melatonin protects against 6-OHDA-induced neurotoxicity in rats: a role for mitochondrial complex I activity. *The FASEB Journal*. 2001;15(1):164-170. doi:10.1096/FJ.00-0129COM;REQUESTEDJOURNAL:JOURNAL:15306860;WGROUP:STRING:PUBLICATION
296. Mayo JC, Sainz RM, Uria H, Antolin I, Esteban MM, Rodriguez C. Melatonin prevents apoptosis induced by 6-hydroxydopamine in neuronal cells: Implications for Parkinson's disease. *J Pineal Res*. 1998;24(3):179-192. doi:10.1111/J.1600-079X.1998.TB00531.X;REQUESTEDJOURNAL:JOURNAL:1600079X
297. Wang ZB, Zhang X, Li XJ. Recapitulation of spinal motor neuron-specific disease phenotypes in a human cell model of spinal muscular atrophy. *Cell Res*. 2013;23(3):378. doi:10.1038/CR.2012.166
298. Ando S, Funato M, Ohuchi K, et al. Edaravone is a candidate agent for spinal muscular atrophy: In vitro analysis using a human induced pluripotent stem cells-derived disease model. *Eur J Pharmacol*. 2017;814:161-168. doi:10.1016/J.EJPHAR.2017.08.005
299. Thelen MP, Wirth B, Kye MJ. Mitochondrial defects in the respiratory complex I contribute to impaired translational initiation via ROS and energy homeostasis in SMA motor neurons. *Acta Neuropathol Commun*. 2020;8(1). doi:10.1186/S40478-020-01101-6
300. Miller N, Shi H, Zelikovich AS, Ma YC. Motor neuron mitochondrial dysfunction in spinal muscular atrophy. *Hum Mol Genet*. 2016;25(16):3395. doi:10.1093/HMG/DDW262
301. Chemello F, Pozzobon M, Tsansizi LI, et al. Dysfunctional mitochondria accumulate in a skeletal muscle knockout model of Smn1, the causal gene of spinal muscular atrophy. *Cell Death & Disease* 2023 14:2. 2023;14(2):1-13. doi:10.1038/s41419-023-05573-x
302. Patitucci TN, Ebert AD. SMN deficiency does not induce oxidative stress in SMA iPSC-derived astrocytes or motor neurons. *Hum Mol Genet*. 2016;25(3):514-523. doi:10.1093/HMG/DDV489
303. El Khoury M, Biondi O, Bruneteau G, et al. NADPH oxidase 4 inhibition is a complementary therapeutic strategy for spinal muscular atrophy. *Front Cell Neurosci*. 2023;17. doi:10.3389/FNCEL.2023.1242828/PDF
304. Hayashi M, Araki S, Arai N, et al. Oxidative stress and disturbed glutamate transport in spinal muscular atrophy. *Brain Dev*. 2002;24(8):770-775. doi:10.1016/S0387-7604(02)00103-1
305. Maxwell GK, Szunyogova E, Shorrock HK, Gillingwater TH, Parson SH. Developmental and degenerative cardiac defects in the Taiwanese mouse model of severe spinal muscular atrophy. *J Anat*. 2018;232(6):965-978. doi:10.1111/joa.12793
306. Shababi M, Habibi J, Ma L, Glascock JJ, Sowers JR, Lorson CL. Partial Restoration of Cardio-Vascular Defects in Rescued Severe Model of Spinal Muscular Atrophy. *J Mol Cell Cardiol*. 2012;52(5):1074. doi:10.1016/J.YJMCC.2012.01.005
307. Majtnerová P, Roušar T. An overview of apoptosis assays detecting DNA fragmentation. *Mol Biol Rep*. 2018;45(5):1469-1478. doi:10.1007/S11033-018-4258-9,

308. Schultz J, Lee SJ, Cole T, et al. The secreted MSP domain of *C. elegans* VAPB homolog VPR-1 patterns the adult striated muscle mitochondrial reticulum via SMN-1. *Development*. 2017;144(12):2175. doi:10.1242/DEV.152025
309. Seo J, Singh NN, Ottesen EW, Sivanesan S, Shishimorova M, Singh RN. Oxidative Stress Triggers Body-Wide Skipping of Multiple Exons of the Spinal Muscular Atrophy Gene. *PLoS One*. 2016;11(4). doi:10.1371/JOURNAL.PONE.0154390
310. Sakla MS, Lorson CL. Induction of full-length survival motor neuron by polyphenol botanical compounds. *Hum Genet*. 2008;122(6):635-643. doi:10.1007/S00439-007-0441-0/FIGURES/6
311. Dayangac-Erden D, Bora-Tatar G, Dalkara S, Demir AS, Erdem-Yurter H. Carboxylic acid derivatives of histone deacetylase inhibitors induce full length SMN2 transcripts: a promising target for spinal muscular atrophy therapeutics. *Arch Med Sci*. 2011;7(2):230. doi:10.5114/AOMS.2011.22072
312. Kelly WK, O'Connor OA, Marks PA. Histone deacetylase inhibitors: From target to clinical trials. *Expert Opin Investig Drugs*. 2002;11(12):1695-1713. doi:10.1517/13543784.11.12.1695,
313. Van Raamsdonk MJ, Hekimi S. Reactive Oxygen Species and Aging in *Caenorhabditis elegans*: Causal or Casual Relationship? *Antioxid Redox Signal*. 2010;13.
314. Brenner S. The Genetics of *Caenorhabditis elegans*. *Genetics*. 1974;77(1):71. doi:10.1093/GENETICS/77.1.71
315. Stiernagle T. Maintenance of *C. elegans*. *WormBook*. Published online 2006:1-11. doi:10.1895/WORMBOOK.1.101.1
316. Stastna JJ, Yiapanas AD, Mandawala AA, Fowler KE, Harvey SC. Cryopreservation produces limited long-term effects on the nematode *Caenorhabditis elegans*. *Cryobiology*. 2020;92:86-91. doi:10.1016/J.CRYOBIOL.2019.11.039
317. Murray KA, Gibson MI. Chemical approaches to cryopreservation. *Nature Reviews Chemistry* 2022 6:8. 2022;6(8):579-593. doi:10.1038/s41570-022-00407-4
318. Ahamefule CS, Ezeudji BC, Ogbonna JC, et al. *Caenorhabditis elegans* as an Infection Model for Pathogenic Mold and Dimorphic Fungi: Applications and Challenges. *Front Cell Infect Microbiol*. 2021;11:751947. doi:10.3389/FCIMB.2021.751947
319. O'Donnell MP, Fox BW, Chao PH, Schroeder FC, Sengupta P. A neurotransmitter produced by gut bacteria modulates host sensory behaviour. *Nature* 2020 583:7816. 2020;583(7816):415-420. doi:10.1038/s41586-020-2395-5
320. Stein KK, Golden A. The *C. elegans* eggshell. *WormBook*. Published online 2018:1-36. doi:10.1895/WORMBOOK.1.179.1
321. Dimitriadis M, Sleight JN, Walker A, et al. Conserved Genes Act as Modifiers of Invertebrate SMN Loss of Function Defects. *PLoS Genet*. 2010;6(10):e1001172. doi:10.1371/JOURNAL.PGEN.1001172
322. Roux AE, Langhans K, Huynh W, Kenyon C. Reversible Age-Related Phenotypes Induced during Larval Quiescence in *C. elegans*. *Cell Metab*. 2016;23(6):1113. doi:10.1016/J.CMET.2016.05.024

323. Aspernig H, Heimbucher T, Qi W, et al. Mitochondrial Perturbations Couple mTORC2 to Autophagy in *C. elegans*. *Cell Rep.* 2019;29(6):1399-1409.e5. doi:10.1016/J.CELREP.2019.09.072/ATTACHMENT/7C9C1C71-D6E3-429E-A957-E15B3549CC25/MMC2.PDF
324. Hsiung KC, Liu KY, Tsai TF, et al. Defects in C1SD-1, a mitochondrial iron-sulfur protein, lower glucose level and ATP production in *Caenorhabditis elegans*. *Biomed J.* 2020;43(1):32. doi:10.1016/J.BJ.2019.07.009
325. Coppa A, Guha S, Fourcade S, et al. The peroxisomal fatty acid transporter ABCD1/PMP-4 is required in the *C. elegans* hypodermis for axonal maintenance: A worm model for adrenoleukodystrophy. *Free Radic Biol Med.* 2020;152:797-809. doi:10.1016/J.FREERADBIOMED.2020.01.177
326. Gandhi S, Santelli J, Mitchell DH, Wesley Stiles J, Rao Sanadi D. A simple method for maintaining large, aging populations of *Caenorhabditis elegans*. *Mech Ageing Dev.* 1980;12(2):137-150. doi:10.1016/0047-6374(80)90090-1
327. Rooney JP, Luz AL, González-Hunt CP, et al. Effects of 5'-fluoro-2-deoxyuridine on mitochondrial biology in *Caenorhabditis elegans*. *Exp Gerontol.* 2014;56:69-76. doi:10.1016/J.EXGER.2014.03.021
328. Anderson EN, Corkins ME, Li JC, et al. *C. elegans* lifespan extension by osmotic stress requires FUDR, base excision repair, FOXO, and sirtuins. *Mech Ageing Dev.* 2016;154:30-42. doi:10.1016/J.MAD.2016.01.004
329. Senchuk M, Dues D, Van Raamsdonk J. Measuring Oxidative Stress in *Caenorhabditis elegans*: Paraquat and Juglone Sensitivity Assays. *Bio Protoc.* 2017;7(1). doi:10.21769/BIOPROTOCOL.2086
330. Zevian SC, Yanowitz JL. Methodological Considerations for Heat Shock of the Nematode *Caenorhabditis elegans*. *Methods.* 2014;68(3):450. doi:10.1016/J.YMETH.2014.04.015
331. Wheeler JM, Thomas JH. Identification of a novel gene family involved in osmotic stress response in *Caenorhabditis elegans*. *Genetics.* 2006;174(3):1327-1336. doi:10.1534/GENETICS.106.059089
332. Scholz M, Lynch DJ, Lee KS, Levine E, Biron D. A scalable method for automatically measuring pharyngeal pumping in *C. elegans*. *J Neurosci Methods.* 2016;274:172-178. doi:10.1016/J.JNEUMETH.2016.07.016
333. AlOkda A, Van Raamsdonk JM. Effect of DMSO on lifespan and physiology in *C. elegans* : Implications for use of DMSO as a solvent for compound delivery. *MicroPubl Biol.* 2022;2022. doi:10.17912/MICROPUB.BIOLOGY.000634,
334. Love MI, Anders S, Kim V, Huber W. RNA-Seq workflow: gene-level exploratory analysis and differential expression. *F1000Res.* 2015;4:1070. doi:10.12688/F1000RESEARCH.7035.1
335. Anders S, Huber W. Differential expression analysis for sequence count data. *Genome Biol.* 2010;11(10):R106. doi:10.1186/GB-2010-11-10-R106
336. Ashburner M, Ball CA, Blake JA, et al. Gene Ontology: tool for the unification of biology. *Nat Genet.* 2000;25(1):25. doi:10.1038/75556
337. Aleksander SA, Balhoff J, Carbon S, et al. The Gene Ontology knowledgebase in 2023. *Genetics.* 2023;224(1):iyad031. doi:10.1093/GENETICS/IYAD031

338. Kanehisa M, Araki M, Goto S, et al. KEGG for linking genomes to life and the environment. *Nucleic Acids Res.* 2007;36(Database issue):D480. doi:10.1093/NAR/GKM882
339. Carlson M. AnnotationDbi: Introduction To Bioconductor Annotation Packages. Bioconductor.
340. Wu T, Hu E, Xu S, et al. clusterProfiler 4.0: A universal enrichment tool for interpreting omics data. *The Innovation.* 2021;2(3):100141. doi:10.1016/J.XINN.2021.100141
341. Yu G, Wang LG, Han Y, He QY. clusterProfiler: an R Package for Comparing Biological Themes Among Gene Clusters. *OMICS.* 2012;16(5):284. doi:10.1089/OMI.2011.0118
342. Mootha VK, Lindgren CM, Eriksson KF, et al. PGC-1 α -responsive genes involved in oxidative phosphorylation are coordinately downregulated in human diabetes. *Nature Genetics* 2003 34:3. 2003;34(3):267-273. doi:10.1038/ng1180
343. Subramanian A, Tamayo P, Mootha VK, et al. Gene set enrichment analysis: A knowledge-based approach for interpreting genome-wide expression profiles. *Proc Natl Acad Sci U S A.* 2005;102(43):15545. doi:10.1073/PNAS.0506580102
344. Zhang Y, Kiryu H. Identification of oxidative stress-related genes differentially expressed in Alzheimer's disease and construction of a hub gene-based diagnostic model. *Scientific Reports* 2023 13:1. 2023;13(1):1-15. doi:10.1038/s41598-023-34021-1
345. Baskoylu SN, Yersak J, O'Hern P, et al. Single copy/knock-in models of ALS SOD1 in *C. elegans* suggest loss and gain of function have different contributions to cholinergic and glutamatergic neurodegeneration. *PLoS Genet.* 2018;14(10). doi:10.1371/journal.pgen.1007682
346. Keith SA, Amrit FRG, Ratnappan R, Ghazi A. The *C. elegans* healthspan and stress-resistance assay toolkit. *Methods.* 2014;68(3):476-486. doi:10.1016/J.YMETH.2014.04.003
347. Sharma A, Kumar V, Shahzad B, et al. Worldwide pesticide usage and its impacts on ecosystem. *SN Appl Sci.* 2019;1(11):1-16. doi:10.1007/S42452-019-1485-1/TABLES/4
348. Clark AM, Jurgens TM, Hufford CD. Antimicrobial activity of juglone. *Phytotherapy Research.* 1990;4(1):11-14. doi:10.1002/PTR.2650040104
349. Sugie S, Okamoto K, Rahman KMW, et al. Inhibitory effects of plumbagin and juglone on azoxymethane-induced intestinal carcinogenesis in rats. *Cancer Lett.* 1998;127(1-2):177-183. doi:10.1016/S0304-3835(98)00035-4
350. Zhang W, Liu A, Li Y, et al. Anticancer activity and mechanism of juglone on human cervical carcinoma HeLa cells. *Can J Physiol Pharmacol.* 2012;90(11):1553-1558. doi:10.1139/Y2012-134
351. Fang F, Chen S, Ma J, et al. Juglone suppresses epithelial-mesenchymal transition in prostate cancer cells via the protein kinase b/glycogen synthase kinase-3 β /snail signaling pathway. *Oncol Lett.* 2018;16(2):2579-2584. doi:10.3892/OL.2018.8885/DOWNLOAD
352. Ahmad T, Suzuki YJ. Juglone in oxidative stress and cell signaling. *Antioxidants.MDPI.* 2019;8(4). doi:10.3390/antiox8040091
353. Bus JS, Gibson JE. *Paraquat: Model for Oxidant-Initiated Toxicity.* Vol 55.; 1984.

354. Dinis-Oliveira RJ, Duarte JA, Sánchez-Navarro A, Remião F, Bastos ML, Carvalho F. Paraquat poisonings: Mechanisms of lung toxicity, clinical features, and treatment. *Crit Rev Toxicol.* 2008;38(1):13-71. doi:10.1080/10408440701669959
355. Ollinger K, Brunmark A. Effect of Hydroxy Substituent Position on 1,4-Naphthoquinone Toxicity to Rat Hepatocytes*. *J Biol Chem.* 1991;266(32):2149621503.
356. Reczek CR, Birsoy K, Kong H, et al. A CRISPR screen identifies a pathway required for paraquat-induced cell death. *Nat Chem Biol.* 2017;13(12):1274-1279. doi:10.1038/nchembio.2499
357. Fukushima T, Yamada K, Isobe A, Shiwaku K, Yamane Y. Mechanism of cytotoxicity of paraquat: I.NADH oxidation and paraquat radical formation via complex I. *Experimental and Toxicologic Pathology.* 1993;45(5-6):345-349. doi:10.1016/S0940-2993(11)80424-0
358. Winterbourn CC. Production of hydroxyl radicals from paraquat radicals and H₂O₂. *FEBS Lett.* 1981;128(2):339-342. doi:10.1016/0014-5793(81)80112-3
359. Gray JP, Heck DE, Mishin V, et al. Paraquat increases cyanide-insensitive respiration in murine lung epithelial cells by activating an NAD(P)H:Paraquat oxidoreductase: Identification of the enzyme as thioredoxin reductase. *Journal of Biological Chemistry.* 2007;282(11):7939-7949. doi:10.1074/JBC.M611817200/ASSET/F51BCCBE-BA2D-4792-82BA-1930445012C1/MAIN.ASSETS/GR8.JPG
360. Muto N, Inouye K, Inada A, Nakanishi T, Tan L. Inhibition of cytochrome P-450-linked monooxygenase systems by naphthoquinones. *Biochem Biophys Res Commun.* 1987;146(2):487-494. doi:10.1016/0006-291X(87)90555-9
361. Anderson WM, Delinck DL, Benninger L, Wood JM, Smiley ST, Chen LB. Cytotoxic effect of thiocarbocyanine dyes on human colon carcinoma cells and inhibition of bovine heart mitochondrial NADH-ubiquinone reductase activity via a rotenone-type mechanism by two of the dyes. *Biochem Pharmacol.* 1993;45(3):691-696. doi:10.1016/0006-2952(93)90144-L
362. Lewis DC, Shibamoto T. Relative metabolism of quinones to semiquinone radicals in xanthine oxidase system. *J Appl Toxicol.* 1989;9(5):291-295. doi:10.1002/JAT.2550090502
363. Zhang RL, Hirsch O, Mohsen M, Samuni A. Effects of Nitroxide Stable Radicals on Juglone Cytotoxicity. *Arch Biochem Biophys.* 1994;312(2):385-391. doi:10.1006/ABBI.1994.1323
364. Keeling PL, Smith LL. Relevance of NADPH depletion and mixed disulphide formation in rat lung to the mechanism of cell damage following paraquat administration. *Biochem Pharmacol.* 1982;31(20):3243-3249. doi:10.1016/0006-2952(82)90557-3
365. Doherty MDA, Rodgers A, Cohen GM. Mechanisms of toxicity of 2- and 5-hydroxy-1,4-naphthoquinone; absence of a role for redox cycling in the toxicity of 2-hydroxy-1,4-naphthoquinone to isolated hepatocytes. *Journal of Applied Toxicology.* 1987;7(2):123-129. doi:10.1002/JAT.2550070209
366. Kappus H, Sies H. Toxic drug effects associated with oxygen metabolism: redox cycling and lipid peroxidation. *Experientia.* 1981;37(12):1233-1241. doi:10.1007/BF01948335
367. Kumbhar AS, Padhye SB, Jitender, Kale RK. Naturally Occurring Hydroxy Naphthoquinones and Their Iron Complexes as Modulators of Radiation Induced Lipid

- Peroxidation in Synaptosomes. *Met Based Drugs*. 1997;4(5):279. doi:10.1155/MBD.1997.279
368. Chao SH, Greenleaf AL, Price DH. Juglone, an inhibitor of the peptidyl-prolyl isomerase Pin1, also directly blocks transcription. *Nucleic Acids Res*. 2001;29(3):767. doi:10.1093/NAR/29.3.767
 369. Suyal S, Choudhury C, Kaur D, Bachhawat AK, Nagar SAS. Identification of Juglone, a 'first-in-class' inhibitor of the human glutathione degrading enzyme, ChaC1, using yeast-based high throughput screens. *bioRxiv*. Published online July 22, 2024:2024.07.21.604522. doi:10.1101/2024.07.21.604522
 370. Kwiecinski MR, Pedrosa RC, Felipe KB, et al. Inhibition of cell proliferation and migration by oxidative stress from ascorbate-driven juglone redox cycling in human bladder-derived T24 cells. *Biochem Biophys Res Commun*. 2012;421(2):268-273. doi:10.1016/J.BBRC.2012.03.150
 371. Paulsen MT, Ljungman M. The natural toxin juglone causes degradation of p53 and induces rapid H2AX phosphorylation and cell death in human fibroblasts. *Toxicol Appl Pharmacol*. 2005;209(1):1-9. doi:10.1016/J.TAAP.2005.03.005
 372. Erkoç-Kaya D, Arikoglu H, Guclu E, Dursunoglu D, Menevse E. Juglone-ascorbate treatment enhances reactive oxygen species mediated mitochondrial apoptosis in pancreatic cancer. *Mol Biol Rep*. 2024;51(1):1-13. doi:10.1007/S11033-024-09254-6/METRICS
 373. Mesalam AA, El-Sheikh M, Joo MD, et al. Induction of Oxidative Stress and Mitochondrial Dysfunction by Juglone Affects the Development of Bovine Oocytes. *Int J Mol Sci*. 2020;22(1):168. doi:10.3390/IJMS22010168
 374. Cui S, Nian Q, Chen G, et al. Ghrelin ameliorates A549 cell apoptosis caused by paraquat via p38-MAPK regulated mitochondrial apoptotic pathway. *Toxicology*. 2019;426. doi:10.1016/j.tox.2019.152267
 375. Jiang F, Li S, Jiang Y, Chen Z, Wang T, Liu W. Fluorofenidone attenuates paraquat-induced pulmonary fibrosis by regulating the PI3K/Akt/mTOR signaling pathway and autophagy. *Mol Med Rep*. 2021;23(6). doi:10.3892/MMR.2021.12044/DOWNLOAD
 376. Liu MW, Su MX, Tang DY, Hao L, Xun XH, Huang YQ. Ligustrazin increases lung cell autophagy and ameliorates paraquat-induced pulmonary fibrosis by inhibiting PI3K/Akt/mTOR and hedgehog signalling via increasing miR-193a expression. *BMC Pulm Med*. 2019;19(1):1-16. doi:10.1186/S12890-019-0799-5/FIGURES/12
 377. Sun Z, Yang Z, Wang M, et al. Paraquat induces pulmonary fibrosis through Wnt/ β -catenin signaling pathway and myofibroblast differentiation. *Toxicol Lett*. 2020;333:170-183. doi:10.1016/J.TOXLET.2020.08.004
 378. Liu X, Yang H, Liu Z. Signaling pathways involved in paraquat-induced pulmonary toxicity: Molecular mechanisms and potential therapeutic drugs. *Int Immunopharmacol.Elsevier B.V*. 2022;113. doi:10.1016/j.intimp.2022.109301
 379. Tang YT, Li Y, Chu P, Ma XD, Tang ZY, Sun ZL. Molecular biological mechanism of action in cancer therapies: Juglone and its derivatives, the future of development. *Biomedicine & Pharmacotherapy*. 2022;148:112785. doi:10.1016/J.BIOPHA.2022.112785

380. Liu X, Chen Y, Zhang Y, et al. Juglone potentiates TRAIL-induced apoptosis in human melanoma cells via activating the ROS-p38-p53 pathway. *Mol Med Rep.* 2017;16(6):9645-9651. doi:10.3892/MMR.2017.7806/DOWNLOAD
381. Wang P, Gao C, Wang W, et al. Juglone induces apoptosis and autophagy via modulation of mitogen-activated protein kinase pathways in human hepatocellular carcinoma cells. *Food Chem Toxicol.* 2018;116(Pt B):40-50. doi:10.1016/J.FCT.2018.04.004
382. Wu J, Zhang H, Xu Y, et al. Juglone induces apoptosis of tumor stem-like cells through ROS-p38 pathway in glioblastoma. *BMC Neurol.* 2017;17(1):70. doi:10.1186/S12883-017-0843-0
383. El-Sheikh M, Mesalam A, Khalil AAK, et al. Downregulation of PI3K/AKT/mTOR Pathway in Juglone-Treated Bovine Oocytes. *Antioxidants.* 2023;12(1). doi:10.3390/antiox12010114
384. Krall J, Bagley AC, Mullenbach GT, Hallewell RA, Lynch RE. Superoxide mediates the toxicity of paraquat for cultured mammalian cells. *Journal of Biological Chemistry.* 1988;263(4):1910-1914. doi:10.1016/s0021-9258(19)77964-2
385. Da Silva MR, Schapochnik A, Leal MP, et al. Beneficial effects of ascorbic acid to treat lung fibrosis induced by paraquat. *PLoS One.* 2018;13(11). doi:10.1371/journal.pone.0205535
386. Hu S, Qiao C, Yuan Z, et al. Therapy with high-dose long-term antioxidant free radicals for severe paraquat poisoning: A pilot study. *Exp Ther Med.* Published online October 2, 2018:5149-5155. Accessed December 6, 2024. <https://www.spandidos-publications.com/10.3892/etm.2018.6823>
387. Sajadimajd S, Yazdanparast R, Roshanzamir F. Augmentation of oxidative stress-induced apoptosis in MCF7 cells by ascorbate–tamoxifen and/or ascorbate–juglone treatments. *In Vitro Cell Dev Biol Anim.* 2016;52(2):193-203. doi:10.1007/S11626-015-9961-4/METRICS
388. Chobot V, Hadacek F. Milieu-dependent pro- and antioxidant activity of juglone may explain linear and nonlinear effects on seedling development. *J Chem Ecol.* 2009;35(3):383-390. doi:10.1007/S10886-009-9609-5/FIGURES/1
389. Leopoldini M, Marino T, Russo N, Toscano M. Antioxidant properties of phenolic compounds: H-atom versus electron transfer mechanism. *Journal of Physical Chemistry A.* 2004;108(22):4916-4922. doi:10.1021/jp037247d
390. Olszowy-Tomczyk M, Wianowska D. Comparison of the Antioxidant Properties of Extracts Obtained from Walnut Husks as well as the Influence of Juglone on Their Evaluation. *Applied Sciences (Switzerland).* 2024;14(7). doi:10.3390/app14072972
391. Cooper JF, Dues DJ, Van Raamsdonk JM. Measuring sensitivity to oxidative stress: the superoxide-generator juglone rapidly loses potency with time. 2016. Accessed December 21, 2024. <http://wbg.wormbook.org/2016/07/14/measuring-sensitivity-to-oxidative-stress-the-superoxide-generator-juglone-rapidly-loses-potency-with-time/>
392. Dues DJ, Andrews EK, Schaar CE, Bergsma AL, Senchuk MM, Van Raamsdonk JM. Aging causes decreased resistance to multiple stresses and a failure to activate specific stress response pathways. *Aging (Albany NY).* 2016;8(4):777. doi:10.18632/AGING.100939

393. Baskoylu SN, Chapkis N, Unsal B, et al. Disrupted autophagy and neuronal dysfunction in *C. elegans* knockin models of FUS amyotrophic lateral sclerosis. *Cell Rep.* 2022;38(4). doi:10.1016/J.CELREP.2021.110195/ATTACHMENT/FEEC30C7-4961-45AD-ACB3-523C4DEFE889/MMC3.PDF
394. Schaar CE, Dues DJ, Spielbauer KK, et al. Mitochondrial and Cytoplasmic ROS Have Opposing Effects on Lifespan. *PLoS Genet.* 2015;11(2):1-24. doi:10.1371/journal.pgen.1004972
395. Labuschagne CF, Brenkman AB. Current methods in quantifying ROS and oxidative damage in *Caenorhabditis elegans* and other model organism of aging. *Ageing Res Rev.* 2013;12(4):918-930. doi:10.1016/j.arr.2013.09.003
396. Ross MF, Kelso GF, Blaikie FH, et al. Lipophilic triphenylphosphonium cations as tools in mitochondrial bioenergetics and free radical biology. *Biochemistry (Moscow).* 2005;70:222-230.
397. Robinson KM, Janes MS, Pehar M, et al. Selective fluorescent imaging of superoxide in vivo using ethidium-based probes. *Proc Natl Acad Sci U S A.* 2006;103(41):15038. doi:10.1073/PNAS.0601945103
398. Zhao H, Kalivendi S, Zhang H, et al. Superoxide reacts with hydroethidine but forms a fluorescent product that is distinctly different from ethidium: Potential implications in intracellular fluorescence detection of superoxide. *Free Radic Biol Med.* 2003;34(11):1359-1368. doi:10.1016/S0891-5849(03)00142-4
399. Zielonka J, Srinivasan S, Hardy M, et al. Cytochrome c-mediated oxidation of hydroethidine and mito-hydroethidine in mitochondria: Identification of homo- and heterodimers. *Free Radic Biol Med.* 2008;44(5):835-846. doi:10.1016/j.freeradbiomed.2007.11.013
400. Bucana C, Saiki I, Nayar R. Uptake and accumulation of the vital dye hydroethidine in neoplastic cells. <http://dx.doi.org/10.1177/3492426339>. 1986;34(9):1109-1115. doi:10.1177/34.9.2426339
401. Zielonka J, Kalyanaraman B. Small-molecule luminescent probes for the detection of cellular oxidizing and nitrating species. *Free Radic Biol Med. Elsevier Inc.* 2018;128:3-22. doi:10.1016/j.freeradbiomed.2018.03.032
402. Funk RHW, Scholkmann F. The significance of bioelectricity on all levels of organization of an organism. Part 1: From the subcellular level to cells. *Prog Biophys Mol Biol. Elsevier Ltd.* 2023;177:185-201. doi:10.1016/j.pbiomolbio.2022.12.002
403. Michalski R, Zielonka J, Hardy M, Joseph J, Kalyanaraman B. Hydropropidine: A novel, cell-impermeant fluorogenic probe for detecting extracellular superoxide. *Free Radic Biol Med.* 2012;54:135. doi:10.1016/J.FREERADBIOMED.2012.09.018
404. Nazarewicz RR, Bikineyeva A, Dikalov SI. Rapid and specific measurements of superoxide using fluorescence spectroscopy. *J Biomol Screen.* 2012;18(4):498. doi:10.1177/1087057112468765
405. Murphy MP, Bayir H, Belousov V, et al. Guidelines for measuring reactive oxygen species and oxidative damage in cells and in vivo. *Nat Metab.* 2022;4(6):651-662. doi:10.1038/s42255-022-00591-z

406. Wehner KA, Ayala L, Kim Y, et al. Survival motor neuron protein in the nucleolus of mammalian neurons. *Brain Res.* 2002;945(2):160-173. doi:10.1016/S0006-8993(02)02750-6
407. Lauria F, Bernabò P, Tebaldi T, et al. SMN-primed ribosomes modulate the translation of transcripts related to spinal muscular atrophy. *Nat Cell Biol.* 2020;22(10):1239-1251. doi:10.1038/S41556-020-00577-7
408. Johnson AB, Barton MC. Hypoxia-induced and stress-specific changes in chromatin structure and function. *Mutat Res.* 2007;618(1-2):149. doi:10.1016/J.MRFMMM.2006.10.007
409. Östman A, Böhmer FD. Regulation of receptor tyrosine kinase signaling by protein tyrosine phosphatases. *Trends Cell Biol.* 2001;11(6):258-266. doi:10.1016/S0962-8924(01)01990-0
410. Zilio E, Piano V, Wirth B. Mitochondrial Dysfunction in Spinal Muscular Atrophy. *Int J Mol Sci.* 2022;23(18). doi:10.3390/IJMS231810878
411. Wang X, Proud CG. The mTOR Pathway in the Control of Protein Synthesis. *Physiology.* 2006;21:362-369.
412. Savino L, Di Marcantonio MC, Moscatello C, et al. Effects of H₂O₂ Treatment Combined With PI3K Inhibitor and MEK Inhibitor in AGS Cells: Oxidative Stress Outcomes in a Model of Gastric Cancer. *Front Oncol.* 2022;12. doi:10.3389/FONC.2022.860760/PDF
413. Dang R, Cai H, Zhang L, et al. Dysregulation of Neuregulin-1/ErbB signaling in the prefrontal cortex and hippocampus of rats exposed to chronic unpredictable mild stress. *Physiol Behav.* 2016;154:145-150. doi:10.1016/J.PHYSBEH.2015.11.023
414. Senchuk MM, Dues DJ, Raamsdonk JM Van. Measuring Oxidative Stress in *Caenorhabditis elegans*: Paraquat and Juglone Sensitivity Assays. *Bio Protoc.* 2017;7(1):e2086. doi:10.21769/BIOPROTOC.2086
415. Altun ZF, Hall DH. Alimentary system, pharynx. . *WormAtlas*. Published online 2009.
416. Dingley S, Polyak E, Lightfoot R, et al. Mitochondrial respiratory chain dysfunction variably increases oxidant stress in *Caenorhabditis elegans*. *Mitochondrion.* 2010;10(2):125-136. doi:10.1016/j.mito.2009.11.003
417. Solouki S, August A, Huang W. Non-receptor tyrosine kinase signaling in autoimmunity and therapeutic implications. *Pharmacol Ther.Elsevier Inc.* 2019;201:39-50. doi:10.1016/j.pharmthera.2019.05.008
418. Kumar SH, Brandt K, Claus P, Jung K. Comparative meta-analysis of transcriptomic studies in spinal muscular atrophy: comparison between tissues and mouse models. *BMC Med Genomics.* 2024;17(1):266. doi:10.1186/s12920-024-02040-0
419. Ren XG, Li W, Li WX, Yu WQ. Mechanism of Histone Arginine Methylation Dynamic Change in Cellular Stress. *Int J Mol Sci.* 2024;25(14). doi:10.3390/ijms25147562
420. Gao X, Xu J, Chen H, et al. Defective expression of mitochondrial, vacuolar H⁺-ATPase and histone genes in a *C. Elegans* Model of SMA. *Front Genet.* 2019;10(MAY). doi:10.3389/fgene.2019.00410

421. Bernabò P, Tebaldi T, Groen EJN, et al. In Vivo Translatome Profiling in Spinal Muscular Atrophy Reveals a Role for SMN Protein in Ribosome Biology. *Cell Rep.* 2017;21(4):953. doi:10.1016/J.CELREP.2017.10.010
422. Sansa A, Hidalgo I, Miralles MP, et al. Spinal Muscular Atrophy autophagy profile is tissue-dependent: differential regulation between muscle and motoneurons. *Acta Neuropathol Commun.* 2021;9(1):1-15. doi:10.1186/S40478-021-01223-5/TABLES/1
423. Kazyken D, Magnuson B, Bodur C, et al. AMPK directly activates mTORC2 to promote cell survival during acute energetic stress. *Sci Signal.* 2019;12(585):eaav3249. doi:10.1126/SCISIGNAL.AAV3249
424. Gems D, Doonan R. *The Nematode Caenorhabditis Elegans: Oxidative Stress and Aging in the Nematode Caenorhabditis Elegans.*; 2008. <http://www.wormbook>.
425. Dues DJ, Schaar CE, Johnson BK, et al. Uncoupling of Oxidative Stress Resistance and Lifespan in Long-lived isp-1 Mitochondrial Mutants in Caenorhabditis elegans. *Free Radic Biol Med.* 2017;108:362. doi:10.1016/J.FREERADBIOMED.2017.04.004
426. Suthammarak W, Somerlot BH, Opheim E, Sedensky M, Morgan PG. Novel Interactions between Mitochondrial Superoxide Dismutases and the Electron Transport Chain. *Aging Cell.* 2013;12(6):10.1111/accel.12144. doi:10.1111/ACEL.12144
427. Van Raamsdonk JM, Hekimi S. Deletion of the Mitochondrial Superoxide Dismutase sod-2 Extends Lifespan in Caenorhabditis elegans. *PLoS Genet.* 2009;5(2):e1000361. doi:10.1371/JOURNAL.PGEN.1000361
428. Crombie TA, Tang L, Choe KP, Julian D. Inhibition of the oxidative stress response by heat stress in Caenorhabditis elegans. *Journal of Experimental Biology.* 2016;219(14):2201-2211. doi:10.1242/JEB.135327/262269/AM/INHIBITION-OF-THE-OXIDATIVE-STRESS-RESPONSE-BY
429. Deng J, Dai Y, Tang H, Pang S. SKN-1 Is a Negative Regulator of DAF-16 and Somatic Stress Resistance in Caenorhabditis elegans. *G3 Genes|Genomes|Genetics.* 2020;10(5):1707-1712. doi:10.1534/G3.120.401203
430. Yun CW, Kim S, Lee JH, Lee SH. Melatonin Promotes Apoptosis of Colorectal Cancer Cells via Superoxide-mediated ER Stress by Inhibiting Cellular Prion Protein Expression. *Anticancer Res.* 2018;38(7):3951-3960. doi:10.21873/ANTICANRES.12681
431. Trujillo M, Alvarez B, Radi R. One- and two-electron oxidation of thiols: mechanisms, kinetics and biological fates. *Free Radic Res.* 2016;50(2):150-171. doi:10.3109/10715762.2015.1089988
432. Winterbourn CC, Metodiewa D. *Reactivity of Biologically Important Thiol Compounds with Superoxide and Hydrogen Peroxide.*; 1999.
433. Benrahmoune M, Théron P, Abedinzadeh Z. The reaction of superoxide radical with N-acetylcysteine. *Free Radic Biol Med.* 2000;29(8):775-782. doi:10.1016/S0891-5849(00)00380-4
434. Aldini G, Altomare A, Baron G, et al. N-Acetylcysteine as an antioxidant and disulphide breaking agent: the reasons why. *Free Radic Res. Taylor and Francis Ltd.* 2018;52(7):751-762. doi:10.1080/10715762.2018.1468564

435. Pedre B, Barayeu U, Ezeriņa D, Dick TP. The mechanism of action of N-acetylcysteine (NAC): The emerging role of H₂S and sulfane sulfur species. *Pharmacol Ther.Elsevier Inc.* 2021;228. doi:10.1016/j.pharmthera.2021.107916
436. Tenório MCDS, Graciliano NG, Moura FA, de Oliveira ACM, Goulart MOF. N-acetylcysteine (Nac): Impacts on human health. *Antioxidants.MDPI.* 2021;10(6). doi:10.3390/antiox10060967
437. Ballatori N, Krance SM, Notenboom S, Shi S, Tieu K, Hammond CL. Glutathione dysregulation and the etiology and progression of human diseases. *Biol Chem.* 2009;390(3):191. doi:10.1515/BC.2009.033
438. Deponte M. Glutathione catalysis and the reaction mechanisms of glutathione-dependent enzymes. *Biochim Biophys Acta Gen Subj.* 2013;1830(5):3217-3266. doi:10.1016/j.bbagen.2012.09.018
439. Radtke KK, Coles LD, Mishra U, Orchard PJ, Holmay M, Cloyd JC. Interaction of n-acetylcysteine and cysteine in human plasma. *J Pharm Sci.* 2012;101(12):4653-4659. doi:10.1002/jps.23325
440. Aoyama K, Watabe M, Nakaki T. Modulation of neuronal glutathione synthesis by EAAC1 and its interacting protein GTRAP3-18. *Amino Acids.* 2012;42(1):163-169. doi:10.1007/S00726-011-0861-Y/METRICS
441. Offen D, Ziv I, Sternin H, Melamed E, Hochman A. Prevention of Dopamine-Induced Cell Death by Thiol Antioxidants: Possible Implications for Treatment of Parkinson's Disease. *Exp Neurol.* 1996;141(1):32-39. doi:10.1006/EXNR.1996.0136
442. Sandhir R, Sood A, Mehrotra A, Kamboj SS. N-acetylcysteine reverses mitochondrial dysfunctions and behavioral abnormalities in 3-nitropropionic acid-induced Huntington's disease. *Neurodegener Dis.* 2012;9(3):145-157. doi:10.1159/000334273
443. Sha D, Chin LS, Li L. Phosphorylation of parkin by Parkinson disease-linked kinase PINK1 activates parkin E3 ligase function and NF- κ B signaling. *Hum Mol Genet.* 2009;19(2):352. doi:10.1093/HMG/DDP501
444. Aoki E, Yano R, Yokoyama H, Kato H, Araki T. Role of nuclear transcription factor kappa B (NF-kappaB) for MPTP (1-methyl-4-phenyl-1,2,3,6-tetrahydropyridine)-induced apoptosis in nigral neurons of mice. *Exp Mol Pathol.* 2009;86(1):57-64. doi:10.1016/J.YEXMP.2008.10.004
445. Sekhon B, Sekhon C, Khan M, Patel SJ, Singh I, Singh AK. N-Acetyl cysteine protects against injury in a rat model of focal cerebral ischemia. *Brain Res.* 2003;971(1):1-8. doi:10.1016/S0006-8993(03)02244-3
446. Yan CYI, Greene LA. *Prevention of PC12 Cell Death by N-Acetylcysteine Requires Activation of the Ras Pathway.*; 1998.
447. Barzegar A, Moosavi-Movahedi AA. Intracellular ROS Protection Efficiency and Free Radical-Scavenging Activity of Curcumin. *PLoS One.* 2011;6(10):e26012. doi:10.1371/JOURNAL.PONE.0026012
448. Yu CW, Wei CC, Liao VHC. Curcumin-mediated oxidative stress resistance in *Caenorhabditis elegans* is modulated by age-1, akt-1, pdk-1, osr-1, unc-43, sek-1, skn-1, sir-2.1, and mev-1. *Free Radic Res.* 2014;48(3):371-379. doi:10.3109/10715762.2013.872779

449. Nguyen HD, Jo WH, Hoang NHM, Kim MS. Curcumin-Attenuated TREM-1/DAP12/NLRP3/Caspase-1/IL1B, TLR4/NF- κ B Pathways, and Tau Hyperphosphorylation Induced by 1,2-Diacetyl Benzene: An in Vitro and in Silico Study. *Neurotox Res.* 2022;40(5):1272-1291. doi:10.1007/S12640-022-00535-1/METRICS
450. Boyao Y, Mengjiao S, Caicai B, Xiaoling L, zhenxing L, Manxia W. Dynamic expression of autophagy-related factors in autoimmune encephalomyelitis and exploration of curcumin therapy. *J Neuroimmunol.* 2019;337. doi:10.1016/j.jneuroim.2019.577067
451. Wang C, Zhang X, Teng Z, Zhang T, Li Y. Downregulation of PI3K/Akt/mTOR signaling pathway in curcumin-induced autophagy in APP/PS1 double transgenic mice. *Eur J Pharmacol.* 2014;740:312-320. doi:10.1016/J.EJPHAR.2014.06.051
452. He HJ, Xiong X, Zhou S, et al. Neuroprotective effects of curcumin via autophagy induction in 6-hydroxydopamine Parkinson's models. *Neurochem Int.* 2022;155:105297. doi:10.1016/J.NEUINT.2022.105297
453. Chang CH, Chen HX, Yü G, Peng CC, Peng RY. Curcumin-Protected PC12 Cells Against Glutamate-Induced Oxidative Toxicity. *Food Technol Biotechnol.* 2014;52(4):468. doi:10.17113/FTB.52.04.14.3622
454. Dong H, Xu L, Wu L, et al. Curcumin abolishes mutant TDP-43 induced excitability in a motoneuron-like cellular model of ALS. *Neuroscience.* 2014;272:141-153. doi:10.1016/J.NEUROSCIENCE.2014.04.032/ASSET/B6EC7D17-93FF-496B-8BCD-4A389DA48FD3/MAIN.ASSETS/GR7.JPG
455. Njus D, Kelley PM, Tu YJ, Schlegel HB. Ascorbic acid: The chemistry underlying its antioxidant properties. *Free Radic Biol Med.* 2020;159:37-43. doi:10.1016/J.FREERADBIOMED.2020.07.013
456. Beyer RE. The role of ascorbate in antioxidant protection of biomembranes: Interaction with vitamin E and coenzyme Q. *J Bioenerg Biomembr.* 1994;26(4):349-358. doi:10.1007/BF00762775/METRICS
457. Li X, Qu ZC, May JM. GSH Is Required to Recycle Ascorbic Acid in Cultured Liver Cell Lines. <https://home.liebertpub.com/ars>. 2004;3(6):1089-1097. doi:10.1089/152308601317203594
458. Ruiz-Ramos M, Alberto Vargas L, Fortoul Van Der Goes TI, Cervantes-Sandoval A, Mendoza-Núñez VM. Supplementation of ascorbic acid and alpha-tocopherol is useful to preventing bone loss linked to oxidative stress in elderly. *J Nutr Health Aging.* 2010;14(6):467-472. doi:10.1007/S12603-010-0099-5
459. Im S, Nam TG, Lee SG, Kim YJ, Chun OK, Kim DO. Additive antioxidant capacity of vitamin C and tocopherols in combination. *Food Sci Biotechnol.* 2014;23(3):693-699. doi:10.1007/S10068-014-0094-4/METRICS
460. Niki E. Interaction of ascorbate and alpha-tocopherol. *Ann N Y Acad Sci.* 1987;498(1):186-199. doi:10.1111/J.1749-6632.1987.TB23761.X
461. KC S, Càrcamo JM, Golde DW. Vitamin C enters mitochondria via facilitative glucose transporter 1 (Glut1) and confers mitochondrial protection against oxidative injury. *FASEB J.* 2005;19(12):1657-1667. doi:10.1096/FJ.05-4107COM

462. Huang J, May JM. Ascorbic acid protects SH-SY5Y neuroblastoma cells from apoptosis and death induced by β -amyloid. *Brain Res.* 2006;1097(1):52-58. doi:10.1016/J.BRAINRES.2006.04.047
463. Li X, Cobb CE, May JM. Mitochondrial recycling of ascorbic acid from dehydroascorbic acid: dependence on the electron transport chain. *Arch Biochem Biophys.* 2002;403(1):103-110. doi:10.1016/S0003-9861(02)00205-9
464. Polyak E, Ostrovsky J, Peng M, et al. N-acetylcysteine and vitamin E rescue animal longevity and cellular oxidative stress in pre-clinical models of mitochondrial complex I disease. *Mol Genet Metab.* 2018;123(4):449-462. doi:10.1016/J.YMGME.2018.02.013
465. Nagano S, Fujii Y, Yamamoto T, et al. The efficacy of trientine or ascorbate alone compared to that of the combined treatment with these two agents in familial amyotrophic lateral sclerosis model mice. *Exp Neurol.* 2003;179(2):176-180. doi:10.1016/S0014-4886(02)00014-6
466. Babri S, Mehrvash F, Mohaddes G, Hatami H, Mirzaie F. Effect of Intrahippocampal Administration of Vitamin C and Progesterone on Learning in a Model of Multiple Sclerosis in Rats. *Adv Pharm Bull.* 2015;5(1):83. doi:10.5681/APB.2015.011
467. Rebec G V., Conroy SK, Barton SJ. Hyperactive striatal neurons in symptomatic Huntington R6/2 mice: Variations with behavioral state and repeated ascorbate treatment. *Neuroscience.* 2006;137(1):327-336. doi:10.1016/J.NEUROSCIENCE.2005.08.062
468. Zeng X, Xu K, Wang J, Xu Y, Qu S. Pretreatment of Ascorbic Acid Inhibits MPTP-Induced Astrocytic Oxidative Stress through Suppressing NF- κ B Signaling. *Neural Plast.* 2020;2020:8872296. doi:10.1155/2020/8872296
469. Frontiñán-Rubio J, Sancho-Bielsa FJ, Peinado JR, et al. Sex-dependent co-occurrence of hypoxia and β -amyloid plaques in hippocampus and entorhinal cortex is reversed by long-term treatment with ubiquinol and ascorbic acid in the 3 \times Tg-AD mouse model of Alzheimer's disease. *Molecular and Cellular Neuroscience.* 2018;92:67-81. doi:10.1016/J.MCN.2018.06.005
470. De Nuccio F, Cianciulli A, Porro C, et al. Inflammatory response modulation by vitamin c in an mptp mouse model of parkinson's disease. *Biology (Basel).* 2021;10(11):1155. doi:10.3390/BIOLOGY10111155/S1
471. Li Y, Darwish WS, Chen Z, et al. Identification of lead-produced lipid hydroperoxides in human HepG2 cells and protection using rosmarinic and ascorbic acids with a reference to their regulatory roles on Nrf2-Keap1 antioxidant pathway. *Chem Biol Interact.* 2019;314. doi:10.1016/j.cbi.2019.108847
472. Xu HJ, Jiang WD, Feng L, et al. Dietary vitamin C deficiency depressed the gill physical barriers and immune barriers referring to Nrf2, apoptosis, MLCK, NF- κ B and TOR signaling in grass carp (*Ctenopharyngodon idella*) under infection of *Flavobacterium columnare*. *Fish Shellfish Immunol.* 2016;58:177-192. doi:10.1016/j.fsi.2016.09.029
473. Somade OT, Adeyi OE, Ajayi BO, et al. Syringic and ascorbic acids prevent NDMA-induced pulmonary fibrogenesis, inflammation, apoptosis, and oxidative stress through the regulation of PI3K-Akt/PKB-mTOR-PTEN signaling pathway. *Metabol Open.* 2022;14:100179. doi:10.1016/J.METOP.2022.100179

474. Zhang P, Zang M, Sang Z, et al. Vitamin C alleviates LPS-induced myocardial injury by inhibiting pyroptosis via the ROS-AKT/mTOR signalling pathway. *BMC Cardiovasc Disord.* 2022;22(1):1-10. doi:10.1186/S12872-022-03014-9/FIGURES/4
475. Yang M, Teng S, Ma C, Yu Y, Wang P, Yi C. Ascorbic acid inhibits senescence in mesenchymal stem cells through ROS and AKT/mTOR signaling. *Cytotechnology.* 2018;70(5):1301-1313. doi:10.1007/s10616-018-0220-x
476. Procházková D, Boušová I, Wilhelmová N. Antioxidant and prooxidant properties of flavonoids. *Fitoterapia.* 2011;82(4):513-523. doi:10.1016/J.FITOTE.2011.01.018
477. Anderson RF, Fisher LJ, Hara Y, et al. Green tea catechins partially protect DNA from ·OH radical-induced strand breaks and base damage through fast chemical repair of DNA radicals. *Carcinogenesis.* 2001;22(8):1189-1193. doi:10.1093/CARCIN/22.8.1189
478. Nanjo F, Mori M, Goto K, Hara Y. Radical Scavenging Activity of Tea Catechins and Their Related Compounds. *Biosci Biotechnol Biochem.* 1999;63(9):1621-1623. doi:10.1271/BBB.63.1621
479. Hou RR, Chen JZ, Chen H, Kang XG, Li MG, Wang BR. Neuroprotective effects of (–)-epigallocatechin-3-gallate (EGCG) on paraquat-induced apoptosis in PC12 cells. *Cell Biol Int.* 2008;32(1):22-30. doi:10.1016/J.CELLBI.2007.08.007
480. Na HK, Kim EH, Jung JH, Lee HH, Hyun JW, Surh YJ. (–)-Epigallocatechin gallate induces Nrf2-mediated antioxidant enzyme expression via activation of PI3K and ERK in human mammary epithelial cells. *Arch Biochem Biophys.* 2008;476(2):171-177. doi:10.1016/J.ABB.2008.04.003
481. Na HK, Surh YJ. Modulation of Nrf2-mediated antioxidant and detoxifying enzyme induction by the green tea polyphenol EGCG. *Food and Chemical Toxicology.* 2008;46(4):1271-1278. doi:10.1016/J.FCT.2007.10.006
482. Abbas S, Wink M. Epigallocatechin gallate inhibits beta amyloid oligomerization in *Caenorhabditis elegans* and affects the daf-2/insulin-like signaling pathway. *Phytomedicine.* 2010;17(11):902-909. doi:10.1016/J.PHYMED.2010.03.008
483. Ehrnhoefer DE, Duennwald M, Markovic P, et al. Green tea (–)-epigallocatechin-gallate modulates early events in huntingtin misfolding and reduces toxicity in Huntington's disease models. *Hum Mol Genet.* 2006;15(18):2743-2751. doi:10.1093/HMG/DDL210
484. Xu Z, Chen S, Li X, Luo G, Li L, Le W. Neuroprotective effects of (–)-epigallocatechin-3-gallate in a transgenic mouse model of amyotrophic lateral sclerosis. *Neurochem Res.* 2006;31(10):1263-1269. doi:10.1007/S11064-006-9166-Z/FIGURES/5
485. Reiter RJ, Guerrero JM, Garcia JJ, Acuña-Castroviejo D. Reactive oxygen intermediates, molecular damage, and aging: Relation to melatonin. In: *Annals of the New York Academy of Sciences.* Vol 854. New York Academy of Sciences; 1998:410-424. doi:10.1111/j.1749-6632.1998.tb09920.x
486. Reiter RJ, Tan DX, Osuna C, Gitto E. *Biomedical Science Review Actions of Melatonin in the Reduction of Oxidative Stress A Review.* Vol 7.; 2000. www.karger.com/journals/jhs
487. Tan D xian, Reiter RJ, Manchester LC, et al. Chemical and Physical Properties and Potential Mechanisms: Melatonin as a Broad Spectrum Antioxidant and Free Radical Scavenger. *Curr Top Med Chem.* 2005;2(2):181-197. doi:10.2174/1568026023394443

488. López-Burillo S, Tan DX, Mayo JC, Sainz RM, Manchester LC, Reiter RJ. Melatonin, xanthurenic acid, resveratrol, EGCG, vitamin C and α -lipoic acid differentially reduce oxidative DNA damage induced by Fenton reagents: A study of their individual and synergistic actions. *J Pineal Res.* 2003;34(4):269-277. doi:10.1034/j.1600-079X.2003.00041.x
489. Yamamoto H, Mohanan P V. Melatonin attenuates brain mitochondria DNA damage induced by potassium cyanide in vivo and in vitro. *Toxicology.* 2002;179(1-2):29-36. doi:10.1016/S0300-483X(02)00244-5
490. Dabbeni-Sala F, Santo S, Franceschini D, D. Skaper S, Pietro G. Melatonin protects against 6-OHDA-induced neurotoxicity in rats: a role for mitochondrial complex I activity. *FASEB J.* 2001;15(1):164-170. doi:10.1096/FJ.00-0129COM
491. Hewitt JE, Pollard AK, Lesanpezeshki L, et al. Muscle strength deficiency and mitochondrial dysfunction in a muscular dystrophy model of *Caenorhabditis elegans* and its functional response to drugs. *Dis Model Mech.* 2018;11(12):dmm036137. doi:10.1242/DMM.036137
492. He L, Du JJ, Zhou JJ, et al. Synthesis of Melatonin Derivatives and the Neuroprotective Effects on Parkinson's Disease Models of *Caenorhabditis elegans*. *Front Chem.* 2022;10:918116. doi:10.3389/FCHEM.2022.918116/FULL
493. Mayo JC, Sainz RM, Uria H, Antolin I, Esteban MM, Rodriguez C. Melatonin prevents apoptosis induced by 6-hydroxydopamine in neuronal cells: Implications for Parkinson's disease. *J Pineal Res.* 1998;24(3):179-192. doi:10.1111/J.1600-079X.1998.TB00531.X
494. Wen X, Tang S, Wan F, Zhong R, Chen L, Zhang H. The PI3K/Akt-Nrf2 Signaling Pathway and Mitophagy Synergistically Mediate Hydroxytyrosol to Alleviate Intestinal Oxidative Damage. *Int J Biol Sci.* 2024;20(11):4258-4276. doi:10.7150/ijbs.97263
495. Reddy NM, Potteti HR, Vegiraju S, Chen HJ, Tamatam CM, Reddy SP. PI3K-AKT signaling via Nrf2 protects against hyperoxia-induced acute lung injury, but promotes inflammation post-injury independent of Nrf2 in mice. *PLoS One.* 2015;10(6). doi:10.1371/journal.pone.0129676
496. Kongsuphol P, Mukda S, Nopparat C, Villarroel A, Govitrapong P. Melatonin attenuates methamphetamine-induced deactivation of the mammalian target of rapamycin signaling to induce autophagy in SK-N-SH cells. *J Pineal Res.* 2009;46(2):199-206. doi:10.1111/J.1600-079X.2008.00648.X
497. Shen Y, Zhang G, Liu L, Xu S. Suppressive Effects of Melatonin on Amyloid- β -induced Glial Activation in Rat Hippocampus. *Arch Med Res.* 2007;38(3):284-290. doi:10.1016/J.ARCMED.2006.10.007
498. Hart A. Behavior. *WormBook.* Published online 2006. doi:10.1895/wormbook.1.87.1
499. Houldsworth A. Role of oxidative stress in neurodegenerative disorders: a review of reactive oxygen species and prevention by antioxidants. *Brain Commun.Oxford University Press.* 2024;6(1). doi:10.1093/braincomms/fcad356
500. Xiong H, Pears C, Woollard A. An enhanced *C. elegans* based platform for toxicity assessment. *Sci Rep.* 2017;7(1):9839. doi:10.1038/S41598-017-10454-3

501. Giunti S, Andersen N, Rayes D, De Rosa MJ. Drug discovery: Insights from the invertebrate *Caenorhabditis elegans*. *Pharmacol Res Perspect*. 2021;9(2):e00721. doi:10.1002/PRP2.721
502. Desjardins D, Cacho-Valadez B, Liu JL, et al. Antioxidants reveal an inverted U-shaped dose-response relationship between reactive oxygen species levels and the rate of aging in *Caenorhabditis elegans*. *Aging Cell*. 2017;16(1):104-112. doi:10.1111/ACEL.12528
503. Moldasheva A, Bakyt L, Bulanin D, Aljofan M. The impact of cellular environment on in vitro drug screening. *Future Sci OA*. 2023;9(9):FSO900. doi:10.2144/FSOA-2023-0027
504. Florido J, Martinez-Ruiz L, Rodriguez-Santana C, et al. Melatonin drives apoptosis in head and neck cancer by increasing mitochondrial ROS generated via reverse electron transport. *J Pineal Res*. 2022;73(3):e12824. doi:10.1111/JPI.12824
505. Bejarano I, Espino J, Barriga C, Reiter RJ, Pariente JA, Rodríguez AB. Pro-Oxidant Effect of Melatonin in Tumour Leucocytes: Relation with its Cytotoxic and Pro-Apoptotic Effects. *Basic Clin Pharmacol Toxicol*. 2011;108(1):14-20. doi:10.1111/J.1742-7843.2010.00619.X
506. Yun SM, Woo SH, Oh ST, et al. Melatonin enhances arsenic trioxide-induced cell death via sustained upregulation of Redd1 expression in breast cancer cells. *Mol Cell Endocrinol*. 2016;422:64-73. doi:10.1016/J.MCE.2015.11.016
507. Chen K, Zhu P, Chen W, Luo K, Shi XJ, Zhai W. Melatonin inhibits proliferation, migration, and invasion by inducing ROS-mediated apoptosis via suppression of the PI3K/Akt/mTOR signaling pathway in gallbladder cancer cells. *Aging (Albany NY)*. 2021;13(18):22502. doi:10.18632/AGING.203561
508. Ding K, Wang H, Xu J, et al. Melatonin stimulates antioxidant enzymes and reduces oxidative stress in experimental traumatic brain injury: the Nrf2–ARE signaling pathway as a potential mechanism. *Free Radic Biol Med*. 2014;73:1-11. doi:10.1016/J.FREERADBIOMED.2014.04.031
509. Zavodnik IB, Domanski A V., Lapshina EA, Bryszewska M, Reiter RJ. Melatonin directly scavenges free radicals generated in red blood cells and a cell-free system: Chemiluminescence measurements and theoretical calculations. *Life Sci*. 2006;79(4):391-400. doi:10.1016/J.LFS.2006.01.030
510. Deng Z, He M, Hu H, et al. Melatonin attenuates sepsis-induced acute kidney injury by promoting mitophagy through SIRT3-mediated TFAM deacetylation. *Autophagy*. 2023;20(1):151. doi:10.1080/15548627.2023.2252265
511. Lecumberri E, Dupertuis YM, Miralbell R, Pichard C. Green tea polyphenol epigallocatechin-3-gallate (EGCG) as adjuvant in cancer therapy. *Clinical Nutrition*. 2013;32(6):894-903. doi:10.1016/j.clnu.2013.03.008
512. Kuriya K, Itoh S, Isoda A, Tanaka S, Nishio M, Umekawa H. Green tea polyphenol EGCg induces cell fusion via reactive oxygen species. *Biochem Biophys Res*. 2023;35:101536. doi:10.1016/J.BBREP.2023.101536
513. Della Via FI, Shiraishi RN, Santos I, et al. (–)-Epigallocatechin-3-gallate induces apoptosis and differentiation in leukaemia by targeting reactive oxygen species and PIN1. *Scientific Reports* 2021 11:1. 2021;11(1):1-11. doi:10.1038/s41598-021-88478-z

514. Dayangac-Erden D, Bora-Tatar G, Dalkara S, Demir AS, Erdem-Yurter H. Carboxylic acid derivatives of histone deacetylase inhibitors induce full length SMN2 transcripts: a promising target for spinal muscular atrophy therapeutics. *Arch Med Sci.* 2011;7(2):230. doi:10.5114/AOMS.2011.22072
515. Sakla MS, Lorson CL. Induction of full-length survival motor neuron by polyphenol botanical compounds. *Hum Genet.* 2008;122(6):635-643. doi:10.1007/S00439-007-0441-0/FIGURES/6
516. Bowerman M, Murray L, Beauvais A, Pinheiro B, Kothary R. A critical smn threshold in mice dictates onset of an intermediate spinal muscular atrophy phenotype associated with a distinct neuromuscular junction pathology. *Neuromuscular Disorders.* 2012;22(3):263-276. doi:10.1016/J.NMD.2011.09.007
517. Kwon DY, Motley WW, Fischbeck KH, Burnett BG. Increasing expression and decreasing degradation of SMN ameliorate the spinal muscular atrophy phenotype in mice. *Hum Mol Genet.* 2011;20(18):3667-3677. doi:10.1093/HMG/DDR288
518. Naryshkin NA, Weetall M, Dakka A, et al. SMN2 splicing modifiers improve motor function and longevity in mice with spinal muscular atrophy. *Science (1979).* 2014;345(6197):688-693. doi:10.1126/SCIENCE.1250127/SUPPL_FILE/NARYSHKIN.SM.REVISION.1.PDF
519. Groen EJN, Perenthaler E, Courtney NL, et al. Temporal and tissue-specific variability of SMN protein levels in mouse models of spinal muscular atrophy. *Hum Mol Genet.* 2018;27(16):2851-2862. doi:10.1093/HMG/DDY195
520. Hua Y, Sahashi K, Rigo F, et al. Peripheral SMN restoration is essential for long-term rescue of a severe spinal muscular atrophy mouse model. *Nature* 2011 478:7367. 2011;478(7367):123-126. doi:10.1038/nature10485
521. Bardaweel SK, Gul M, Alzweiri M, Ishaqat A, Alsalamat HA, Bashatwah RM. Reactive Oxygen Species: the Dual Role in Physiological and Pathological Conditions of the Human Body. *Eurasian J Med.* 2018;50(3):193. doi:10.5152/EURASIANJMED.2018.17397
522. Kozlov A V., Javadov S, Sommer N. Cellular ROS and Antioxidants: Physiological and Pathological Role. *Antioxidants.* 2024;13(5):602. doi:10.3390/ANTIOX13050602
523. Liu R, Bian Y, Liu L, Liu L, Liu X, Ma S. Molecular pathways associated with oxidative stress and their potential applications in radiotherapy (Review). *Int J Mol Med.Spandidos Publications.* 2022;49(5). doi:10.3892/IJMM.2022.5121
524. Tejchman K, Kotfis K, Sieńko J. Biomarkers and Mechanisms of Oxidative Stress—Last 20 Years of Research with an Emphasis on Kidney Damage and Renal Transplantation. *Int J Mol Sci.* 2021;22(15):8010. doi:10.3390/IJMS22158010
525. Priya Dharshini LC, Vishnupriya S, Sakthivel KM, Rasmi RR. Oxidative stress responsive transcription factors in cellular signalling transduction mechanisms. *Cell Signal.* 2020;72:109670. doi:10.1016/J.CELLSIG.2020.109670
526. Lin Y, Lin C, Cao Y, Chen Y. Caenorhabditis elegans as an in vivo model for the identification of natural antioxidants with anti-aging actions. *Biomedicine & Pharmacotherapy.* 2023;167:115594. doi:10.1016/J.BIOPHA.2023.115594

527. Back P, Braeckman BP, Matthijssens F. ROS in aging *Caenorhabditis elegans*: Damage or signaling? *Oxid Med Cell Longev*. Preprint posted online 2012. doi:10.1155/2012/608478
528. Murphy CT, Hu PJ. Insulin/insulin-like growth factor signaling in *C. elegans* - WormBook - NCBI Bookshelf. WormBook. doi:doi/10.1895/wormbook.1.164.1
529. Ogg S, Paradis S, Gottlieb S, et al. The Fork head transcription factor DAF-16 transduces insulin-like metabolic and longevity signals in *C. elegans*. *Nature* 1997 389:6654. 1997;389(6654):994-999. doi:10.1038/40194
530. Zhang YP, Zhang WH, Zhang P, et al. Intestine-specific removal of DAF-2 nearly doubles lifespan in *Caenorhabditis elegans* with little fitness cost. *Nature Communications* 2022 13:1. 2022;13(1):1-18. doi:10.1038/s41467-022-33850-4
531. Kimura KD, Tissenbaum HA, Liu Y, Ruvkun G. daf-2, an insulin receptor-like gene that regulates longevity and diapause in *Caenorhabditis elegans*. *Science*. 1997;277(5328):942-946. doi:10.1126/SCIENCE.277.5328.942
532. Zheng S, Chiu H, Boudreau J, Papanicolaou T, Bendena W, Chin-Sang I. A functional study of all 40 *Caenorhabditis elegans* insulin-like peptides. *Journal of Biological Chemistry*. 2019;293(43):16912-16922. doi:10.1074/JBC.RA118.004542/ATTACHMENT/3D7375C2-422F-4C32-BC05-9ECE282D3EDC/MMC1.DOCX
533. Morris JZ, Tissenbaum HA, Ruvkun G. A phosphatidylinositol-3-OH kinase family member regulating longevity and diapause in *Caenorhabditis elegans*. *Nature*. 1996;382(6591):536-539. doi:10.1038/382536A0
534. Wolkow CA, Muñoz MJ, Riddle DL, Ruvkun G. Insulin receptor substrate and p55 orthologous adaptor proteins function in the *Caenorhabditis elegans* daf-2/insulin-like signaling pathway. *Journal of Biological Chemistry*. 2002;277(51):49591-49597. doi:10.1074/jbc.M207866200
535. Paradis S, Ailion M, Toker A, Thomas JH, Ruvkun G. A PDK1 homolog is necessary and sufficient to transduce AGE-1 PI3 kinase signals that regulate diapause in *Caenorhabditis elegans*. *Genes Dev*. 1999;13(11):1438. doi:10.1101/GAD.13.11.1438
536. Toker A, Newton AC. Cellular Signaling: Pivoting around PDK-1. *Cell*. 2000;103(2):185-188. doi:10.1016/S0092-8674(00)00110-0
537. Henderson ST, Johnson TE. daf-16 integrates developmental and environmental inputs to mediate aging in the nematode *Caenorhabditis elegans*. *Curr Biol*. 2001;11(24):1975-1980. doi:10.1016/S0960-9822(01)00594-2
538. Padmanabhan S, Mukhopadhyay A, Narasimhan SD, Tesz G, Czech MP, Tissenbaum HA. A PP2A regulatory subunit regulates *C. elegans* insulin/IGF-1 signaling by modulating AKT-1 phosphorylation. *Cell*. 2009;136(5):939-951. doi:10.1016/J.CELL.2009.01.025
539. Rouault JP, Kuwabara PE, Sinilnikova OM, Duret L, Thierry-Mieg D, Billaud M. Regulation of dauer larva development in *Caenorhabditis elegans* by daf-18, a homologue of the tumour suppressor PTEN. *Current Biology*. 1999;9(6):329-334. doi:10.1016/S0960-9822(99)80143-2
540. McElwee J, Bubb K, Thomas JH. Transcriptional outputs of the *Caenorhabditis elegans* forkhead protein DAF-16. *Aging Cell*. 2003;2(2):111-121. doi:10.1046/J.1474-9728.2003.00043.X

541. Honda Y, Tanaka M, Honda S. Modulation of longevity and diapause by redox regulation mechanisms under the insulin-like signaling control in *Caenorhabditis elegans*. *Exp Gerontol*. 2008;43(6):520-529. doi:10.1016/J.EXGER.2008.02.009
542. Yanase S, Yasuda K, Ishii N. Interaction between the ins/IGF-1 and p38 MAPK signaling pathways in molecular compensation of sod genes and modulation related to intracellular ROS levels in *C. elegans*. *Biochem Biophys Res*. 2020;23:100796. doi:10.1016/J.BBREP.2020.100796
543. Yanase S, Yasuda K, Ishii N. Adaptive responses to oxidative damage in three mutants of *Caenorhabditis elegans* (age-1, mev-1 and daf-16) that affect life span. *Mech Ageing Dev*. 2002;123(12):1579-1587. doi:10.1016/S0047-6374(02)00093-3
544. Hsu AL, Murphy CT, Kenyon C. Regulation of aging and age-related disease by DAF-16 and heat-shock factor. *Science* (1979). 2003;300(5622):1142-1145. doi:10.1126/SCIENCE.1083701/SUPPL_FILE/HSU.SOM.PDF
545. Meléndez A, Tallóczy Z, Seaman M, Eskelinen EL, Hall DH, Levine B. Autophagy genes are essential for dauer development and life-span extension in *C. elegans*. *Science*. 2003;301(5638):1387-1391. doi:10.1126/SCIENCE.1087782
546. Oh SW, Mukhopadhyay A, Svrzikapa N, Jiang F, Davis RJ, Tissenbaum HA. JNK regulates lifespan in *Caenorhabditis elegans* by modulating nuclear translocation of forkhead transcription factor/DAF-16. *Proc Natl Acad Sci U S A*. 2005;102(12):4494-4499. doi:10.1073/PNAS.0500749102/SUPPL_FILE/00749FIG11.PDF
547. Greer EL, Dowlathshahi D, Banko MR, et al. An AMPK-FOXO Pathway Mediates Longevity Induced by a Novel Method of Dietary Restriction in *C. elegans*. *Current Biology*. 2007;17(19):1646-1656. doi:10.1016/J.CUB.2007.08.047
548. Murphy CT. The search for DAF-16/FOXO transcriptional targets: Approaches and discoveries. *Exp Gerontol*. 2006;41(10):910-921. doi:10.1016/J.EXGER.2006.06.040
549. Walker AK, See R, Batchelder C, et al. A conserved transcription motif suggesting functional parallels between *Caenorhabditis elegans* SKN-1 and Cap'n'Collar-related basic leucine zipper proteins. *Journal of Biological Chemistry*. 2000;275(29):22166-22171. doi:10.1074/jbc.M001746200
550. Bowerman B, Eaton BA, Priess JR. skn-1, a maternally expressed gene required to specify the fate of ventral blastomeres in the early *C. elegans* embryo. *Cell*. 1992;68(6):1061-1075. doi:10.1016/0092-8674(92)90078-Q
551. An JH, Blackwell TK. SKN-1 links *C. elegans* mesendodermal specification to a conserved oxidative stress response. *Genes Dev*. 2003;17(15):1882. doi:10.1101/GAD.1107803
552. Tullet JMA, Hertweck M, An JH, et al. Direct inhibition of the longevity promoting factor SKN-1 by Insulin-like signaling in *C. elegans*. *Cell*. 2008;132(6):1025. doi:10.1016/J.CELL.2008.01.030
553. Li X, Matilainen O, Jin C, Glover-Cutter KM, Holmberg CI, Blackwell TK. Specific SKN-1/Nrf Stress Responses to Perturbations in Translation Elongation and Proteasome Activity. *PLoS Genet*. 2011;7(6):e1002119. doi:10.1371/JOURNAL.PGEN.1002119

554. Inoue H, Hisamoto N, Jae HA, et al. The C. elegans p38 MAPK pathway regulates nuclear localization of the transcription factor SKN-1 in oxidative stress response. *Genes Dev.* 2005;19(19):2278. doi:10.1101/GAD.1324805
555. Staab TA, Griffen TC, Corcoran C, Evgrafov O, Knowles JA, Sieburth D. The Conserved SKN-1/Nrf2 Stress Response Pathway Regulates Synaptic Function in Caenorhabditis elegans. *PLoS Genet.* 2013;9(3):e1003354. doi:10.1371/JOURNAL.PGEN.1003354
556. Staab TA, Egrafv O, Knowles JA, Sieburth D. Regulation of Synaptic nlG-1/Neuroigin Abundance by the skn-1/Nrf Stress Response Pathway Protects against Oxidative Stress. *PLoS Genet.* 2014;10(1):e1004100. doi:10.1371/JOURNAL.PGEN.1004100
557. Bishop NA, Guarente L. Two neurons mediate diet-restriction-induced longevity in C. elegans. *Nature* 2007 447:7144. 2007;447(7144):545-549. doi:10.1038/nature05904
558. Park SK, Tedesco PM, Johnson TE. Oxidative Stress and Longevity in C.elegans as Mediated by SKN-1. *Aging Cell.* 2009;8(3):258. doi:10.1111/J.1474-9726.2009.00473.X
559. Oliveira RP, Abate JP, Dilks K, et al. Condition-adapted stress and longevity gene regulation by Caenorhabditis elegans SKN-1/Nrf. *Aging Cell.* 2009;8(5):524. doi:10.1111/J.1474-9726.2009.00501.X
560. Sheng Y, Yang G, Casey K, et al. A novel role of the mitochondrial iron-sulfur cluster assembly protein ISCU-1/ISCU in longevity and stress response. *Geroscience.* 2021;43(2):691-707. doi:10.1007/S11357-021-00327-Z/METRICS
561. Paek J, Lo JY, Narasimhan SD, et al. Mitochondrial SKN-1/Nrf Mediates a Conserved Starvation Response. *Cell Metab.* 2012;16(4):526-537. doi:10.1016/J.CMET.2012.09.007
562. Tullet JMA, Green JW, Au C, et al. The SKN-1/Nrf2 transcription factor can protect against oxidative stress and increase lifespan in C. elegans by distinct mechanisms. *Aging Cell.* 2017;16(5):1191-1194. doi:10.1111/ACEL.12627
563. Schuster E, McElwee JJ, Tullet JMA, et al. DamID in C. elegans reveals longevity-associated targets of DAF-16/FoxO. *Mol Syst Biol.* 2010;6. doi:10.1038/MSB.2010.54
564. Li J, Ebata A, Dong Y, Rizki G, Iwata T, Siu SL. Caenorhabditis elegans HCF-1 Functions in Longevity Maintenance as a DAF-16 Regulator. *PLoS Biol.* 2008;6(9):e233. doi:10.1371/JOURNAL.PBIO.0060233
565. Senchuk MM, Dues DJ, Schaar CE, et al. Activation of DAF-16/FOXO by reactive oxygen species contributes to longevity in long-lived mitochondrial mutants in Caenorhabditis elegans. *PLoS Genet.* 2018;14(3):e1007268. doi:10.1371/JOURNAL.PGEN.1007268
566. Houthoofd K, Braeckman BP, Johnson TE, Vanfleteren JR. Life extension via dietary restriction is independent of the Ins/IGF-1 signalling pathway in Caenorhabditis elegans. *Exp Gerontol.* 2003;38(9):947-954. doi:10.1016/S0531-5565(03)00161-X
567. Yanase S, Onodera A, Tedesco P, Johnson TE, Ishii N. SOD-1 Deletions in Caenorhabditis elegans Alter the Localization of Intracellular Reactive Oxygen Species and Show Molecular Compensation. *The Journals of Gerontology: Series A.* 2009;64A(5):530-539. doi:10.1093/GERONA/GLP020
568. Libina N, Berman JR, Kenyon C. Tissue-Specific Activities of C. elegans DAF-16 in the Regulation of Lifespan. *Cell.* 2003;115(4):489-502. doi:10.1016/S0092-8674(03)00889-4/ATTACHMENT/892E5581-A7C8-4257-9B09-E158A4C7251D/MMC5.JPG

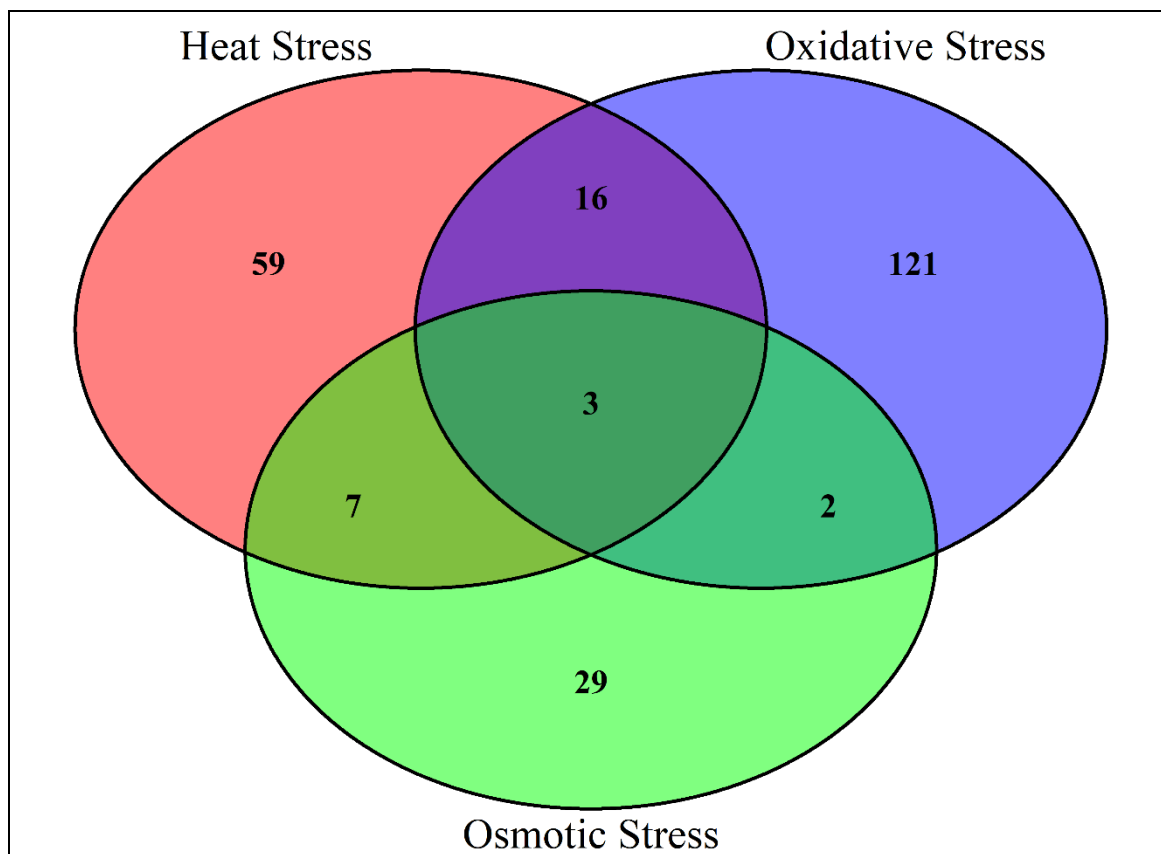
569. Paavanen-Huhtala S, Kalichamy K, Pessi AM, et al. Biomonitoring of Indoor Air Fungal or Chemical Toxins with *Caenorhabditis elegans* nematodes. *Pathogens*. 2023;12(2):161. doi:10.3390/PATHOGENS12020161/S1
570. Panowski SH, Wolff S, Aguilaniu H, Durieux J, Dillin A. PHA-4/Foxa mediates diet-restriction-induced longevity of *C. elegans*. *Nature* 2007 447:7144. 2007;447(7144):550-555. doi:10.1038/nature05837
571. Meng J, Lv Z, Qiao X, et al. The decay of Redox-stress Response Capacity is a substantive characteristic of aging: Revising the redox theory of aging. *Redox Biol*. 2016;11:365. doi:10.1016/J.REDOX.2016.12.026
572. Cabreiro F, Ackerman D, Doonan R, et al. Increased life span from overexpression of superoxide dismutase in *Caenorhabditis elegans* is not caused by decreased oxidative damage. *Free Radic Biol Med*. 2011;51(8):1575. doi:10.1016/J.FREERADBIOMED.2011.07.020
573. Hamaguchi T, Sato K, Vicente CSL, Hasegawa K. Nematicidal actions of the marigold exudate α -terthienyl: oxidative stress-inducing compound penetrates nematode hypodermis. *Biol Open*. 2019;8(4):bio038646. doi:10.1242/BIO.038646
574. Petriv OI, Rachubinski RA. Lack of Peroxisomal Catalase Causes a Progeric Phenotype in *Caenorhabditis elegans*. *Journal of Biological Chemistry*. 2004;279(19):19996-20001. doi:10.1074/JBC.M400207200
575. Hekimi S, Burgess J, Bussière F, Meng Y, Bénard C. Genetics of lifespan in *C. elegans*: molecular diversity, physiological complexity, mechanistic simplicity. *Trends Genet*. 2001;17(12):712-718. doi:10.1016/S0168-9525(01)02523-9
576. Sakamoto T, Maebayashi K, Nakagawa Y, Imai H. Deletion of the four phospholipid hydroperoxide glutathione peroxidase genes accelerates aging in *Caenorhabditis elegans*. *Genes to Cells*. 2014;19(10):778-792. doi:10.1111/GTC.12175
577. Sakamoto T, Maebayashi, Tsunoda Y, Imai H. Inhibition of lipid peroxidation during the reproductive period extends the lifespan of *Caenorhabditis elegans*. *J Clin Biochem Nutr*. 2020;66(2):116. doi:10.3164/JCBN.19-51
578. Sternberg PW, Van Auken K, Wang Q, et al. WormBase 2024: status and transitioning to Alliance infrastructure. *Genetics*. 2024;227(1). doi:10.1093/GENETICS/IYAE050
579. Song S, Zhang X, Wu H, et al. Molecular Basis for Antioxidant Enzymes in Mediating Copper Detoxification in the Nematode *Caenorhabditis elegans*. *PLoS One*. 2014;9(9):e107685. doi:10.1371/JOURNAL.PONE.0107685
580. Ferguson GD, Bridge WJ. The glutathione system and the related thiol network in *Caenorhabditis elegans*. *Redox Biol*. 2019;24:101171. doi:10.1016/J.REDOX.2019.101171
581. Oláhová M, Taylor SR, Khazaipoul S, et al. A redox-sensitive peroxiredoxin that is important for longevity has tissue- and stress-specific roles in stress resistance. *Proc Natl Acad Sci U S A*. 2008;105(50):19839-19844. doi:10.1073/PNAS.0805507105/SUPPL_FILE/0805507105SI.PDF
582. Isermann K, Liebau E, Roeder T, Bruchhaus I. A Peroxiredoxin Specifically Expressed in Two Types of Pharyngeal Neurons is Required for Normal Growth and Egg Production in

- Caenorhabditis elegans. *J Mol Biol.* 2004;338(4):745-755. doi:10.1016/J.JMB.2004.03.021
583. Ranjan M, Grubern J, Ng LF, Halliwell B. Repression of the mitochondrial peroxiredoxin antioxidant system does not shorten life span but causes reduced fitness in *Caenorhabditis elegans*. *Free Radic Biol Med.* 2013;63:381-389. doi:10.1016/J.FREERADBIOMED.2013.05.025
 584. Bhatla N, Horvitz HR. Light and Hydrogen Peroxide Inhibit *C.elegans* Feeding through Gustatory Receptor Orthologs and Pharyngeal Neurons. *Neuron.* 2015;85(4):804-818. doi:10.1016/J.NEURON.2014.12.061/ATTACHMENT/3647EE27-8D34-4463-ABF3-F08FE94F2F7B/MMC4.PDF
 585. Olahova M, Veal EA. A peroxiredoxin, PRDX-2, is required for insulin secretion and insulin/IIS-dependent regulation of stress resistance and longevity. *Aging Cell.* 2015;14(4):558. doi:10.1111/ACEL.12321
 586. Gaudet J, Mango SE. Regulation of organogenesis by the *Caenorhabditis elegans* FoxA protein PHA-4. *Science (1979).* 2002;295(5556):821-825. doi:10.1126/SCIENCE.1065175/SUPPL_FILE/GUADETTABLE3.PDF
 587. Zárate-Potes A, Yang W, Pees B, et al. The *C. elegans* GATA transcription factor elt-2 mediates distinct transcriptional responses and opposite infection outcomes towards different *Bacillus thuringiensis* strains. *PLoS Pathog.* 2020;16(9). doi:10.1371/JOURNAL.PPAT.1008826
 588. Dowell P, Otto TC, Adi S, Lane MD. Convergence of peroxisome proliferator-activated receptor gamma and Foxo1 signaling pathways. *J Biol Chem.* 2003;278(46):45485-45491. doi:10.1074/JBC.M309069200
 589. Brena D, Bertran J, Porta-de-la-Riva M, et al. Ancestral function of Inhibitors-of-kappaB regulates *Caenorhabditis elegans* development. *Scientific Reports* 2020 10:1. 2020;10(1):1-13. doi:10.1038/s41598-020-73146-5
 590. Barnham KJ, Masters CL, Bush AI. Neurodegenerative diseases and oxidative stress. *Nat Rev Drug Discov.Nature Publishing Group.* 2004;3(3):205-214. doi:10.1038/nrd1330
 591. Chen X, Guo C, Kong J. Oxidative stress in neurodegenerative diseases. *Neural Regen Res.* 2012;7(5):376-385. doi:10.3969/j.issn.1673-5374
 592. Barbo M, Koritnik B, Leonardis L, Blagus T, Dolžan V, Ravnik-Glavač M. Genetic Variability in Oxidative Stress, Inflammatory, and Neurodevelopmental Pathways: Impact on the Susceptibility and Course of Spinal Muscular Atrophy. *Cell Mol Neurobiol.* 2024;44(1):71. doi:10.1007/S10571-024-01508-Y
 593. Zhang Y, Kiryu H. Identification of oxidative stress-related genes differentially expressed in Alzheimer's disease and construction of a hub gene-based diagnostic model. *Scientific Reports* 2023 13:1. 2023;13(1):1-15. doi:10.1038/s41598-023-34021-1
 594. Zhu Z, Jiang H. Identification of oxidative stress-related biomarkers associated with the development of acute-on-chronic liver failure using bioinformatics. *Scientific Reports* 2023 13:1. 2023;13(1):1-15. doi:10.1038/s41598-023-44343-9
 595. Gu Y, Yu W, Qi M, et al. Identification and validation of hub genes and pathways associated with mitochondrial dysfunction in hypertrophy of ligamentum flavum. *Front Genet.* 2023;14:1117416. doi:10.3389/FGENE.2023.1117416

596. Yang W, Hekimi S. A Mitochondrial Superoxide Signal Triggers Increased Longevity in *Caenorhabditis elegans*. *PLoS Biol.* 2010;8(12):e1000556. doi:10.1371/JOURNAL.PBIO.1000556
597. Wu S, Lei L, Song Y, et al. Mutation of *hop-1* and *pink-1* attenuates vulnerability of neurotoxicity in *C. elegans*: the role of mitochondria-associated membrane proteins in Parkinsonism. *Exp Neurol.* 2018;309:67. doi:10.1016/J.EXPNEUROL.2018.07.018
598. Taylor SKB, Minhas MH, Tong J, Selvaganapathy PR, Mishra RK, Gupta BP. *C. elegans* electrotaxis behavior is modulated by heat shock response and unfolded protein response signaling pathways. *Scientific Reports* 2021 11:1. 2021;11(1):1-17. doi:10.1038/s41598-021-82466-z
599. Ji P, Li H, Jin Y, Peng Y, Zhao L, Wang X. *C. Elegans* as an in vivo model system for the phenotypic drug discovery for treating paraquat poisoning. *PeerJ.* 2022;10:e12866. doi:10.7717/PEERJ.12866/SUPP-9
600. Baskoylu SN, Yersak J, O'Hern P, et al. Single copy/knock-in models of ALS SOD1 in *C. elegans* suggest loss and gain of function have different contributions to cholinergic and glutamatergic neurodegeneration. *PLoS Genet.* 2018;14(10). doi:10.1371/journal.pgen.1007682
601. Horspool AM, Chang HC. Superoxide dismutase SOD-1 modulates *C. elegans* pathogen avoidance behavior. *Sci Rep.* 2017;7:45128. doi:10.1038/SREP45128
602. Byrne JJ, Soh MS, Chandhok G, et al. Disruption of mitochondrial dynamics affects behaviour and lifespan in *Caenorhabditis elegans*. *Cellular and Molecular Life Sciences.* 2019;76(10):1967-1985. doi:10.1007/S00018-019-03024-5/FIGURES/8
603. Guha S, Cheng A, Carroll T, et al. Selective disruption of Drp1-independent mitophagy and mitolysosome trafficking by an Alzheimer's disease relevant tau modification in a novel *Caenorhabditis elegans* model. *Genetics.* 2022;222(1). doi:10.1093/GENETICS/IYAC104
604. Scholtes C, Bellemin S, Martin E, et al. DRP-1-mediated apoptosis induces muscle degeneration in dystrophin mutants. *Scientific Reports* 2018 8:1. 2018;8(1):1-16. doi:10.1038/s41598-018-25727-8
605. Zhou H, Singh H, Parsons ZD, et al. The biological buffer bicarbonate/CO₂ potentiates H₂O₂-mediated inactivation of protein tyrosine phosphatases. *J Am Chem Soc.* 2011;133(40):15803-15805. doi:10.1021/JA2077137/SUPPL_FILE/JA2077137_SI_001.PDF
606. Tanner JJ, Parsons ZD, Cummings AH, Zhou H, Gates KS. Redox Regulation of Protein Tyrosine Phosphatases: Structural and Chemical Aspects. <https://home.liebertpub.com/ars>. 2011;15(1):77-97. doi:10.1089/ARS.2010.3611
607. Kim JS, Saengsirisuwan V, Sloniger JA, Teachey MK, Henriksen EJ. Oxidant stress and skeletal muscle glucose transport: Roles of insulin signaling and p38 MAPK. *Free Radic Biol Med.* 2006;41(5):818-824. doi:10.1016/J.FREERADBIOMED.2006.05.031
608. Weinkove D, Halstead JR, Gems D, Divecha N. Long-term starvation and ageing induce AGE-1/PI 3-kinase-dependent translocation of DAF-16/FOXO to the cytoplasm. *BMC Biol.* 2006;4(1):1-13. doi:10.1186/1741-7007-4-1/FIGURES/7

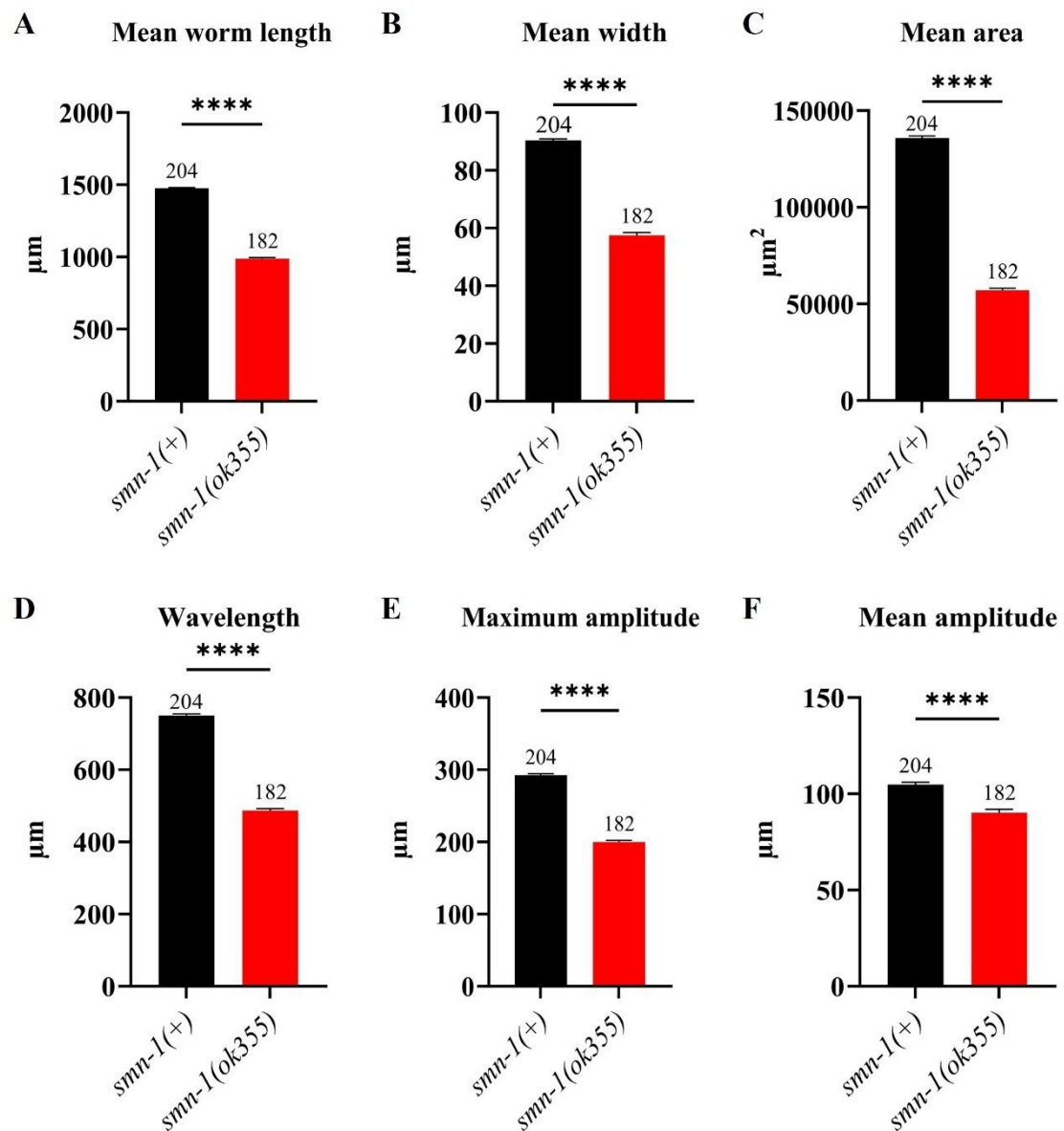
609. Doonan R, McElwee JJ, Matthijssens F, et al. Against the oxidative damage theory of aging: superoxide dismutases protect against oxidative stress but have little or no effect on life span in *Caenorhabditis elegans*. *Genes Dev.* 2008;22(23):3236-3241. doi:10.1101/GAD.504808
610. Wu CY, Gagnon DA, Sardin JS, et al. Enhancing GABAergic Transmission Improves Locomotion in a *Caenorhabditis elegans* Model of Spinal Muscular Atrophy. *eNeuro.* 2019;5(6):ENEURO.0289-18.2018. doi:10.1523/ENEURO.0289-18.2018
611. Kye MJ eong, Niederst ED, Wertz MH, et al. SMN regulates axonal local translation via miR-183/mTOR pathway. *Hum Mol Genet.* 2014;23(23):6318-6331. doi:10.1093/HMG/DDU350
612. Rashid S, Dimitriadi M. Autophagy in spinal muscular atrophy: from pathogenic mechanisms to therapeutic approaches. *Front Cell Neurosci.* 2024;17:1307636. doi:10.3389/FNCEL.2023.1307636
613. Biondi O, Branchu J, Salah A Ben, et al. IGF-1R Reduction Triggers Neuroprotective Signaling Pathways in Spinal Muscular Atrophy Mice. *The Journal of Neuroscience.* 2015;35(34):12063. doi:10.1523/JNEUROSCI.0608-15.2015
614. Bosch-Marcé M, Wee CD, Martinez TL, et al. Increased IGF-1 in muscle modulates the phenotype of severe SMA mice. *Hum Mol Genet.* 2011;20(9):1844-1853. doi:10.1093/HMG/DDR067,
615. Mahadev K, Motoshima H, Wu X, et al. The NAD(P)H Oxidase Homolog Nox4 Modulates Insulin-Stimulated Generation of H₂O₂ and Plays an Integral Role in Insulin Signal Transduction. *Mol Cell Biol.* 2004;24(5):1844. doi:10.1128/MCB.24.5.1844-1854.2004

Anexo I



Supplementary Figure 1. Venn diagram illustrating the overlap of molecular components involved in the oxidative, heat and osmotic stress responses in *C. elegans*

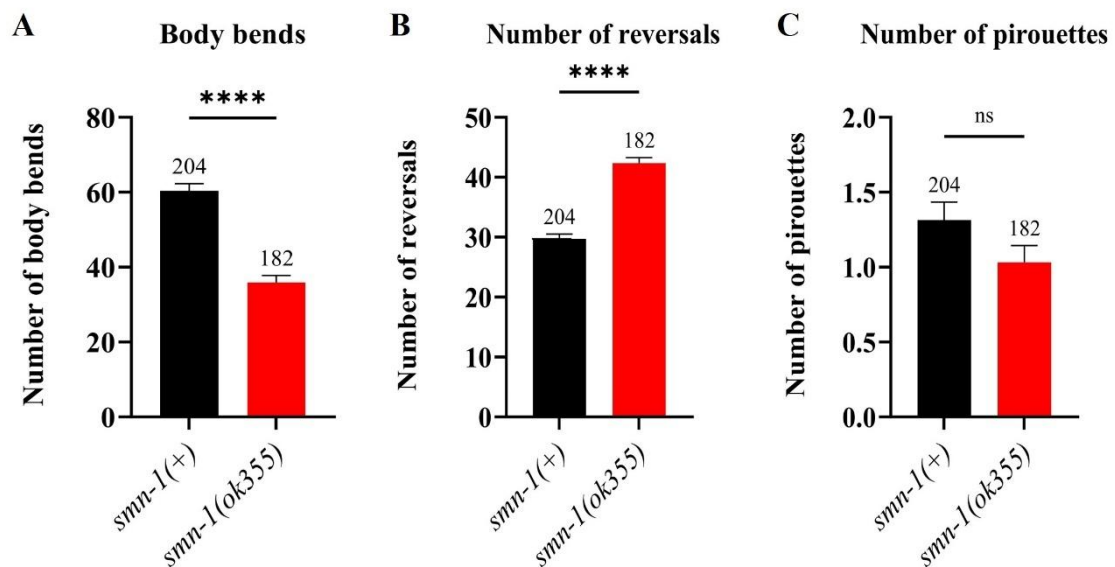
The list of genes associated with each stress response were obtained from the Gene Ontology (GO) database under the identifiers GO:0006979 (oxidative stress response), GO:0009408 (heat stress response) and GO:0006970 (osmotic stress response). Only 3 genes were common to all three stress responses, whereas 121, 59, and 29 genes were specific to oxidative, heat, and osmotic stress, respectively. This limited overlap supports the notion that stress responses are partially independent, and may explain why certain mutants display selective sensitivity to specific stressors.



Supplementary Figure 2. WormLab shape-based parameters

At day 3 post-hatching, the length (A), width (B), and area (C) of *smn-1(ok355)* nematodes were significantly smaller than those of *smn-1(+)* animals ($P < 0.0001$, $P < 0.0001$, and $P < 0.0001$, respectively). Similarly, parameters related to the sinusoidal curvature of the body of the animals while crawling, such as wavelength (D), maximum amplitude (E), and mean amplitude (F), were also significantly reduced in *smn-1(ok355)* animals in comparison to healthy *smn-1(+)* ($P < 0.0001$, $P < 0.0001$, and $P < 0.0001$, respectively), as such parameters are dependent on the size (length, width, and area) of the animals. Therefore, these parameters were not taken into consideration for the study herein.

Data are presented as the mean \pm SEM from at least ten independent trials. Statistical significance was determined using Mann-Whitney unpaired test. **** $P < 0.0001$. The sample size (n) for each condition is shown above of the corresponding error bar.



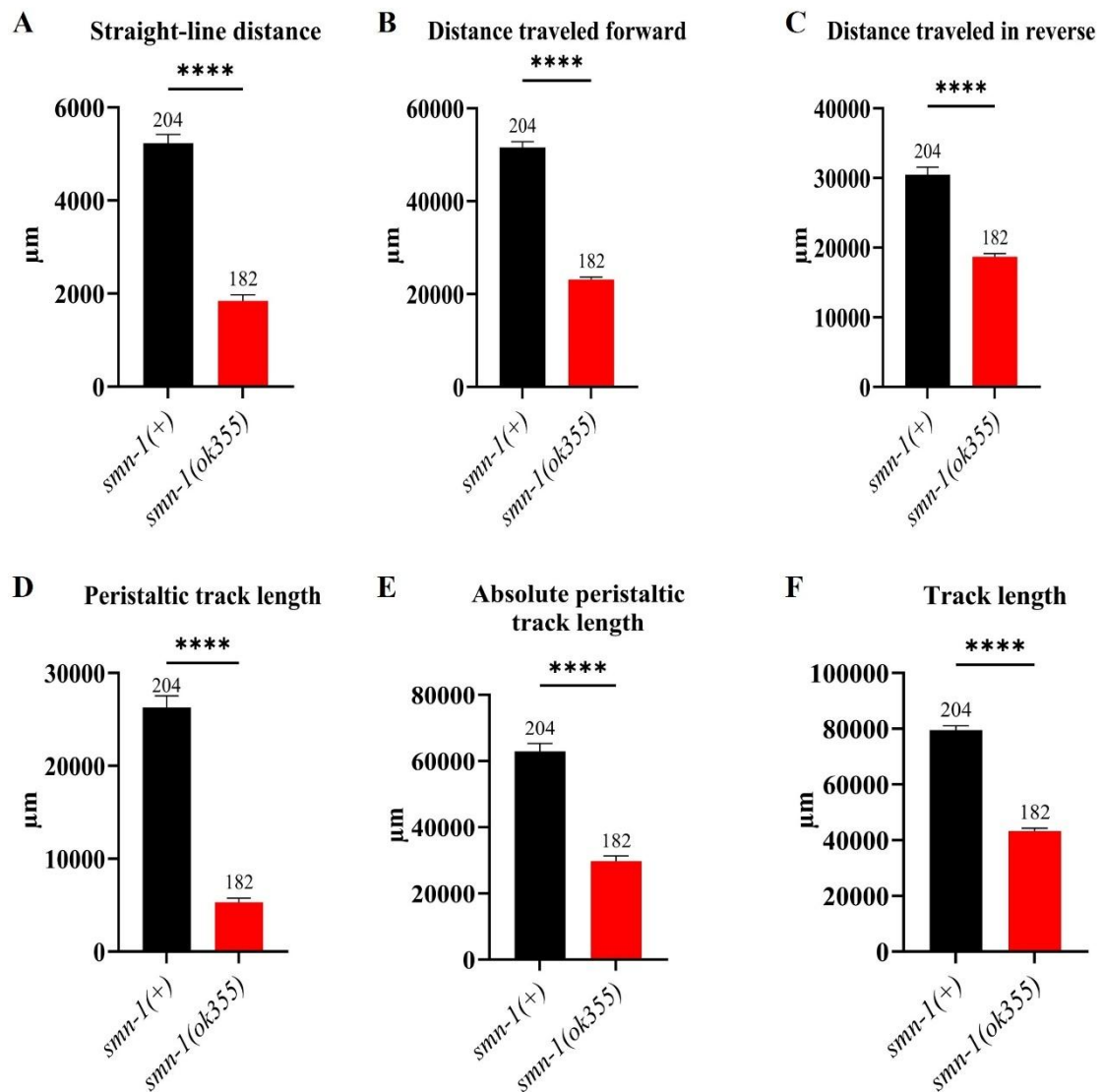
Supplementary Figure 3. WormLab movement-behaviour parameters

(A) The number of body bends is a general measure of a nematode's body angle during crawling. One body bend is defined as the bending angle between the head and tail of the nematode of at least 20 degrees amplitude, maintained for at least five frames. During a five-minutes recording, *smn-1(ok355)* animals had significantly fewer body bends than *smn-1(+)* animals ($P < 0.0001$).

(B) *C. elegans* has two types of motion: forward and reverse. The number of reversals refers to the number of times *C. elegans* changed from forward to reverse locomotion. Our analysis revealed that *smn-1(ok355)* animals exhibited an increased number of reversals compared to *smn-1(+)* nematodes ($P < 0.0001$).

(C) *C. elegans* can undergo sudden changes in direction through pirouettes. A pirouette is defined as a reversal movement followed by a bending angle between the head and tail of the nematode of at least 90 degrees amplitude (omega shape Ω conformation). Our analysis revealed no significant differences in the number of pirouettes between *smn-1(ok355)* and *smn-1(+)* animals ($P = 0.8815$).

Data are presented as the mean \pm SEM from at least ten independent trials. Statistical significance was determined using Mann-Whitney unpaired test. ns $P > 0.05$; **** $P < 0.0001$. The sample size (n) for each condition is shown above of the corresponding error bar.



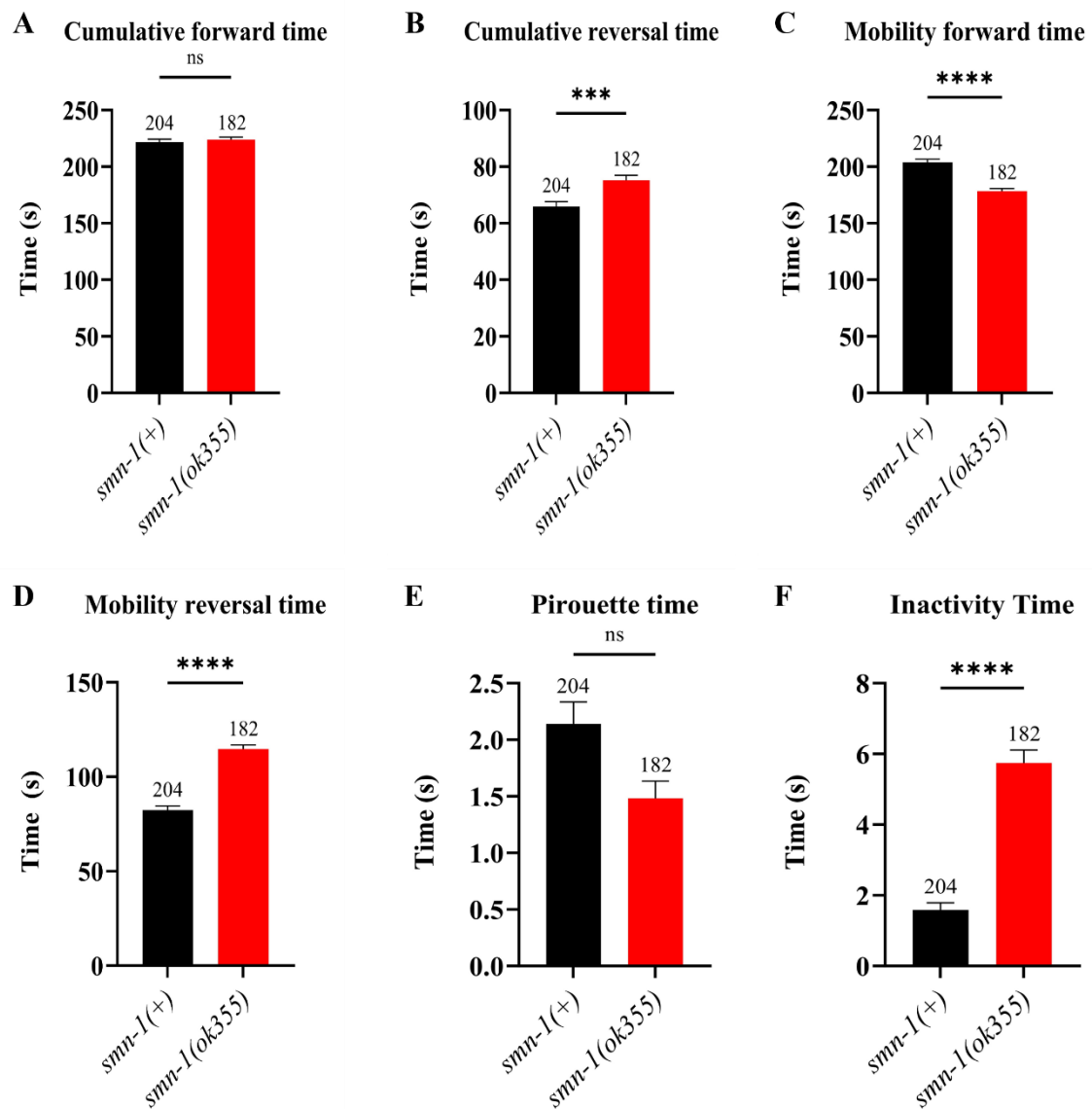
Supplementary Figure 4. WormLab distance-travelled parameters

The straight-line distance (A) is defined as the length of an imaginary straight line drawn from the initial position “X” occupied by the animal assessed at the beginning of the filming, until the final position “Y” occupied by the same animal at the end of the filming. Our analysis revealed that the length of the straight-line travelled by *smn-1(ok355)* animals during a five-minute film was significantly lower than that of *smn-1(+)* nematodes ($P < 0.0001$). Moreover, the total distance travelled in forward locomotion (B) and reverse locomotion (C) during the same period was reduced in *smn-1(ok355)* mutants compared to that of healthy *smn-1(+)* nematodes ($P < 0.0001$ and $P < 0.0001$, respectively).

WormLab generates additional distance-travelled parameters derived from (A), (B) and (C) measurements. The peristaltic track length (D) is the total distance travelled in forward locomotion minus the total distance travelled in reverse locomotion ($D = B - C$). The absolute peristaltic track length (E) is the total distance travelled in forward locomotion plus the total distance travelled in reverse locomotion ($E = B + C$). Finally, the track length (F) parameter is very similar to the absolute peristaltic track length parameter, except that *C. elegans* movement behaviour needs to be maintained for a minimum number of frames for the locomotion to be considered either forward or reverse. This threshold was not considered when calculating (D) or (E), which is why the track length was always slightly higher than the absolute peristaltic track length (F). Our analysis revealed that *smn-1(ok355)* exhibited decreased peristaltic track length

(D), absolute peristaltic track length (E) and track length (F) in comparison with healthy *smn-1(+)* animals ($P < 0.0001$, $P < 0.0001$, and $P < 0.0001$, respectively)

Data are presented as the mean \pm SEM from at least ten independent trials. Statistical significance was determined using Mann-Whitney unpaired test. **** $P < 0.0001$. The sample size (n) for each condition is shown above of the corresponding error bar.



Supplementary Figure 5. WormLab time-based parameters

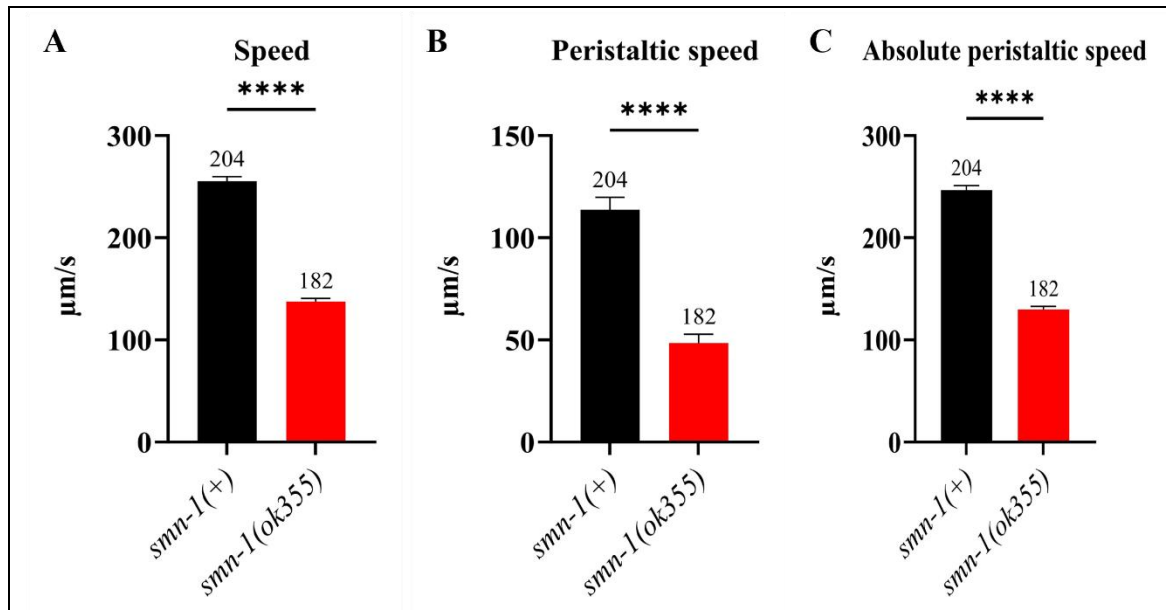
The cumulative forward time (A) encompasses all periods during which the animal assessed is engaged in forward locomotion, with no threshold for the minimum number of frames to be maintained to define forward locomotion. There was no significant difference in cumulative forward time (A) between *smn-1(ok355)* mutants and *smn-1(+)* healthy animals ($P = 0.4851$). The cumulative reversal time (B) encompasses all periods during which the animal assessed is engaged in reverse locomotion, with no threshold for the minimum number of frames to be maintained to define reverse locomotion. Our analysis revealed that the cumulative reversal time (B) was significantly increased in *smn-1(ok355)* nematodes compared to that in *smn-1(+)* animals ($P < 0.001$).

The mobility forward time (C) refers to the total amount of time during which the animal is actively moving forward, with the requirement that the behaviour needs to be maintained for a minimum number of frames for the locomotion to be considered forward. Our analysis revealed that *smn-1(ok355)* animals exhibited significantly lower mobility forward time than *smn-1(+)* animals ($P < 0.0001$). The mobility reversal time (D) refers to the total amount of time during which the animal is actively moving in reverse, with the requirement that the behaviour needs to be maintained for a minimum number of frames for locomotion to be considered reversal. Our

analysis revealed that *smn-1(ok355)* animals exhibited significantly greater mobility reversal time than *smn-1(+)* animals ($P < 0.0001$).

WormLab also calculated the time that the animals spent engaging in pirouette behaviour (E), with no statistically significant differences found between *smn-1(ok355)* and *smn-1(+)* animals ($P = 0.0610$). Finally, the mobility idle time, defined as the total amount of time that the animals spent inactive during the film, was significantly higher in *smn-1(ok355)* animals than in *smn-1(+)* healthy nematodes ($P < 0.0001$).

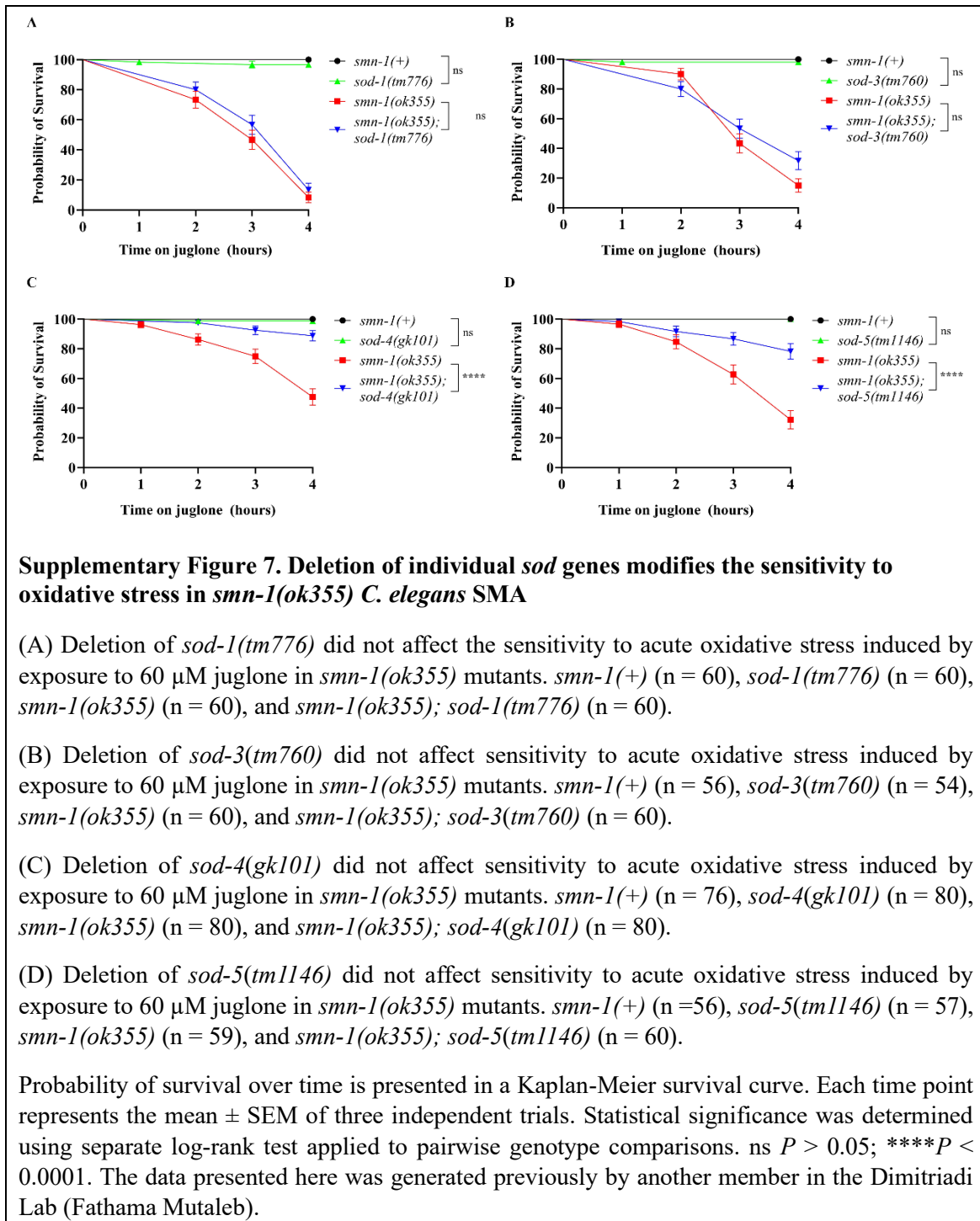
Data are presented as the mean \pm SEM from at least ten independent trials. Statistical significance was determined using Mann-Whitney unpaired test. ns $P > 0.05$; *** $P < 0.001$; **** $P < 0.0001$. The sample size (n) for each condition is shown above of the corresponding error bar.

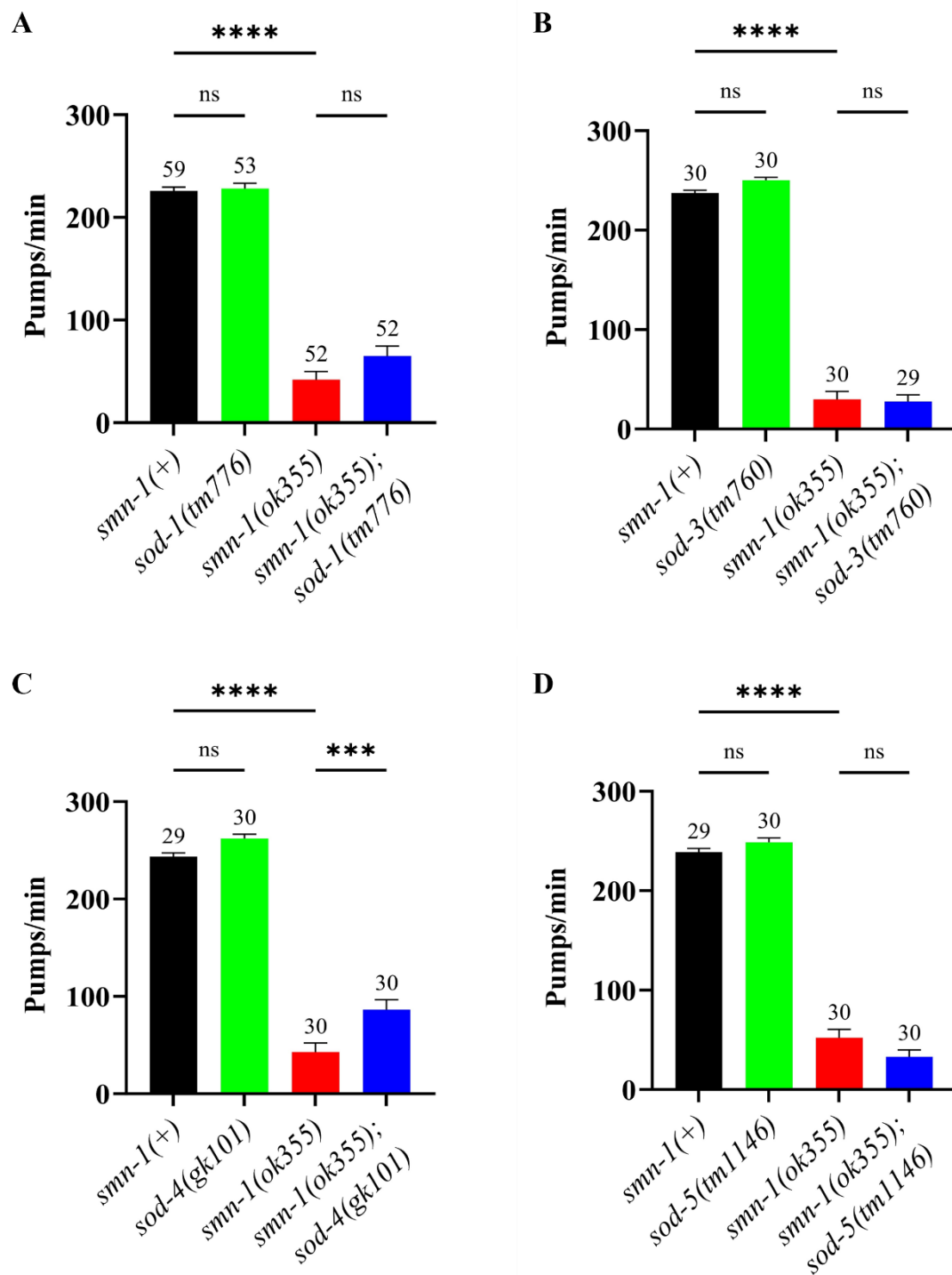


Supplementary Figure 6. WormLab speed measurements

WormLab calculated three different speed measurements derived from different distance-travelled parameters divided by the total duration of the film. Speed (A) uses the distance calculated in the track length parameter, peristaltic speed (B) uses the distance calculated in the peristaltic track length parameter, and absolute peristaltic speed (C) uses the distance calculated in the absolute peristaltic track length parameter. Our analysis revealed that all three parameters of speed (A), (B), and (C) were significantly reduced in *smn-1(ok355)* animals compared to *smn-1(+)* healthy nematodes ($P < 0.0001$, $P < 0.0001$, and $P < 0.0001$, respectively).

Data are presented as the mean \pm SEM from at least ten independent trials. Statistical significance was determined using Mann-Whitney unpaired test. **** $P < 0.0001$. The sample size (n) for each condition is shown above of the corresponding error bar.





Supplementary Figure 8. Deletion of *sod-4* gene can modify *smn-1(ok355)* *C. elegans* neuromuscular defects

(A) Deletion of *sod-1(tm776)* did not affect the pharyngeal pumping rate of *smn-1(ok355)* mutants.

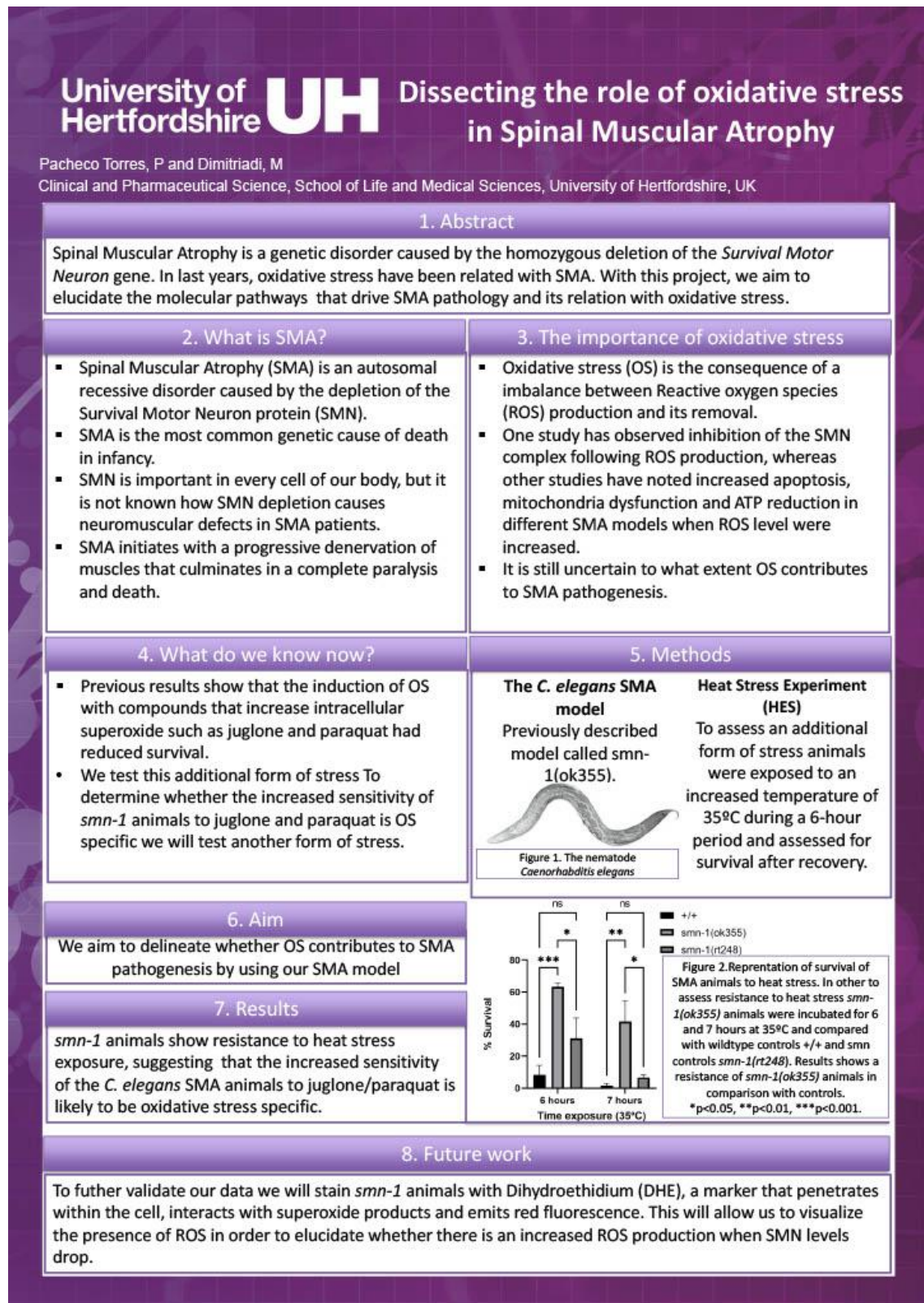
(B) Deletion of *sod-3(tm760)* did not affect the pharyngeal pumping rate of *smn-1(ok355)* mutants.

(C) Deletion of *sod-4(gk101)* increased the number of pumps/min of *smn-1(ok355)* mutants.

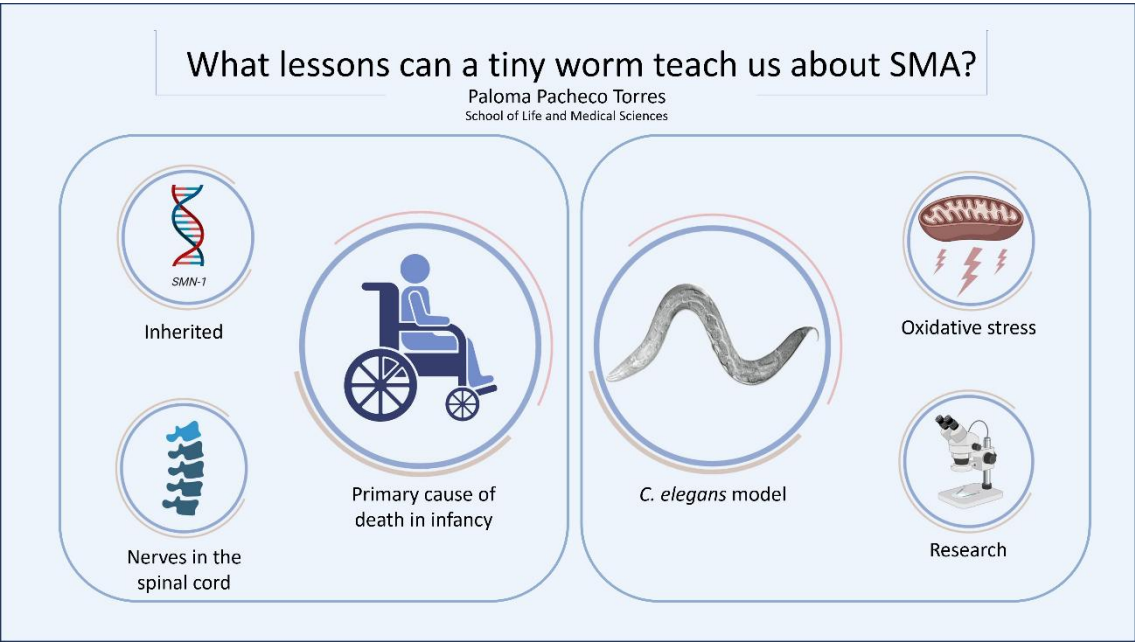
(D) Deletion of *sod-5(tm1146)* did not affect the pharyngeal pumping rate of *smn-1(ok355)* mutants.

Data are presented as the mean \pm SEM from at least two independent trials. Statistical significance was determined using one-way ANOVA ($P < 0.0001$, $P < 0.0001$, $P < 0.0001$, and $P < 0.0001$, for A, B, C, and D, respectively), followed by Sidak's multiple comparison test. ns $P > 0.05$; *** $P < 0.001$; **** $P < 0.0001$. The sample size (n) for each condition is shown above of the corresponding error bar. The data presented here was generated previously by another member in the Dimitriadi Lab (Fathama Mutaleb).

Anexo II



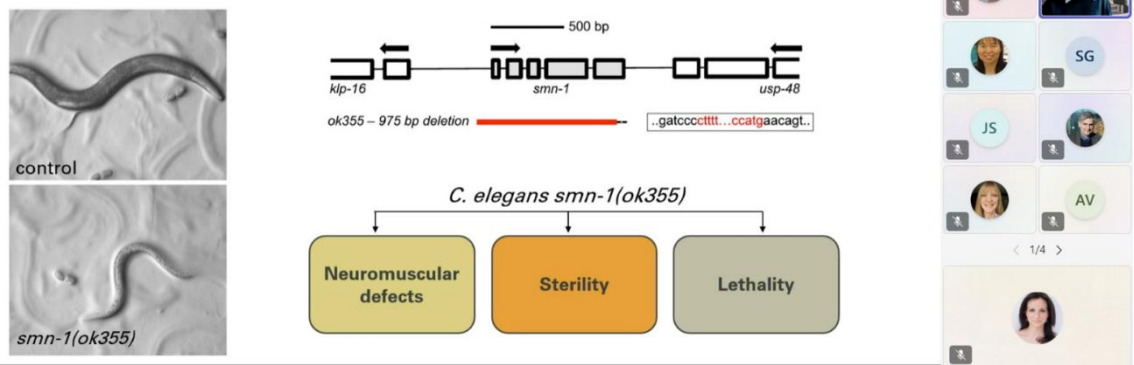




A5. Life and Medical School Annual Research Conference 2024 – 11 Jun 2024 – University of Hertfordshire, Hatfield, United Kingdom – Presentation.

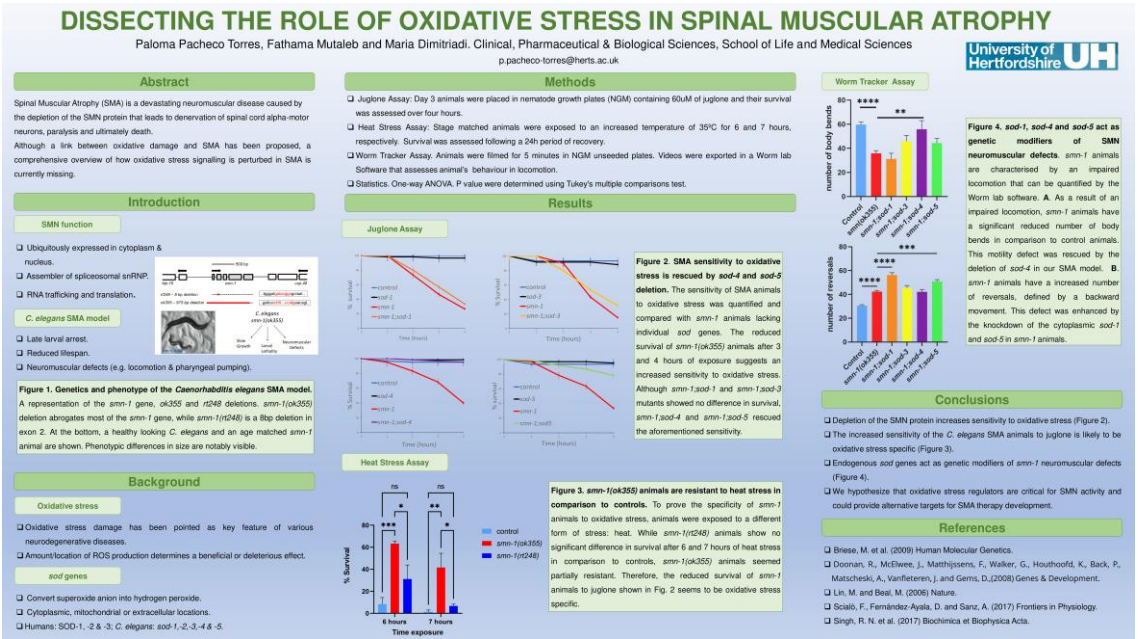


The *C. elegans* SMA model

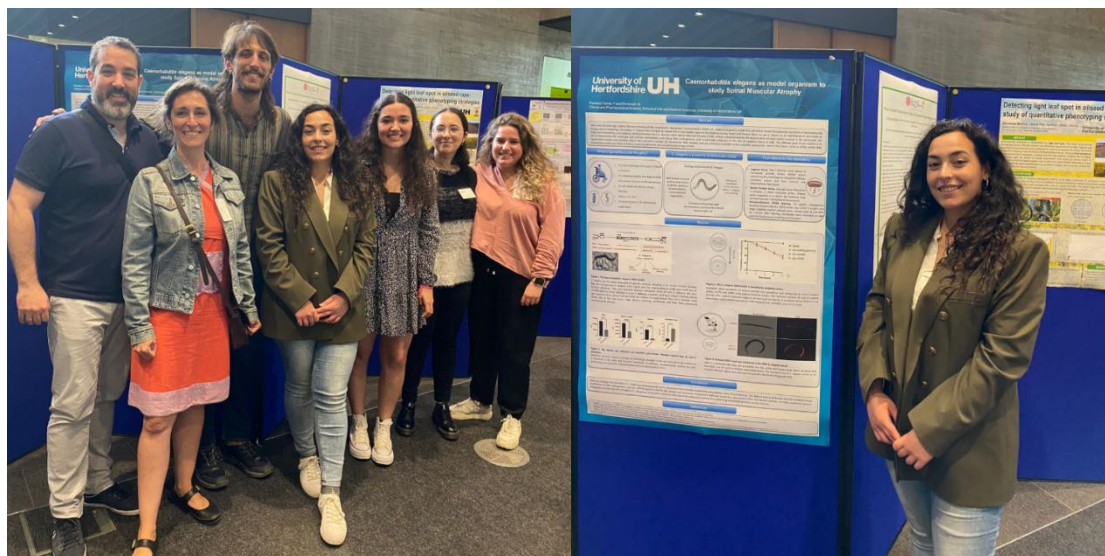


B1. Worm Club Seminars 2021 – 3 Nov 2021 – The London Worm Club (online), United Kingdom – Presentation.

The screenshot shows a Zoom meeting interface. At the top, a status bar indicates 'You are viewing Paloma Pacheco's screen'. Below this, a row of participant thumbnails is visible, including Maria Dimitriadi, Paloma Pacheco, Rachel Wilson, Arantza Barrios, QueeLim Ch'ng, and Tom O'Brien. The main area of the screen displays a presentation slide with a dark background and a blue wavy line graphic. The slide title is 'Spinal Muscular Atrophy' in large white text. Below the title, it says 'DISSECTING THE ROLE OF OXIDATIVE STRESS'. At the bottom of the slide, the presenters are listed as 'Paloma Pacheco Torres & Fathama Mutaleb' and 'Dimitriadi Lab'. The University of Hertfordshire logo (UH) is in the top right corner of the slide. The Zoom interface at the bottom shows controls for Unmute, Start Video, Participants (43), Chat, Share Screen, Live Transcript, Reactions, and a red Leave button.



B3. IX International Symposium SRUK – 1-3 July 2022 – Spanish Researchers in the UK, Oxford, United Kingdom – Poster presentation.



IX INTERNATIONAL SYMPOSIUM SRUK/CERU | OXFORD 2022



Paloma Pacheco Torres

has been awarded the

Best Poster Award

for their contribution to the IX International Symposium SRUK/CERU



FUNDACIÓN
RAMÓN ARECES



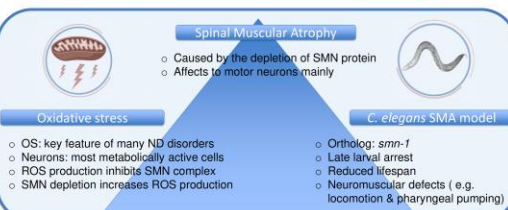
B4. SRUK Ageing and Diseases Conference – 9 Jun 2023 – Spanish Researchers in the United Kingdom, Cambridge, United Kingdom – Presentation.



Abstract

Spinal muscular atrophy (SMA) is the most common monogenic cause of death in infancy, triggered by the depletion of the ubiquitously expressed survival motor neuron protein (SMN). It is still unknown which are the molecular mechanisms involved in this disorder and why specifically alpha-motor neurons are mainly affected. A role of oxidative stress (OS) in SMA has been proposed with various SMA models depicting an increase in reactive oxygen species (ROS) production; ROS induction has also been correlated with the inhibition of the SMN complex, apoptosis and impaired *SMN2* gene splicing. Despite this growing body of evidence, a comprehensive overview of how oxidative stress signalling is perturbed in SMA is missing. The focus of the project proposed herein is to utilise the powerful genetic tools of *C. elegans* and a range of functional assays and pharmacological challenges to delineate the mechanism(s) by which oxidative stress perturbations control SMN function.

Introduction



Methods

- Oxidative stress sensitivity assay.** Day 3 animals were placed in nematode growth media (NGM) plates containing 60 μ M of Juglone or 4mM of Paraquat (drugs that induce oxidative stress) and their survival was assessed over time.
- Osmotic stress assay.** Day 3 animals were placed in hyperosmotic plates containing 450 mM NaCl and incubated at 20°C for 24h. Following this, animals were washed and transferred to isotonic plates (50mM NaCl) and after a 24h period of recovery their survival was assessed.
- Heat stress assay.** L4 animals were picked on the day and incubated at 35°C for 6 or 7 hours. Following this, plates were moved to 20°C and after a 24h period of recovery survival was assessed.
- Antioxidant treatment.** Day 3 animals were raised in NGM plates containing different concentrations of N-Acetyl-L-cysteine (NAC) or Vitamin C (VitC) and filmed for 10 seconds. Rate of pumps was determined by counting the number of grinder contractions in any axis.
- Statistical analysis.** Analysis were performed in GraphPad Prism 9.3.1. Error bars indicate \pm SEM. Mann-Whitney U test: * $P < 0.05$; ** $P < 0.01$; *** $P < 0.001$; n.s., not significant. One-way ANOVA and Log-rank test test: * $P < 0.1$, ** $P < 0.01$, *** $P < 0.001$

Results

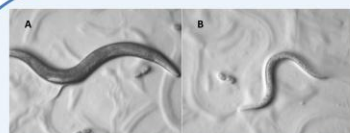


Figure 1. The *Caenorhabditis elegans* SMA model

C. elegans can be easily amenable to genetic analysis, allowing us to 'mimic' human diseases. A healthy looking *smn-1(+)* (A) and an age-matched *smn-1(ok355)* animal (B) are shown. Depletion of *smn-1* causes slow movement, larval arrest and prominent neuromuscular defects. The endogenous *C. elegans smn-1* gene (C) and the representative *ok355* (D) and *rt248* (E) loss-of-function deletions are depicted. The *smn-1(ok355)* deletion abrogates most of *smn-1*, whereas the *smn-1(rt248)* allele encompasses an 8 bp deletion in exon 2.

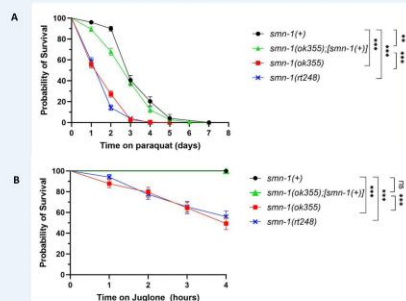


Figure 2. The *C. elegans* SMA model is sensitive to oxidative stress.

Oxidative stress sensitivity of *smn-1(+)* control animals was quantified and compared to *smn-1* mutant alleles *ok355* and *rt248* using paraquat (A) or juglone (B) sensitivity assays. The reduced survival of *smn-1* animals following either juglone or paraquat exposure suggests an increased sensitivity to oxidative stress; an observation that is not evident in either control or in the *smn-1(+)* single copy insertion strain *smn-1(ok355); [smn-1(+)]*. Data was analysed with Log-Rank test.

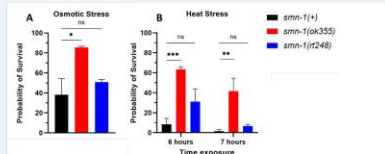


Figure 3. *smn-1(ok355)* animals display increased tolerance to osmotic and heat stress.

smn-1(ok355) mutants exhibited increased survival to both osmotic (A) and heat stress (B) compared with *smn-1(+)* control animals. Contrary, the *smn-1(rt248)* mutant mirrors *smn-1(+)* controls which are sensitive to both osmotic and heat stress. Data was analysed with One-way ANOVA test.

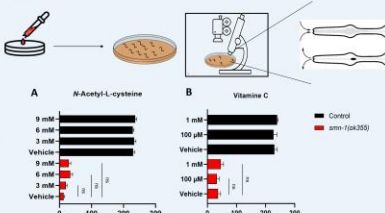


Figure 4. N-Acetyl-L-cysteine and Vitamin C do not ameliorate *smn-1* pharyngeal pumping defects.

SMN depletion causes defective neuromuscular function that can be assessed by the pharyngeal pumping assay while feeding. Treatment with 3, 6 and 9mM NAC (A) or 0.1 and 1mM Vitamin C (B) did not modify the pharyngeal pumping rates of *smn-1(ok355)* animals. Data was analysed with Mann-Whitney U test, two-tailed.

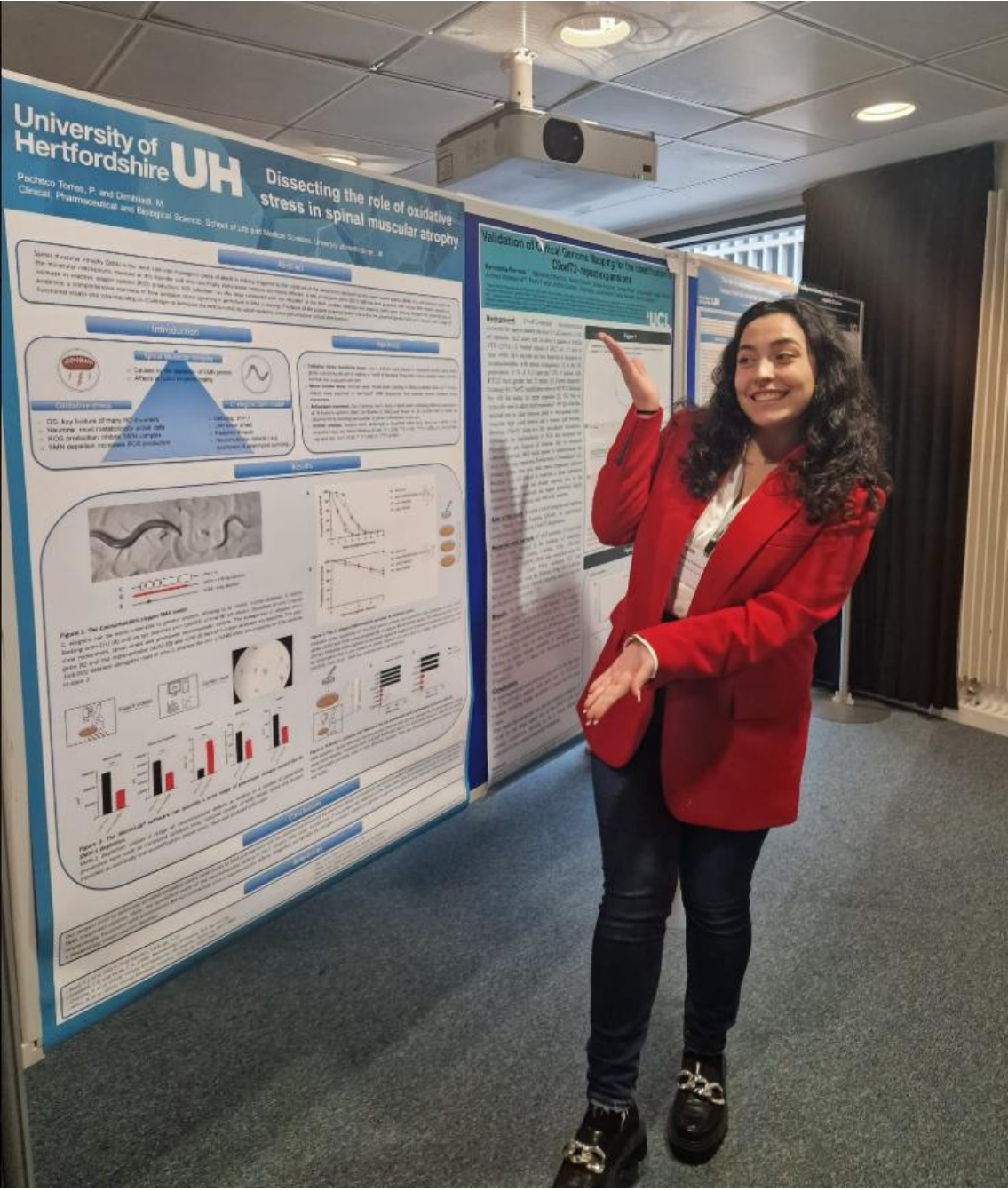
Conclusions

Our project aims to delineate whether oxidative stress contributes to SMA pathogenesis with the ultimate goal to identify the conserved cellular and molecular mechanisms needed to spearhead further therapeutic avenues for SMA treatment options. Here, we show that the depletion of the SMN protein leads to increased sensitivity that is likely to be oxidative stress as is suggested for an increased tolerance of *smn-1* animals to other type of stresses. Interestingly, treatment with antioxidants did not ameliorate *smn-1* neuromuscular defects. Altogether, we highlight the strengths of using *C. elegans* as a genetic *in vivo* tool to understand the molecular mechanisms underlying a devastating motor neuron disorder.

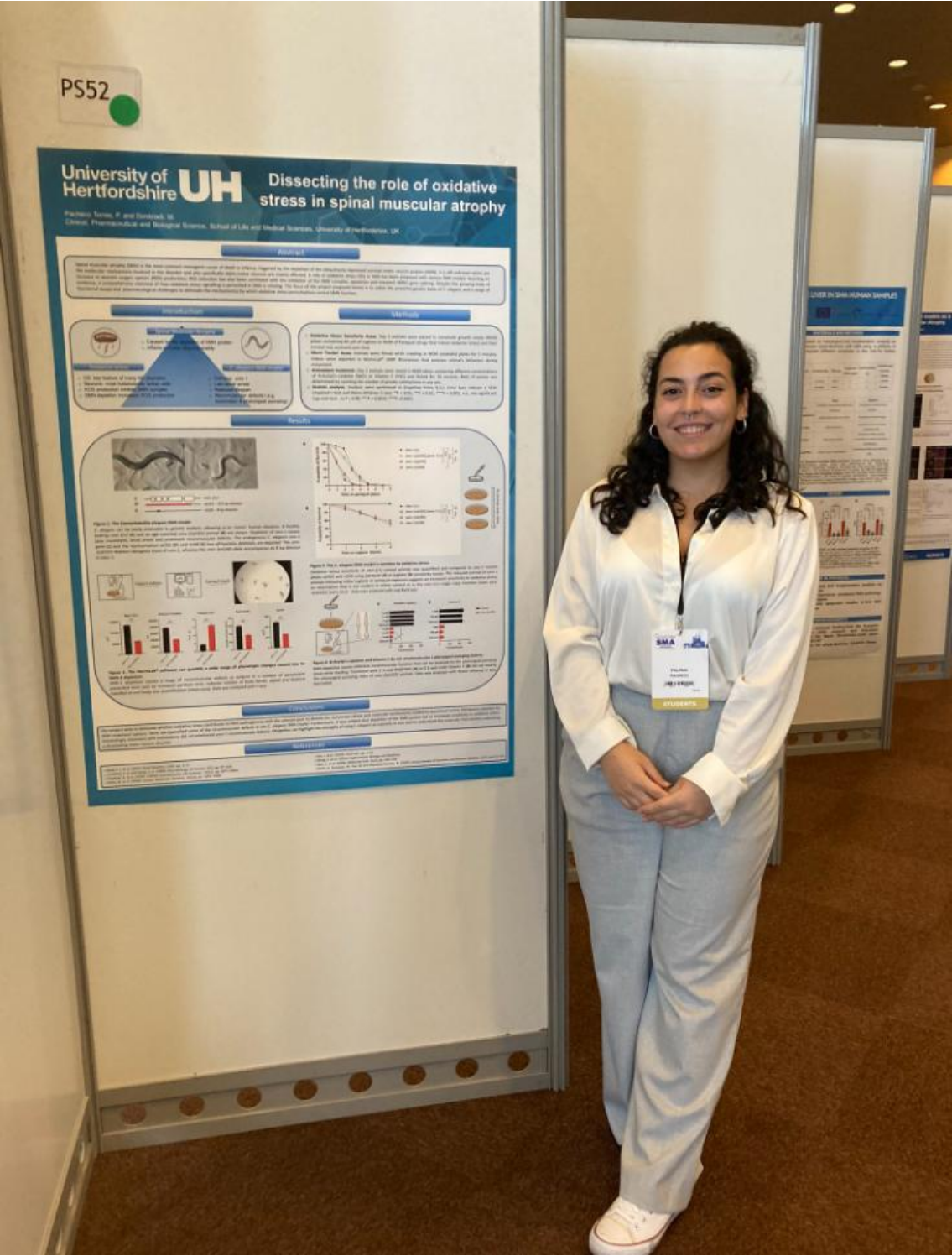
References

- Boyd, P. J. et al. (2017). PLoS Genetics, 13(4), pp. 1–27.
- Crawford, T. O. and Pardo, C. A. (1996). Neurobiology of Disease, 3(2), pp. 97–110.
- Chaytow, H. et al. (2018). Cellular and Molecular Life Sciences, 75(21), pp. 3877–3894.
- Miller, N. et al. (2016). Human Molecular Genetics, 25(16), pp. 3395–3406.
- Seo, J. et al. (2016). PLoS one, pp. 1–31.
- Wang, C. et al. (2013). Experimental Biology and Medicine.
- Wan, L. et al. (2008). Molecular Cell, 31(2), pp. 244–254.
- Wirth, B., Karakaya, M., Kye, M. and Mendoza-Ferreira, N. (2020). Annual Review of Genomics and Human Genetics, 21(1), pp. 231–261.

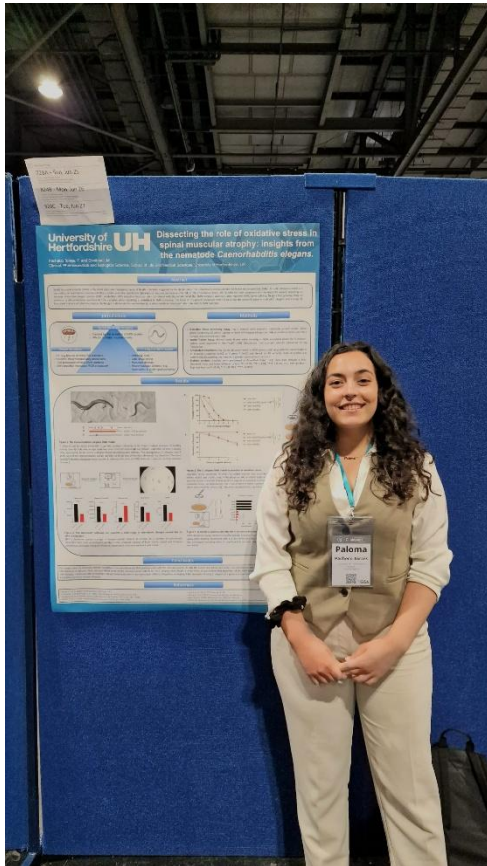
B6. 16th UK Neuromuscular Translational Research Conference – 29-30 Mar 2023 – Muscular Dystrophy UK, University College London, London, United Kingdom – Poster presentation.



C1. 3rd International Scientific Congress on Spinal Muscular Atrophy – 21-23 October 2022 – SMA Europe, Barcelona, Spain – Poster presentation.



C2. 24th International *C. elegans* Conference – 24-28 June 2023 – Genetics Society of America, Glasgow, Scotland – Poster presentation.



C3. 4th International Scientific Congress on Spinal Muscular Atrophy – 14-16 March 2024 – SMA Europe, Ghent, Belgium – Poster presentation.

